

MUC1 MEDIATED SIGNALING IN PANCREATIC DUCTAL ADENOCARCINOMA

by

Priyanka Grover

A dissertation submitted to the faculty of
The University of North Carolina at Charlotte
in partial fulfillment of the requirements
for the degree of Doctor of Philosophy in
Biological Sciences

Charlotte

2019

Approved by:

Dr. Pinku Mukherjee

Dr. Didier Dréau

Dr. Valery Grdzlishvili

Dr. Andrew Truman

Dr. Juan Vivero-Escoto

ABSTRACT

PRIYANKA GROVER. MUC1 Mediated Signaling in Pancreatic Ductal Adenocarcinoma. (Under the direction of DR. PINKU MUKHERJEE)

In 2019, Pancreatic Cancer (PC) is the 3rd leading cause of cancer-related deaths in the USA with 94% dying within 5 years of diagnosis. 90% of PC is Pancreatic Ductal Adenocarcinoma (PDA), of which >80% overexpress a hypo-glycosylated form the membrane-bound glycoprotein of Mucin-1 (tMUC1). While overexpression of tMUC1 is associated with metastasis and poor prognosis, the mechanism remains unclear. Transforming growth factor- β 1 (TGF- β) is a cytokine with dual functionality. Within normal cells and during early carcinogenesis, TGF- β 1 functions as a tumor suppressor through the engagement of the TGF- β Receptor 1 (TGF- β RI) and the activation of the canonical Smad pathway. In contrast, during the later stages of cancer, TGF- β 1 acts as a tumor promoter activating the non-canonical Erk1/2 pathway. We establish the mechanistic connection between tMUC1 and TGF- β signaling in PDA and hypothesize that tMUC1 is the switch that turns TGF- β 1 from a tumor suppressor into a tumor promoter. We have shown a correlation between tMUC1 expression and TGF- β signaling within an exogenous tMUC1 model of PDA. We specifically tested the hypothesis that the tyrosine kinases present in the cytoplasmic tail of tMUC1 are signaling between tMUC1 and TGF- β 1, thus leading to enhanced metastasis. Data reported here indicate that tMUC1 influences TGF- β signaling in an exogenous tMUC1 PDA model (Chapter 2) and in endogenous MUC1 PDA cells both *in vitro* and *in vivo* (Chapter 3). The data support tMUC1 as a promising biomarker for TGF- β mediated therapies.

DEDICATION

To my papa, Dr. Arun Grover

my mom, Rosy Grover

my sister, Kajal Grover

my brother, Kurren Grover

and our baby doggo, Luca Grover

for being there for me every step of the way.

And making me laugh the entire time.

To my grandparents, Tilak Grover, Satvinder Grover, Hirde Kailwoo, and Anoop Kailwoo, for always supporting me.

And to all my family members around the world who were my cheerleaders...thanks guys.

ACKNOWLEDGEMENTS

This entire journey was only possible because Dr. Pinku Mukherjee took a chance on a very “unsure of herself” girl in August 2011. She has been the constant guardian angel on an arduous journey to find myself (and get a Ph.D. in the process). Without her, I would not have gone from a quiet volunteer to the President of the Graduate & Professional Student Government on campus. At certain points of this journey, I was dragged to the next stage because I had so much uncertainty in myself. For that I would like to acknowledge my parents, my sister, my brother, my grandparents, and my dog for lifting me up. I would like to thank my committee: Dr. Didier Dreau, Dr. Andrew Truman, Dr. Valery Grdzlishvili, and Dr. Juan Vivero-Escoto. Without each one of you, I would not have realized my potential. I am honored and grateful to have you all on my committee. Thank you to the Department of Biological Sciences faculty and employees and the UNC Charlotte vivarium staff. You all made this crazy ride so much more enjoyable. Thank you to my second family: The Mukherjee Lab. I lucked out having you all in my life during my graduate career. Without the love and support of Mahboubeh Yazdanifar (my sister), Laura Jeffords Moore (my confidant), Chelsea Maccow, Benjamin Jacques, Chiagoziem Ngwadam, Nitika (let’s face it, you’re an honorary member), Dr. Shu-ta Wu, Dr. Ru Zhou (our ringleader), Dr. Timothy Erick, Dr. Lopamudra Das Roy, Dr. Lloye Dillion, Dr. Sritama Nath, Dr. Jennifer Curry, and all past and present members of the Mukherjee Lab, I might have gone insane. The friendships and mentorships I have developed through the Department of Biological Sciences and the Graduate & Professional Student Government mean the world to me.

P.S. I owe the department a Dissertation Fellowship and Dr. Truman a centrifuge. And a garden for the lovely Ru.

TABLE OF CONTENTS

LIST OF FIGURES	viii
LIST OF ABBREVIATIONS	x
CHAPTER 1: INTRODUCTION	1
CHAPTER 2: SMAD4-INDEPENDENT ACTIVATION OF TGF- β SIGNALING BY MUC1 IN A HUMAN PANCREATIC CANCER CELL LINE	17
2.1 Introduction	17
2.2 Results	20
2.3 Discussion	27
2.4 Experimental Procedures	31
2.5 Figures	35
CHAPTER 3: MUC1 REGULATES TGF- β IN PANCREATIC DUCTAL ADENOCARCINOMA	45
3.1 Introduction	45
3.2 Results	47
3.3 Discussion	52
3.4 Experimental Procedures	56
3.5 Figures	61
CHAPTER 4: DISSERTATION SUMMARY	67
CHAPTER 5: SUPPLEMENTAL	75
THE EFFECTS OF KRAS ACTIVATION ON THE REGULATION OF TUMOR ASSOCIATED MUC1	75
5.1 Introduction	75
5.2 Results	78

	vii
5.3 Discussion	80
5.4 Experimental Procedures	80
5.5 Figures	82
REFERENCES	85
APPENDIX	
Publications	95
Contributions, Honors, and Awards	167

LIST OF FIGURES

Chapter 1

Figure 1. Schematic of Pancreas	2
Figure 2. Early mutations in pancreatic neoplasms	7
Figure 3. Schematic of MUC1	9
Figure 4. Sequence of MUC1-CT	10
Figure 5. Glycosylation differences in MUC1	12
Figure 6. Schematic of the TGF- β pathway	16

Chapter 2

Figure 1. tMUC1 overexpressing cells release significantly higher amounts of active TGF- β 1 when compared to tMUC1-low expressing cells	35
Figure 2. tMUC1 overexpressing cells resist apoptosis in response to treatment with TGF- β 1 with corresponding decrease in cleaved caspase 3 when compared to tMUC1 low expressing cells	36
Figure 3. tMUC1 overexpressing cells undergo significantly higher levels of invasion in response to TGF- β 1 treatment	37
Figure 4. TGF- β 1 mediated invasiveness is dependent upon signaling through the tyrosines in tMUC1-CT	38
Figure 5. C-Src inhibition negates the aggressiveness of TGF- β mediated invasion in MUC1 expressing cells	39
Figure 6. A schematic of the proposed mechanism of MUC1 mediating TGF- β signaling	40
Supplementary Figure 1. Western blotting showing EMT and Apoptosis associated markers in BxPC3.Y0 cells	41
Supplementary Figure 2. N-terminus of MUC1 expression in BxPC3.Neo, BxPC3.MUC1, and BxPC3.Y0	42
Supplementary Figure 3. BxPC3 variation cells undergoing invasion	43

Supplementary Figure 4. Endogenous tMUC1 high and low cells undergoing invasion	44
Chapter 3	
Figure 1. MUC1 high expression positively correlates to TGF- β RII and negatively correlates to TGF- β RI levels and leads to activation of Erk pathway	61
Figure 2. TGF- β 1 exposure increases cell death in endogenously low MUC1 cells	62
Figure 3. C-Src has increased activation in endogenously high MUC1 cells in the presence of TGF- β 1	63
Figure 4. TGF- β effects MUC1 phosphorylation and protein expression in MUC1 high cells	64
Figure 5. Neutralizing TGF- β signaling decreases tMUC1 high tumor growth in vivo	65
Figure 6. Updated schematic of tMUC1-TGF- β crosstalk	66
Supplemental	
Figure 1. Western Blot shows positive correlation between MUC1 and GTP-active mutant KRAS (codons 12, 13, and 61) in a panel of PDA cell lines	82
Figure 2. CRISPR-Cas9 generates GFP positive cells	83
Figure 3. The HEK.293G12D and HEK.293G12V cells were more proliferative than the untreated and Px.458 plasmid alone HEK.293 cells	84

LIST OF ABBREVIATIONS

BxPC3.MUC1	BxPC3 cell line overexpressing human MUC1 protein
BxPC3.Y0	BxPC3 cell line expressing Mucin 1 protein where all 7 tyrosines are mutated
CHO	Chinese Hamster Ovarian cell line
CHO.MUC1	Chinese Hamster Ovarian cell line overexpressing human MUC1 protein
CHO.Y0	Chinese Hamster Ovarian cell line expressing Mucin1 protein with 7 mutated tyrosines
COX-2	cyclooxygenase-2
CRISPR	Clustered Regularly Interspaced Short Palindromic Repeats
CT	cytoplasmic tail
EMT	Epithelial – Mesenchymal Transition
FOLFIRINOX	Folinic acid, Fluorouracil, Irinotecan, Oxaliplatin
HEK	Human Embryonic Kidney
KRAS	Kirsten Rat Sarcoma virus
LTBP1	Latent Transforming Growth Factor Beta Binding Protein
MUC1	Mucin 1
MUC1.CT	Mucin 1 cytoplasmic tail
PC	Pancreatic Cancer
PDA	Pancreatic Ductal Adenocarcinoma
PanIN	Pancreatic intraepithelial lesions
PDGF	Platelet Derived Growth Factor
PP2	c-Src inhibitor
TGF- β	Transforming Growth Factor Beta
TGF- β 1	Transforming Growth Factor Beta Isotype 1
TGF β RI	Transforming Growth Factor Beta Receptor I
TGF β RII	Transforming Growth Factor Beta Receptor II

VEGF

Vascular Endothelial Growth Factor

Y0

all tyrosines mutated

CHAPTER 1: INTRODUCTION

1.1 Pancreas

The pancreas is a glandular organ located in the abdomen behind the stomach. It is anatomically separated into the head, body, and tail [1]. The main and accessory pancreatic ducts run through the body, joining with the common bile duct. The pancreas secretes hormones and peptides into the descending part of the duodenum for its role in the digestive system or into the bloodstream for its role in the endocrine system [2]. The pancreas is comprised of exocrine and endocrine cells, which serve different functions and have unique morphologies (schematically represented in Fig 1).

The endocrine pancreas is comprised of the islets of Langerhans, which constitute 1-2% of the total pancreatic volume [3]. The islet cells include alpha, beta, delta, epsilon, and gamma cells [4]. These cells release hormones directly into the bloodstream. Alpha cells release glucagon when insulin levels are low [5]. Glucagon is a peptide hormone that raises the concentration of glucose and fatty acids in the bloodstream. Beta cells, the prominent group in the islets of Langerhans, release insulin and amylin. Diminishing function in beta cells can lead to type 1 or type 2 diabetes [6]. Delta cells produce somatostatin, which can reduce stomach acid production. It can act directly on the acid-producing parietal cells, as well as, indirectly by preventing the release of other hormones, such as gastrin and secretin [7]. Epsilon cells produce ghrelin, a neuropeptide that increases hunger and gastric acid secretion [8]. Lastly, gamma cells produce

pancreatic polypeptide, which self-regulate pancreatic secretion whether endocrine or exocrine [9].

The exocrine pancreas is made up of acinar cells, which secrete digestive enzymes. These enzymes include trypsin and chymotrypsin to digest proteins, amylase to digest carbohydrates, and lipase to break down fats [10]. The enzymes accumulate in the intralobular ducts, which lead to the pancreatic ducts. The pancreatic ducts join the common bile duct to form the ampulla of Vater, which leads to the duodenum [11].

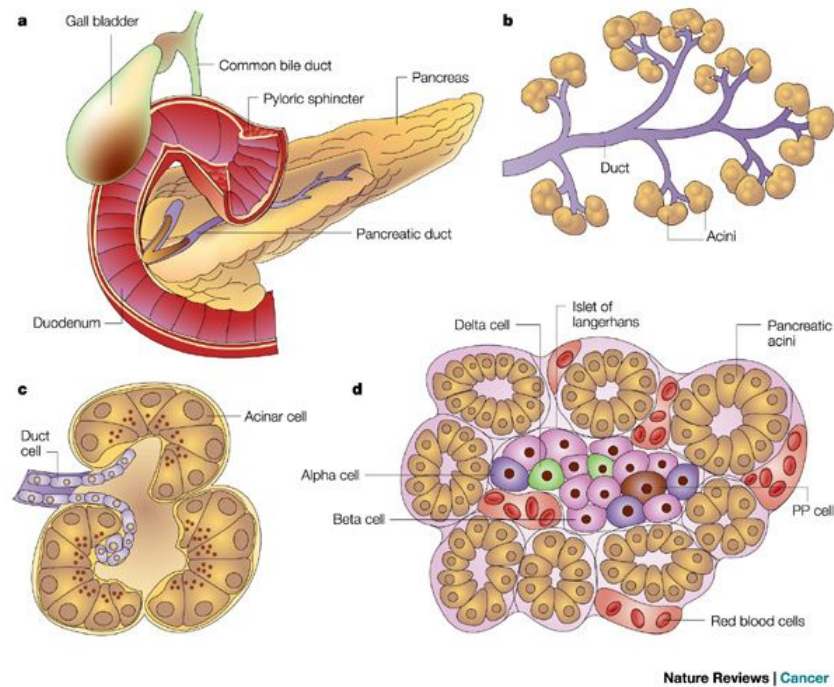


Figure 1. The pancreas secretes hormones and peptides generated by the islets of Langerhorns via the pancreatic ducts. The endocrine pancreas produces regulatory hormones and peptides. They are secreted via ducts that are lined with pancreatic ductal cells [12].

1.2 Pancreatic Cancer

Pancreatic Cancer (PC) is the third leading cause of cancer-related deaths in the United States, with a five-year survival rate at nine percent and a median rate of six months [13]. By 2020, PC is estimated to become the second leading cause of cancer-related deaths by overtaking colorectal cancers [14]. The majority of patients present with stage IV at diagnosis with an overall five-year survival of three percent [15]. Its mortality rate nearly matches its incidence rate [16]. In 2018, the NCI SEER program showed there were an estimated 55,440 new PC cases with 44,330 patients succumbing to the disease [17]. The incidence and mortality rates have been relatively stable for the past ten years [17]. It affects men and women indiscriminately. In the United States, the median age for PC diagnosis is 71 years [18]. Only 20% develop PC before the age of 60 [19], and less than 3% of cases are in individuals younger than 45.

There are several risk factors for PC such as familial history, cigarette smoking, chronic pancreatitis, and diabetes mellitus [20]. About 10% of PC cases have a familial basis, and family history significantly increases the chances of developing PC [21]. However, the genetic basis of familial-linked PC has not yet been established. Germline mutations in BRCA2 can cause increased risk of breast, ovarian, and pancreatic cancer [22], and BRCA1 mutations could be associated with familial PC risk [23]. Cigarette smoking is a consistent risk factor for PC, and it may contribute to the development of about 20% of PC cases [24]. It has been linked with a reduction in survival among PC patients [25]. Chronic pancreatitis has also been shown to greatly increase the risk of developing PC. In fact, five years after diagnosis, chronic pancreatitis patients have

nearly eight-fold increased risk of PC [26]. Chronic pancreatitis in conjunction with other risk factors, such as cigarette smoking and older age, greatly increases the inherent risk of developing PC [27]. Diabetes has also been closely tied to PC. 68% of PC patients had concurrent diabetes [28] and 74-88% of the patients received their diabetes diagnosis less than 24 months prior to the PC diagnosis [29]. Diabetes and PDA have often been studied as “dual causalities”; however, the mechanism between this relationship remains unclear.

Most PC do not present symptoms in the early stage. Later-stage PC has been associated with the following symptoms: weight loss, abdominal pain, nausea and vomiting, bloating, dyspepsia, onset of diabetes, changes in bowel habit, pruritus, lethargy, back pain, shoulder pain, and jaundice [20]. Since most of these symptoms are common for other less acute ailments, many patients do not suspect PC until it is too late. It has been shown that diabetes (97%) and abdominal pain (78-82%) due to cancer-nerve interaction are frequently reported in advanced late stage PC [30].

Diagnosing PC in the early stages is difficult. As stated above, most classical symptoms are not present in the early stage, and so the disease is asymptomatic until it has progressed significantly. PC is considered extremely lethal due to its aggressive growth and rapid development that leads to metastasis [31]. The pancreas is near several main arteries, which cancer cells use to traverse to distant areas to form secondary tumors. There are many diagnostic methods to determine the presence of PC. The most common is serum carbohydrate antigen (CA) 19-9 [32]. It has been combined with other protein biomarkers to significantly increase the detection of PC, such as a protein biomarker panel of CA125, CA19-9, and laminin γ C (LAMC2) [33]. CA19-9 and CA125 has 95% specificity together, which raised the CA19-9 alone sensitivity by 20% [34].

Treatment of PC generally includes surgery, chemotherapy, and radiotherapy. The treatment options are dependent on the stage and spread of PC upon diagnosis. Surgery is the only treatment that can potentially cure the patient. Unfortunately, only twenty percent of cases are eligible for surgical resection [35]. The primary tumor must be localized with no distant metastases, and it cannot be near the major veins and arteries neighboring the pancreas. Currently, the standard of care for metastatic PDA is combination cytotoxic therapy, namely FOLFIRINOX or gemcitabine plus nab-paclitaxel [15]. FOLFIRINOX has been shown to respond better and increase overall survival in patients with metastatic PC [36]. However, there are physiological complications, such as sensory neuropathy [37]. The emerging field of immunotherapy has provided new treatment avenues. New developments within the field might play important roles in the future treatment of PC. Some interesting approaches include chimeric antigen receptor T cell therapy and antibody guided nanoparticles [38, 39]. However, it is still early in the research and development phase. Therefore, it is imperative to develop and evaluate novel targeted therapeutic treatments to improve patient outcome in this deadly disease.

1.3 Pancreatic Ductal Adenocarcinoma

There are two main types of pancreatic neoplasms: neuroendocrine and exocrine. Pancreatic neuroendocrine neoplasms (pNENs) are a heterogeneous group of tumors, including pancreatic neuroendocrine tumors and neuroendocrine carcinomas, and have better prognosis than exocrine pancreatic cancer [40]. pNENs comprise only 1-2% of all pancreatic neoplasms, leaving the exocrine group the most common type [41].

The most frequent type of exocrine PC is pancreatic ductal adenocarcinoma (PDA), which represents about 95% of all pancreatic cancers [42, 43]. It arises from genetic mutations within the epithelial ductal cells that line the pancreatic ducts. KRAS point mutations lead to the initiation and development of 95% of PDA [44]. 98% of KRAS point mutations develop at G12 (glycine), while G13 (glycine) and Q61 (glutamine) account for 1% each [45]. The most common KRAS mutation is G12D (glycine to aspartic acid). RAS mutations are present in about one third of all cancer cases, regardless of organ origin or type [46]. The oncogenic mutant KRAS present early in the progression of the disease [47, 48]. It has been shown to drive pancreatic neoplasia [49]. KRAS typically requires sustained expression for cancer cell survival; however, the molecular oncogene dependency is not clearly understood [50]. It is seen that knocking down mutant KRAS in non-small cell lung cancers suppress tumor growth [51]. However, KRAS knockdown was not considered sufficient treatment to destroy the cancer, as tumors have been shown to escape this mutant KRAS addiction, or dependency. Very few studies have been done studying KRAS addiction in PDA. One study showed that reoccurring PDA may escape the addiction of mutant KRAS to relapse [52].

Other genetic mutations have also been identified to play a role in the development of PDA, such as CDKN2A, TP53, and SMAD4/DPC4 [12]. These mutations seem to occur in a temporal sequence in progressive pancreatic intraepithelial neoplasia stages (PanIN). Full blown PDA arise from these PanINs. These lesions are categorized as PanIN-1A, PanIN-1B, PanIN-2, and PanIN-3 according to the histological atypia after pathology [53] (Schematically represented in Figure 2). Ductal epithelial

cells are normally cuboidal in shape. They have an apical surface, which faces the duct and has mucins to protect the cell from bacterial invasion or mechanical damage. Normal epithelial cells also have a basement membrane near the blood supply where growth factors accumulate. In PanIN-1 lesions, the epithelial ductal cells start to lose their key morphological cuboidal shape and become elongated. Here, they start to overexpress mucins. In PanIN-2 lesions, the cells start to lose its polarity and detaches from the basement membrane. The nucleus also becomes atypical. PanIN-3 lesions lead to invagination of the cells, which then start to bud off and is sometimes termed as carcinoma-in-situ. PanIN-4 is considered full onset invasive carcinoma. It can take about twenty years from the initiating gene mutation in KRAS in a pancreatic ductal epithelial cell to progress to full blown PDA [54].

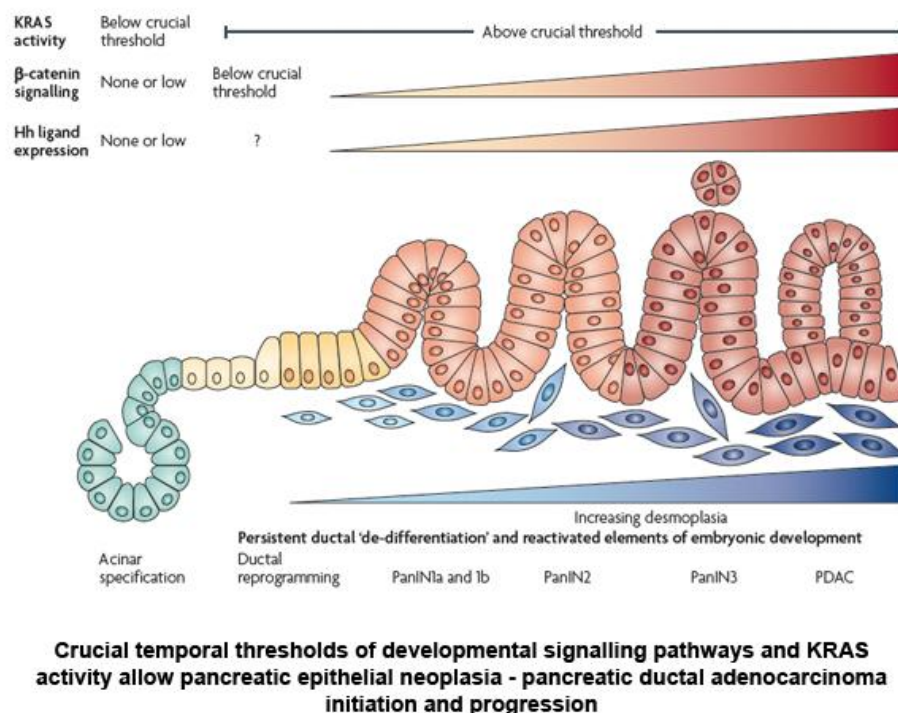


Figure 2. Oncogenic KRAS mutation drives early pancreatic neoplasia leading to the development of PanIN lesions [55].

1.4 MUC1

Mucin1 (MUC1), found on chromosome 1q21, is a single pass type I transmembrane protein with a heavily glycosylated extracellular domain that extends up to 200-500 nm from the cell surface [56]. It is normally expressed in the glandular or luminal epithelial cells that line the digestive, respiratory, and reproductive tracts, such as esophagus, stomach, duodenum, pancreas, uterus, prostate, mammary glands, and lungs [57]. MUC1 protects the apical surface of the epithelial cells by creating a physical barrier that prevents bacteria from entering the cell. Mucins are made of over 50% carbohydrates which are O-linked to the protein core through serine and threonine residues [58]. The hydrophilic, negatively charged sugar branches oligomerize to form a mucinous gel that lubricates and protects the underlying epithelia from desiccation, pH changes, pollutants, and microbes [59]. MUC1 comprises of a N-terminal protein sequence, followed by a sequence called the variable number of tandem repeats (VNTR), a transmembrane region, and finally a cytoplasmic tail. The larger extracellular portion consists of the N-terminus (104 amino acids) and the VNTR sequence (20 amino acids) that is repeated 25-125 times due to polymorphism. The VNTR segment has 5 prolines and up to 5 O-linked glycans due to serine and threonine residues. The C-terminus consists of 170 amino acids. The MUC1-C consists of an extracellular region (58 amino acids), a transmembrane region (28 amino acids), and a cytoplasmic tail (72 amino acids) [60]. The cytoplasmic tail (also known as CT) is mostly conserved across various species, although the rest of the molecule is not. The Sea Urchin Sperm protein enterokinase and

agrin (SEA) domain is the extracellular region adjacent to the transmembrane domain. It anchors the N-terminus to the C-terminus via stable hydrogen bonds [61]. The SEA domain contains cleavage sites that can release the extracellular N-terminus (Schematically represented in Figure 3).

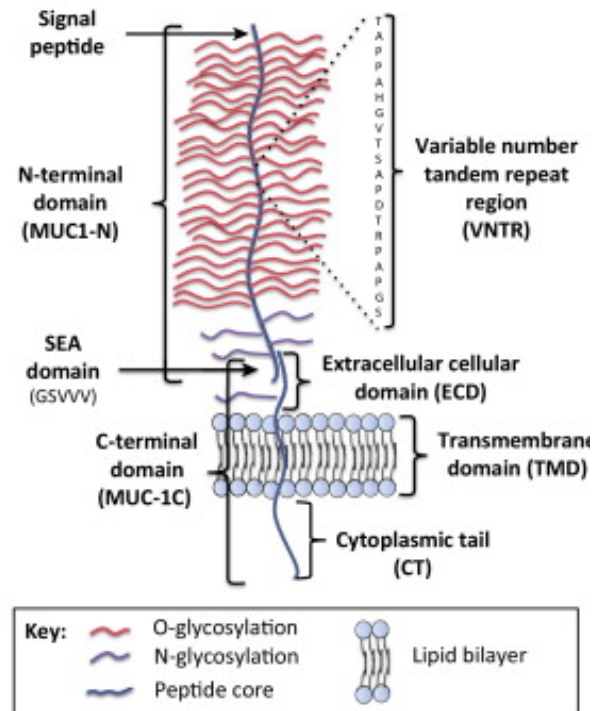


Figure 3. Schematic of glycosylated MUC1 N-terminus bound to C-terminus. MUC1 on normal cells has O- and N- glycosylation, protecting the VNTR region of the N-terminus. It is bound via hydrogen bonds to the extracellular SEA domain of the C-terminus. Adapted from Nath et al 2014 [56].

The tumor associated MUC1 (tMUC1) plays a critical role in tumor progression and metastasis in PDA [56]. tMUC1 is different from normal MUC1. tMUC1 is not only overexpressed in PDA but is aberrantly glycosylated in over 80% of PDA cases [56, 59, 62-64]. In normal epithelial cells lining the ducts, MUC1 is localized on the apical

surface and plays the role of protective barrier. However, when normal cells transform to malignant cells and lose their polarity, MUC1 is no longer restricted to the apical surface; it becomes hypo-glycosylated, and comes in close proximity to several growth factor receptors [65] (Schematically represented in Figure 4). This allows tMUC1 to play an important role in oncogenic signaling [62, 66-68].

It is well established that the oncogenic signal transduction occurs through the cytoplasmic tail of MUC1 (tMUC1-CT) [69, 70]. Once the tMUC1-CT is phosphorylated, it associates with β -catenin and other transcription factors, and becomes released from the N-terminus of tMUC1, leading it to translocate to the nucleus and subsequently activate downstream signaling pathways [66, 67, 71]. tMUC1-CT is 72 amino acids long and is highly conserved with 7 tyrosine residues that are phosphorylated by intracellular kinases. tMUC1-CT in PDA acts as a binding site for these molecules, such as c-Src, a proto-oncogene linked to cancer progression [56, 72].

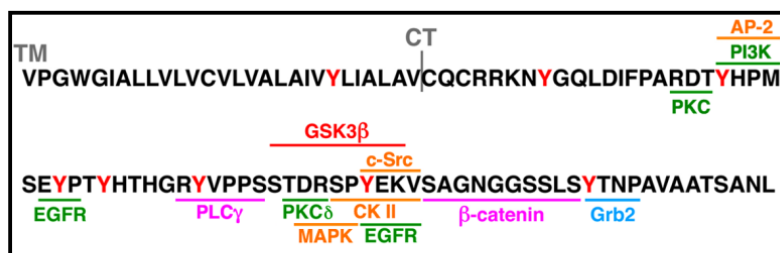


Figure 4. Sequence of MUC1-CT with binding sites for tyrosine kinase receptors [73].

Studies have linked overexpression of tMUC1 in tumors with enhanced epithelial to mesenchymal transition (EMT) leading to increased invasiveness, metastasis, and drug resistance [56, 74, 75]. In fact, tMUC1 has been shown to enhance invasiveness of

pancreatic cancer cells by inducing EMT [63]. tMUC1 has also been shown to increase cell proliferation, cell migration and invasion, cell survival, and decrease cell apoptosis via p42/44 MAPK, Akt, Bcl-2, and MMP13 pathways [76]. tMUC1 induces increased production of prostaglandin (Cox-2) and growth factors, platelet-derived growth factor-A (PDGF-A) and vascular endothelial growth factor (VEGF), which leads to enhanced invasiveness of cells mainly through induction of EMT related genes [62, 63, 68, 77]. The increase in Cox-2, including IDO, correlated with an increased percentage of regulatory T cells and myeloid-derived suppressor cells in pancreatic tumors and tumor draining lymph nodes [64]. tMUC1 has also been implicated in the metabolic reprogramming that occurs in PDA. It has been shown to control cancer cell metabolism to aid growth properties of cancer cells. tMUC1 occupies the promoter elements (and thereby regulates the expression) of multiple genes that are directly involved in glucose metabolism. It also enhances glycolytic activity and increases glucose uptake in PC cells [78]. By controlling autophagy, reactive oxygen species levels, and metabolite flux, it has been shown that tMUC1 influences cancer cell survival under hypoxic and nutrient-deprived conditions [79].

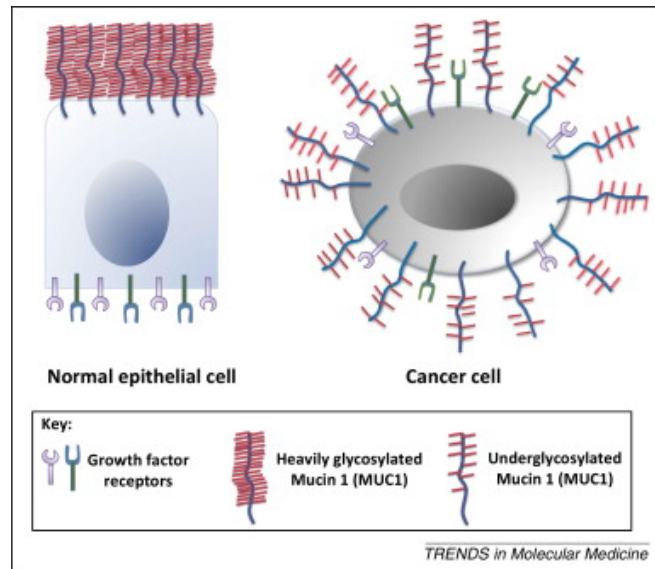


Figure 5. Tumor associated MUC1 becomes aberrantly glycosylated and overexpressed. MUC1 and the growth factors are no longer bound to their respective regions. tMUC1 becomes overexpressed on the surface of the cancer cell and develops close proximity to growth factors. Adapted from [56].

1.5 Transforming Growth Factor Beta

The transforming growth factor – beta (TGF- β) signaling pathway is involved in many cellular processes from embryogenesis to the adult organism. Members of the TGF- β family are found in a wide range of species, such as insects, amphibians, birds, and humans [80]. It is involved in, but not limited to, cell growth, cell differentiation, cell cycle regulation, apoptosis, and cellular homeostasis. The TGF- β superfamily consists of more than 40 members, including bone morphogenetic proteins (BMPs), growth and differentiation Factors (GDFs), Activin, Nodal, and TGF- β s [80] (schematically represented in Figure 6).

The TGF- β ligand family consists of three different, highly homologous isoforms in mammals: TGF- β 1, TGF- β 2, and TGF- β 3 [81-83]. The most abundant isoform is TGF- β 1 [84]. About 90% of total TGF- β isoform is TGF- β 1. Each are synthesized with latent precursor protein Latent Transforming Growth Factor – Beta Protein 1 (LTBP1), forming the complex latent transforming growth factor – beta (LTGF- β), which regulates TGF- β 1 cytokine activation via association with the latency-associated proteins [85]. This complex forms the latent precursor protein, LTGF- β , which can be cleaved by Furin into the latency-associated peptide (LAP) and the shorter region which forms the mature inactive TGF- β dimer [86]. LAP is noncovalently associated with the mature TGF- β 1 and serves as a chaperone during exocytosis. This leads TGF- β into the extracellular matrix through its interaction with LTBP1. This process is exceptionally important during wound healing when the dimer is in close proximity to myofibrils [87]. Once the LTBP1 dissociates by either proteolytic cleavage by proteases or physical interactions of LAP with proteins, TGF- β 1 becomes active [86].

The receptors for TGF- β cytokines are divided into two categories: Type I (R1) and Type II (R2). Both are single membrane span glycoproteins that have an intrinsic serine/threonine kinase domain in the C-terminus. Type II receptors phosphorylate type I receptors. There are five type II receptors and seven type I receptors. Type I receptors are also called Activin-like receptors (ALKs). Type I receptors are categorized according to sequence similarities. The main Type I receptors are ALK5 (TGF- β Receptor I), ALK4 (Activin receptor), ALK7 (Nodal receptor), ALK3 and ALK 6 (BMP type I receptors), and ALK1 and ALK2 which interacts with various TGF- β superfamily members [88, 89]. The most common isoform is ALK5 [90]. TGF- β RIII, (also known as betaglycan) which

is a proteoglycan-containing glycoprotein, has also been identified as a receptor that binds to various TGF- β receptors. However, it is not directly involved in TGF- β signal transduction [91].

In normal tissue development and early oncogenesis, the TGF- β signaling complex regulates the cell cycle and induces apoptosis. Signaling, generally, involves binding of cytokines with their respective TGF- β type II receptor dimer. The canonical pathway of TGF- β signaling starts with binding of two TGF- β receptor type II (TGF- β RII), a serine/threonine receptor, to two TGF- β receptor type I (TGF- β RI), a serine/threonine receptor, to activate the SMAD pathway [92, 93]. TGF- β and activins phosphorylate SMAD 2 and SMAD 3, which are activin/TGF- β -specific R-Smads, and BMPs induce phosphorylation of SMAD 1, SMAD 5, and SMAD 8 (BMP-specific R-Smads) [94]. The receptors dimerize, forming a hetero-tetrameric complex with the ligand [95]. When the ligand binds, it triggers the activation of TGF- β RI kinase activity and switches it to a docking site for SMAD proteins [96]. SMAD 2 and SMAD 3 are activated by the TGF- β RI [97]. Once phosphorylated by TGF- β RI, SMAD 2 and 3 dimerize, forming the SMAD 2/3 complex [84]. The SMAD 2/3 dimer joins with SMAD 4, creating a hetero-hexameric complex [84]. The newly created complex translocates to the nucleus, allowing for the transcriptional regulation of target genes that regulate cellular processes, such as induction of apoptosis [98]. However, it has been shown in a SMAD 4 null cell line that SMAD 2 and SMAD 3 are still able to translocate to the nucleus [99]. SMAD 4 is often mutated or deleted in about 55% of PDA cases showcasing the importance of studying SMAD 4 independent mechanisms of PDA

development [100]. Loss of functional SMAD 4 in PDA interferes with the TGF- β /SMAD pathway leading to decreased growth inhibition [101].

TGF- β has a dichotomous role in oncogenesis. In later stages of cancer, a switch occurs and the TGF- β signaling pathway becomes a tumor promoter, inducing invasion and metastasis. TGF- β 1 stimulates EMT through the activation of the ERK/MAPK pathway and phosphoinositide 3-kinase (PI3K)/Akt pathway in a Smad independent manner [102-104]. As reviewed in Kalluri et al, EMT is a biological process that transforms an epithelial cell to a mesenchymal cell phenotype, which can lead to resistance to apoptosis [105]. Increased migration and invasion of cancer cells has also been associated with EMT [106]. TGF- β receptors activate transcription factors associated with EMT, such as ZEB1, ZEB2, Snail, and Slug [107]. It has also been established that TGF- β activates the Erk/MAPK pathway through Ras [108]. ShcA is phosphorylated by the TGF- β receptor complex, which recruits Grb2/SOS/Ras complex to activate the Erk/MAPK pathway [109]. The mechanism is poorly understood [110]. Understanding the downstream effects of TGF- β 1 mediated Smad-independent cellular activation will help us establish more efficient treatment regimens. The TGF- β switch in function from a tumor suppressor, via apoptosis, to a tumor promoter, via EMT, is elusive but holds high importance in treatment refractory cancers like PDA [111]. TGF- β is considered an important target for cancer therapy, and there are multiple anti-TGF- β compounds in clinical trials [112].

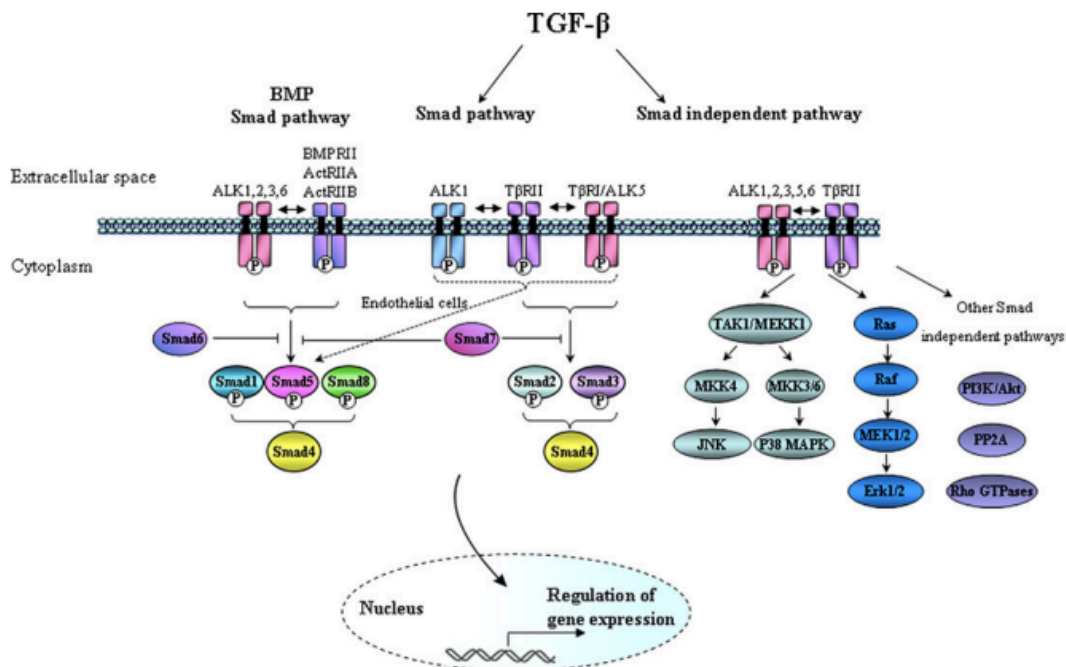


Figure 6. Schematic representation of TGF- β signaling pathways [113].

CHAPTER 2: SMAD4-independent activation of TGF- β signaling by MUC1 in a human pancreatic cancer cell line

This chapter has been published: Grover et al, 2018 Oncotarget [73].

2.1 Introduction

Pancreatic Ductal Adenocarcinoma (PDA) is the fourth leading cause of cancer related deaths in the United States with a median survival rate of less than six months and a 5-year survival rate of a dismal 7% [114], [115]. By 2030, PDA is predicted to be the second leading cause of cancer-related deaths in the United States [14]. Its mortality rate nearly matches its incidence rate [16].

Transforming Growth Factor Beta (TGF- β) is a cytokine with a dichotomous role in oncogenesis. In normal tissue development and early oncogenesis, the TGF- β signaling complex is a cell cycle regulator and induces apoptosis. The canonical pathway of TGF- β signaling starts with binding of two TGF- β Receptor type II (TGF- β RII) to two TGF- β Receptor type I (TGF- β RI) to activate the SMAD pathway [92, 93]. The receptors dimerize, when the ligand binds, triggering the activation of TGF- β RI kinase activity and switching it to a docking site for SMAD proteins [96]. SMAD 2 and SMAD 3 are activated by the TGF- β RI [97]. Once phosphorylated by TGF- β RI, SMAD 2 and 3 dimerize forming the SMAD 2/3 complex [84]. The SMAD 2/3 dimer joins with SMAD 4, creating a heterohexameric complex [84]. The newly created complex translocates to the nucleus, allowing for the transcriptional regulation of target genes which regulate

cellular processes, such as induction of apoptosis [98]. However, it has been shown that in a SMAD 4 null cell line SMAD2 and SMAD3 are still able to translocate to the nucleus [99]. SMAD 4 is often mutated or deleted in about 55% of PDA cases showcasing the importance of studying SMAD4 independent mechanisms of PDA development [100]. Loss of functional SMAD 4 in PDA interferes with the TGF- β /SMAD pathway leading to decreased growth inhibition [101].

In later stages of cancer, a switch occurs and the TGF- β signaling pathway becomes a tumor promoter, inducing invasion and metastasis. TGF- β 1 stimulates Epithelial-to-Mesenchymal Transition (EMT) through the activation of the ERK pathway [102]. As reviewed in Kalluri et al, EMT is a biological process that transforms an epithelial cell to a mesenchymal cell phenotype, which can lead to resistance to apoptosis [105]. Increased migration and invasion of cancer cells has also been associated with EMT [106]. The TGF- β switch in function from a tumor suppressor, via apoptosis, to a tumor promoter, via EMT, is elusive but holds high importance in treatment refractory cancers like PDA [111]. The TGF- β ligand family consists of three different, highly homologous isoforms: TGF- β 1, TGF- β 2, and TGF- β 3 [81-83]. The most abundant isoform is TGF- β 1 [84]. TGF- β is considered an important target for cancer therapy, and there are multiple anti-TGF- β compounds in clinical trials [112].

Mucin-1 (MUC1), a transmembrane glycoprotein that plays a critical role in tumor progression and metastasis in PDA [56]. In normal epithelial cells lining the ducts, MUC1 is localized on the apical surface and provides a protective barrier. However, when normal cells transform to malignant cells and lose their polarity, MUC1 is no longer restricted to the apical surface; it becomes hypo-glycosylated, and comes in close

proximity to several growth factor receptors including TGF- β receptors [65]. The tumor-associated form of MUC1 (tMUC1) plays an important role in oncogenic signaling [62, 66-68]. Studies have linked overexpression of tMUC1 in tumors with enhanced EMT leading to increased invasiveness, metastasis, and drug resistance [56, 74, 75]. tMUC1 induces increased production of prostaglandin (Cox-2) and growth factors (PDGF and VEGF), which leads to enhanced invasiveness of cells mainly through induction of EMT related genes [62, 63, 68, 77]. Importantly, tMUC1 is overexpressed and aberrantly glycosylated in over 80% of PDA cases [56, 59, 62-64]. It is well established that the oncogenic signal transduction occurs through the cytoplasmic tail of tMUC1 (tMUC1-CT) [69, 70]. Once the tMUC1-CT is phosphorylated, it associates with β -catenin and other transcription factors, and becomes released from the N-terminus of tMUC1, leading it to translocate to the nucleus and subsequently activate downstream signaling pathways [66, 67, 71]. tMUC1-CT is 72 amino acids long and is highly conserved with seven tyrosine residues that are phosphorylated by intracellular kinases. The phosphotyrosine residues act as binding sites for molecules, such as c-Src, a proto-oncogene linked to cancer progression [56, 72].

In this study, we show that overexpression of tMUC1 in human SMAD4 deleted PDA cell line BxPC3, plays an important role in the switch of TGF- β 1 from a tumor suppressor to a tumor promoter, via a SMAD4 independent mechanism. Similar data is also reported in CHO cells. This study is the first to show that overexpression of tMUC1 directly reduces TGF- β 1 induced apoptosis and increases invasive potential in BxPC3 and CHO cells via signaling through the tyrosines in tMUC1-CT.

2.2 Results

Overexpression of tMUC1 in BxPC3 and CHO cells significantly increases the amount of TGF- β 1 produced without altering levels of the TGF- β receptors or SMAD2/3. For this study, we selected Chinese hamster ovarian cell line (CHO) that is null for human tMUC1 and a human PDA cell line BxPC3 that express low levels of endogenous human tMUC1 and has SMAD4 independent TGF- β signaling. CHO cells have intact canonical TGF- β signaling pathway and were selected as a control cell line to investigate the effects of tMUC1 on TGF- β signaling and phenotypic outcomes. Using a retroviral gene delivery system, we overexpressed the full-length human MUC1 transgene in BxPC3 and CHO cells creating two tMUC1 high cell lines: BxPC3.MUC1 and CHO.MUC1. An empty vector, which does not carry the human MUC1 gene, was used to create the control cell lines BxPC3.Neo and CHO.Neo. Western blotting was performed to confirm the expression of human tMUC1 in these cell lines. Cell lysates probed with CT2 antibody that recognizes the last 17 amino acids (SSLSYNTPAVAATSANL) of the cytoplasmic tail (CT) [116] revealed that BxPC3.MUC1 and CHO.MUC1 cells expressed high levels of human tMUC1, while BxPC3.Neo and CHO.Neo did not (Fig. 1A and 1B). Next, we tested expression of the key signaling components of the canonical TGF- β pathway, TGF- β RI, TGF- β RII, SMAD 2/3, and SMAD4 (expressed in CHO cells) [117]. We found that the levels of these signaling proteins were not significantly altered in the BxPC3.MUC1 compared to BxPC.Neo (Fig. 1B) or in CHO.MUC1 compared to CHO.Neo (Fig. 1A). Densitometric

arbitrary units are shown in Figure 1A and B representing the levels of protein normalized to their β -actin loading control.

To investigate if overexpression of tMUC1 alters SMAD4 independent TGF- β signaling, we first looked for differences in TGF- β 1 secretion by these cells. Specific ELISA was used to determine the TGF- β 1 concentration in the supernatant of these cells. Our data showed significantly higher levels of TGF- β 1 in the supernatants of CHO.MUC1 at 48 hours and BxPC3.MUC1 at 6, 12, and 24 hours when compared to the control cell lines that expressed low levels of endogenous tMUC1 (Fig. 1C, $p < 0.01$ and 1D, $p < 0.001$), suggesting that MUC1 is a major contributor to the abundant release of TGF- β 1. (Note: Only 48h time point is shown for CHO cells as earlier time points had very low undetectable levels of TGF- β 1 release). Thus, we concluded that tMUC1 overexpression increases TGF- β 1 released but does not affect the expression of the receptors or the downstream signaling component.

Overexpression of tMUC1 protects PDA cells from TGF- β 1-mediated apoptosis.

We determined the effect of exogenous TGF- β 1 on induction of apoptosis in CHO and BxPC3 cells in context of tMUC1 expression. Apoptosis was measured by performing Annexin V/7AAD staining followed by flow cytometry. Treatment with TGF- β 1 induced a 2-fold induction of apoptosis in the CHO.Neo cells compared to 0.5-fold induction of apoptosis in CHO.MUC1 cells (Figure 2A, $p < 0.05$). Similarly, BxPC3.MUC1 cells were completely protected from TGF- β 1 induced apoptosis compared to 5-fold induction of apoptosis in BxPC3.Neo cells (Figure 2B, $p < 0.05$). Furthermore, we found that TGF- β 1 treatment activated cleavage of Caspase 3 more in the BxPC3.Neo cells than in the

BxPC3.MUC1 cells (Fig. 2C and 2D, $p < 0.0001$) even though total Caspase 3 was significantly higher in the BxPC3.MUC1 versus the Neo cells (Fig. 2C and 2E, $p < 0.001$). Caspase 3 is a death protease commonly associated with changes in cell morphology, and induction of apoptosis [118]. tMUC1 expression has been shown to reduce stress induced apoptosis by blocking activation of Caspase 8, which is known to interact and activate Caspase 3 [119]. It has also been shown to inhibit apoptosis under genotoxic stress via JNK1 activation [75, 120]. Upon comparing overall Caspase 3 activation, we observed that BxPC3.Neo has a statistically significant increase when compared to BxPC3.MUC1 in the presence of TGF- β 1 (Fig. 2C and 2F, $p < 0.0001$). We did not observe any significant difference in cleaved Caspase 7 between BxPC3.Neo and MUC1 cells in response to TGF- β 1 treatment (Fig. 2C and 2G). However, when we compared the ratio of cleaved Caspase 7 versus total Caspase 7, a significant decrease in cleaved Caspase 7 in the tMUC1-overexpressing cells was noted when exposed to TGF- β 1 (Fig. 2I, $p < 0.01$). As with Caspase 3, Caspase 7 levels were significantly higher in BxPC3.MUC1 when compared to BxPC3.Neo cells (Fig. 2C and 2H, $p < 0.05$). Etoposide was used as the positive control for inducing Caspase 3 and 7 cleavage and activation. However, we did not observe any significant difference in Caspase 3 and 7 cleavages, because both BxPC3.MUC1 and BxPC3.Neo cells were equally sensitive to high concentration (100uM) of etoposide. Therefore, we suggest that cleaved caspases may regulate TGF- β 1 induced apoptosis in the absence of tMUC1. The densitometric arbitrary unit shown in Figures D, E, G, and H represent levels of protein normalized to their β -actin loading control while F and I represent levels of cleaved caspase/total caspase.

Treatment with TGF- β 1 increases invasive properties of tMUC1-overexpressing cells as compared to their Neo counterparts. We hypothesized that TGF- β 1 may induce invasiveness in tMUC1-high but not tMUC1-low cells by activating EMT. To test this hypothesis, we determined the invasive properties of BxPC3.MUC1 and CHO.MUC1 versus BxPC3.Neo and CHO.Neo cells in response to TGF- β 1. Results show 20-fold higher levels of invasion in CHO.MUC1 when compared to CHO.Neo (Fig. 3A, $p < 0.0001$,) and 1.5-fold higher in BxPC3.MUC1 when compared to BxPC3.Neo (Fig. 3B, $p < 0.05$,). We recognize that CHO cells that are SMAD4 positive respond better to TGF- β 1. However, to further explore whether SMAD4 deletion plays a role, we also tested the invasive potential of Wild Type SMAD4 PDA cell lines HPAF-II and MIA PaCa-2 (Supplemental Figure 4). HPAF-II, an endogenously high tMUC1 line significantly increases its invasive potential when exposed to TGF- β 1. Following the trends established, MIA PaCa-2, an endogenously low tMUC1 line, significantly decreases its invasive potential in the presence of TGF- β 1. These cell lines, in relation to their endogenous tMUC1 levels, will be further studied. Overall, the results suggest that there is synergistic interaction between tMUC1 and TGF- β signaling resulting in increased motility and invasiveness. Next, we assessed the levels of EMT associated proteins by western blotting in TGF- β 1 treated versus untreated cells. Twenty four post TGF- β 1 treatment, levels of Snail, Slug, Vimentin, and N-Cadherin was determined. The percent change in density of the bands due to TGF- β 1 treatment is significantly higher in the BxPC3.MUC1 compared to BxPC3.Neo for all the EMT associated proteins except for Snail (Figure 3C-G). Percent change was determined by formula (TGF- β 1 treated – No treatment/No treatment) * 100. If the final answer was negative, this was percentage

decrease (suggesting that the protein level remained unchanged with treatment). We observed no difference in the activation of the ERK pathway when examining levels of phospho-ERK between MUC1 and Neo cells. Presently, we do not know why that is, however we suspect that in the absence of SMAD4 in the tMUC1 overexpressing BxPC3 cell line that the ERK pathway may not be activated [121].

TGF- β 1 mediated functions require signaling through the tyrosines present in tMUC1-CT. We next investigated if the functional differences of TGF- β were manifestations of signaling crosstalk between the TGF- β signaling components and tMUC1-CT. tMUC1 associated non-canonical regulation of TGF- β signaling in a SMAD4 independent mechanism is responsible for the activation of other transcription factors via their interaction with the cytoplasmic tail of tMUC1 [122]. Therefore, we hypothesized that the interaction of tMUC1-CT with the TGF- β signaling pathway regulates the differences in apoptosis and induction of EMT independently of SMAD4. To test this hypothesis, we generated a phosphomutant form of tMUC1 (CHO.Y0 and BxPC3.Y0), where all seven tyrosines of tMUC1-CT were mutated to phenylalanine. The tMUC1 Y0 mutant is considered ‘a non-functional form’ of tMUC1-CT as it lacks the tyrosines for phosphorylation, a precursor for downstream signal transduction (Fig. 4A). Western blots show the expression levels of tMUC1-CT in Neo, MUC1, and Y0 cells (Figure 4B and C). As previously observed, TGF- β 1 treatment increases invasiveness in the tMUC1-overexpressing cells when compared to the Neo cells. However, when comparing phosphomutant BxPC3.Y0 or CHO.Y0 cells to the full-length tMUC1-overexpressing cells, we observed a complete reversal of the enhanced invasion when

exposed to TGF- β 1 (Fig. 4D and E). The only difference between the full length tMUC1 and tMUC1.Y0 expressing cells is the ability to signal through the tyrosine residues of tMUC1-CT. Therefore, we postulate that the tyrosine residues of tMUC1-CT are critical for the synergistic cross talk between tMUC1 and TGF- β signaling that results in the TGF- β 1 associated apoptosis and invasion. To our surprise we observed an increase in Vimentin in the BxPC3.Y0 cells post TGF- β 1 treatment (Supplemental Figure 1A); however, it was striking to note that there were no cleaved caspases 3 or 7 in these cells post TGF- β 1 treatment suggesting that the tyrosines play a major role in the TGF- β 1 induced apoptotic pathway (Supplemental Figure 1B). To confirm that treatment itself did not cause any changes in the tMUC1 levels, we conducted western blotting for tMUC1 extracellular domain expression pre and post-TGF- β 1 or etoposide treatment in BxC3.Neo, MUC1, and Y0 cells (Supplemental Figure 2). Treatment did not result in any change in the expression levels of tMUC1 in the cells. Due to the changes in tyrosine to phenylalanine, the Y0 cells always run smaller in size and has been published extensively [123].

C-Src inhibition negates TGF- β 1 mediated invasion in tMUC1-overexpressing cells. It has been shown that when Dasatinib, a Src inhibitor, was used on PDA cell lines PANC-1 and Colo-357, it inhibited TGF- β 1 induced SMAD phosphorylation, migration, and invasion, therefore it is a tyrosine to consider [124]. c-Src is also associated with tMUC1-CT and plays a vital role in tMUC1 induced tumor metastasis [56, 72, 125]. Therefore, when BxPC3.MUC1 cells were treated with PP2, a c-Src inhibitor, the invasiveness of the cells in response to TGF- β 1 was decreased (Fig. 5B and D, $p < 0.05$).

However, PP2 treatment did not affect the invasive potential of BxPC3.Neo cells (Fig. 5B and C). Although the BxPC3.Y0 cells had lower percent invasion than BxPC3.MUC1 and BxPC3.Neo cells, it is interesting that PP2 treatment further decreased invasiveness in BxPC3.Y0 cells (Fig. 5B and E, $p < 0.001$, $p < 0.05$). The fact that PP2 inhibition affected the Y0 cells may be because PP2 is non-selective and is known to weakly inhibit EGFR and many other kinases with similar affinities [126, 127]. Overall, the results suggest that overexpression of tMUC1 in these cell lines drive the anti-apoptotic oncogenic functions of TGF- β 1 in a SMAD4 independent manner, and that this is partially via signaling interaction of c-Src with tMUC1-CT. Further investigations need to be conducted to better understand the mechanisms and importance of tMUC1-CT tyrosines and the interaction with other oncogenic signaling pathways. In a pilot study, we established the tMUC1-CT expression levels and the natural invasive potential of a variety of tMUC1-CT mutated BxPC3 cells (Supplemental Figure 3A and B). In BxPC3.Y2 and 5; BxPC3.Y6; BxPC3.Y7; and BxPC3.Y3, 6 and 7 cell lines where either single or multiple tyrosines are mutated to phenylalanine, the results show that these cells behave similarly to BxPC3.Y0. These results further establish the critical oncogenic role of tMUC1-CT as reviewed in [122].

It must be noted that the levels that we report for the endogenous TGF- β 1 production is in picograms/ml and what we add exogenously is in ngs/ml. In the CHO.MUC1 cells, the level is only 0.1ngs and in BxPC3.MUC1, it is 0.6ngs (Figure 1). Therefore, the functional differences we report in Figures 2-5 is due predominantly through the exogenous addition of TGF- β (10ngs).

2.3 Discussion

In a noncancerous pancreas, tMUC1 is expressed in low levels on the luminal surface of the ductal epithelial cells. Yet, an exponential increase in tMUC1 expression occurs during early stages of pancreatic cancer development. Even in early stage pancreatic intraepithelial neoplasia (PanIN) lesions, there is an observed increase in tMUC1 expression [68, 128, 129]. It is also shown that TGF- β 1 mediated response changes from apoptotic and cell growth regulatory to increasing invasiveness and migration in cancer [84]. The data presented herein suggests that tMUC1's interaction with components of the TGF- β signaling pathway, in a SMAD4 independent mechanism, increases the oncogenic features of anti-apoptosis, increased EMT signaling, and more invasion. This has important clinical relevance, because tMUC1 may be a biomarker for anti-TGF- β therapies in PDA cells. Tumors with high tMUC1 expression can now be considered for TGF- β neutralizing strategies, while tMUC1 low expressing tumors should not be considered for the same.

Using a SMAD4 independent PDA cell model, we demonstrate that tMUC1 increases TGF- β 1 secretion, without affecting expression of the key components of the TGF- β signaling in a SMAD-4 deleted cell line (Fig. 1). We believe that the increase in TGF- β 1 secretion in the tMUC1 overexpressing cells (Fig. 1) may be due to the 3-fold increase in latent TGF-beta binding protein 1 (LTBP-1) gene expression in the

BxPC3.MUC1 when compared to the Neo cells (from our microarray data¹ (data not shown)). LTBP-1 activates TGF- β secretion. This targets latent complexes of TGF- β 1 to the extracellular matrix, where the latent cytokine is subsequently activated by various mechanisms. It has been previously shown that tMUC1 expression increased TGF- β 1 expression at the mRNA and protein levels in human hepatocellular carcinoma cells [130]. In dry eye disease, it has also been shown that tMUC1 increases basal TGF- β 1 expression [131]. Recently, it has been shown that TGF- β signaling and deletion of SMAD 4 can alter AGR2 expression, which in turn positively correlates with tMUC1 expression [132]. These studies support our findings that in a tMUC1-overexpressing SMAD 4 deleted PDA cell line model, tMUC1 increases TGF- β 1 expression and release. The mechanisms for upregulation of TGF- β 1 are unknown. However, once malignant cells lose their growth inhibitory response to TGF- β 1 and produce high levels of these protein, the increased expression of TGF- β 1 provides a selective advantage for tumor cell survival as TGF- β 1 are also angiogenic and have potent immunosuppressive effects [117].

During the early phases of tumorigenesis, TGF- β 1 inhibits primary tumor development and growth by inducing cell cycle arrest and apoptosis [133, 134]. Apoptosis is characterized by morphological and biochemical changes [135]. When the role of TGF- β 1 changes from tumor suppressor to tumor promoter, as reviewed in Lebrun 2012, the tumor promoting effects of TGF- β 1 includes induction of EMT, resistance to apoptosis, migration, invasion, and tumor metastasis [136]. It has been shown that SMAD-4 deleted WT BxPC3 cells constitutively activates ERK, has an increased anti-

¹ Preliminary data from our lab not shown

apoptotic response but does not promote invasiveness [137, 138]. Finally, it has also been shown that tMUC1 expression can confer resistance of epithelial cancer cells to cell death via anoikis [139]. Data from our study indicates that tMUC1-overexpressing cells are resistant to TGF- β mediated apoptosis, (Fig. 2) and become highly invasive in a SMAD4-independent manner (Fig. 3). We have also shown similar results in an endogenously tMUC1 high Wild Type SMAD4 PDA cell line (Supplemental Figure 4). Another study reported that inhibiting TGF- β downstream signaling reduces invasiveness in PANC-1 PDA cell line that is known to express tMUC1 [140]. Thus, our data correlates with that study, showing that the tMUC1-over expressing cell lines, BxPC3.MUC1 and CHO.MUC1, have significantly reduced TGF- β 1-induced invasiveness when downstream signaling is blocked in the tMUC1 phosphomutant Y0 cells or in PP2 treated cells (Fig. 4 and 5). The blocking of tMUC1-CT downstream signaling in SMAD4 - negative pancreatic cancer cell line reduces the effects previously seen in the tMUC1-high expressing cells, establishing the importance of tMUC1-CT. This is significant for the 55% of PDA cases where SMAD4 is deleted. It is important to note that tMUC1 expression level does not change with TGF- β 1 treatment or in cells with tMUC1-CT tyrosines mutated to phenylalanine (Supplemental Figure 2). Therefore, the effects are not a reflection of differences in tMUC1 expression levels. Although tMUC1 is known to confer resistance to apoptosis in response to several genotoxic drugs in PDA and other cancer cells [75, 119, 120], this is the first study that shows tMUC1 blocks TGF- β 1 induced apoptosis. Signaling through the MUC1-CT is critical for cleavage of caspases and apoptosis (Supplemental Figure 1B).

Previous studies have shown that the clinical efficiency of inhibition of c-Src in PDA cells is due to inhibition of tumor-promoting TGF- β signaling [124]. Our data supports this interaction by providing evidence that in BxPC3.MUC1 cells treated with c-Src inhibitor PP2 significantly reduced TGF- β 1-induced invasion (Fig. 5). However, it is also shown that PP2 can be non-selective by weakly inhibit EGFR and have other off-target effects [126, 141]. Further array analysis can be performed to understand the complete mechanism. Solving the mystery of the molecular interactions with other oncogenic signaling pathways associated with SMAD4 independent TGF- β signaling will provide great insight into the functional switch of TGF- β 1 from a tumor suppressor to a promoter of tumor development. This knowledge may potentially enable anti-TGF- β therapies in combination with standard therapies and/or immunotherapy to become more efficiently used in the clinic. For example, although certain TGF- β inhibitory treatments have worked *in vivo* using mouse models, the results have not been particularly promising in clinical trials [142]. Targeting TGF- β signaling carries a substantial risk as this pathway is implicated in multiple homeostatic processes and is known to have tumor-suppressor functions. Establishing the mechanism, and determining a potential biomarker, should be priority before continuing anti-TGF- β clinical trials. The mechanisms for upregulation of TGF- β 1 remain unknown. However, once malignant cells lose their growth inhibitory response to TGF- β 1 and produce massive amounts of TGF- β 1 (as seen in the tMUC1-high cells-Figure 1), the increased expression of TGF- β 1 provides a discerning advantage for tumor cell survival. If tMUC1 can be shown as a correlative biomarker, as our data suggests, we may alleviate some of the complications associated with anti-TGF- β therapies, especially in SMAD4 independent PDA cases. The

data presented here is just the beginning in establishing why certain patients may be more suitable candidates for TGF- β targeted therapies than others may. We conclude that signaling through tMUC1-CT plays a critical role in the switch of SMAD4 independent TGF- β 1 function from a pro-apoptotic to a pro-invasion cytokine (Fig. 6).

2.4 Experimental Procedures

Cell Lines and culture. CHO.MUC1, CHO.Neo, CHO. Y0, BxPC3.MUC1, BxPC3.Neo, BxPC3.Y0 were generated as previously described [63]. HPAF-II and MIA Paca-2 were obtained from American Type Culture Collection and cultured as instructed. Cell lines were maintained in Roswell Park Memorial Institute 1640 medium (RPMI; with, L-glutamine; ThermoFisher). RPMI was supplemented with 10% fetal bovine serum (FBS; Hyclone), 3.4 mM L-glutamine, 90 units (U) per ml penicillin, 90 μ g/ml streptomycin, and 1% Non-essential amino acids (Cellgro). RPMI was also supplemented with Geneticin (G418; Invitrogen, Carlsbad, CA, USA). Cells were kept in a 5% CO₂ atmosphere at 37°C. The antibiotic G418 (50 mg/ml) was added to every passage of BxPC3.Neo and BxPC3.MUC1 to ensure positive selection of MUC1 positive cells. For all experiments, cell lines were passaged no more than 10 times.

Western blotting. Cellular lysate preparation and Western blotting was done as previously described [63]. The cells were either treated as such: no treatment, 10 ng/ml of TGF- β 1 (Peprotech, Rocky Hill, NJ, USA), or 100 μ M of Etoposide for 48 hours due to more pronounced signaling. 1:500 Armenian hamster monoclonal anti-human tMUC1 cytoplasmic tail (CT2) antibody was used to probe for tMUC1 in phosphate- buffered-

saline-Tween 20 (PBS-T) with 5% BSA. CT2 antibody recognizes the last 17 amino acids (SSLSYNTPAVAATSANL) of the cytoplasmic tail (CT) of human MUC1 [116]. 1:10,000 TAB004 (OncoTAb, Charlotte, NC) was used to detect the N-terminus extracellular domain of MUC1[62, 143]. Membranes were also probed with the following antibodies from Cell Signaling (1:1000): Smad4 (Rabbit, 38454), Smad 2/3 (Rabbit, 5678), Vimentin (Rabbit, 5741), Snail (Rabbit, 3879), Slug (Rabbit, 9585), N-cadherin (Rabbit, 13116), Cleaved Caspase 3 (Rabbit, 9664), Caspase 3 (Rabbit, 9665), Cleaved Caspase 7 (Rabbit, 8438), Caspase 7 (Rabbit, 12827), and β -Actin (Mouse, 3700). Other antibodies used include TGF- β RI (Abcam, 1:200, Rabbit, ab31013) and TGF- β RII (Abcam, 1:1000, Rabbit, ab61213). Densitometric analysis was conducted using the ImageJ software and percent change is calculated accordingly: First, each density unit for the particular protein was normalized to their respective β -actin density. Percent change was determined by formula $(\text{TGF-}\beta\text{1 treated} - \text{No treatment/No treatment}) * 100$. If the final answer was negative, this was percentage decrease (suggesting that the protein level remained unchanged with treatment).

ELISA. Cells plated in duplicates in 6 well plates were cultured for 6, 12, and 24 hours. At the indicated time point, the culture supernatant was collected and concentrated using Amicon ultra-centrifugal filters (3KDa cutoff). The protein retentate was reconstituted up to 0.5ml with PBS. TGF- β 1 levels in the supernatant were assessed using a specific ELISA (R&D systems, Minneapolis, MN), according to the manufacturer's recommended protocol. The total protein concentration was determined by BCA. The TGF- β 1 levels were normalized to the total protein content of each sample. Results were expressed as TGF- β 1 pg/ml concentration.

Apoptosis Assay. Cells that were serum starved for 18 hours were left untreated or treated with 10ng/ml of TGF- β 1 (Peprotech, Rocky Hill, NJ, USA) and 100 μ M of Etoposide (as a positive control). 24 hours after treatment began; the cells were harvested and stained with Annexin V and PI (Annexin V/Dead Cell Apoptosis Kit, Life Technologies, Eugene, Oregon). The cells were analyzed using BD FORTESSA and FlowJo Version 8.8.7. Fold-change was calculated as TGF- β treated percent apoptosis/control percent invasion.

Invasion Assay. Cells were serum starved 18 hours before plating for the invasion assay. 50,000 cells in serum-free media were plated over transwell inserts (BD Biosciences, San Jose, CA, USA) precoated with diluted reduced growth factor Matrigel in serum free media, plus or minus TGF- β 1 (Peprotech, Rocky Hill, NJ, USA). The cells were allowed to invade through the Matrigel[®] for 48 hours towards the serum contained in the bottom chamber. After 48 hours, only the control wells were swabbed with a cotton swab, followed by staining of all inserts with Coomassie blue. The excess stain was washed off and the inserts were allowed to dry. The membrane was cut and dipped in 10% acetic acid for 10 minutes to elute the dye, which was read by UV/Vis Spectrophotometer at 562 μ M. Percent invasion was calculated as sample absorbance/control absorbance X 100. Fold-change was calculated as TGF- β 1 treated percent invasion/untreated percent invasion.

Treatment with c-Src Inhibitor. BxPC3.MUC1, Neo, and Y0 cells were serum starved 18 hours before plating for the invasion assay. 50,000 cells were plated as in the invasion assay protocol. Cells were either left untreated, treated with 10 ng/ml of TGF- β 1

(Peprotech, Rocky Hill, NJ, USA), or the c-Src inhibitor PP2 (Tocris), or a combination of 10 ng/ml of TGF- β 1 and PP2. The invasion assay was performed as described above.

Statistics. GraphPad Prism 5 and ImageJ were used to analyze the western data. GraphPad Prism 5 was used to generate the graphs and perform statistical analysis.

2.5 Figures

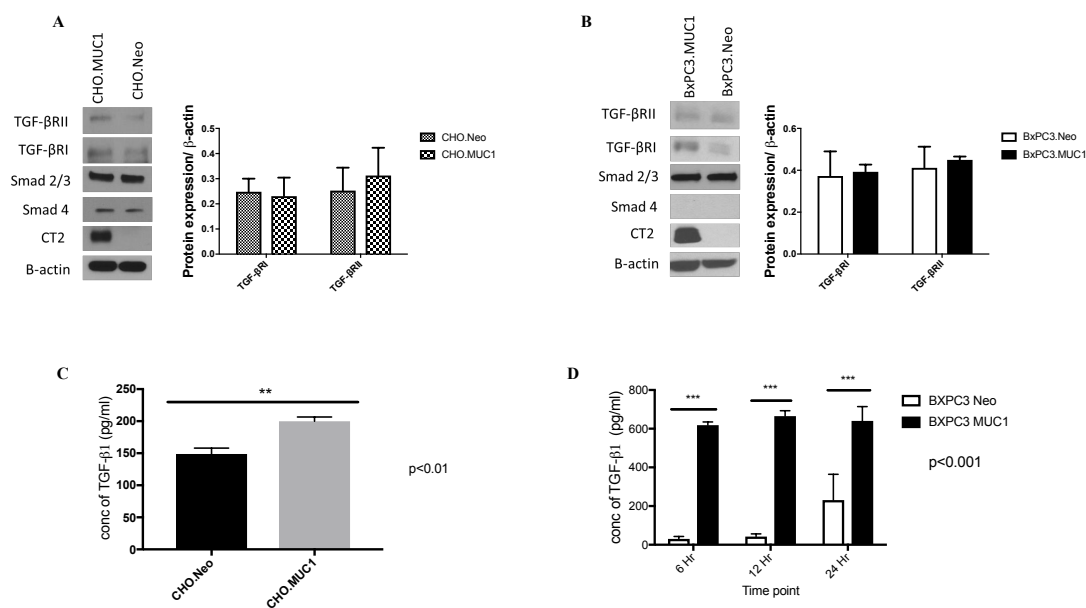


Figure 1. tMUC1 overexpressing cells release significantly higher amounts of active TGF-β1 when compared to tMUC1-low expressing cells. A and B. Western blotting detecting expression of MUC1-CT, TGF-βRI, TGF-βRII, SMAD 2/3, and SMAD4 in CHO and BxPC3 cells. Corresponding densitometric analysis for the TGF-β receptors. **C and D.** TGF-β1 specific ELISA of supernatants from CHO and BxPC3 cells cultured in serum free medium for the indicated times. Results are presented as means +/- SEM of n=3. ** p < 0.01, *** p < 0.001.

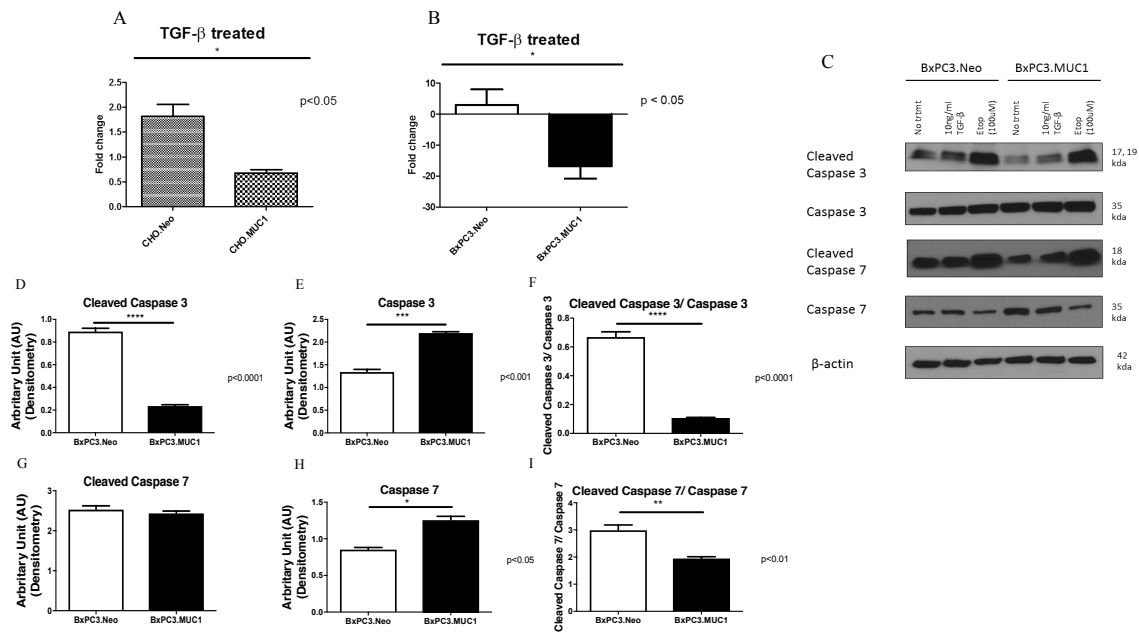


Figure 2. tMUC1 overexpressing cells resist apoptosis in response to treatment with TGF- β 1 with corresponding decrease in cleaved caspase 3 when compared to tMUC1 low expressing cells. **A and B.** Apoptosis was determined at 48 hours post treatment with TGF- β 1 by Annexin V+/7AAD staining and flow cytometry. Data is presented as fold change in apoptosis from untreated cells. **C.** Western blotting of apoptotic markers (cleaved Caspase 3 and 7) in BxPC3 cells 48 hours post TGF- β 1 treatment. **D-I.** Corresponding densitometric analysis of C is presented. **D and G:** Arbitrary densitometric unit of cleaved caspase 3 and cleaved caspase 7 normalized to β -actin respectively; **E and H:** Arbitrary densitometric unit of total caspase 3 and caspase 7 normalized to β -actin; **2F:** Ratio of cleaved caspase 3 and 7 normalized to total caspase 3 and 7. Results are presented as means +/- SEM of n=3. * p < 0.05, ** p < 0.01, *** p<0.001, **** p<0.0001.

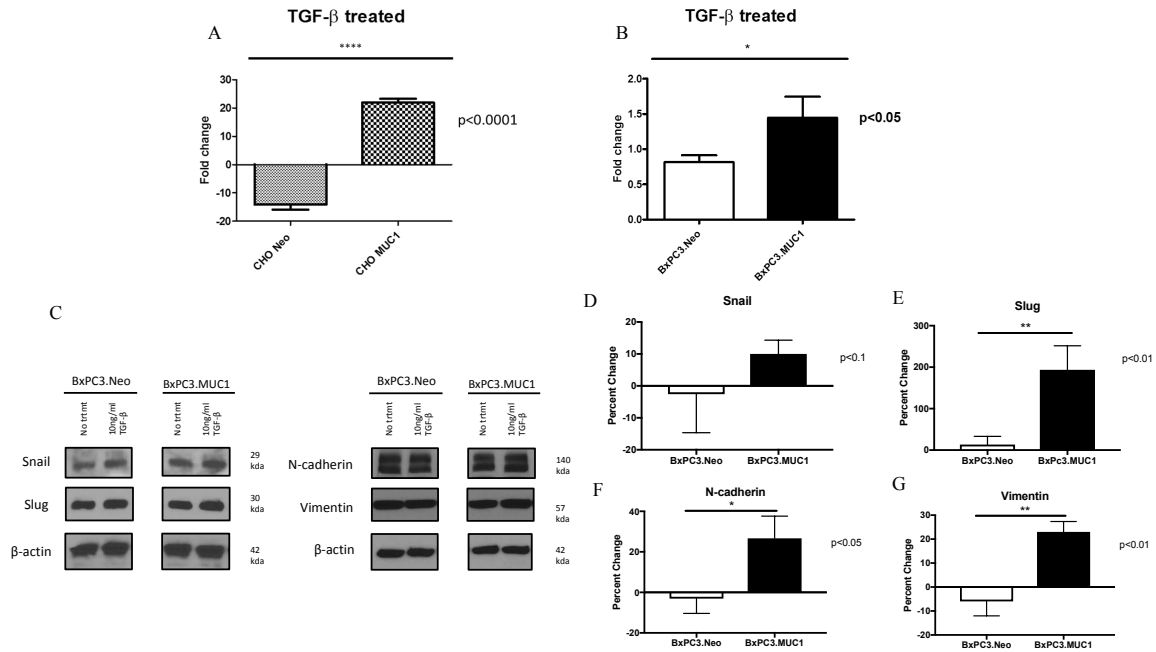


Figure 3. tMUC1 overexpressing cells undergo significantly higher levels of invasion in response to TGF- β 1 treatment. **A and B.** Invasion was determined by standard transwell assay at 48h time point. Results are presented as fold change from untreated. **C.** Western blots to detect EMT markers 48 hours post TGF- β 1 treatment. **D-G.** Corresponding densitometric analysis of C is presented. Percent change from untreated is presented. All values are first normalized to its corresponding β -actin levels. Results are presented as means \pm SEM of n=3. * p < 0.05, ** p < 0.01, **** p<0.0001. **D-G calculation** First the density value of each protein was normalized to their respective β -actin density value. Next the percent change was calculated by the formula: $(\text{TGF-}\beta\text{1 treated} - \text{No treatment/No treatment}) * 100$. If the final answer was negative, this was percentage decrease.

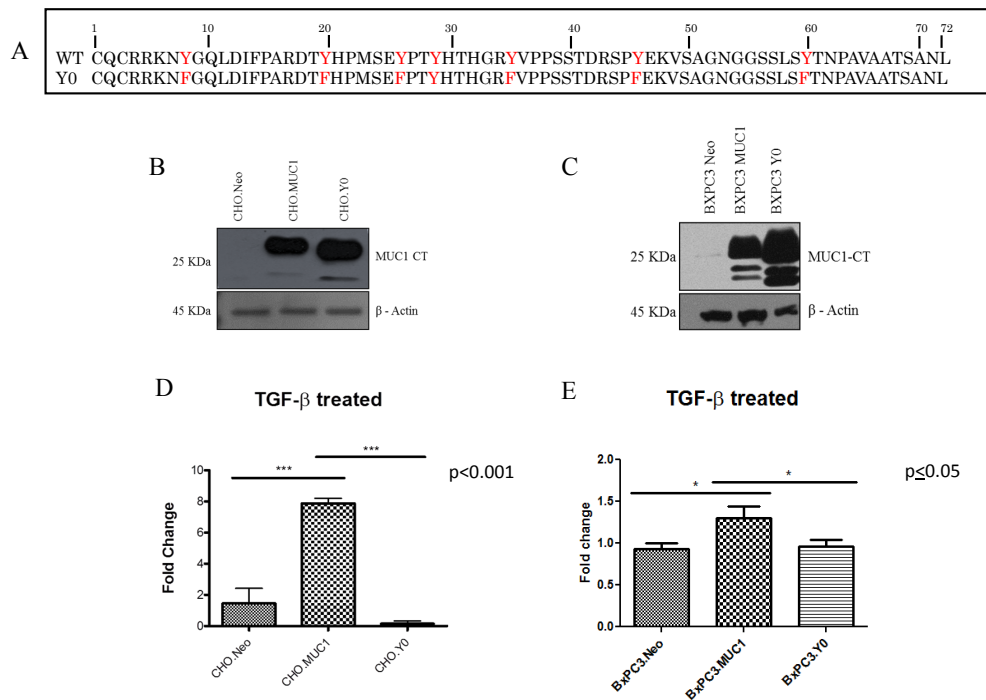


Figure 4. TGF- β 1 mediated invasiveness is dependent upon signaling through the tyrosines in tMUC1-CT. **A.** Amino Acid sequence of tMUC1 CT WT and tMUC1 CT Y0 where tyrosines are mutated to phenylalanine. **B and C.** Western blots to detect tMUC1 using the tMUC1-CT antibody in CHO.Neo, MUC1, and Y0 cells as well as BxPC3.Neo, MUC1, and Y0 cells. **D and E.** 48-hour invasion in response to TGF- β 1 treatment presented as fold change from untreated cells. Results are presented as means \pm SEM of $n=3$. * $p<0.05$, *** $p<0.001$.

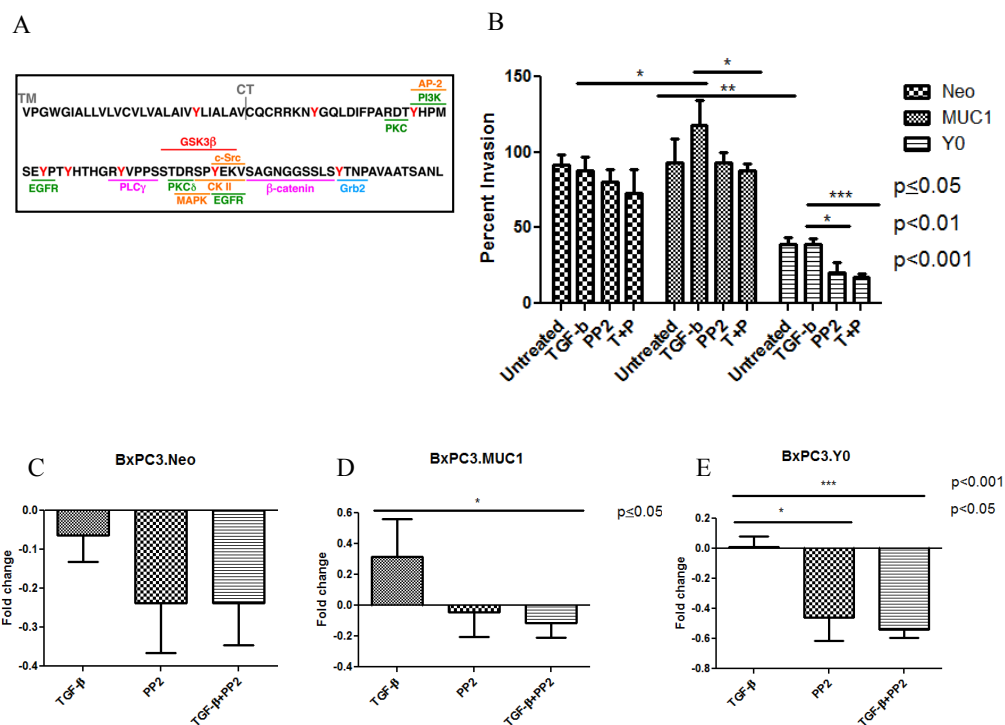


Figure 5. C-Src inhibition negates the aggressiveness of TGF- β 1 mediated invasion in tMUC1 expressing cells. **A.** Schematic of tMUC-CT amino acid sequence and the potential kinase binding sites. **B.** Percent invasion was determined by standard transwell assay at 48 hours post treatment with TGF- β 1 \pm PP2 as indicated in the figure. **C-E.** Each treatment is compared to the untreated within each individual cell line. Results of the invasion assay are presented as means \pm SEM of $n=3$. * $p<0.05$, *** $p<0.001$.

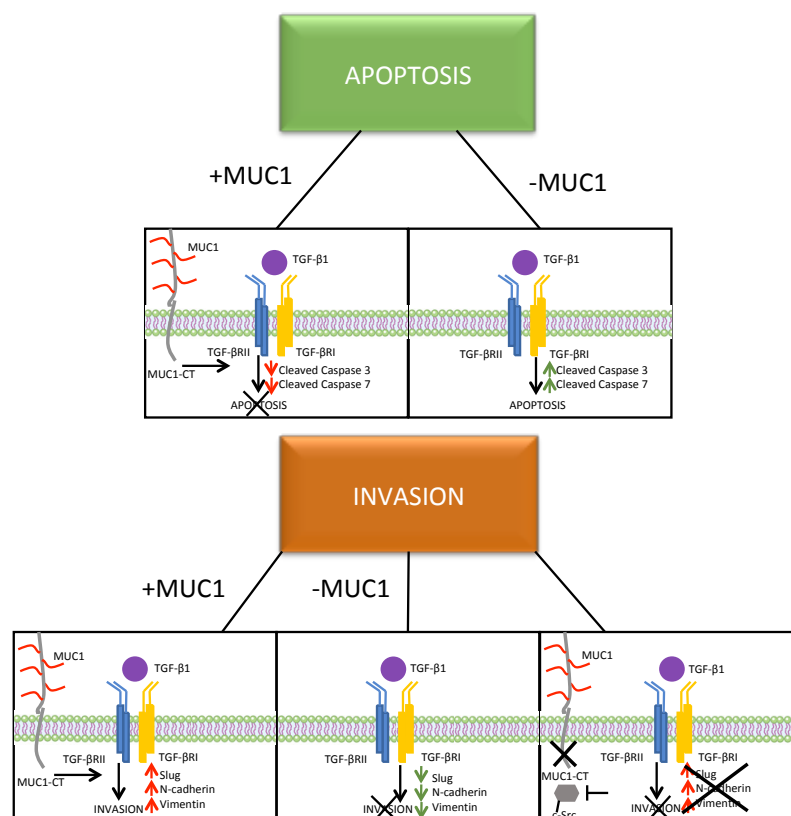
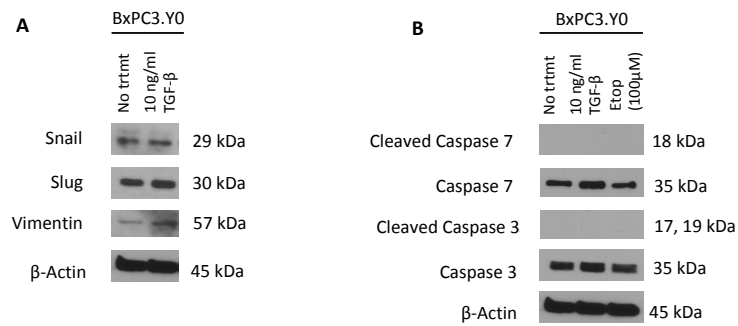
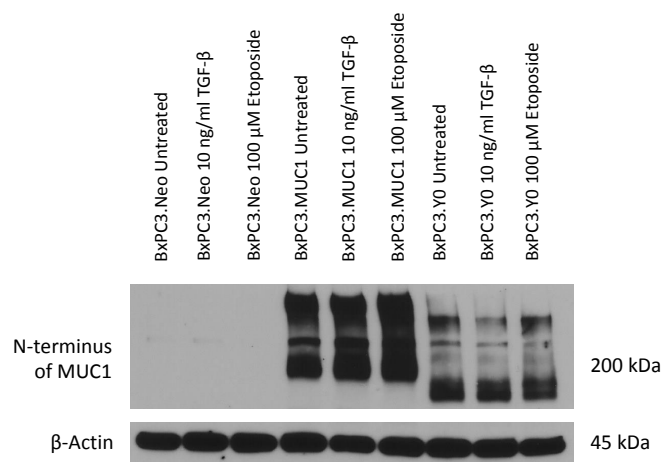


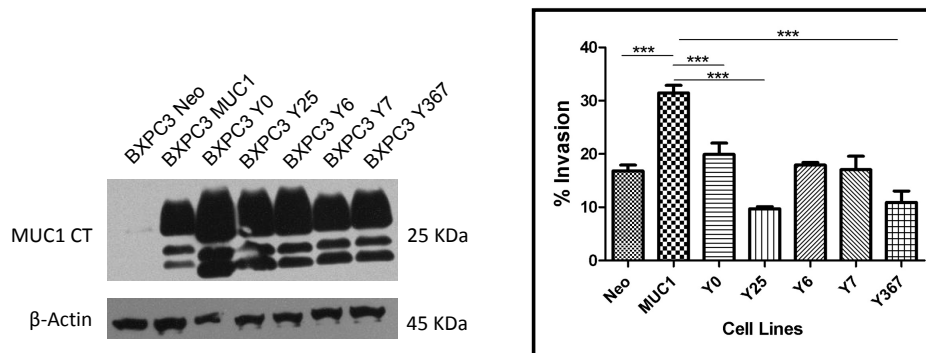
Figure 6. A schematic of the proposed mechanism of tMUC1 mediating TGF- β signaling. Schematic showing that tMUC1-CT plays an important role in switching the role of TGF- β from a tumor suppressor to a tumor promoter in PDA, specifically in BxPC3 cells.



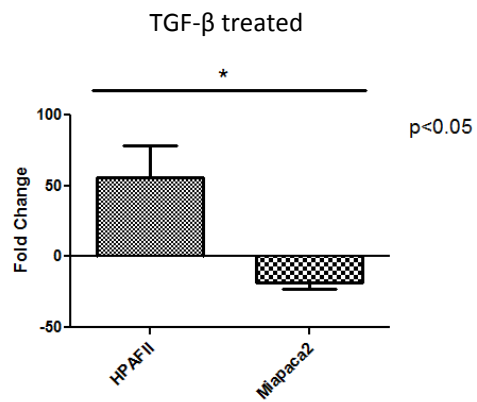
Supplementary Figure 1. Western blotting showing A) EMT and B) Apoptosis associated markers in BxPC3.Y0 cells in response to exogenous TGF- β 1.



Supplementary Figure 2. N-terminus of tMUC1 expression in BxPC3.Neo, BxPC3.MUC1, and BxPC3.Y0 under various conditions was analyzed by Western Blot. Due to the changes of tyrosine to phenylalanine, the Y0 cells always run smaller in size.



Supplementary Figure 3. A. tMUC1 expression in BXPC3 cells infected with full length tMUC1 or various mutants of tMUC1-CT was analyzed by Western Blot. **B.** BXPC3 cells stably expressing the various mutants of tMUC1-CT were plated over transwell inserts pre-coated with reduced growth factor Matrigel[®], and were allowed to invade the matrix towards serum contained in the bottom chamber for 48 hours. Percent invasion was calculated as absorbance of samples/absorbance of controls \times 100.



Supplementary Figure 4. HPAFII and Mia-PaCa2 were plated over transwell inserts pre-coated with reduced growth factor Matrigel[®], and were allowed to invade the matrix towards serum contained in the bottom chamber for 24 hours. Percent invasion was calculated as absorbance of samples/absorbance of controls \times 100.

CHAPTER 3: tMUC1 Regulates Transforming Growth Factor beta 1 (TGF- β 1) function in Pancreatic Ductal Adenocarcinoma

3.1 Introduction

Pancreatic ductal adenocarcinoma (PDA) is currently the third leading cause of cancer-related deaths in the United States. By 2030, it will become the second leading cause [14]. PDA has a median survival rate of less than six months and a five-year survival rate of 9% in the US [144]. Worldwide, the overall five-year survival rate ranges from 2% to 9% [145]. It has a mortality rate that nearly matches its incidence rate [18].

TGF- β 1 is a member of the TGF superfamily of secreted cytokines. It signals through its receptors and performs many cellular functions such as cell growth, apoptosis, differentiation, immune response, angiogenesis, and inflammation [146-148]. Dysregulation of this pathway can lead to cancer, among other ailments [149]. In normal environments and early cancers, TGF- β 1 regulates epithelial cells as a tumor suppressor by regulating the cell cycle and inducing apoptosis. However, a switch occurs and TGF- β 1 becomes a tumor promoter. TGF- β 1 can induce invasion and migration and eventually lead to epithelial-to-mesenchymal transition (EMT) [117]. This process helps facilitate the migration and invasion of cancer cells to distant locations leading to metastasis, the major cause of cancer-related deaths [150].

Canonical TGF- β 1 signaling is initiated by the binding of a cytokine to a pair of specific transmembrane receptors [151]. This activates the cytoplasmic serine/threonine kinase domains of the receptors [152]. This leads to further activation downstream. In normal environments, TGF- β 1 binds to its specific receptors TGF- β RII and TGF- β RI,

respectively. This leads to the phosphorylation of SMAD 2/3 via the cytoplasmic Serine/Threonine kinase domain of TGF- β RI [153]. SMAD2 has been identified as a tumor suppressor and mediator of the anti-proliferative TGF- β 1 and activin responses [154]. SMAD 2/3 trilocates with SMAD 4 which leads the complex to the nucleus to induce transcriptional changes. However, frequent alterations and changes in the TGF- β 1 pathway occur in cancer. Noncanonical TGF- β 1 signaling has been shown to activate Erk1/2 via tyrosine kinase signaling [109]. SMAD 4 mutations and deletions are particularly common in PDA. SMAD 4 is inactivated in about half of PDA cases. Homozygous deletions account for 30% of PDA cases and loss of heterozygosity accounts for 20% of all PDA cases [155].

Tumor Associated Mucin-1 (tMUC1) is a Type I transmembrane O-glycosylated protein that is overexpressed and differently glycosylated, thus influencing tumor progression and metastasis in PDA [56]. tMUC1 is overexpressed and aberrantly glycosylated in more than 80% of PDA cases [56, 59, 62-64]. In normal environments, MUC1 is expressed on the apical surface of ductal cells to provide a protective barrier [156]. However, when the cells become cancerous, tMUC1 expression is no longer restricted to the apical surface. Glycosylation is decreased and the protein becomes overexpressed [59]. Due to loss of polarity in tumor cells, tMUC1 comes into close vicinity of many growth factor receptors. tMUC1 oncogenic signaling, which plays an important role in increased metastasis and invasion, occurs through the cytoplasmic tail (tMUC1-CT). The tMUC1-CT is a highly conserved 72 amino acid long section with seven tyrosine residues that are phosphorylated by tyrosine receptor kinases, such as c-Src [69, 70]. This intracellular kinase is a proto-oncogene that plays an important role in

cancer progression. c-Src has been shown to mediate breast cancer cell proliferation and invasion via regulation of mitogen-activated protein kinase (MAPK) activation [157].

In our previous publication, we have shown tMUC1 controls TGF- β 1 signaling in genetically identical PDA cell lines that are engineered to stably overexpress tMUC1 [73]. We also established that the signaling is dependent upon tyrosine phosphorylation of the tMUC1-CT. We further proved that c-Src is partially responsible for the phosphorylation of tMUC1-CT and neutralizing c-Src led to rescue of TGF- β 1 signaling. In this follow-up report, we confirm our findings in genetically distinct PDA cell lines that express endogenously high and low MUC1. We establish that MUC1 plays a definitive role in switching TGF- β 1's function from a tumor suppressor to a tumor promoter. In the presence of high tMUC1, TGF- β 1 activates the Erk pathway, increases c-Src phosphorylation, and increases the apoptotic resistance of the cells. In contrast, in PDA cells with low levels of tMUC1, TGF- β 1 activates the SMAD pathway, decreases c-Src phosphorylation, and induces cell death by apoptosis. This study is the first to implicate tMUC1 as a potential predictor of response to neutralizing TGF- β therapies.

3.2 Results

tMUC1 high expression positively correlates to TGF- β RII and negatively correlates to TGF- β RI expression levels and leads to activation of Erk pathway. It has been established that tMUC1 and TGF- β 1 is overexpressed in PDA and is linked to metastasis and enhanced invasion. To determine if high tMUC1 in PDA regulates TGF- β 1 associated oncogenic signaling, we first examined a panel of PDA cell lines, with

varying levels of tMUC1, KRAS, SMAD 4 and p53 mutations/deletion status (Table in Figure 1A), for expression of tMUC1, TGF- β RI, TGF- β RII, and SMAD 4 by western blotting. Cells expressing high endogenous levels of tMUC1 displayed high levels of TGF- β RII and low levels of TGF- β RI, while cells expressing low endogenous levels of tMUC1 expressed high levels of TGF- β RI and low levels of TGF- β RII (Figure 1B). Particularly, we observed a stark separation between high and low tMUC1 levels in relation to levels of TGF- β RI as represented in Figure 1C.

To assess if signaling downstream is affected by the differences in TGF- β R levels, we determined the phosphorylation of SMAD 2/3 and Erk 1/2, along with the total levels of the proteins in response to 10ng/ml of TGF- β 1. We observed that cells with high endogenous levels of tMUC1 showed increased phosphorylation of Erk 1/2 while cells with low endogenous levels of tMUC1 showed increased phosphorylation of SMAD 2/3 (Figure 1D). The data suggests that PDA cells expressing high levels of tMUC1 lead to activation of the Erk pathway while cells expressing endogenous low levels of tMUC1 lead to activation of the SMAD pathway.

TGF- β 1 exposure increases cell death in endogenously low tMUC1 expressing PDA cells. We next investigated the effects of TGF- β 1 on the cell cycle of PDA cells with high and low tMUC1 expression. To this end, we exposed endogenously high and low tMUC1 cells to TGF- β 1 for 48 hours. HPAF-II and CFPAC, (high MUC1 cell lines), have very little differences in the G2/M, S, G1/G0, and SubG0/G1 phases of the cell cycle in the presence or absence of TGF- β 1 (Figure 2A and B). However, Panc1 and Mia-PaCa2 (low MUC1 cell lines) showed a dramatic increase in Sub-G0/G1 phase of the cell

cycle in response to TGF- β 1 (Figure 2C and D). *The Sub-G0/G1 phase represents apoptotic/dead cells.* The increase in dead cells confirms that tMUC1 low PDA cells respond well to the anti-tumor effects of TGF- β 1 treatment. Apoptosis was confirmed with AnnexinV/PI staining and flow cytometry (data not shown).

Increased phosphorylation of c-Src in endogenously high tMUC1 cells in the response of TGF- β 1. Src and Src-family protein-tyrosine kinases (including c-Src) are regulatory proteins that play key roles in cell differentiation, proliferation, and survival. Phosphorylation sites of c-Src include an activating phosphotyrosine 416 that results from autophosphorylation, and an inhibiting phosphotyrosine 527 that results from phosphorylation by C-terminal Src kinase (Csk). Dephosphorylation of phosphotyrosine 527 increases Src kinase activity. Thus, we examined the phosphorylation of the c-Src at tyrosines 416 and 527 in high and low MUC1 cells in response to TGF- β 1. We exposed high (HPAF-II and CFPAC) and low MUC1 (Mia-PaCa2) cells to 10 and 50ngs/ml of TGF- β 1 for 30 minutes. After 30 minutes of TGF- β 1 exposure, we observed increased phosphorylation of c-Src at Tyrosine 416 (pC-SrcTry416), signifying increased autophosphorylation in tMUC1 high cells. As expected, we observed decreased pC-SrcTry416 in tMUC1 low cells in response to TGF- β 1. The fold change from untreated cells (represented as densitometry arbitrary unit (A.U.)) is presented in Figure 3A. In contrast to pC-SrcTry416, we observed a decrease in phosphorylation of c-Src at Tyrosine 527 (pC-SrcTry527), signifying decreased dephosphorylation in the tMUC1-high cells in response to TGF β 1 while an increase in pC-SrcTry527 in tMUC1 low cell

line (Fig. 3B). This signifies that c-Src becomes dephosphorylated in low tMUC1 cells in response to TGF- β 1.

TGF- β 1 affects tMUC1 phosphorylation and protein expression. We established that c-Src, a tyrosine receptor kinase that interacts with tMUC1-CT, has increased phosphorylation in endogenously high tMUC1 cells. To determine if TGF- β 1 affects tMUC1 oncogenic signaling, we treated BxPC3.Neo, MUC1, and Y0 cells (where all 7 tyrosines of tMUC1-CT is mutated to phenylalanine) with TGF- β 1 to determine the effects on tMUC1 phosphorylation. Upon 30 minutes of treatment with TGF- β 1, BxPC3.MUC1 cells had increased phosphorylation (Figure 4). However, BxPC3.Neo and Y0 had no difference between control and TGF- β 1 treated. We also noticed a peculiar result. BxPC3.MUC1 cells increased their total tMUC1 levels in the cells after exposure to TGF- β 1 after a short 30 minutes. Further experiments need to be conducted to evaluate this finding. We hypothesize that TGF- β 1 inhibits tMUC1 protein degradation, therefore increasing total tMUC1 protein expression. This result signifies a possible loop between tMUC1 overexpression and TGF- β 1 signaling. This further confirms the importance of the tyrosines in tMUC1-CT for oncogenic signaling and in modulating TGF- β 1 dual function during tumorigenesis.

Neutralizing TGF- β 1 signaling decreases tMUC1 high tumor growth in vivo. We demonstrated MUC1 influences TGF- β 1 signaling *in vitro*, therefore we moved to determine if the same is true *in vivo*. Athymic Nude-Foxn1nu immune compromised mice bearing tMUC1 high (HPAF-II) or tMUC1 low (Mia-PaCa2) established tumors

were injected intra-tumorally with either control IgG or neutralizing TGF- β 1 antibody three times a week for two weeks. The tumors were then measured with calipers over 28 days. tMUC1 low (Mia-PaCa2) tumors treated with neutralizing TGF- β 1 were seen to grow very similarly to the IgG treated tumors (Figure 5A). We did notice an interesting trend when we compared the tumor wet weight at endpoint. In tMUC1 high (HPAF-II) tumors, the α -TGF- β 1 antibody treated tumors weighed significantly less than the control IgG tumors. In tMUC1 low (Mia-PaCa2) tumors, the α -TGF- β 1 antibody treated tumors weighed more than the control IgG treated tumors, however not statistically significant. This is in accordance with our hypothesis.

As expected, α -TGF- β 1 antibody treated tMUC1 high (HFAF-II) tumors had dramatically lower tumor growth when compared to the IgG treated tumors (Figure 5A). When comparing the tumor wet weight, the IgG treated tumors were double the size of the α -TGF- β 1 antibody treated tumors (Figure 5B). The data clearly show that high tMUC1 tumors significantly decrease in size if exposed to neutralizing α -TGF- β 1 antibody therapies but tMUC1-low tumors will not respond to the treatment.

To show clinical relevance and significance of our findings, we generated a heatmap using the TCGA data with high and low MUC1 patient PDA. The correlation heatmap (Figure 5C) demonstrates the correlation between each of the genes in low MUC1 expression samples and moderate/high MUC1 expression samples. The genes included (other than MUC1) were all significantly correlated with MUC1 in PDA samples. Observing the row with MUC1 shows the correlation of each gene with MUC1 in the low MUC1 expression samples. The MUC1 column is a visual of the correlation of each gene with MUC1 in the moderate/high MUC1 expression samples. Comparing the

color block of each gene with itself in the MUC1 row versus column is a visual demonstration of the correlation change between the genes dependent on MUC1 expression. *CDKN2B* and *RHOA* show a slightly stronger positive correlation in the moderate/high MUC1 expression group. *RAF1* shows a very similar correlation in both groups. *SRC* and *ID4* genes have stronger correlations in the low MUC1 expression group; *SRC* is a slightly stronger positive correlation and *ID4* is a slightly stronger negative correlation. The *SMAD4* gene is the only gene to show a noticeable change in correlation. Only a slight small positive correlation is detected between *SMAD4* and MUC1 in the low expression group; however, in the moderate/high expression group there is a strong negative correlation. *SMAD4* is negatively correlated with MUC1 when MUC1 expression is moderate/high but almost no correlation is observed when MUC1 expression is low.

Using the TCGA data, we determined that tMUC1 high PDA cases have higher levels of c-Src when compared to tMUC1 low PDA cases. This validates the importance of c-Src as a mediator in tMUC1 high PDA cases.

3.3 Discussion

In 2009, the National Cancer Institute of NIH chose tMUC1 as the second most targetable biomarker in cancer [158]. tMUC1 is overexpressed in about 80% of all PDA cases [56]. TGF- β signaling has also been shown to play an important role in established cancers [117]. The data presented suggests that tMUC1 and TGF- β closely interact with one another via c-Src. This data has important clinical relevance because tMUC1 can be

used as a prominent biomarker to determine the possible efficacy of TGF- β treatments and help choose between antibody or neutralization treatments.

Using a panel of PDA cell lines (Fig. 1A), we demonstrate the stark connection between tMUC1 and TGF- β receptors (Fig. 1B). We see that tMUC1 is highly positively correlated with TGF- β RII expression. This is important due to TGF- β RII's interaction with pathways significant in cellular proliferation and invasion. tMUC1 is also highly negatively correlated with TGF- β RI expression, which is the receptor that activates the SMAD pathway (Fig. 1C). This pathway plays an important role in apoptosis. We see that low tMUC1 cells are positively correlated with TGF- β RI expression and negatively correlated with TGF- β RII expression. This supports our findings from our previous publication and leads to a possible mechanism for this tMUC1 – TGF- β interaction. Data from our study further suggests downstream pathway differences in our tMUC1 high and low cells when in the presence of TGF- β 1 (Fig. 1D). The tMUC1 high cells have, overall, higher phosphorylation of Erk 1/2. This pathway is important in metastasis and invasion. In the tMUC1 low cells, we see a general increase in the phosphorylation of Smad2/3, which can lead to apoptosis.

To determine if TGF- β 1 functionally affects cells, we analyzed the differences in the cell cycle of the high and low endogenous tMUC1 cells with and without TGF- β 1 (Fig. 2). Our data supports our hypothesis. The high endogenous tMUC1 cells had no increase in sub-G0/G1 cells, signifying no cell death. However, the low endogenous tMUC1 cells had an increase in sub-G0/G1 cells. This established that TGF- β 1 exposure in low endogenous tMUC1 cells leads to more apoptosis.

We further established that the key regulator from our exogenous tMUC1 model, c-Src, is also the regulator in our endogenously high tMUC1 cells (Fig. 3). In a relatively short time, TGF- β 1 exposure in the endogenously high tMUC1 cells, HPAF-II and CFPAC, increased c-Src phosphorylation dramatically. In an interesting twist, we also see c-Src with significant dephosphorylation in endogenously low tMUC1 cells. This establishes the importance of c-Src in this mechanism.

To prove the mechanism is through the tMUC1-CT, we observed the phosphorylation levels of the tMUC1-CT in the presence of TGF- β 1 (Fig. 4). We immediately noticed that BxPC3.MUC1 had increased phosphorylation and overall tMUC1 protein expression. However, we did not see this difference in BxPC3.Y0. This proves that TGF- β 1 is signaling via the tyrosines of the tMUC1-CT, possibly through the tyrosine receptor kinase c-Src. However, the increase in overall tMUC1 protein expression is perplexing. In our previous publication, we found no difference in tMUC1 expression levels after 48 hours of TGF- β 1 exposure [73]. Therefore, we determined that TGF- β 1 affects tMUC1 levels immediately upon treatment. However, due to no more TGF- β 1 being added after initial exposure, the cells' tMUC1 levels return to normal. The data signifies an intricate connection between tMUC1 and TGF- β 1. It could be possible that constant a barrage of TGF- β 1 leads to tMUC1 overexpression in cancer cells.

Lastly, we investigated whether our hypothesis and findings were viable *in vivo* (Fig. 5A). After neutralizing TGF- β 1 in our tMUC1 high tumor, we saw a stark decrease in tumor size and wet weight when compared to the IgG control. We established neutralizing TGF- β treatments as a viable course of action for tMUC1 high PDA tumors.

We further confirmed the importance of c-Src in tMUC1 human PDA cases within our TCGA heatmap (Fig. 5B). The TCGA heatmap also further elucidated some interesting trends within PDA cases when separated by MUC1 expression. In MUC1 low cases, SMAD4 had low interaction with MUC1. However, MUC1 high cases showed SMAD4 had higher interaction with MUC1. For CDKN2B, we see CDKN2B-RAF1 interactions are relatively lower in MUC1 high cases when compared to MUC1 low. CDKN2B-SRC interactions are lower in high MUC1 PDA cases when compared to low MUC1 PDA cases. We see a stark difference in CDKN2B-SMAD4 interactions. MUC1 high PDA cases have higher levels of CDKN2B-SMAD4 interactions, while MUC1 low PDA cases have extremely low CDKN2B-SMAD4 interactions. This interaction will be studied further. We also noticed RHOA interactions with ID4 and SMAD4 also increased in MUC1 high PDA cases. In MUC1 high PDA cases, RAF interacts more with ID4 and SMAD4 when compared to MUC1 low PDA cases. For SRC interactions, besides MUC1-SRC interactions increasing in MUC1 high PDA cases, SRC also interacts with SMAD4 in MUC1 high PDA tumors. Oddly enough, ID4 interacts with SMAD4 less in MUC1 high PDA cases when compared to MUC1 low PDA tumors. Overall, we see that SMAD4 has higher interactions in MUC1 high PDA cases when compared to MUC1 low PDA cases. This increase in activity in MUC1 high environments will require further study. As seen in previous genomic screenings of PDA, protein profiling helps identify efficient pathways to target [159]. Our data helps elucidate c-Src and TGF- β as potential targets in tMUC1 high PDA cases. SMAD4 interactions were also shown to increase in tMUC1 high PDA cases. The connection between SMAD4 and tMUC1 will need to be further studied.

We had previously established the interaction between tMUC1 and TGF- β 1 in a tMUC1 exogenous model. Within this follow-up work, we establish this interaction and mechanism using endogenously high and low tMUC1 cells. We found that short-term exposure to TGF- β 1 leads to an initial increase in tMUC1 tyrosine phosphorylation and overall tMUC1 expression. Therefore, we have established a crosstalk between tMUC1 and TGF- β (Fig. 6). This warrants further study. We also determined a possible treatment route for tMUC1 high PDA tumors with neutralizing TGF- β antibodies. The data presented here establishes tMUC1 as a biomarker for TGF- β treatments in clinical settings.

3.4 Experimental Procedures

Cell Lines and Culture. BxPC3.MUC1, BxPC3.Neo, and BxPC3.Y0 were generated as previously described [63]. Human cell lines (CFPAC, HPAC, HPAF-II, Capan1, Capan2, Panc1, Mia-PaCa2, Su86.86) were obtained from American Type Culture Collection and cultured as instructed. Panc02.MUC1 and Panc02.Neo were originally gifted by Dr. Hollingsworth (University of Nebraska), and maintained in medium containing Geneticin (G418; Invitrogen, Carlsbad, CA, USA). KCM and KCKO were developed in our lab [160]. Cell lines were maintained in Dulbecco's Modified Eagle Medium (DMEM; Gibco), Minimal Essential Media (MEM; Gibco), or Roswell Park Memorial Institute 1640 medium (RPMI; with, L-glutamine; ThermoFisher). All media was supplemented with 10% fetal bovine serum (FBS; Gibco or Hyclone), 3.4 mM L-glutamine, 90 units (U) per ml penicillin, 90 ug/ml streptomycin, and 1% Non-essential

amino acids (Cellgro). RPMI was also supplemented with Geneticin. Cells were kept in a 5% CO₂ atmosphere at 37 degrees Celsius. The antibiotic G418 (50 mg/ml) was added to every passage of BxPC3 transfected cells to ensure positive selection. For all experiments, cell lines were passaged no more than 10 times.

Western Blotting. Cellular lysate preparation and Western blotting were performed as previously described [63]. The cells were divided into different treatment groups: no treatment, 10 ng/ml of TGF- β 1 (Peprotech, Rocky Hill, NJ, USA), or drugs at various concentrations for 48 hours due to more pronounced signaling. 1:500 Armenian hamster monoclonal anti-human MUC1 cytoplasmic tail (CT2) antibody was used to probe for tMUC1 in phosphate- buffered-saline-Tween 20 (PBS-T) with 5% BSA. CT2 antibody recognizes the last 17 amino acids (SSLSYNTPAVAATSANL) of the cytoplasmic tail (CT) of human MUC1 [116]. 1:10,000 TAB004 (OncoTAb, Charlotte, NC) was used to detect the N-terminus extracellular domain of MUC1 [129, 161]. Membranes were also probed with the following antibodies from Cell Signaling Technology (1:1000): SMAD 4 (Rabbit, 38454), p-SMAD 2/3 (Rabbit, 5678), total SMAD (Rabbit, 3102), p-Erk1/2 (Rabbit, 9101), total Erk (Rabbit, 9102), p-Src Family Tyr416 (Rabbit, 6943), Non-p-Src Tyr416 (Mouse, 2102), p-Src Tyr527 (Rabbit, 2105), Non-p-Src (Rabbit, 2107), and β -Actin (Mouse, 3700). Other antibodies used include TGF- β RI (Abcam, 1:200, Rabbit, ab31013) and TGF- β RII (Abcam, 1:1000, Rabbit, ab61213). Densitometric analysis was conducted using the ImageJ software and percent change was calculated accordingly: First, each density unit for the particular protein was normalized to their respective β -actin density. Percent change was determined by formula (TGF- β 1 treated – No treatment/No treatment) X 100. If the final answer was negative,

this was percentage decrease (suggesting that the protein level remained unchanged with treatment).

Cell Cycle. To determine the effect of TGF- β 1 on the cell cycle, cell lines were cultured as described above until ~80% confluent and then serum starved for 18 hours. Cells were then given 50 ng/ml of TGF- β 1 in serum-free media for 24 and 48 hours. Cells were detached with trypsin and fixed in cold 70% ethanol in phosphate buffered saline (1x PBS) overnight. Once the cells were centrifuged, they were then stained with 50 microgram/ml Propidium Iodide (PI) with 20 microgram/ml of RNase A in 1x PBS at room temperature for 30 minutes. Approximately 30,000 cells/sample were acquired using BD LSR Fortessa flow cytometer (BD Biosciences). The data was analyzed with FLOJO software (version 10).

Proteomics. Twenty-nine pancreatic adenocarcinoma RNA-Seq sample data were downloaded from the Genomic Data Commons data portal [162, 163]. All tumor samples were from the PAAD project data generated by The Cancer Genome Atlas (TCGA) Research Network: <http://cancergenome.nih.gov/>. The FPKM gene expression files from these samples were analyzed to identify gene correlations with MUC1. Genes were prefiltered based on a defined list containing genes of interest, including genes involved in the TGFB pathway. Differential Gene Correlation Analysis (DGCA – version 1.0.1) package and psych_1.8.12 package in R were used to identify genes correlated with MUC1 in the tumor samples. Genes with a false discovery rate adjusted p-value of less than 0.05 were considered significantly correlated with MUC1. The tumor samples were then separated into two groups based on their MUC1 expression: MUC1 low expression group and MUC1 moderate/high expression group. A heatmap was generated for

expression of significant genes and MUC1 in the 29 tumor samples. There were 7 samples that showed clear visual low expression in the heatmap compared to the other samples; these were selected for the low expression group. The other 22 samples were included in the mod/high expression group. A heatmap showing correlation of tumor significant correlated genes with MUC1 was plotted using DGCA, separated by the MUC1 expression groups.

Phos-tag. BxPC3 cells were serum starved for 18 hours and then treated with 10 ng/ml of TGF- β for 48 hours. Untreated cells were used as controls. Whole cell lysate was extracted from the cells. Lysate protein concentrations were measured using the Bicinchoninic Acid Assay. 30 micrograms of samples were boiled for 5 minutes prior to loading into a SGS-PAGE gel containing 50 mM Phos-tag and 50 mM MnCl₂. Gels were soaked in 1mM EDTA for 10 minutes prior to transfer onto a nitrocellulose membrane [164].

Mouse Strains. Athymic Nude-Foxn1nu mice were purchased from Charles River Laboratories and housed at UNC Charlotte's vivarium.

Subcutaneous Mouse Model. Athymic Nude-Foxn1nu mice were injected subcutaneously with tumor cells. 3×10^6 HPAFII cells (50ul) or 5×10^6 Mia-PaCa2 cells (50ul) were injected with Matrigel[®] (50ul) (total=100ul) subcutaneously into the flank of male or female Athymic Nude-Foxn1nu mice [165]. Once the tumors reached a palpable size (~3x3mm, ~5 days post tumor inoculation), mice were separated into 4 different groups (n=6). Groups 1 and 3 were treated with the isotype control IgG antibody (20ug/100ul per mouse) three times a week for two weeks. Groups 2 and 4 were treated with the neutralizing TGF- β antibody (20ug/100ul per mouse) three times a week for two

weeks. Mice were monitored daily for general health and tumors were palpated. Caliper measurements were taken three times a week until endpoint (tumor size: ~15x15mm).

This study and all procedures were performed after approval from the Institutional Animal Care and Use Committee of UNC Charlotte.

3.5 Figures

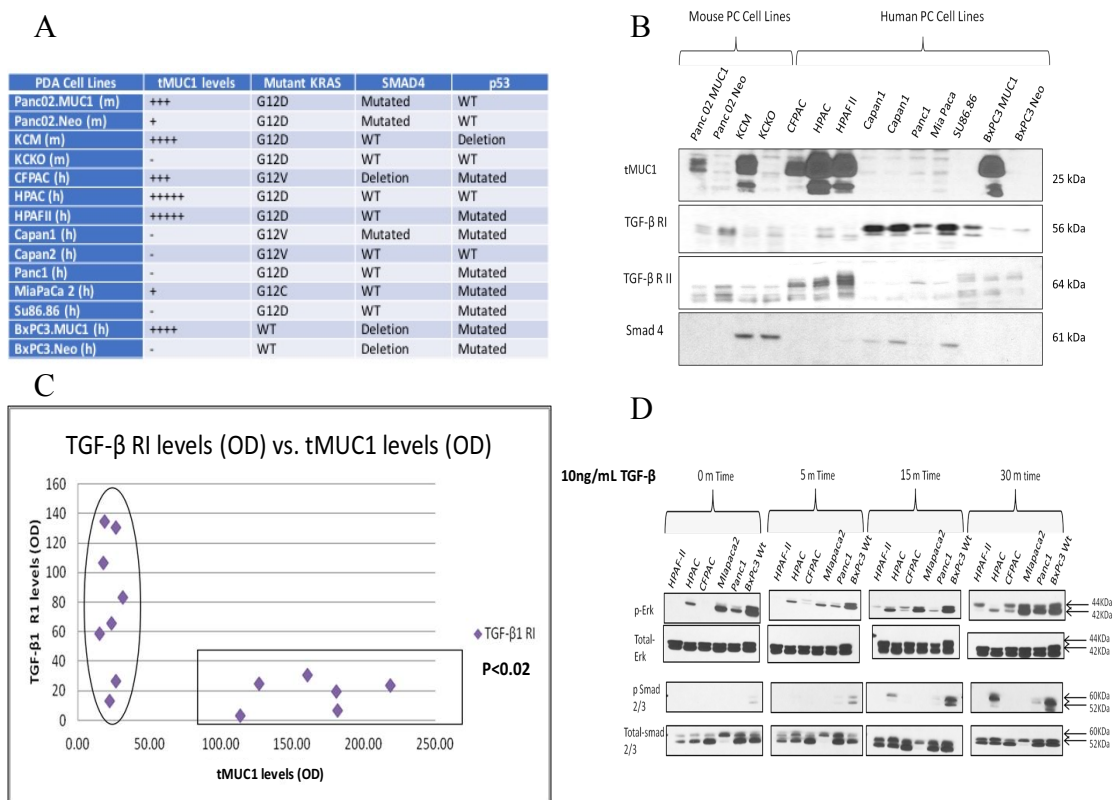


Figure 1. tMUC1 high expression positively correlates to TGF- β RII and negatively correlates to TGF- β R I levels and leads to activation of Erk pathway.

A. Panel of PDA cell lines used in Western blot. **B.** Western blot detecting expression of tMUC1-CT, TGF- β R I, TGF- β R II, and SMAD4 in panel of PDA cell lines. **C.** Densitometric analysis of tMUC1 expression compared to TGF- β R I expression. **D.** Western blot expression of phosphorylation of Erk1/2 and Smad2/3 compared to total Erk 1/2 and SMAD 2/3. Results are presented as n=3.

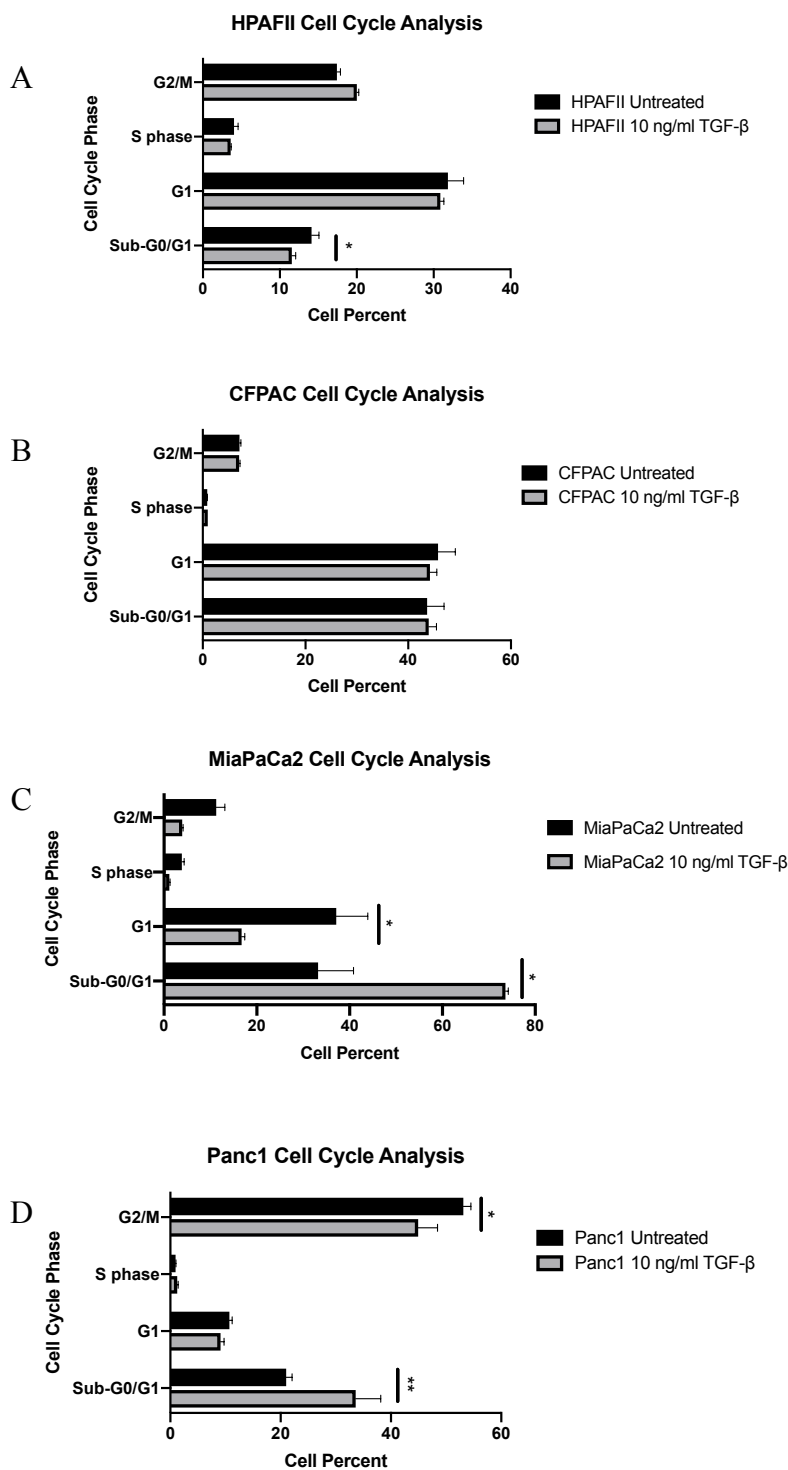


Figure 2. TGF- β 1 exposure increases cell death in endogenously low tMUC1 cells. Cell cycle analysis of tMUC1 high (Fig. 2A and 2B) and low (Fig. 2C and 2D) cell lines when exposed to 10ng/ml of TGF- β 1. Results are presented as means \pm SEM of n=3. * $p < 0.05$, ** $p < 0.01$

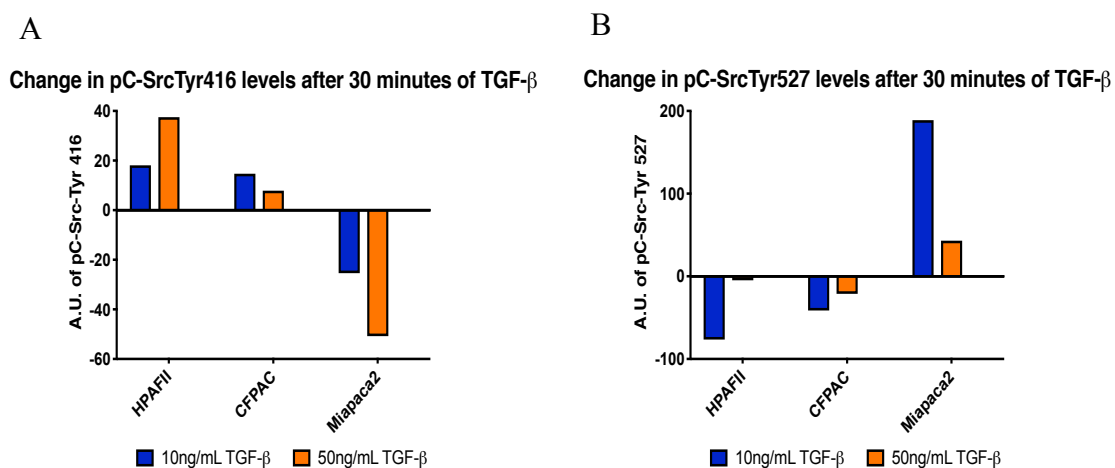


Figure 3. C-Src has increased activation in endogenously high tMUC1 cells in the presence of TGF- β 1. After 30 minutes of exposure to 10ng/ml of TGF- β 1, c-Src phosphorylation increases in the tMUC1 high cells while decreasing in the tMUC1 low cells using Western blot. Densitometric analysis is shown. Results are presented as n=3.

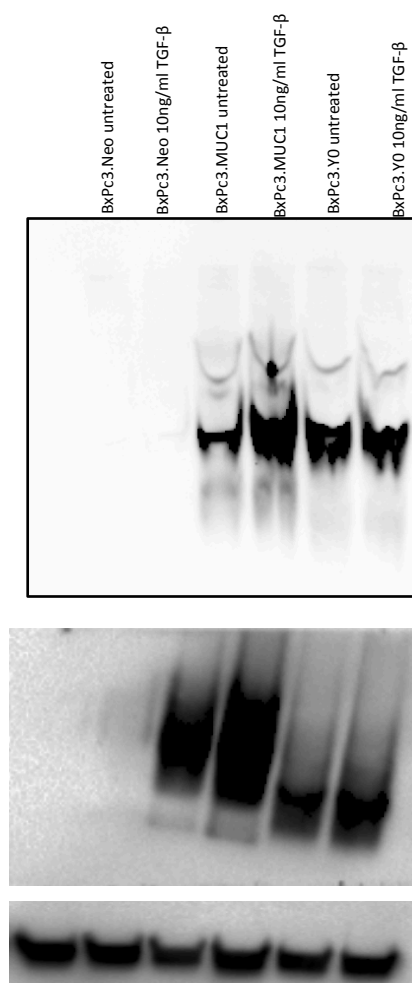


Figure 4. TGF- β 1 effects MUC1 phosphorylation and protein expression in tMUC1 high cells. Phos-tag is used to look at the phosphorylation of tMUC1-CT in BxPC3.Neo, BxPC3.MUC1, and BxPC3.Y0 after 30 minutes of treatment with TGF- β 1. Western blot expression of tMUC1-CT of the Phos-tag is provided. β -actin is the loading control. Results are presented as n=3.

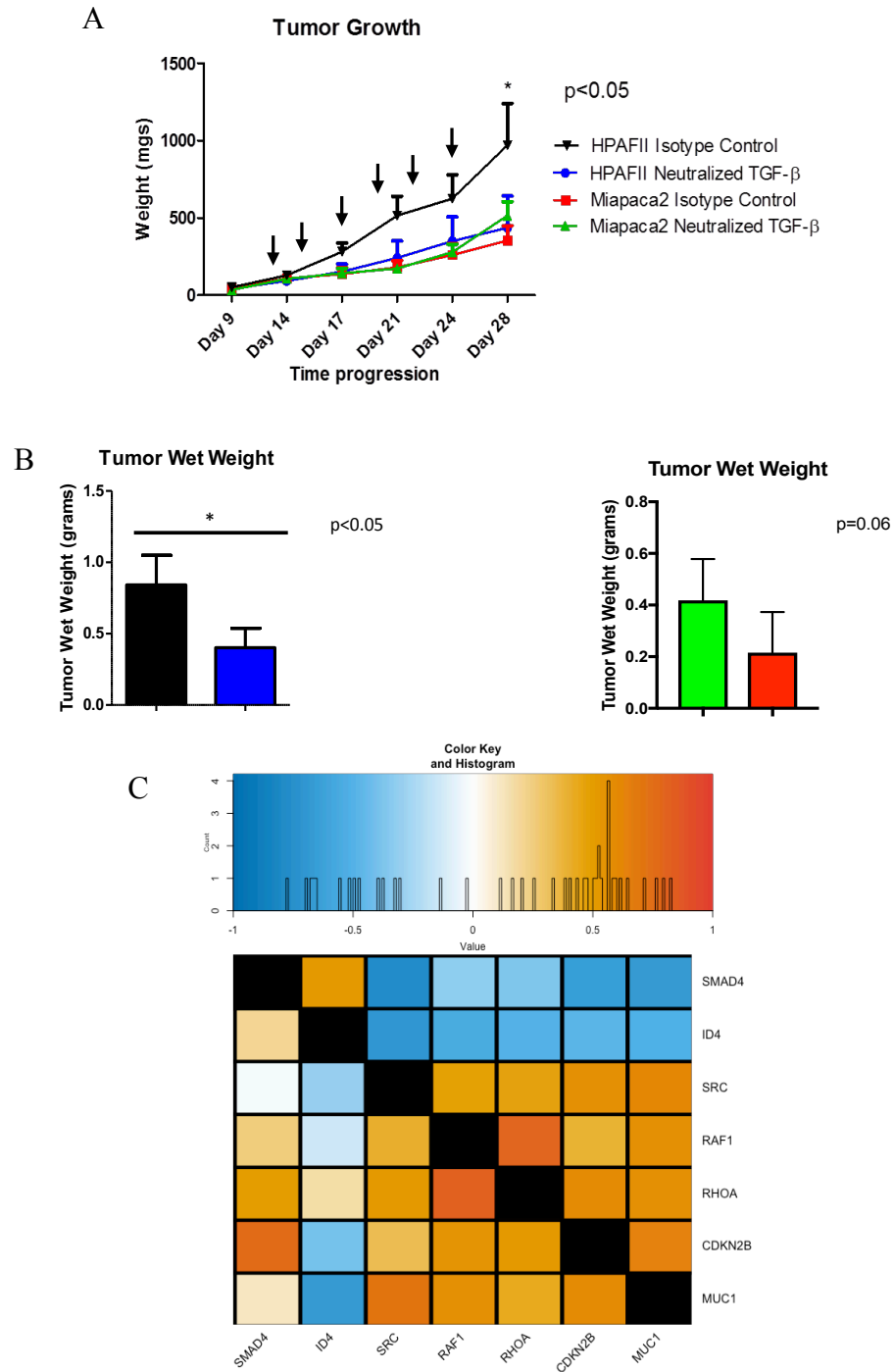


Figure 5. Neutralizing TGF- β signaling decreases tMUC1 high tumor growth in vivo. Neutralizing TGF- β antibody used to treat tMUC1 high and tMUC1 low tumors in vivo. * $p < 0.5$. TCGA correlation heatmap showing the importance of c-Src in high MUC1 PDA cases.

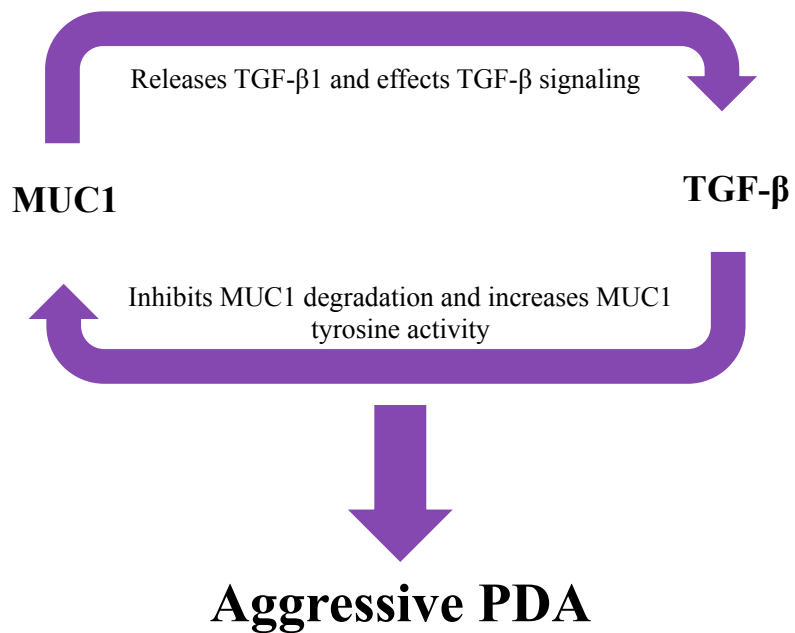


Figure 6. A schematic of the updated mechanism of tMUC1 - TGF-β crosstalk. Updated schematic showing the newly proposed mechanism of the tMUC1 – TGF-β crosstalk. tMUC1 releases TGF-β1 which increases the TGF-β signaling. TGF-β inhibits tMUC1 degradation.

CHAPTER 4: Dissertation Summary

This PhD dissertation aimed to study the interaction between tMUC1 and TGF- β 1 in PDA. Understanding the mechanistic switch of TGF- β 1 will lead to the development of more efficient treatments of PDA tumors. The first part of my dissertation (Chapter 2) establishes the effects of TGF- β 1 in an exogenous tMUC1 model. This study was the first to demonstrate the possible mechanistic switch of TGF- β 1 from a tumor suppressor to a tumor promoter in any solid cancer. The second part of my dissertation (Chapter 3) unravels the mechanistic interaction of tMUC1 and TGF- β 1 in a panel of endogenously high and low tMUC1 PDA cells. The findings were furthered *in vivo* by establishing tMUC1 as a possible marker to efficiently select TGF- β mediated therapies.

Within Chapter 2, it is suggested that tMUC1's interaction with components of the TGF- β signaling pathway increases the oncogenic features of anti-apoptosis, increases EMT signaling, and increases invasion. Using a SMAD 4 independent PDA cell model, it is demonstrated that tMUC1 increases TGF- β 1 secretion, without affecting expression of the key components of the TGF- β signaling in SMAD-4 deleted cells (Fig. 1). Data from Chapter 2 also indicated that tMUC1-overexpressing cells are resistant to TGF- β mediated apoptosis, (Fig. 2) and become highly invasive in a SMAD 4-independent manner (Fig. 3). Furthermore, the data also establish that tMUC1-overexpressing cells have significantly reduced TGF- β 1-induced invasiveness when downstream signaling is blocked in the tMUC1 phosphomutant Y0 cells or in c-Src inhibited cells (Fig. 4 and 5). The blocking of tMUC1-CT downstream signaling in a SMAD 4 – negative pancreatic cancer cell line reduced the effects previously seen in the tMUC1-high expressing cells, highlighting the key signaling role of tMUC1-CT.

In Chapter 3, data gathered in the exogenous model (see above) were further assessed using endogenous models i.e., high and low tMUC1-expressing PDA cells. We established the clear connection between high tMUC1 protein expression and the positive correlation to TGF- β RII, as well as the negative correlation to TGF- β RI. Alternatively, low tMUC1 protein expression was correlated positive and negatively with TGF- β RI and TGF- β RII respectively. In tMUC1 high cells, the phosphorylation of Erk 1/2 was increased, while in tMUC1 low cells, the phosphorylation of SMAD 2/3 was increased (Fig. 1). The functional differences in the cell cycle for endogenously low MUC1 cell lines were further established. We see that these cell lines have an increase in cell death when exposed to TGF- β 1. However, the cell cycles of tMUC1 high cell lines are not affected by TGF- β 1 (Fig. 2). Further, the data show that TGF- β 1 exposure increases phosphorylation of c-Src in tMUC1 high cell lines but dephosphorylates c-Src in tMUC1 low cells (Fig. 3). To detail the mechanism involved, the phosphorylation of tMUC1-CT was assessed using Phos-tag gels. Interestingly, tMUC1 phosphorylation and protein expression both increased after 30 minutes of TGF- β 1 exposure (Fig. 4). In contrast, tMUC1 phosphorylation and protein expression remained unchanged in BxPC3.Y0 cells after 30 minutes of TGF- β 1 exposure (Fig. 4). One possible explanation may be that TGF- β 1 inhibits tMUC1 protein degradation, which would lead to the increase in total tMUC1 protein expression. These findings also indicate that the TGF- β signaling is occurring through the tyrosines of tMUC1-CT. Additionally, tMUC1 protein expression did not increase after a 48-hour exposure to exogenous TGF- β 1 (Chapter 2; Supp. Fig 2). This suggests that initial exposure to TGF- β 1 immediately inhibits tMUC1 protein degradation, and therefore, increases total tMUC1-CT tyrosine phosphorylation levels.

However, over time, tMUC1 protein expression levels decrease to normal levels. Further experiments are required to elucidate this mechanistic loop. This data might be pertinent in understanding tMUC1 degradation in PDA tumor cells. TGF- β 1 is released via autocrine and paracrine methods. Therefore, tumor cells are exposed to TGF- β 1 most of the time. One possible explanation is that TGF- β 1 inhibits tMUC1 degradation in PDA tumors leading to increased total protein expression of the tMUC1-CT. This increased activity can increase oncogenic signaling in cancer cells, ultimately leading to an aggressive tumor.

Finally, we determined the efficacy of neutralizing TGF- β in tMUC1 high and low tumors (Fig. 5). A stark decrease in tumor size (to roughly 50% of IgG treated controls) when we neutralized TGF- β in tMUC1 high tumors was observed. Interestingly, we noticed that the size of tMUC1 low tumors treated with neutralizing TGF- β antibody slowly increased compared to control tumors. The importance of c-Src in tMUC1 high PDA cases was confirmed by the c-Src increased expression observed in the TCGA data of high tMUC1 PDA cases.

PDA is a deadly cancer. Moreover, treatments for the disease are limited. With a five-year survival rate of only 9% in the United States, PDA has limited treatment options. The only possible curative treatment of PDA is surgery, but less than 20% of patients have operable tumors, and less than 30% of those patients survive surgery [14, 22, 166]. Other treatments include chemotherapy and radiotherapy, which only allows for the overall median survival rate of six months. In order to develop more effective treatments, it is important to understand the molecular signaling in PDA. About 97% of PDA have gene alterations, such as amplifications, deletions, translocations, inversions,

frameshifts, and substitutions [22]. In PDA, gene disruptions are almost universal in about 70 – 98% of patients, depending on the gene [22, 167, 168]. PDA is initiated by oncogenic mutant KRAS and present early in the progression of the disease [47, 48]. KRAS has been shown to drive pancreatic neoplasia [49]. 98% of mutant KRAS driven PDA has a KRAS mutation at codon G12, G13, or Q61 [45]. The most common KRAS mutation is G12 with over 98% of total mutation. The most common G12 is G12D, which accounts for about 50% of PDA cases [49].

Aberrantly expressed tMUC1 is an important biomarker and oncogenic protein in adenocarcinomas. tMUC1 is developmentally regulated and aberrantly over-expressed in many human adenocarcinomas, including those of the pancreas, breast, colon, and ovaries [57, 65]. tMUC1 is often over-expressed and/or aberrantly glycosylated in pancreatic cancers, and is associated with increased invasiveness, metastasis, and poor prognosis [169]. In many of these tumor types, tMUC1 is correlated with aggressive, metastatic disease, poor response to therapy, and poor survival [170]. tMUC1 overexpression is prevalent in PDA and a major player in oncogenic signaling via its cytoplasmic tail [62, 66-68, 171]. Once the tMUC1-CT is phosphorylated, it associates with β -catenin and other transcription factors, and becomes released from the N-terminus of tMUC1. The complex translocates to the nucleus and subsequently activates downstream signaling pathways [66, 67, 71]. tMUC1-CT is 72 amino acids long and is highly conserved with seven tyrosine residues that are phosphorylated by intracellular kinases. The phosphotyrosine residues act as binding sites for molecules, such as c-Src, a proto-oncogene linked to cancer progression [56, 72].

Very little is known about tMUC1 degradation. It has been shown in apoptotic resistant cells that tMUC1 lysosomal degradation was blocked which led to an increase in overall tMUC1 expression [172]. ILK negatively regulated protein kinase C (PKC) – δ has also been shown to control the phosphorylation and subsequent proteasomal degradation of tMUC1-CT [173]. This supports our findings (Chapter 3). TGF- β signaling inhibiting MUC1 degradation is extremely novel and can establish a new mechanism to make PDA more aggressive.

Transforming Growth Factor Beta (TGF- β) is a cytokine with a dichotomous role in oncogenesis. In normal tissue development and early oncogenesis, the TGF- β signaling complex is a cell cycle regulator and induces apoptosis. In later stages of cancer, a switch occurs and the TGF- β signaling pathway becomes a tumor promoter, inducing invasion and metastasis. TGF- β 1 stimulates Epithelial-to-Mesenchymal Transition (EMT) through the activation of the ERK pathway [102]. As reviewed in Kalluri et al, EMT is a biological process that transforms an epithelial cell to a mesenchymal cell phenotype, which can lead to resistance to apoptosis [105]. Increased migration and invasion of cancer cells has also been associated with EMT [106]. The TGF- β 1 switch in function from a tumor suppressor, via apoptosis, to a tumor promoter, via EMT, is elusive but holds high importance in treatment refractory cancers like PDA [111]. The TGF- β ligand family consists of three different, highly homologous isoforms: TGF- β 1, TGF- β 2, and TGF- β 3 [81-83]. The most abundant isoform is TGF- β 1 [84]. TGF- β is considered an important target for cancer therapy, and there are multiple anti-TGF- β compounds in clinical trials such as neutralizing TGF- β antibodies [112]. However, the efficacy of the

treatments has not been clear. Establishing a biomarker for TGF- β mediated therapies can increase the success of the trials.

An expansion in TGF- β mediated therapies is imminent and several TGF- β pathway inhibitors are now undergoing clinical assessments. These small-molecules inhibit TGF- β receptors and are based on mostly a dihydropyrrolopyrazole scaffold (LY550410, LY580276 Eli Lilly Research) or imidazole scaffolds (SB-505124 GlaxoSmithKline) [174]. Undergoing phase II trials, the most advanced small molecule inhibitor is galunisertib (LY2157299 Monohydrate Eli Lilly Research). So far, galunisertib has very safe toxicity profile with no dose-limiting limitations [174]. The combination treatment galunisertib plus gemcitabine increased the median survival rate to 8.9 months from 7.1 months (gemcitabine plus placebo) [175].

As stated above, neutralizing TGF- β antibodies have also been explored. For example, fresolimumab (GC1008) has been developed as a treatment for idiopathic pulmonary fibrosis and focal segmental glomerulosclerosis [176]. Since fresolimumab blocks TGF- β 1 and TGF- β 2, it is now being considered for treatment of cancers. Another neutralizing TGF- β antibody is XOMA089, which has also been shown to bind and block TGF- β 1 and TGF- β 2 [174]. As shown in the *in vivo* experiment, neutralizing TGF- β can be an efficient treatment to slow tumor growth in tMUC1 high tumors.

Vaccines have also been developed for TGF- β mediated therapies. Unfortunately, the most advanced vaccine, Belagenpumatucel-L, failed the double blind, randomized phase III trial in stage III/IV non-small cell lung cancer patients after frontline platinum-based induction chemotherapy with optional irradiation [177]. Currently, a newer vaccine called Gemogenovatumel-T has showed promising results. It is in a phase II/III trial in

stage III/IV ovarian cancer patients who have responded to primary surgery and adjuvant chemotherapy (NCT02346747) [174]. This maintenance treatment has increased median relapse-free survival to 13.3 months compared to 3.1 months for placebo. This clinical trial is currently ongoing.

TGF- β biomarkers have also been tested. Considering the numerous members of the TGF- β superfamily, finding reliable biomarkers has been difficult. Galunisertib has been shown to inhibit the phosphorylation of SMAD 2 in peripheral blood mononuclear cells in about 64% of patients in a phase I study [178]. However, using phosphorylated biomarkers in cells has extreme limitations in the clinic due to the difficulties of studying this within patients. Difficulties include off target effects.

It is important to establish signaling connections to expand TGF- β mediated therapies. Establishing tMUC1 as a potential biomarker for TGF- β signaling would greatly benefit the field, especially for TGF- β related biomarkers and neutralizing TGF- β antibodies. Exploring the mechanism between tMUC1 and TGF- β 1 could create new avenues to treat PDA. Establishing tMUC1 as a reliable predictive biomarker in PDA to identify patients who would benefit from TGF- β mediated treatments would be one approach to increase the survival rate in many PDA cases.

Future studies should further our understanding of why TGF- β 1 treatment increases total tMUC1 protein expression rapidly (~ 30 minutes) and then decreases it to control levels (after 48 hours). One option is that TGF- β 1 inhibits tMUC1 degradation. The constant exposure of tumors to TGF- β 1 could maintain the aggressive nature of PDA tumors via tMUC1 overexpression, which, in turn, leads to increased tyrosine phosphorylation of the tMUC1-CT. This data is both intriguing and highly novel. To

evaluate the above hypothesis, I will inhibit proteasome degradation, with and without TGF- β 1, and assess the tMUC1-CT protein expression. I will also determine if the tMUC1 N-terminus follows the same trend as the tMUC1-CT after 30 minutes of exposure to TGF- β 1. Furthermore, I will also repeat the experiment with neutralizing TGF- β antibody to determine the effects on tMUC1-CT after 30 minutes. I hypothesize that there will be no increase in total tMUC1-CT protein expression once we neutralize TGF- β .

Through my dissertation work, I have established a novel biomarker for TGF- β mediated therapies that could be used to increase the efficiency of PDA clinical trials. Through this novel connection between tMUC1 and TGF- β , I hope to increase the overall survival rate of PDA from the single digits into, finally, the double digits.

SUPPLEMENTAL

The Effects of KRAS Activation on the Regulation of Tumor Associated MUC1

5.1 Introduction

PDA has become the third leading cause of cancer-related deaths in the United States with a median survival rate of less than six months and a 5-year survival rate of a dismal 9% [114, 115]. By 2030, it is estimated to become the second leading cause. Its mortality rate nearly matches its incidence rate [16]. Only 20% of patients are eligible for surgery, the only therapy to fully cure [166]. In recent years, there has been an explosive expansion in the field of immunotherapy and the use of small molecule inhibitors. Within Pancreatic Cancer, the main target has been KRAS, the main initiating oncogene. However, it is considered “undruggable” due to its size, protein folding structure, and overall lack of knowledge of this protein and its effects [49]. Studying and evaluating the KRAS pathway and its downstream effects is of utmost importance to understand this deadly disease.

PDA is initiated by oncogenic mutant KRAS and present early in the progression of the disease [47, 48]. It has been shown to drive pancreatic neoplasia [49]. 98% of mutant KRAS driven PDA has a KRAS mutation at codon G12, G13, and Q61 [45]. With point mutations at codon 12, 13, or 61, the initiating oncogene KRAS is responsible for about 99% of all Pancreatic Ductal Adenocarcinoma (PDA) cases [48, 49]. RAS mutations are present in about one third of all cancer cases, regardless of organ origin or type. Given the severity of Ras mutations in cancers and the lack of direct targeting, there needs to be mechanistic understanding of Ras pathways and its effects downstream [46].

PDA cell lines derived from tumors mostly have mutant KRAS. Rarely, a PDA cell line will have Wild Type KRAS (WT KRAS). One predominantly used cell line is BxPC3. KRAS typically requires sustained expression for cancer cell survival; however, the molecular oncogene dependency is not clearly understood [50]. It is seen that knocking down mutant KRAS in Non-Small Cell Lung Cancers suppress tumor growth [51]. It also affects invasive pathways and receptors, such as the Akt pathway and Epidermal Growth Factor Receptors. However, this was not considered sufficient treatment to destroy the cancer. The tumors have been shown to escape this mutant KRAS addiction, or dependency. Very few studies have been done studying KRAS addiction within PC. One study shows that reoccurring pancreatic tumors escape the addiction of mutant KRAS to relapse [52]. Yet, the mechanism involved is not clear. Given the essential roles of oncogenic KRAS in PDA initiation and maintenance, mutant KRAS and the related signaling pathways have become a main focus within cancer research, especially PDA.

Tumor associated Mucin-1 (tMUC1) is a transmembrane glycoprotein that plays a critical role in tumor progression and metastasis in PDA [56]. In normal epithelial cells lining the ducts, MUC1 is localized on the apical surface and plays the role of protective barrier. However, when normal cells transform to malignant cells and lose their polarity, tMUC1 is no longer restricted to the apical surface; it becomes hypo-glycosylated, and comes in close proximity to several growth factor receptors [65]. tMUC1 plays an important role in oncogenic signaling [62, 66-68]. tMUC1 serves as a target for cancer intervention and was named the 2nd most targetable tumor antigen by NCI in 2009 [158]. Studies have linked overexpression of tMUC1 in tumors with enhanced EMT leading to

increased invasiveness, metastasis, and drug resistance [56, 74, 75]. tMUC1 induces increased production of prostaglandin (Cox-2) and growth factors (PDGF and VEGF), which leads to enhanced invasiveness of cells mainly through induction of EMT related genes [62, 63, 68, 77]. Importantly, tMUC1 is overexpressed and aberrantly glycosylated in over 80% of PDA cases [56, 59, 62-64]. It is well established that the oncogenic signal transduction occurs through the cytoplasmic tail of MUC1 (tMUC1-CT) [69, 70]. Once the tMUC1-CT is phosphorylated, it associates with β -catenin and other transcription factors, and becomes released from the N-terminus of tMUC1, leading it to translocate to the nucleus and subsequently activate downstream signaling pathways [66, 67, 71]. tMUC1-CT is 72 amino acids long and is highly conserved with 7 tyrosine residues that are phosphorylated by intracellular kinases. tMUC1 in PDA acts as a binding site for molecules, such as c-Src, a proto-oncogene linked to cancer progression [56, 72]. Understanding the upstream mechanisms involved in tMUC1 regulation is important.

However, the transformation from ordinary MUC1 to tumor-associated MUC1 is not known. A connection has been seen between tMUC1 and mutant KRAS in other cancers. In non-small cell lung cancers, targeting tMUC1 allowed for mutant KRAS independence, while inhibiting tumor growth [179]. In Ovarian Cancer, conditional activation of mutant KRAS leads to diminished tMUC1 expression [180]. Therefore, PDA may escape KRAS addiction, or dependence, through tMUC1 signaling promoting cancer proliferation and growth. Understanding whether the tMUC1 pathway is involved in pancreatic cancer cell proliferation and growth following escape from KRAS addiction is imperative to expand our knowledge of how to treat this disease.

We hypothesize that the oncogenic mutant KRAS plays a role in MUC1 transformation in PDA. tMUC1 may also play a role in escaping KRAS addiction leading to possible reoccurrence of the primary tumor without significant KRAS signaling initiation.

To test our hypothesis, we transfected HEK.293 and BxPC3 cells using CRISPR-Cas9 technology to induce a point mutation of either G12D or G12V. HEK.293 was selected as it has been extensively assessed using CRISPR technology. A CRISPR-Cas9 plasmid, Px.458, was engineered to include KRAS single guide RNA (KRAS sgRNA) that efficiently targets the KRAS gene. The entrance of the plasmid in cells was monitored through the expression of the Green Fluorescent Protein (GFP) a part of the Px.458 plasmid. To induce a point mutation of either G12D or G12V, ultramers or single strand oligo donor nucleotides i.e., SSODN) of KRAS with either specific point mutation were generated. The SSODN were added along CRISPR-Cas9 Px.458 plasmid to OPTI-MEM media with Lipofectamine 3000 and its enhancer and cells incubated with the mixture in complete media for 6 hours. The media was removed and fresh complete media added.

5.2 Results

tMUC1 expression is positively correlated with mutant KRAS protein expression. Western Blot investigations of tMUC1 and mutant KRAS in panel of cancerous cells and of cell overexpressing MUC1 were conducted (Fig. 1). Mutant KRAS non-transfected PDA cells expressing high levels of tMUC1 also express high levels of mutant KRAS (GTP-activate KRAS). Conversely, the cells with low levels of tMUC1

also express low levels of mutant KRAS. To assess whether the mutant KRAS regulates tMUC1 expression or alternatively tMUC1 regulate mutant KRAS, Panc02 overexpressing tMUC1 were generated i.e., Panc02.MUC1 along with a control cell transfected with the empty vector i.e., Panc02.Neo. No significant change in mutant KRAS expression was detected in Panc02.MUC1 supporting the hypothesis that mutant KRAS is upstream of tMUC1. We also transfected the WT KRAS PDA cell, BxPC3 to determine whether WT KRAS expression are altered following tMUC1 overexpression. No significant change was measured in mutant KRAS protein levels, suggesting that tMUC1 is not associated with the conversion of WT KRAS to mutant KRAS. Finally, in Chinese Hamster Ovarian (CHO) cells transfected with KRAS mutant expressed low levels of tMUC1 and extremely high levels of mutant supporting the hypothesis that mutant KRAS activation prevents tMUC1 upregulation [180].

HEK.293 cells were successfully transfected with CRISPR-Cas9 technology.

HEK.293 cells were transfected with Px.458 plasmid alone, Px.458 plasmid with G12D SSODN, or Px.458 plasmid with G12V SSODN. Untreated HEK.293 cells were used as control. After 48 hours, all transfected wells had a significant number of GFP positive cells. Due to the aggressive nature of the KRAS point mutations and the stressful process of sorting cells, the KRAS mutation cells did overgrow the negative cells. Once the cells were 90% confluent, the cells were reseeded at a 10% confluency and regrown. We expect that over time the positive KRAS mutation cells would become the majority.

HEK.293G12D and HEK.293G12V cells are more proliferative. Clonogenic growth assays indicated that HEK.293G12D and HEK.293G12V cells had far more colonies when compared to HEK.293untreated and HEK.293Px.458 cells. We confirmed that the KRAS point mutations led to more aggressive and proliferative HEK.293 cells.

5.3 Discussion

In our exploratory experiments, we see a clear positive correlation between the activation of mutant KRAS and tMUC1 levels (Fig.1). This connection should be fully investigated to determine if KRAS is the upstream mechanism that induces normal MUC1 into tumor associated MUC1. To begin this line of study, we mutated KRAS to either G12D or G12V in HEK cells (Fig. 2). We immediately see that KRAS point mutations lead to cells becoming far more proliferative and aggressive (Fig. 3).

For future directions, we will test tMUC1 expression levels via Western Blot and Flow cytometry. CRISPR will also be completed on BxPC3 cells, a human WT KRAS PDA cell line. This will help us determine if only the KRAS point mutation is sufficient to activate tumor associated MUC1 in PDA.

5.4 Experimental Procedures

Cell Culture. HEK.293 cells were gifted by Dr. Andrew Truman (Department of Biological Sciences, University of North Carolina at Charlotte) and maintained in Dulbecco's Modified Eagle Medium (DMEM; Gibco). Media was supplemented with

10% fetal bovine serum (FBS; Gibco or Hyclone), 3.4 mM L-glutamine, 90 units (U) per ml penicillin, 90 ug/ml streptomycin, and 1% Non-essential amino acids (Cellgro).

CRISPR-Cas9. Cells were seeded in 6 well plates. The experiment began when the cells were 90% confluent. 5 micrograms of Crispr-Cas9 plasmid with KRAS guideRNA, G12D or G12V single-strand oligo donor nucleotides (SSODN), and Lipofectamine 3000 with enhancer were added in OPTI-MEM media and placed in complete media within the wells. After 6 hours, the media was taken out and replaced with fresh media. The cells were observed for GFP for up to 72 hours and sorted by FACS-Aria.

Clonogenic Growth Assay. HEK.293untreated, HEK.293Px.458, HEK.293G12D, and HEK.293G12V cells were seeded in 6-well plates (1,000 cells/well) in triplicates. The cells were incubated for 10-14 days in complete media. Cells were washed with 1xPBS and fixed with methanol: acetic acid (3:1) for 5 minutes. Cells were then stained with 0.5% crystal violet (w/v in methanol) for 15 minutes. Once washed with tap water, the plates were left to dry. Colonies were individually counted and then dissolved in 10% glacial acetic acid to measure the Optical Density (O.D.) at 560nm.

5.5 Figures

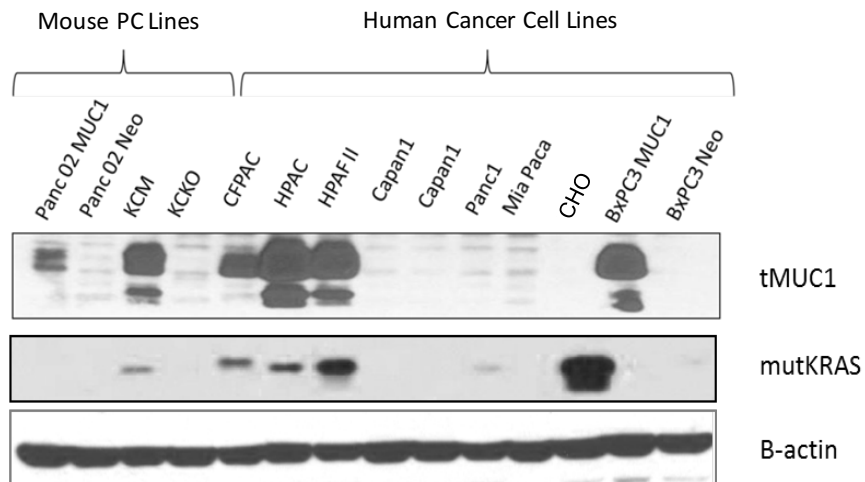


Figure 1. Western Blot shows positive correlation between tMUC1 and GTP-active mutant KRAS (codons 12, 13, and 61) in a panel of PDA cell lines. Mutant KRAS was determined by the activation of GTP-KRAS via a pan-mutant KRAS antibody.

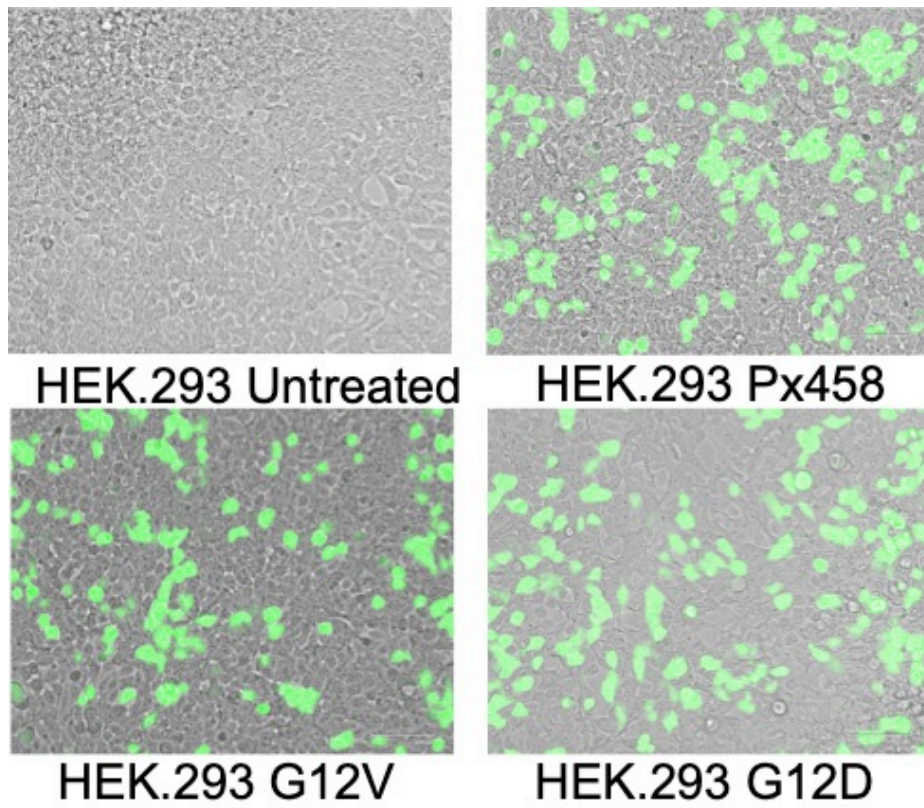


Figure 2. CRISPR-Cas9 generates GFP positive cells. The GFP positive cells were successfully created in HEK.293 cells. The G12D and G12V cells were also exposed to the appropriate SSODNs.

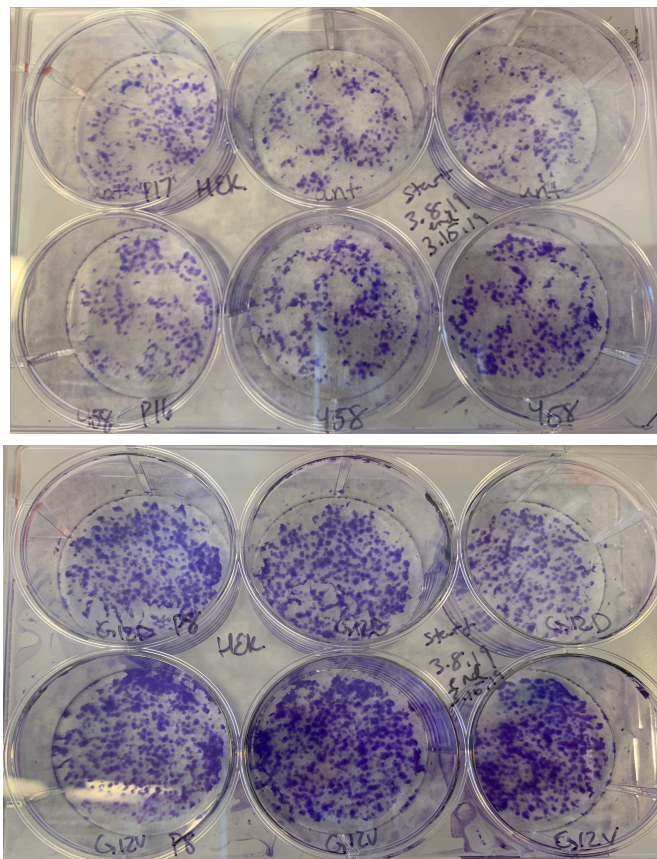


Figure 3. The HEK.293G12D and HEK.293G12V cells were more proliferative than the untreated and Px.458 plasmid alone HEK.293 cells. The clonogenic growth assay starkly shows that the mutant KRAS HEK.293 cell lines are far more proliferative and aggressive when compared to the wild type KRAS HEK.293 cells.

REFERENCES

1. Gittes, G.K., Developmental biology of the pancreas: A comprehensive review. *Developmental Biology*, 2009. 326(1): p. 4-35.
2. Puri, S., Alexandra E. Folias, and M. Hebrok, Plasticity and Dedifferentiation within the Pancreas: Development, Homeostasis, and Disease. *Cell Stem Cell*, 2015. 16(1): p. 18-31.
3. Hellman, B.O., Actual Distribution of the Number and Volume of the Islets of Langerhans in Different Size Classes in Non-diabetic Humans of Varying Ages. *Nature*, 1959. 184(4697): p. 1498-1499.
4. Mastracci, T.L. and L. Sussel, The Endocrine Pancreas: insights into development, differentiation and diabetes. *Wiley interdisciplinary reviews. Membrane transport and signaling*, 2012. 1(5): p. 609-628.
5. Gromada, J., I. Franklin, and C.B. Wollheim, Alpha-cells of the endocrine pancreas: 35 years of research but the enigma remains. *Endocr Rev*, 2007. 28(1): p. 84-116.
6. Cnop, M., et al., Mechanisms of Pancreatic β -Cell Death in Type 1 and Type 2 Diabetes. *Diabetes*, 2005. 54(suppl 2): p. S97.
7. Ludvigsen, E., Somatostatin receptor expression and biological functions in endocrine pancreatic cells: review based on a doctoral thesis. *Ups J Med Sci*, 2007. 112(1): p. 1-20.
8. Müller, T.D., et al., Ghrelin. *Molecular metabolism*, 2015. 4(6): p. 437-460.
9. Da Silva Xavier, G., The Cells of the Islets of Langerhans. *J Clin Med*, 2018. 7(3).
10. Williams, J.A., Regulation of acinar cell function in the pancreas. *Current opinion in gastroenterology*, 2010. 26(5): p. 478-483.
11. Avisse, C., J.B. Flament, and J.F. Delattre, Ampulla of Vater. Anatomic, embryologic, and surgical aspects. *Surg Clin North Am*, 2000. 80(1): p. 201-12.
12. Bardeesy, N. and R.A. DePinho, Pancreatic cancer biology and genetics. *Nature Reviews Cancer*, 2002. 2(12): p. 897.
13. Kindler, H.L., A Glimmer of Hope for Pancreatic Cancer. *New England Journal of Medicine*, 2018. 379(25): p. 2463-2464.
14. Rahib, L., et al., Projecting Cancer Incidence and Deaths to 2030: The Unexpected Burden of Thyroid, Liver, and Pancreas Cancers in the United States. *Cancer Research*, 2014.
15. Chiaravalli, M., M. Reni, and E.M. O'Reilly, Pancreatic ductal adenocarcinoma: State-of-the-art 2017 and new therapeutic strategies. *Cancer Treat Rev*, 2017. 60: p. 32-43.
16. Siegel, R.L., K.D. Miller, and A. Jemal, Cancer statistics, 2016. *CA: A Cancer Journal for Clinicians*, 2016. 66(1): p. 7-30.
17. Siegel, R.L., K.D. Miller, and A.A.-O.h.o.o. Jemal, Cancer statistics, 2018. (1542-4863 (Electronic)).
18. Noone AM, H.N., Krapcho M, Miller D, Brest A, Yu M, Ruhl J, Tatalovich Z, Mariotto A, Lewis DR, Chen HS, Feuer EJ, Cronin KA (eds). *SEER Cancer Statistics Review, 1975-2015*, National Cancer Institute. 2018; based on

- November 2017 SEER data submission, posted to the SEER web site, April 2018.]. Available from: https://seer.cancer.gov/csr/1975_2015/.
19. Raimondi, S., et al., Early onset pancreatic cancer: evidence of a major role for smoking and genetic factors. *Cancer Epidemiol Biomarkers Prev*, 2007. 16(9): p. 1894-7.
 20. Kamisawa, T., et al., Pancreatic cancer. *The Lancet*, 2016. 388(10039): p. 73-85.
 21. Matsubayashi, H., et al., Familial pancreatic cancer: Concept, management and issues. *World journal of gastroenterology*, 2017. 23(6): p. 935-948.
 22. Cicens, J., et al., KRAS, TP53, CDKN2A, SMAD4, BRCA1, and BRCA2 Mutations in Pancreatic Cancer. *Cancers*, 2017. 9(5).
 23. Stadler, Z.K., et al., Prevalence of BRCA1 and BRCA2 mutations in Ashkenazi Jewish families with breast and pancreatic cancer. *Cancer*, 2012. 118(2): p. 493-9.
 24. Iodice, S., et al., Tobacco and the risk of pancreatic cancer: a review and meta-analysis. *Langenbecks Arch Surg*, 2008. 393(4): p. 535-45.
 25. Yuan, C., et al., Cigarette Smoking and Pancreatic Cancer Survival. *J Clin Oncol*, 2017. 35(16): p. 1822-1828.
 26. Kirkegard, J., F.V. Mortensen, and D. Cronin-Fenton, Chronic Pancreatitis and Pancreatic Cancer Risk: A Systematic Review and Meta-analysis. *Am J Gastroenterol*, 2017. 112(9): p. 1366-1372.
 27. Hao, L., et al., Incidence of and risk factors for pancreatic cancer in chronic pancreatitis: A cohort of 1656 patients. *Digestive and Liver Disease*, 2017. 49(11): p. 1249-1256.
 28. Aggarwal, G., P. Kamada, and S.T. Chari, Prevalence of diabetes mellitus in pancreatic cancer compared to common cancers. *Pancreas*, 2013. 42(2): p. 198-201.
 29. Pannala, R., et al., Prevalence and clinical profile of pancreatic cancer-associated diabetes mellitus. *Gastroenterology*, 2008. 134(4): p. 981-7.
 30. Li, J., et al., Early manifestations of pancreatic cancer: the effect of cancer-nerve interaction. *Med Hypotheses*, 2013. 81(2): p. 180-2.
 31. Das, S. and S.K. Batra, Pancreatic cancer metastasis: are we being pre-EMT'ed? *Current pharmaceutical design*, 2015. 21(10): p. 1249-1255.
 32. Chen, Y.F., et al., The diagnostic significance of carbohydrate antigen CA 19-9 in serum and pancreatic juice in pancreatic carcinoma. *Chin Med J (Engl)*, 1989. 102(5): p. 333-7.
 33. Chan, A., et al., Validation of biomarkers that complement CA19.9 in detecting early pancreatic cancer. *Clin Cancer Res*, 2014. 20(22): p. 5787-95.
 34. O'Brien, D.P., et al., Serum CA19-9 is significantly upregulated up to 2 years before diagnosis with pancreatic cancer: implications for early disease detection. *Clin Cancer Res*, 2015. 21(3): p. 622-31.
 35. Griffin, J.F., K.E. Poruk, and C.L. Wolfgang, Pancreatic cancer surgery: past, present, and future. *Chinese journal of cancer research = Chung-kuo yen cheng yen chiu*, 2015. 27(4): p. 332-348.
 36. Conroy, T., et al., FOLFIRINOX versus Gemcitabine for Metastatic Pancreatic Cancer. *New England Journal of Medicine*, 2011. 364(19): p. 1817-1825.

37. Marthey, L., et al., FOLFIRINOX for locally advanced pancreatic adenocarcinoma: results of an AGEO multicenter prospective observational cohort. *Ann Surg Oncol*, 2015. 22(1): p. 295-301.
38. Yu, Y. and J. Cui, Present and future of cancer immunotherapy: A tumor microenvironmental perspective. *Oncology letters*, 2018. 16(4): p. 4105-4113.
39. Brigger, I., C. Dubernet, and P. Couvreur, Nanoparticles in cancer therapy and diagnosis. *Advanced Drug Delivery Reviews*, 2012. 64: p. 24-36.
40. Ro, C., et al., Pancreatic neuroendocrine tumors: biology, diagnosis, and treatment. *Chinese journal of cancer*, 2013. 32(6): p. 312-324.
41. Sun, J., Pancreatic neuroendocrine tumors. *Intractable & rare diseases research*, 2017. 6(1): p. 21-28.
42. Adamska, A., A. Domenichini, and M. Falasca, Pancreatic Ductal Adenocarcinoma: Current and Evolving Therapies. *International journal of molecular sciences*, 2017. 18(7): p. 1338.
43. Delpu, Y., et al., Genetic and epigenetic alterations in pancreatic carcinogenesis. *Curr Genomics*, 2011. 12(1): p. 15-24.
44. Zeitouni, D., et al., KRAS Mutant Pancreatic Cancer: No Lone Path to an Effective Treatment. *Cancers*, 2016. 8(4): p. 45.
45. Collins, M.A. and M. Pasca di Magliano, Kras as a key oncogene and therapeutic target in pancreatic cancer. *Frontiers in Physiology*, 2013. 4: p. 407.
46. Marcus, K. and C. Mattos, Direct Attack on RAS: Intramolecular Communication and Mutation-Specific Effects. *Clin Cancer Res*, 2015. 21(8): p. 1810-8.
47. Deer, E.L., et al., Phenotype and Genotype of Pancreatic Cancer Cell Lines. *Pancreas*, 2010. 39(4): p. 425-435.
48. Eser, S., et al., Oncogenic KRAS signalling in pancreatic cancer. *Br J Cancer*, 2014. 111(5): p. 817-22.
49. Bryant, K.L., et al., KRAS: feeding pancreatic cancer proliferation. *Trends Biochem Sci*, 2014. 39(2): p. 91-100.
50. Shao, D.D., et al., KRAS and YAP1 converge to regulate EMT and tumor survival. *Cell*, 2014. 158(1): p. 171-84.
51. Sunaga, N., et al., Knockdown of Oncogenic KRAS in Non-Small Cell Lung Cancers Suppresses Tumor Growth and Sensitizes Tumor Cells to Targeted Therapy. *Molecular cancer therapeutics*, 2011. 10(2): p. 336-346.
52. Kapoor, A., et al., Yap1 activation enables bypass of oncogenic Kras addiction in pancreatic cancer. *Cell*, 2014. 158(1): p. 185-197.
53. Yonezawa, S., et al., Precursor lesions of pancreatic cancer. *Gut and liver*, 2008. 2(3): p. 137-154.
54. Bournet, B., et al., Targeting KRAS for diagnosis, prognosis, and treatment of pancreatic cancer: Hopes and realities. *European Journal of Cancer*, 2016. 54: p. 75-83.
55. Morris, J.P.t., S.C. Wang, and M. Hebrok, KRAS, Hedgehog, Wnt and the twisted developmental biology of pancreatic ductal adenocarcinoma. *Nat Rev Cancer*, 2010. 10(10): p. 683-95.
56. Nath, S. and P. Mukherjee, MUC1: a multifaceted oncoprotein with a key role in cancer progression. *Trends in Molecular Medicine*. 20(6): p. 332-342.

57. Gendler, S.J., MUC1, the renaissance molecule. *J Mammary Gland Biol Neoplasia*, 2001. 6(3): p. 339-53.
58. Apostolopoulos, V. and I.F. McKenzie, Cellular mucins: targets for immunotherapy. *Crit Rev Immunol*, 1994. 14(3-4): p. 293-309.
59. Kufe, D.W., Mucins in cancer: function, prognosis and therapy. *Nature reviews. Cancer*, 2009. 9(12): p. 874-885.
60. Merlo, G.R., et al., Frequent alteration of the DF3 tumor-associated antigen gene in primary human breast carcinomas. *Cancer Res*, 1989. 49(24 Pt 1): p. 6966-71.
61. Levitin, F., et al., The MUC1 SEA module is a self-cleaving domain. *J Biol Chem*, 2005. 280(39): p. 33374-86.
62. Zhou, R., et al., A novel association of neuropilin-1 and MUC1 in pancreatic ductal adenocarcinoma: role in induction of VEGF signaling and angiogenesis. *Oncogene*, 2016.
63. Roy, L.D., et al., MUC1 enhances invasiveness of pancreatic cancer cells by inducing epithelial to mesenchymal transition. *Oncogene*, 2011. 30(12): p. 1449-59.
64. Tinder, T.L., et al., MUC1 enhances tumor progression and contributes toward immunosuppression in a mouse model of spontaneous pancreatic adenocarcinoma. *J Immunol*, 2008. 181(5): p. 3116-25.
65. Kufe, D.W., Functional targeting of the MUC1 oncogene in human cancers. *Cancer Biol Ther*, 2009. 8(13): p. 1197-203.
66. Li, Y., et al., The Epidermal Growth Factor Receptor Regulates Interaction of the Human DF3/MUC1 Carcinoma Antigen with c-Src and β -Catenin. *Journal of Biological Chemistry*, 2001. 276(38): p. 35239-35242.
67. Li, Y., et al., The c-Src Tyrosine Kinase Regulates Signaling of the Human DF3/MUC1 Carcinoma-associated Antigen with GSK3 β and β -Catenin. *Journal of Biological Chemistry*, 2001. 276(9): p. 6061-6064.
68. Sahraei, M., et al., MUC1 Regulates PDGFA Expression During Pancreatic Cancer Progression. *Oncogene*, 2012. 31(47): p. 4935-4945.
69. Singh, P.K. and M.A. Hollingsworth, Cell surface-associated mucins in signal transduction. *Trends in Cell Biology*, 2006. 16(9): p. 467-476.
70. Thompson, E.J., et al., Tyrosines in the MUC1 cytoplasmic tail modulate oncogenic signaling pathways. *Cancer Research*, 2005. 65(9 Supplement): p. 222-222.
71. Hollingsworth, M.A. and B.J. Swanson, Mucins in cancer: protection and control of the cell surface. *Nat Rev Cancer*, 2004. 4(1): p. 45-60.
72. Ren, J., et al., MUC1 Oncoprotein Functions in Activation of Fibroblast Growth Factor Receptor Signaling. *Molecular Cancer Research*, 2006. 4(11): p. 873-883.
73. Grover, P., et al., SMAD4-independent activation of TGF-beta signaling by MUC1 in a human pancreatic cancer cell line. *Oncotarget*, 2018. 9(6): p. 6897-6910.
74. Kaur, S., et al., Mucins in pancreatic cancer and its microenvironment. *Nature reviews. Gastroenterology & hepatology*, 2013. 10(10): p. 607-620.
75. Nath, S., et al., MUC1 induces drug resistance in pancreatic cancer cells via upregulation of multidrug resistance genes. *Oncogenesis*, 2013. 2: p. e51.

76. Tréhoux, S., et al., The MUC1 oncomucin regulates pancreatic cancer cell biological properties and chemoresistance. Implication of p42–44 MAPK, Akt, Bcl-2 and MMP13 pathways. *Biochemical and Biophysical Research Communications*, 2015. 456(3): p. 757-762.
77. Nath, S., et al., Mucin 1 Regulates Cox-2 Gene in Pancreatic Cancer. *Pancreas*, 2015. 44(6): p. 909-17.
78. Chaika, N.V., et al., MUC1 mucin stabilizes and activates hypoxia-inducible factor 1 alpha to regulate metabolism in pancreatic cancer. *Proc Natl Acad Sci U S A*, 2012. 109(34): p. 13787-92.
79. Mehla, K. and P.K. Singh, MUC1: a novel metabolic master regulator. *Biochimica et biophysica acta*, 2014. 1845(2): p. 126-135.
80. Santibanez, J.F., M. Quintanilla, and C. Bernabeu, TGF-beta/TGF-beta receptor system and its role in physiological and pathological conditions. *Clin Sci (Lond)*, 2011. 121(6): p. 233-51.
81. Assoian, R.K., et al., Transforming growth factor-beta in human platelets. Identification of a major storage site, purification, and characterization. *J Biol Chem*, 1983. 258(11): p. 7155-60.
82. Ikeda, T., M.N. Lioubin, and H. Marquardt, Human transforming growth factor type beta 2: production by a prostatic adenocarcinoma cell line, purification, and initial characterization. *Biochemistry*, 1987. 26(9): p. 2406-10.
83. Derynck, R., et al., A new type of transforming growth factor-beta, TGF-beta 3. *The EMBO Journal*, 1988. 7(12): p. 3737-3743.
84. Katz, L.H., et al., Targeting TGF-beta signaling in cancer. *Expert Opin Ther Targets*, 2013. 17(7): p. 743-60.
85. Saharinen, J. and J. Keski-Oja, Specific sequence motif of 8-Cys repeats of TGF-beta binding proteins, LTBP, creates a hydrophobic interaction surface for binding of small latent TGF-beta. *Molecular biology of the cell*, 2000. 11(8): p. 2691-2704.
86. ten Dijke, P. and H.M. Arthur, Extracellular control of TGFbeta signalling in vascular development and disease. *Nat Rev Mol Cell Biol*, 2007. 8(11): p. 857-69.
87. Klingberg, F., et al., Prestress in the extracellular matrix sensitizes latent TGF-beta1 for activation. *The Journal of Cell Biology*, 2014. 207(2): p. 283-297.
88. ten Dijke, P., et al., Activin receptor-like kinases: a novel subclass of cell-surface receptors with predicted serine/threonine kinase activity. *Oncogene*, 1993. 8(10): p. 2879-87.
89. ten Dijke, P., et al., Characterization of type I receptors for transforming growth factor-beta and activin. *Science*, 1994. 264(5155): p. 101-4.
90. Verrecchia, F. and A. Mauviel, Transforming growth factor-beta and fibrosis. *World J Gastroenterol*, 2007. 13(22): p. 3056-62.
91. Andres, J.L., et al., Binding of two growth factor families to separate domains of the proteoglycan betaglycan. *J Biol Chem*, 1992. 267(9): p. 5927-30.
92. Macías-Silva, M., et al., MADR2 Is a Substrate of the TGFbeta Receptor and Its Phosphorylation Is Required for Nuclear Accumulation and Signaling. *Cell*, 1996. 87(7): p. 1215-1224.
93. Zhang, Y., et al., Receptor-associated Mad homologues synergize as effectors of the TGF-beta response. *Nature*, 1996. 383(6596): p. 168-72.

94. Morikawa, M., R. Derynck, and K. Miyazono, TGF-beta and the TGF-beta Family: Context-Dependent Roles in Cell and Tissue Physiology. *Cold Spring Harb Perspect Biol*, 2016. 8(5).
95. Wrana, J.L., et al., TGF-beta signals through a heteromeric protein kinase receptor complex. *Cell*, 1992. 71(6): p. 1003-1014.
96. Shi, Y. and J. Massague, Mechanisms of TGF-beta signaling from cell membrane to the nucleus. *Cell*, 2003. 113(6): p. 685-700.
97. Souchelnytskyi, S., et al., Phosphorylation of Ser465 and Ser467 in the C terminus of Smad2 mediates interaction with Smad4 and is required for transforming growth factor-beta signaling. *J Biol Chem*, 1997. 272(44): p. 28107-15.
98. Neuzillet, C., et al., Targeting the TGF-beta pathway for cancer therapy. *Pharmacology & Therapeutics*, 2015. 147: p. 22-31.
99. Fink, S.P., et al., TGF-beta-induced nuclear localization of Smad2 and Smad3 in Smad4 null cancer cell lines. *Oncogene*, 2003. 22(9): p. 1317-23.
100. Hahn, S.A., et al., DPC4, A Candidate Tumor Suppressor Gene at Human Chromosome 18q21.1. *Science*, 1996. 271(5247): p. 350-353.
101. Hansel, D.E., S.E. Kern, and R.H. Hruban, Molecular pathogenesis of pancreatic cancer. *Annu Rev Genomics Hum Genet*, 2003. 4: p. 237-56.
102. Xie, L., et al., Activation of the Erk Pathway Is Required for TGF-beta-1-Induced EMT In Vitro. *Neoplasia*, 2004. 6(5): p. 603-610.
103. Yu, J.S., et al., PI3K/mTORC2 regulates TGF-beta/Activin signalling by modulating Smad2/3 activity via linker phosphorylation. *Nat Commun*, 2015. 6: p. 7212.
104. Singha, P.K., et al., TGF-beta induced TMEM16A/PMEM16A1 inhibits canonical Smad signaling through R-Smad sequestration and promotes non-canonical PI3K/Akt signaling by reducing PTEN in triple negative breast cancer. *Genes Cancer*, 2014. 5(9-10): p. 320-36.
105. Kalluri, R. and R.A. Weinberg, The basics of epithelial-mesenchymal transition. *The Journal of Clinical Investigation*, 2009. 119(6): p. 1420-1428.
106. Thiery, J.P., Epithelial-mesenchymal transitions in tumour progression. *Nat Rev Cancer*, 2002. 2(6): p. 442-454.
107. Liu, S., S. Chen, and J. Zeng, TGF-beta signaling: A complex role in tumorigenesis (Review). *Mol Med Rep*, 2018. 17(1): p. 699-704.
108. Mulder, K.M., Role of Ras and Mapks in TGF-beta signaling. *Cytokine Growth Factor Rev*, 2000. 11(1-2): p. 23-35.
109. Lee, M.K., et al., TGF-beta activates Erk MAP kinase signalling through direct phosphorylation of ShcA. *Embo j*, 2007. 26(17): p. 3957-67.
110. Chapnick, D.A., et al., Partners in crime: the TGF-beta and MAPK pathways in cancer progression. *Cell & Bioscience*, 2011. 1(1): p. 42.
111. Truty, M.J. and R. Urrutia, Basics of TGF-beta and Pancreatic Cancer. *Pancreatology*, 2007. 7(5): p. 423-435.
112. Buijs, J.T., K.R. Stayrook, and T.A. Guise, The role of TGF-beta in bone metastasis: novel therapeutic perspectives. *BoneKEY Rep*, 2012. 1(6).

113. Lifshitz, V. and D. Frenkel, Chapter 225 - TGF- β , in Handbook of Biologically Active Peptides (Second Edition), A.J. Kastin, Editor. 2013, Academic Press: Boston. p. 1647-1653.
114. Hezel, A.F., et al., Genetics and biology of pancreatic ductal adenocarcinoma. *Genes Dev*, 2006. 20(10): p. 1218-49.
115. Howlander N, N.A., Krapcho M, Miller D, Bishop K, Altekruse SF, Kosary CL, Yu M, Ruhl J, Tatalovich Z, Mariotto A, Lewis DR, Chen HS, Feuer EJ, Cronin KA (eds), SEER Cancer Statistics Review, 1975-2013. National Cancer Institute, 2016.
116. Croce, M.V., et al., MUC1 cytoplasmic tail detection using CT33 polyclonal and CT2 monoclonal antibodies in breast and colorectal tissue. *Histol Histopathol*, 2006. 21(8): p. 849-55.
117. Massague, J., TGFbeta in Cancer. *Cell*, 2008. 134(2): p. 215-30.
118. Porter, A.G. and R.U. Janicke, Emerging roles of caspase-3 in apoptosis. *Cell Death Differ*, 1999. 6(2): p. 99-104.
119. Agata, N., et al., MUC1 oncoprotein blocks death receptor-mediated apoptosis by inhibiting recruitment of caspase-8. *Cancer Res*, 2008. 68(15): p. 6136-44.
120. Chen, Q., et al., MUC1 activates JNK1 and inhibits apoptosis under genotoxic stress. *Biochem Biophys Res Commun*, 2013. 440(1): p. 179-83.
121. Moz, S., et al., SMAD4 loss enables EGF, TGF β 1 and S100A8/A9 induced activation of critical pathways to invasion in human pancreatic adenocarcinoma cells. *Oncotarget*, 2016. 7(43): p. 69927-69944.
122. Carson, D.D., The cytoplasmic tail of MUC1: a very busy place. *Sci Signal*, 2008. 1(27): p. pe35.
123. Thompson, E.J., et al., Tyrosines in the MUC1 cytoplasmic tail modulate transcription via the extracellular signal-regulated kinase 1/2 and nuclear factor-kappaB pathways. *Mol Cancer Res*, 2006. 4(7): p. 489-97.
124. Bartscht, T., et al., Dasatinib blocks transcriptional and promigratory responses to transforming growth factor-beta in pancreatic adenocarcinoma cells through inhibition of Smad signalling: implications for in vivo mode of action. *Mol Cancer*, 2015. 14: p. 199.
125. Al Masri, A. and S.J. Gendler, Muc1 affects c-Src signaling in PyV MT-induced mammary tumorigenesis. *Oncogene*, 2005. 24(38): p. 5799-808.
126. Kong, L., et al., Src family kinase inhibitor PP2 efficiently inhibits cervical cancer cell proliferation through down-regulating phospho-Src-Y416 and phospho-EGFR-Y1173. *Mol Cell Biochem*, 2011. 348(1-2): p. 11-9.
127. Brandvold, K.R., et al., Development of a highly selective c-Src kinase inhibitor. *ACS Chem Biol*, 2012. 7(8): p. 1393-8.
128. Nagata, K., et al., Mucin expression profile in pancreatic cancer and the precursor lesions. *J Hepatobiliary Pancreat Surg*, 2007. 14(3): p. 243-54.
129. Curry, J.M., et al., The Use of a Novel MUC1 Antibody to Identify Cancer Stem Cells and Circulating MUC1 in Mice and Patients With Pancreatic Cancer. *Journal of surgical oncology*, 2013. 107(7): p. 10.1002/jso.23316.
130. Li, Q., et al., Mucin1 mediates autocrine transforming growth factor beta signaling through activating the c-Jun N-terminal kinase/activator protein 1

- pathway in human hepatocellular carcinoma cells. *Int J Biochem Cell Biol*, 2015. 59: p. 116-25.
131. Imbert-Fernandez, Y., et al., MUC1/A and MUC1/B splice variants differentially regulate inflammatory cytokine expression. *Experimental Eye Research*, 2011. 93(5): p. 649-657.
 132. Norris, A.M., et al., AGR2 is a SMAD4-suppressible gene that modulates MUC1 levels and promotes the initiation and progression of pancreatic intraepithelial neoplasia. *Oncogene*, 2013. 32(33): p. 3867-76.
 133. Jakowlew, S.B., Transforming growth factor-beta in cancer and metastasis. *Cancer Metastasis Rev*, 2006. 25(3): p. 435-57.
 134. Kim, T.-A. and S.-J. Kim, Mechanisms of TGF- β -Induced Apoptosis in Cancer Cells, in *Transforming Growth Factor- β in Cancer Therapy, Volume I: Basic and Clinical Biology*. 2008, Humana Press: Totowa, NJ. p. 199-211.
 135. Kerr, J.F., A.H. Wyllie, and A.R. Currie, Apoptosis: a basic biological phenomenon with wide-ranging implications in tissue kinetics. *Br J Cancer*, 1972. 26(4): p. 239-57.
 136. Lebrun, J.-J., The Dual Role of TGF in Human Cancer: From Tumor Suppression to Cancer Metastasis. *ISRN Molecular Biology*, 2012. 2012: p. 28.
 137. Moz, S., et al., SMAD4 loss enables EGF, TGFbeta1 and S100A8/A9 induced activation of critical pathways to invasion in human pancreatic adenocarcinoma cells. *Oncotarget*, 2016. 7(43): p. 69927-69944.
 138. Fullerton, P.T., C.J. Creighton, and M.M. Matzuk, Insights Into SMAD4 Loss in Pancreatic Cancer From Inducible Restoration of TGF- β Signaling. *Molecular Endocrinology*, 2015. 29(10): p. 1440-1453.
 139. Zhao, Q., et al., MUC1 extracellular domain confers resistance of epithelial cancer cells to anoikis. *Cell Death & Disease*, 2014. 5(10): p. e1438.
 140. Gaspar, N.J., et al., Inhibition of transforming growth factor beta signaling reduces pancreatic adenocarcinoma growth and invasiveness. *Mol Pharmacol*, 2007. 72(1): p. 152-61.
 141. Brandvold, K.R., et al., Development of a Highly Selective c-Src Kinase Inhibitor. *ACS Chemical Biology*, 2012. 7(8): p. 1393-1398.
 142. Connolly, E.C., J. Freimuth, and R.J. Akhurst, Complexities of TGF- β Targeted Cancer Therapy. *International Journal of Biological Sciences*, 2012. 8(7): p. 964-978.
 143. Curry, J.M., et al., The use of a novel MUC1 antibody to identify cancer stem cells and circulating MUC1 in mice and patients with pancreatic cancer. *Journal of Surgical Oncology*, 2013. 107(7): p. 713-722.
 144. McGuigan, A., et al., Pancreatic cancer: A review of clinical diagnosis, epidemiology, treatment and outcomes. *World journal of gastroenterology*, 2018. 24(43): p. 4846-4861.
 145. Ilic, M. and I. Ilic, Epidemiology of pancreatic cancer. *World journal of gastroenterology*, 2016. 22(44): p. 9694-9705.
 146. Isabel, F., et al., TGF-beta Signaling in Cancer Treatment. *Current Pharmaceutical Design*, 2014. 20(17): p. 2934-2947.

147. Carcamo, J., et al., Type I receptors specify growth-inhibitory and transcriptional responses to transforming growth factor beta and activin. *Mol Cell Biol*, 1994. 14(6): p. 3810-21.
148. Shi, Y., Structural insights on Smad function in TGF β signaling. *BioEssays*, 2001. 23(3): p. 223-232.
149. Colak, S. and P. ten Dijke, Targeting TGF- β ; Signaling in Cancer. *Trends in Cancer*, 2017. 3(1): p. 56-71.
150. Mittal, V., Epithelial Mesenchymal Transition in Tumor Metastasis. *Annual Review of Pathology: Mechanisms of Disease*, 2018. 13(1): p. 395-412.
151. Massague, J. and Y.G. Chen, Controlling TGF-beta signaling. *Genes Dev*, 2000. 14(6): p. 627-44.
152. Wrana, J.L., et al., Mechanism of activation of the TGF- β receptor. *Nature*, 1994. 370(6488): p. 341-347.
153. Tsukazaki, T., et al., SARA, a FYVE Domain Protein that Recruits Smad2 to the TGF β Receptor. *Cell*, 1998. 95(6): p. 779-791.
154. Eppert, K., et al., MADR2 Maps to 18q21 and Encodes a TGF β -Regulated MAD-Related Protein That Is Functionally Mutated in Colorectal Carcinoma. *Cell*, 1996. 86(4): p. 543-552.
155. Schutte, M., et al., DPC4 gene in various tumor types. *Cancer Res*, 1996. 56(11): p. 2527-30.
156. Kato, K., et al., MUC1: The First Respiratory Mucin with an Anti-Inflammatory Function. *J Clin Med*, 2017. 6(12).
157. Galliher, A.J. and W.P. Schiemann, Src Phosphorylates Tyr²⁸⁴ in TGF- β Type II Receptor and Regulates TGF- β Stimulation of p38 MAPK during Breast Cancer Cell Proliferation and Invasion. *Cancer Research*, 2007. 67(8): p. 3752.
158. Cheever, M.A., et al., The prioritization of cancer antigens: a national cancer institute pilot project for the acceleration of translational research. *Clin Cancer Res*, 2009. 15(17): p. 5323-37.
159. Integrated Genomic Characterization of Pancreatic Ductal Adenocarcinoma. *Cancer Cell*, 2017. 32(2): p. 185-203.e13.
160. Besmer, D.M., et al., Pancreatic ductal adenocarcinoma mice lacking mucin 1 have a profound defect in tumor growth and metastasis. *Cancer Res*, 2011. 71(13): p. 4432-42.
161. Zhou, R., et al., A Novel Association of Neuropilin-1 and MUC1 in Pancreatic Ductal Adenocarcinoma: Role in Induction of VEGF Signaling and Angiogenesis. *Oncogene*, 2016. 35(43): p. 5608-5618.
162. Grossman, R.L., et al., Toward a Shared Vision for Cancer Genomic Data. *New England Journal of Medicine*, 2016. 375(12): p. 1109-1112.
163. McKenzie, A.T., et al., DGCA: A comprehensive R package for Differential Gene Correlation Analysis. *BMC systems biology*, 2016. 10(1): p. 106-106.
164. Sha, H., et al., The IRE1 α -XBP1 pathway of the unfolded protein response is required for adipogenesis. *Cell Metab*, 2009. 9(6): p. 556-64.
165. Murphy, A.M., et al., Vesicular stomatitis virus as an oncolytic agent against pancreatic ductal adenocarcinoma. *J Virol*, 2012. 86(6): p. 3073-87.

166. Carrato, A., et al., A Systematic Review of the Burden of Pancreatic Cancer in Europe: Real-World Impact on Survival, Quality of Life and Costs. *J Gastrointest Cancer*, 2015. 46(3): p. 201-11.
167. Smit, V.T., et al., KRAS codon 12 mutations occur very frequently in pancreatic adenocarcinomas. *Nucleic Acids Res*, 1988. 16(16): p. 7773-82.
168. Redston, M.S., et al., p53 mutations in pancreatic carcinoma and evidence of common involvement of homocopolymer tracts in DNA microdeletions. *Cancer Res*, 1994. 54(11): p. 3025-33.
169. Singh, R. and D. Bandyopadhyay, MUC1: a target molecule for cancer therapy. *Cancer Biol Ther*, 2007. 6(4): p. 481-6.
170. Horm, T.M. and J.A. Schroeder, MUC1 and metastatic cancer: expression, function and therapeutic targeting. *Cell adhesion & migration*, 2013. 7(2): p. 187-198.
171. Xu, H., et al., Expression of KL-6/MUC1 in pancreatic cancer tissues and its potential involvement in tumor metastasis. *Oncol Rep*, 2011. 26(2): p. 371-6.
172. Wells, A., et al., A signaling pathway consisting of miR-551b, catalase and MUC1 contributes to acquired apoptosis resistance and chemoresistance. *Carcinogenesis*, 2014. 35(11): p. 2457-2466.
173. Huang, H.L., et al., Role of integrin-linked kinase in regulating the protein stability of the MUC1-C oncoprotein in pancreatic cancer cells. *Oncogenesis*, 2017. 6: p. e359.
174. de Gramont, A., S. Faivre, and E. Raymond, Novel TGF- β inhibitors ready for prime time in onco-immunology. *Oncoimmunology*, 2016. 6(1): p. e1257453-e1257453.
175. Melisi, D., et al., Galunisertib plus gemcitabine vs. gemcitabine for first-line treatment of patients with unresectable pancreatic cancer. *Br J Cancer*, 2018. 119(10): p. 1208-1214.
176. Vincenti, F., et al., A Phase 2, Double-Blind, Placebo-Controlled, Randomized Study of Fresolimumab in Patients With Steroid-Resistant Primary Focal Segmental Glomerulosclerosis. *Kidney international reports*, 2017. 2(5): p. 800-810.
177. Giaccone, G., et al., A phase III study of belagenpumatucel-L, an allogeneic tumour cell vaccine, as maintenance therapy for non-small cell lung cancer. *Eur J Cancer*, 2015. 51(16): p. 2321-9.
178. Rodon, J., et al., Pharmacokinetic, pharmacodynamic and biomarker evaluation of transforming growth factor-beta receptor I kinase inhibitor, galunisertib, in phase 1 study in patients with advanced cancer. *Invest New Drugs*, 2015. 33(2): p. 357-70.
179. Akriti Kharbanda, H.R., Caining Jin, Maroof Alam, Kwok-Kin Wong, Donald Kufe, MUC1-C confers EMT and KRAS independence in mutant KRAS lung cancer cells. *Oncotarget*, 2014. 5(19): p. 13.
180. Zhang, L., et al., Effects of Kras activation and Pten deletion alone or in combination on MUC1 biology and epithelial-to-mesenchymal transition in ovarian cancer. *Oncogene*, 2016. 35(38): p. 5010-20.

APPENDIX

PUBLICATIONS – IN CHRONOLOGICAL ORDER

OPEN

Citation: *Oncogenesis* (2013) 2, e51; doi:10.1038/oncsis.2013.16
© 2013 Macmillan Publishers Limited All rights reserved 2157-9024/13

www.nature.com/oncsis

ORIGINAL ARTICLE

MUC1 induces drug resistance in pancreatic cancer cells via upregulation of multidrug resistance genes

S Nath, K Daneshvar, LD Roy, P Grover, A Kidiyoor, L Mosley, M Sahraei and P Mukherjee

MUC1 (CD227), a membrane tethered mucin glycoprotein, is overexpressed in >60% of human pancreatic cancers (PCs), and is associated with poor prognosis, enhanced metastasis and chemoresistance. The objective of this study was to delineate the mechanism by which MUC1 induces drug resistance in human (BxPC3 and Capan-1) and mouse (KCKO, KCM) PC cells. We report that PC cells that express high levels of MUC1 exhibit increased resistance to chemotherapeutic drugs (gemcitabine and etoposide) in comparison with cells that express low levels of MUC1. This chemo resistance was attributed to the enhanced expression of multidrug resistance (MDR) genes including *ABCC1*, *ABCC3*, *ABCC5* and *ABCB1*. In particular, levels of MRP1 protein encoded by the *ABCC1* gene were significantly higher in the MUC1-high PC cells. In BxPC3 and Capan-1 cells MUC1 upregulates MRP1 via an Akt-dependent pathway, whereas in KCM cells MUC1-mediated MRP1 upregulation is via an Akt-independent mechanism. In KCM, BxPC3 and Capan-1 cells, the cytoplasmic tail motif of MUC1 associates directly with the promoter region of the *Abcc1/ABCC1* gene, indicating a possible role of MUC1 acting as a transcriptional regulator of this gene. This is the first report to show that MUC1 can directly regulate the expression of MDR genes in PC cells, and thus confer drug resistance.

Oncogenesis (2013) 2, e51; doi:10.1038/oncsis.2013.16; published online 17 June 2013**Subject Categories:** molecular oncology**Keywords:** pancreatic cancer; mucin1 tandem repeat; mucin 1 cytoplasmic tail; multidrug resistance; PI3K/Akt; *ABCC1* (MRP1)

INTRODUCTION

Pancreatic cancer (PC) is the fourth leading cause of cancer-related deaths in the United States. The 5-year survival rate is ~3% and the median survival rate is <6 months.¹ The current therapeutic interventions include surgical resection, radiation therapy, chemotherapy and immunotherapy.² Less than 20% of PC patients are eligible for surgery because the disease is often diagnosed in late stages.³ However, in most cases where surgery is an option, the tumor recurs within 1–2 years and patients develop hepatic metastasis.⁴ In case of patients with inoperable PC, the standard treatment is chemotherapy that includes gemcitabine. In this group of patients the survival is increased by a dismal 5 weeks.⁵ The poor outcome of chemotherapy is partly due to the drug-resistant phenotype of PC cells. Thus, failure of effective chemotherapeutic treatment results in high mortality in PC patients.⁵ This underscores the importance of understanding the mechanism of drug resistance and developing strategies that would improve the outcome of chemotherapy.

Drug resistance can be classified into two categories: *de novo* resistance or acquired resistance. Cancer patients that exhibit *de novo* resistance do not respond to chemotherapy from the start. However, in acquired resistance, the cancer cells initially respond to a chemotherapeutic drug but eventually acquire resistance to it. The cells might also show cross-resistance to other structurally and mechanistically unrelated drugs—a phenomenon commonly known as multi drug resistance (MDR).⁶ Owing to acquisition of MDR, treatment regimens that combine multiple agents with different targets are no longer effective.^{5,7}

One of the primary mechanisms by which cancer cells attain drug resistance is via upregulation of a family of ATP-binding

cassette (ABC) transporters. These transporters or drug efflux pumps contribute to the MDR phenotype in cancer cells by increasing the efflux of anticancer drugs, thereby reducing their accumulation inside the cancer cells.⁸ P-glycoprotein, MRP1-9 and BCRP are some of the ABC transporters that have been positively linked to the MDR phenotype in cancer cells. The *Mdr1* (or *ABCB1/Abcb1*) gene, which encodes for P-gp, is a well-characterized *mdr* gene. The *ABCC/Abcc* (1–9) gene encodes for the MRP family of multidrug transporters that are responsible for the acquired drug resistance. The *ABCC1/Abcc1* gene encodes for MRP1, which is structurally very similar to P-gp.⁹ Overexpression of the *mdr* genes in cancer cells is considered to be the primary determinant of the MDR phenotype. Another common mechanism of acquiring drug resistance is through enhanced activation of PI3K/Akt and Erk1/2 pathways. These pro-survival pathways inhibit induction of apoptosis in cancer cells. Interestingly, it has recently been shown that PI3K/Akt activation regulates expression of the *ABCC1* gene in prostate cancer cells.¹⁰ Studies have shown that in MUC1-overexpressing cancer cells both Erk1/2 and PI3K pathways are overstimulated.^{11,12} These reports indicate a possible role of these pathways in conferring drug resistance in MUC1-overexpressing PC cells.

MUC1 is a transmembrane mucin glycoprotein that is expressed at the apical surface of epithelial cells.¹³ In over 80% of human pancreatic adenocarcinomas (PDA), a differentially glycosylated form of MUC1 is predominantly overexpressed.^{14,15} MUC1 is a heterodimer, which consists of a unique N-terminal extracellular domain and a C-terminal intracellular domain. The N-terminal domain consists of variable number tandem repeats of 20 amino acids that are extensively modified by O-glycosylation.

Department of Biology, University of North Carolina at Charlotte, Charlotte, NC, USA. Correspondence: Professor P Mukherjee, Department of Biology, Irwin Belk Distinguished Professor of Cancer Research, University of North Carolina-Charlotte, 9201 University City Blvd, Charlotte, NC 28223, USA.
E-mail: pmukherj@uncc.edu

Received 20 February 2013; revised 22 April 2013; accepted 8 May 2013



2

The C-terminal domain includes a 53-amino-acid-long extracellular region, a 28-amino-acid-long transmembrane domain and a 72-amino-acid-long cytoplasmic tail (CT).^{16–18} The transmembrane (TM) and the seven tyrosine residues of MUC1 CT are highly conserved (88% and 100% identical, respectively) among different species, suggesting important functional roles. MUC1 CT serves as an adaptor protein that brings together kinases and other proteins for the propagation of signals, which leads to increased cell proliferation, changes in adhesive state of the cell, invasion into the extracellular matrix and deregulation of apoptosis.^{11,19,20} Importantly, studies have shown that MUC1-overexpressing breast, colon and thyroid cancer cells are unresponsive to chemotoxic agents.^{11,12}

Thus, the goal of the present study was (1) to determine if MUC1-overexpressing PC cells are resistant to chemotherapeutic drugs and (2) to delineate the mechanism by which MUC1-associated resistance occur. We report that MUC1 regulates the *mdr* gene expression via both Akt-dependent and -independent pathways, which confers the MDR phenotype to PC cells. This is the first report that demonstrates a direct relationship between expression of MUC1 and *mdr* genes, in particular *ABCC1* in PC.

RESULTS

PC cells expressing high levels of MUC1 are less sensitive to chemotherapeutic drugs that are reversed upon MUC1 downregulation

To determine the relative expression of endogenous MUC1 in BxPC3 and Capan-1 cell lines, immunohistochemical analysis of cells grown in chamber slides was performed using an antibody against the tandem repeat of MUC1 (HMFG2). Immunohistochemical staining showed that Capan-1 cells have higher endogenous MUC1 expression as compared with BxPC3 cells (Figure 1a). This was confirmed using western blotting assay using antibodies against the tandem repeat (HMFG2) and CT of MUC1 (CT2). Both antibodies showed that Capan-1 cells have higher endogenous MUC1 compared with BxPC3 cells (Figure 1b). Next, we show MUC1 expression in Capan-1 cells following treatment with control and MUC1-specific siRNA (small interfering RNA) by western blot. Complete knockdown of MUC1 is observed in Capan-1 cells post 48-h treatment with MUC1-specific siRNA (Figure 1c and Supplementary Table 1).

To determine the effect of MUC1 in drug resistance, BxPC3 and Capan-1 cells were treated with etoposide and gemcitabine, and proliferation post treatment was determined using H³-thymidine

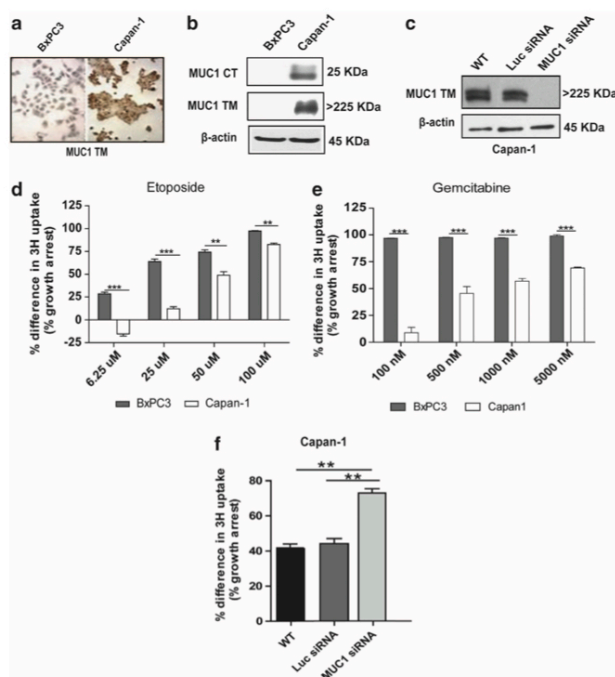


Figure 1. MUC1 expression and drug sensitivity of a panel of cancer cells. (a) Staining of endogenous MUC1 expression in BxPC3 and Capan-1 cells using HMFG2 antibody, Capan-1 expresses high levels as depicted by the brown staining whereas BxPC3 cells have negligible levels of MUC1 staining. (b) Western blot analysis of MUC1 expression in BxPC3 and Capan-1 cells by western blot using HMFG2 and CT2 antibody. (c) Western blot analysis of MUC1 expression in Capan-1 cells following treatment with MUC1-specific siRNA (48 h). (d, e) H³-thymidine incorporation to measure proliferation in PC cells following 24 h treatment with etoposide and gemcitabine ($n = 4$). Significantly higher proliferation was observed in Capan-1 cells, which express high levels of MUC1 ($***P < 0.001$). (f) Percent difference in H³-thymidine uptake in control siRNA and MUC1 siRNA treated cells as a function of Capan-1 WT cells. Cells were treated for 24 h with 500 nM of gemcitabine ($n = 4$). Cells treated with MUC1 siRNA showed significantly reduced proliferation in response to gemcitabine as compared with untreated or control siRNA treated cells ($**P < 0.05$).

incorporation assay. Etoposide is a topoisomerase II inhibitor, whereas gemcitabine is a nucleoside analog. Low MUC1-expressing BxPC3 cells showed greater sensitivity to etoposide and gemcitabine compared with high MUC1-expressing Capan-1 cells. At 25 μM dose of etoposide, we observed a 62.8% growth arrest in BxPC3 cells. In contrast, at the same dose, only 12.14% growth arrest was observed in Capan-1 cells (Figure 1d). Similarly, at 500 nM dose of gemcitabine, ~100% growth arrest was observed in BxPC3 cells, compared with only 50% growth arrest in Capan-1 cells (Figure 1e). Further, when Capan-1 cells treated with MUC1 siRNA were exposed to 500 nM of gemcitabine, a 31% increase in growth arrest was observed compared with untreated cells or cells transfected with control scrambled siRNA (Figure 1f).

For further investigations, mouse PDA primary cells genetically lacking Muc1 (KCKO) and ones expressing human MUC1 (KCM) were included in this study. Upon using the CT2 antibody that recognizes the CT of both mouse and human MUC1, KCM cells showed high expression of MUC1 while KCKO cells showed no detectable levels (Figure 2a and Supplementary Table 2). To further validate the effect of MUC1 in drug resistance, KCKO and KCM cells were treated with etoposide and gemcitabine. We found 76% and 88% of growth arrest upon treatment of KCKO cells with 1.25 μM and 2.5 μM of etoposide, respectively. In contrast, only 52% and 57% of growth arrest was observed in KCM cells at 1.25 and 2.5 μM of etoposide, respectively, indicating that KCM cells were more resistant to etoposide (Figure 2b, left panel). At 5 μM of etoposide, both cell lines irrespective of their MUC1 status were sensitive. Similar resistance of KCM cells to gemcitabine was observed. At 3 nM of gemcitabine, 60% of growth arrest was

observed in KCKO cells compared with only 34% of growth arrest in KCM cells. At higher doses, there was no difference in growth arrest between KCKO and KCM cells (Figure 2b, right panel). MTT assay was also performed to validate the cytotoxic effects of these drugs on the same cell lines. At 50 μM of etoposide, 48% of cell death was observed in KCKO cells compared with only 27% cell death in KCM cells (Figure 2c, left panel). Similarly, at 150 nM of gemcitabine, 53.3% of cell death was observed in KCKO cells compared with only 40% cell death in KCM cells (Figure 2c, right panel).

To further confirm that the effect was due to MUC1 expression, we stably expressed full-length MUC1 in BxPC3 cells that have low levels of endogenous MUC1 (BxPC3.MUC1), and as control we transfected BxPC3 cells with empty vector that contains the neomycin resistance gene (BxPC3.Neo). First we show the relative expression of MUC1 in these cells (Figure 3a and Supplementary Table 3). BxPC3 MUC1 cells express high levels of MUC1 while BxPC3 Neo cells have negligible levels. BxPC3 MUC1 cells were significantly resistant to both the genotoxic drugs as compared with the BxPC3 Neo cells. At 25, 50 and 75 μM of etoposide, cells with low MUC1 showed significantly higher growth arrest compared with cells expressing high levels of MUC1 (Figure 3b, left panel). Similar results were observed with 6.25–25 nM of gemcitabine (Figure 3b, right panel). MTT assay was performed to validate the cytotoxic effects of etoposide and gemcitabine on both cell lines. At 75 μM of etoposide, 64% of cell death was observed in BxPC3 Neo cells compared with only 39.6% cell death in BxPC3 MUC1 cells (Figure 3c, left panel). Similarly, at 50 nM of gemcitabine, 42.7% of cell death was observed in BxPC3 Neo cells

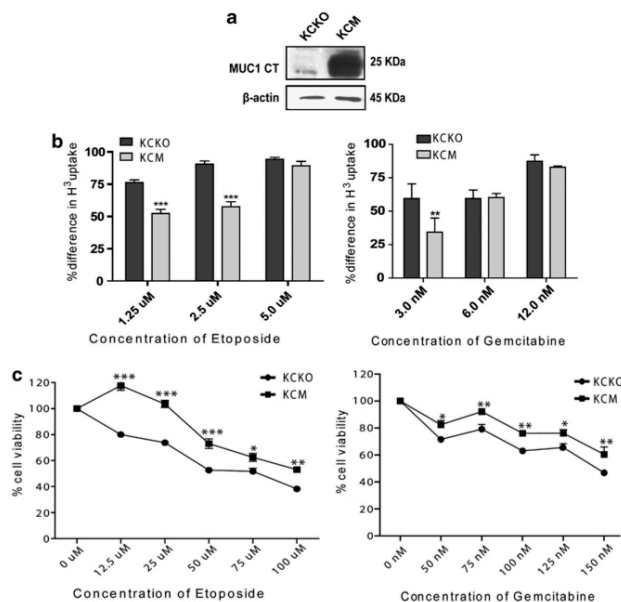


Figure 2. Endogenous expression of MUC1 in PC cells confers resistance to cytotoxic drugs. (a) Western blot analysis of endogenous Muc1/MUC1 expression in mouse cells lines, KCKO and KCM using CT2 antibody. Note: CT2 is the only antibody that recognizes both mouse and human Muc1/MUC1. (b) Percent difference in H^3 -thymidine uptake in KCKO and KCM cells following 24 h treatment with etoposide and gemcitabine. Significant differences between KCKO and KCM cells at varying concentrations of the drugs are shown as *P*-values ($n=4$) (** $P<0.01$, *** $P<0.001$). (c) Cell viability in KCKO and KCM cells following 24 h treatment with etoposide and gemcitabine. Significant differences between KCKO and KCM cells at varying concentrations of the drugs are shown as *P*-values ($n=6$) (* $P<0.1$, ** $P<0.01$, *** $P<0.001$).

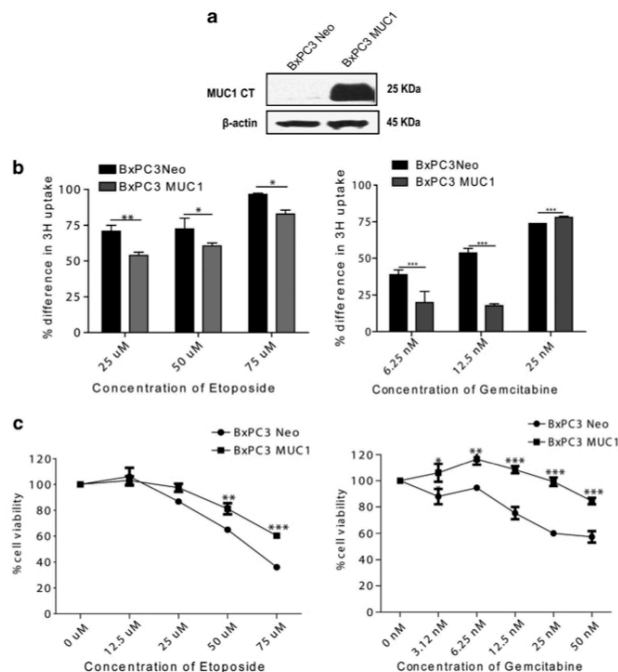


Figure 3. Exogenous expression of MUC1 in BxPC3 cells confers resistance to cytotoxic drugs. (a) Western blotting analysis of MUC1 expression in BxPC3 cells using CT2. (b) Percent difference in H^3 -thymidine uptake of BxPC3 Neo and MUC1 cells following 24 h treatment with etoposide and gemcitabine ($n=4$). Significant differences between BxPC3 Neo and MUC1 are shown (** $P<0.01$). (c) Cell viability in BxPC3 Neo and BxPC3 MUC1 cells following 24-h treatment with etoposide and gemcitabine. Significant differences between BxPC3 Neo and BxPC3 MUC1 cells at varying concentrations of the drugs are shown as P -values ($n=6$) (* $P<0.1$, ** $P<0.01$, *** $P<0.001$).

compared with only 15.5% cell death in BxPC3 MUC1 cells (Figure 3c, right panel). These results suggested that MUC1 confers resistance to gemcitabine and etoposide in PC cells.

MUC1 regulates expression of multidrug resistance genes in PC cells *in vitro*

Previously we have published proteomics data that showed KCM cells express eightfold higher P-glycoprotein, fourfold higher MRP-1 and twofold higher MRP-5 protein compared with KCKO cells.¹⁹ Therefore, we first determined the mRNA level of some of these MDR genes. Consistent with those results, we found significantly higher mRNA levels of the *Abcc1*, *Abcc3*, *Abcc5*, *Abcb1a* and *Abcb1b* genes in KCM vs KCKO cells using RT-PCR (Figure 4a, left panel). Similarly, in BxPC3 MUC1, the mRNA levels of *ABCC1*, *ABCC3*, *ABCC5* and *ABCB1* genes were significantly higher compared with BxPC3 Neo cells (Figure 4a, right panel). To validate this finding, we determined the protein expression of MRP-1 by western blotting, and, as expected, we observed significantly higher expression of MRP-1 in KCM cells compared with KCKO cells, and in BxPC3 MUC1 compared with BxPC3 Neo cells (Figure 4b and Supplementary Table 4).

Tumors lacking MUC1 or expressing low levels of MUC1 have lower expression of MRP-1

All of the data so far have been shown in cells grown *in vitro*. To answer if this is true *in vivo*, we determined the MRP-1 protein

expression in spontaneously occurring PDA.MUC1 (KCM) and PDA.Muc1KO (KCKO) tumors, as well as in BxPC3 Neo and MUC1 tumors grown in nude mice. Immunohistochemical analysis was performed on tumor sections from ~16-week-old KCM and ~24-week-old KCKO mice, and a representative section from each tumor type is shown in Figure 4c (left panel). Significantly higher expression of MRP-1 protein was observed in KCM as compared with KCKO tumor sections (Figure 4c). MRP1 levels in the tumor lysates isolated from BxPC3 Neo and BxPC3 MUC1-xenografted tumors were determined by western blotting. BxPC3 MUC1 tumors showed higher MRP-1 expression compared with BxPC3 Neo tumors (Figure 4d). Interestingly, the tumor sample (sample 3) that had higher MUC1 expression compared with the other MUC1-positive tumor sample (sample 4) also showed higher MRP-1 expression (Supplementary Table 5). The data suggest that a positive correlation exists between MUC1 overexpression and upregulation of *mdr* genes in PC cells.

Knockdown of Akt decreases MRP1 expression in MUC1 high PC cells and sensitizes them to chemotherapeutic drugs

Often in tumor cells, reduced sensitivity to chemotherapeutic drugs is due to enhanced activation of the anti-apoptotic or pro-survival pathways, which includes the PI3K/Akt pathway. We first determined the activation status of PI3K/Akt pathway in KCKO, KCM, BxPC3.Neo and BxPC3.MUC1 cells. Protein lysates from these cell lines were subjected to immunoblotting using

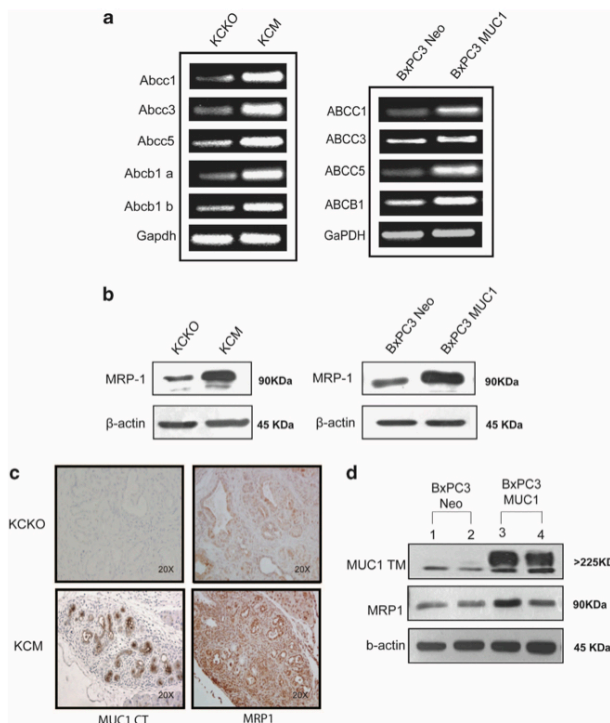


Figure 4. MUC1-positive PC cells express elevated levels of MDR genes *in vitro* and *in vivo*. **(a)** RT-PCR data showing fold changes in the mRNA level of MDR genes that are associated with multidrug resistance. **(b)** Levels of MRP1 protein in BxPC3 Neo, MUC1, KCKO and KCM cell lysates analyzed by western blot. **(c)** Immunohistochemical analysis of MRP1 expression in the tumor sections from KCKO (24-week-old) and KCM (16-week-old) mice. Note: Two different time points were deliberately selected, as the tumor burden in the KCKO mice at 24 weeks is equivalent to the tumor burden in 16-week-old KCM mice. **(d)** Levels of MRP1 protein in BxPC3 Neo and MUC1 tumor lysates were determined by western blot.

anti-phospho-Akt (p-Akt) and Akt antibodies. Significantly higher levels of pAkt were found in MUC1-positive PC cells (KCM and BxPC3 MUC1) compared with MUC1-low or -null PC cells (KCKO and BxPC3 Neo) (Figure 5a and Supplementary Table 5). The levels of total Akt remained same in all cell lines, indicating enhanced activation of the PI3K/Akt pathway in KCM and BxPC3 MUC1 cells. This finding positively correlates with the results presented previously in MUC1-overexpressing fibroblasts.¹¹

To test the contribution of Akt on MRP1 expression and drug resistance, we transiently knocked down Akt and evaluated the levels of MRP1 expression by western blot and drug sensitivity by MTT assay. The levels of Akt, MRP1 and MUC1 are shown in Figures 5b–d. Upon Akt knockdown, we observed a 5.4-fold decrease in MRP1 expression in Capan-1 cells and 4.6-fold decrease in MRP1 expression in BxPC3 MUC1 cells (Figures 5b and c, and Supplementary Tables 7 and 8). Furthermore, ~40% and 25% increase in cytotoxicity was observed in Akt siRNA-treated BxPC3 MUC1 cells upon treatment with 50 μ M of etoposide and 25 nM of gemcitabine, respectively (Figure 5e). These data indicated that Akt pathway had an important role in MUC1-induced MRP1 expression, and drug resistance in Capan1 and BxPC3 cells.

Interestingly, we also observed a subsequent decrease in MUC1 expression upon downregulation of Akt in Capan-1 and BxPC3 MUC1 cells (Figures 5b and c). When Akt was transiently knocked down in Capan-1 and BxPC3 MUC1 cells, a respective 3.2-fold and 2.5-fold decrease in MUC1 expression was observed (Supplementary Tables 7 and 8). These data indicate that MUC1 gene is also under regulation of PI3K/Akt pathway. Hence, abrogation of the Akt pathway causes a significant decrease in MUC1 expression, which in turn negatively affects MRP1 expression.

However, we did not see a significant decrease in MUC1 and MRP1 expression in KCM cells upon Akt knockdown (1.2-fold decrease) (Figure 5d and Supplementary Table 9). Consequently, we did not detect a significant increase in cytotoxicity in Akt siRNA-treated KCM cells upon treatment with etoposide and gemcitabine (data not shown). These data indicate that in KCM cells, MUC1 gene is not strongly regulated by PI3K/Akt pathway. This observation further led to the possibility that in KCM cells, an Akt-independent mechanism must be involved in MUC1-induced MRP1 expression and drug resistance. It is of interest that BxPC3 and Capan-1 are human cells while KCM is a mouse cell line.

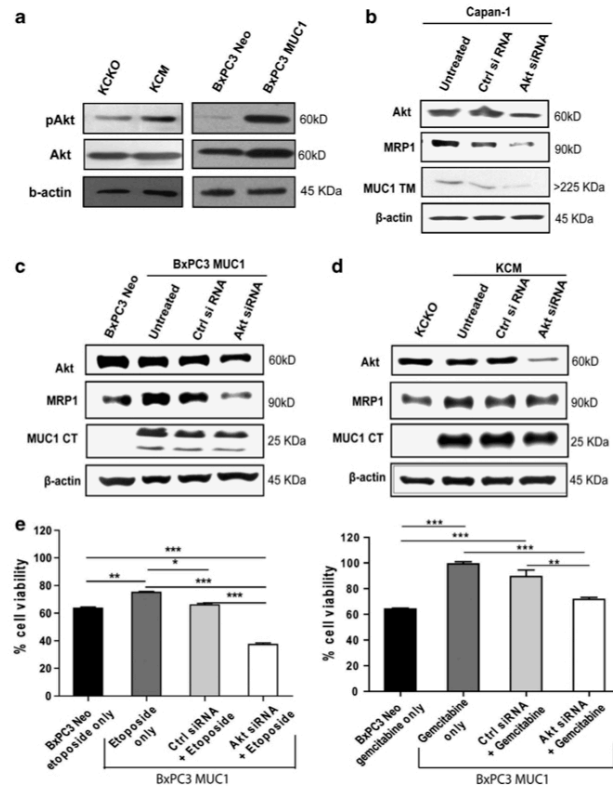


Figure 5. Enhanced activation of the prosurvival pathways in MUC1-positive PC cells. MUC1 induces MRP1 expression via Akt-dependent and -independent pathways. (a) BxPC3 Neo, MUC1, KCKO and KCM cell lysates were subjected to western blot analysis to determine phosphorylation of Akt. Level of unphosphorylated Akt served as control for phosphorylation. β-Actin served as loading control. (b–d) Cells were treated with with 100 nM of Akt siRNA for 48 h, and the lysates were immunoblotted to evaluate the levels of Akt, MRP1 and MUC1. β-Actin served as a loading control. (e) Cells growing in a 6-well plate were left untreated (WT) or treated with either control siRNA or Akt siRNA (100 nM). Thirty-six hours post treatment, cells were trypsinized, and equal number of cells were re-plated in a 96-well plate. The cells were allowed to adhere and, at 48 h, were left untreated or treated with 50 μM of etoposide and 25 nM of gemcitabine. MTT assay was performed to measure cytotoxicity 24 h post drug treatment.

MUC1.CT interacts within the promoter region of the *ABCC1* gene. Several studies have shown that MUC1 CT associates with mediators of signal transduction and transcriptional regulation, and thereby modifies the expression of specific target genes.^{21,22} In this study, we wanted to investigate the occupancy of MUC1 CT in the promoter region of *ABCC1/Abcc1* gene, which can be indicative of MUC1's role as a modulator of *ABCC1/Abcc1* gene expression. First, we demonstrate that MUC1 CT localizes to the nucleus of MUC1-positive PC cells. Nuclear and cytosolic fractions were extracted from KCKO, KCM, BxPC3 Neo and BxPC3 MUC1 cells, and the lysates were immunoblotted to determine the cellular localization of MUC1 CT in these PC cells. As expected, we found MUC1 CT localizing to the nucleus of KCM cells (Figure 6a, left top panel) and BxPC3 MUC1 cells (right top panel Figure 6a). Lamin A/C and MEK1 served as controls for the extraction process. Lamin A/C is a nuclear protein, and hence is found only in the nuclear fractions (middle panels, Figure 6a).

MEK1 is a cytosolic protein and is found only in the cytosolic fractions (bottom panels Figure 6a).

Next, we evaluated the occupancy of MUC1 CT in the genomic regions of the *ABCC1/Abcc1* gene upstream the transcription start site (Figure 6b). Sheared DNA was immunoprecipitated using MUC1 CT specific antibody CT2. IgG antibody was used as a control. The immunoprecipitated DNA was amplified by PCR using primers spanning around 1000 bp upstream (ChIP region I) and 2000 bp upstream (ChIP region II) of the *ABCC1/Abcc1* gene transcription start site (Figure 6b). In Capan-1 cells, we observed a strong interaction between MUC1 CT and ChIP region I of *ABCC1* gene (6.5-fold enrichment with CT2 antibody relative to IgG) (Figure 6c and Supplementary Table 10). Similarly, in KCM cells, a strong interaction was observed between MUC1 CT and ChIP region I of *Abcc1* gene (3.2-fold enrichment with CT2 antibody relative to IgG) (Figure 6c and Supplementary Table 11). However, no interaction was observed between MUC1 CT and ChIP region II

in Capan-1 and KCM cells (Figure 6c). KCKO cells, which are null for MUC1, did not show any interaction between MUC1 CT, and ChIP region I and II of *Abcc1* gene (Figure 6c). These data indicated that the interaction of MUC1 CT with the promoter region of *ABCC1/Abcc1* gene around ChIP region I is specific. However, in BxPC3 MUC1 cells, a very weak interaction between MUC1 CT and ChIP region I of *ABCC1* gene was observed (1.1-fold enrichment compared with IgG, Supplementary Table 12 and Figure 6c). BxPC3 Neo cell also showed weak binding of MUC1 CT around the same gene locus. This is most likely because BxPC3 cells express low levels of endogenous MUC1 and are not null for the same (Figure 6c). The interaction between MUC1 CT and ChIP region II was not observed in BxPC3 cells (Figure 6b).

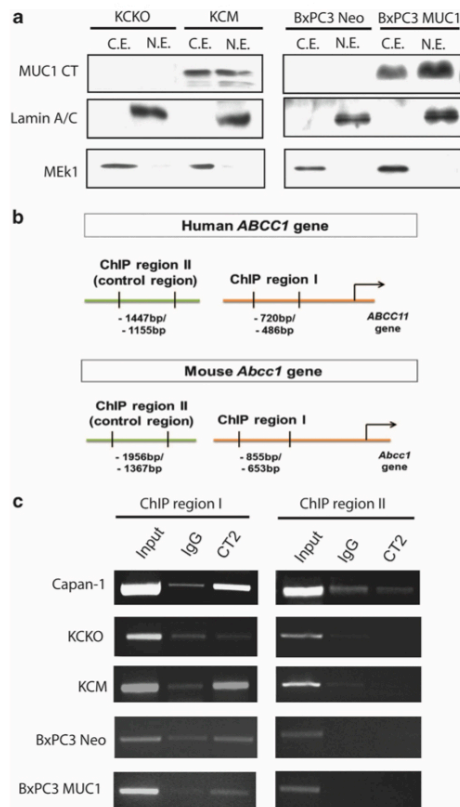


Figure 6. ChIP-PCR assay reveals an interaction between the MUC1 CT and the *ABCC1* promoter region. (a) Nuclear lysates of KCKO, KCM, BxPC3 Neo and BxPC3 MUC1 cells were subjected to immunoblotting to determine the nuclear localization of MUC1 CT. Lamin and MEK1 were used as controls for nuclear and cytosolic fractions, respectively. (b) Schematic representation of the primers that were designed to PCR amplify the promoter region of human *ABCC1* gene (top panel) and mouse *Abcc1* gene (bottom panel) in ChIP assay. (c) ChIP-PCR; lanes include: Input DNA, DNA precipitated using control IgG and CT2, and amplified by PCR using Taq polymerase and separated by 2% agarose gel.

DISCUSSION

The ability of tumor cells to escape the cytotoxic effect of chemotherapeutic agents may result from genetic alterations that affect cell cycle, apoptosis or accumulation of drugs inside the cell. Several studies in breast, colon and thyroid cancers have shown that MUC1 attenuates stress-induced or chemotoxic agents-induced apoptosis by blocking the release of cytochrome *c* from mitochondria.^{11,12,23} In this study, we demonstrate additional mechanisms by which MUC1 enables PC cells to escape chemotherapeutic drug-mediated cell death.

We found that cells expressing full-length MUC1 are less sensitive to genotoxic drugs than cells lacking or expressing low levels of MUC1, indicating a direct correlation between MUC1 expression and chemoresistance in PC (Figures 1, 2 and 3).

Here, for the first time, we provide evidence that in PC cells, *mdr* gene expression is directly correlated with MUC1 expression (Figure 4). Previous work has shown that hyperactivation of PI3K/Akt pathway is able to regulate expression of *mdr* genes, including *ABCC1*, *ABCC3*, *ABCC5* and *ABCB1* genes.¹⁰ Studies have demonstrated that MUC1 oncoprotein induces transformation in rat fibroblasts or desensitizes thyroid cancer cells to chemotherapy induced apoptosis through activation of Jak/Stat and PI3K/Akt pathways.^{11,12} So, we evaluated if MUC1 induced expression of the *mdr* gene *ABCC1/Abcc1* via activating the PI3K/Akt pathway. We found that in a subset of human PC cells (BxPC3 MUC1 and Capan-1), MUC1-induced MRP1 expression was via the Akt pathway with a pattern that suggests increased refractoriness of these cells to genotoxic drugs. Accordingly, abrogation of the PI3K/Akt pathway resulted in increased responsiveness of these cells to etoposide and gemcitabine (Figure 5). We also found the evidence for existence of a positive feedback loop between MUC1 expression and PI3K/Akt signaling cascade. PC cells with high MUC1 expression exhibited hyperactivation of the PI3K/Akt pathway, which in turn upregulated MUC1 expression in those PC cells. However, it is beyond the scope of the current study to determine how Akt pathway regulates MUC1 expression. In the future, we would like to investigate the mechanism in further

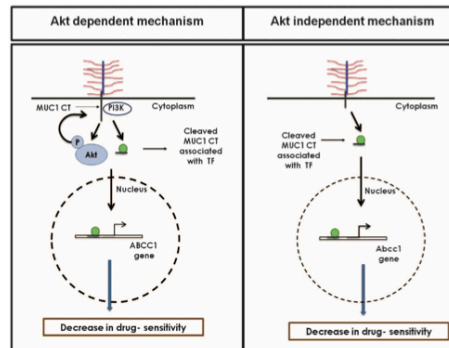


Figure 7. Schematic illustration of the two possible pathways by which MUC1 regulates MRP1 gene expression in PC cells. In human PC cell lines, Capan-1 and BxPC3 MUC1, MUC1-induced *ABCC1* gene expression is dependent on PI3K/Akt pathway. The CT of MUC1 stimulates the PI3K/Akt pathway, which in turn increases MUC1 expression (left panel). In murine PC cell line, KCM, MUC1-induced MRP1 expression is independent of the PI3K/Akt pathway (right panel). The CT of MUC1 translocates to the nucleus and binds to the promoter of *ABCC1/Abcc1* gene, possibly acting as a part of the transcriptional complex that drives the expression of this gene (left and right panels).



detail. Interestingly, in the mouse PC cells, KCM, MUC1-induced MRP1 expression was independent of PI3K/Akt pathway even though the pAkt was significantly higher in the KCM vs KCKO cells. These data underscored the possibility of involvement of an alternative mechanism involved in MUC1-induced MRP1 expression (Figure 6). Thus, we report for the first time that two alternate mechanisms may be involved in MUC1-induced MRP1 expression in PC cells (Figure 7).

Interestingly, we found a strong association between MUC1 CT and the promoter region of the *ABCC1/Abcc1* gene (Figure 6). These preliminary data raise a possibility that MUC1 might be part of the transcriptional complex that regulates expression of the *ABCC1/Abcc1* gene. The 5'-untranslated promoter region of the human *ABCC1* gene contains several putative binding sites, such as GC elements (-91 to +103) that bind Sp1, AP1 sites (-511 to -492) that bind a complex of cJun/cFos and E box elements (-1020 to -2008) that bind N-myc.²³⁻²⁵ We found MUC1 CT associating with the promoter region of the *ABCC1/Abcc1* gene within ChIP region I. Both mouse and human ChIP region I contain putative AP1, CREB1, GATA1, c-Ets1 and MZF1 binding motifs, as predicted by the transcription factor binding site prediction tools that uses TRANSFAC and JASPAR core databases (data not shown). MUC1 as such does not have a DNA-responsive domain, and studies so far have shown that it binds to DNA via transcription factors such as NF- κ B, cJun, β -catenin and HIF-1 α .^{21,26,27} Thus, in future we intend to investigate in detail what MUC1 CT is doing at the promoter region of *ABCC1/Abcc1* gene and also the transcription factor that is involved in MUC1-mediated *MRP1* gene expression.

Taken together, our study shows that, in PC cells, MUC1 overexpression leads to chemoresistance, and that MUC1 CT associates directly with the promoter region of the *ABCC1/Abcc1* gene. Thus, the data provide new insights into the mechanisms by which MUC1 can interfere with the effectiveness of chemotherapy in PC. As MUC1 acts as a vital component that minimizes the efficacy of chemotherapy, it could be considered as a key molecular target for sensitizing cancer cells to conventional or novel treatments. The CT of MUC1 can be targeted to inhibit its ability to initiate signaling cascades, and also to block its nuclear translocation and subsequent binding to the promoter regions of its target genes. MDR modulators did not gain much popularity in the clinic owing to their ability to regulate more than one transporter and subsequently causing severe side effects in patients.⁶ As an alternative strategy, MUC1 CT can be targeted to downregulate the expression of *mdr* genes or the activity of these efflux pumps.

MATERIALS AND METHODS

Cell culture and establishment of stable cell lines expressing MUC1
BxPC3 cells (American Type Culture Collection, Manassas, VA, USA) are a human PC cell line that express very little endogenous MUC1. For retroviral infection, GP2-293 packaging cells (stably expressing the gag and pol proteins) were co-transfected with the full-length MUC1 construct or an empty vector expressing the VSV-G envelope protein as previously described.^{20,28} Cells were treated with 0.5 mg/ml of G418, beginning 48 h post infection. Three independent infections of the constructs were carried out with similar results. Expression of the constructs was stable throughout the span of experiments. Cells infected with vector alone were used as control and designated Neo. For MUC1-infected cells, MUC1-positive cells were sorted using the FACS Aria (BD Biosciences, San Jose, CA, USA). For Neo-infected cells, MUC1-negative cells were sorted. Capan-1 is a human PC cell line that expresses high levels of endogenous MUC1.

Mouse model and mouse cell lines

In our laboratory, mice that develop spontaneous pancreatic ductal adenocarcinoma (PDA) were generated by mating the P48-Cre with the LSL-KRAS^{G12D} mice.²⁹ PDA mice were further mated with the MUC1.Tg mice (that express human MUC1) to generate PDA.MUC1 mice or with the Muc1 knockout mice to generate PDA.MUC1KO mice.^{19,30} All these mice

were on the C57/B6 background. Cell lines were generated from the primary tumors of PDA.MUC1 and PDA.Muc1 KO mice, and were designated as KCM and KCKO, respectively.

Transient knockdown using siRNA

The method is previously described in Sahraei et al.²⁸ In brief, cells were seeded in a six-well plate and were allowed to reach 40% confluency. The cells were then transfected with 100 nm of MUC1 siRNA (Smart genome pool) or 100 nm of Akt siRNA (Santa Cruz Biotechnology, Santa Cruz, CA, USA and Cell Signaling, Boston, MA, USA). Cells of the control group were treated with 100 nm of scrambled siRNA (Dharmacon, Thermo Fischer Scientific, CO, USA; Santa Cruz and Cell Signaling). Lipofectamine (Invitrogen, San Diego, CA, USA) was used for the delivery of siRNA into the cells over a period of 5–6 h in serum-free Opti-MEM. Forty-eight hours post transfection, MUC1 and Akt expression were evaluated by western blot. For MTT assay, 36 h post siRNA treatment, cells were trypsinized, replated in a 96-well plate and treated with or without the drugs. MTT assay was performed 24 h post drug treatment. The calculations were done as follows.

The viability of each treatment group without drug treatment (that is, WT alone, control siRNA alone and Akt siRNA alone) was considered as 100%. The viability following drug treatment on each of these treatment groups was calculated using the following expression:

$$\% \text{ viability of drug-treated WT cells} = (\text{OD of drug-treated WT cells} / \text{OD of WT cells}) \times 100\%$$

$$\% \text{ viability of drug + control (or Akt) siRNA-treated cells} = (\text{OD of drug + control (or Akt) siRNA treated cells} / \text{OD of control (or Akt) siRNA treated cells}) \times 100\%$$

Preparation of nuclear extract

Cells were grown in a 10-cm plate. When the cells reached around 80% confluency, they were scraped off the plate, and a nuclear extraction kit (EMD Millipore, Billerica, MA, USA) was used to isolate the nuclear and cytosolic fractions.

Western blots

Equal quantities of cell lysates were loaded on SDS-PAGE gels. MUC1 antibodies were a gift from Dr Sandra Gendler. pAkt and Akt antibodies were purchased from Cell Signaling Technology (Danvers, MA, USA), MRP-1, Lamin A/C and β -actin were purchased from Santa Cruz (CA, USA), and MEK1 was purchased from Abcam (Boston, MA, USA). The antibodies were used according to the manufacturer's recommendations.

MTT assay and H³-thymidine incorporation assays

10×10^3 cells were plated in quadruplicate in normal growth medium in 96-well plates and were permitted to grow for 18 h. Cells were left untreated or treated with etoposide (Sigma-Aldrich, St Louis, MO, USA) and gemcitabine (Sigma-Aldrich) for 24 h. Next, MTT (Biotium) solution was added (10 μ l per well) to the cells, incubated for additional 3–4 h. In the final step, media was removed, formazan was dissolved in DMSO (200 μ l per well) and the absorbance was read on an ELISA plate reader.

For H³-thymidine assay, 5×10^3 cells were plated and treated as described above. Twenty-four hours post drug treatment, H³-thymidine (Perkin Elmer, Waltham, MA, USA) was added in fresh medium (1 μ Ci per well), and cells were permitted to grow for another 24 h. At this time, cells were washed to remove excess radioactivity, trypsinized and harvested onto a filter plate, which was then read on a TopCount plate reader. The data have been represented as % difference in H³-thymidine uptake, which represents the % decrease in proliferation or % in growth arrest. The following formula was used for calculations:

$$\% \text{ difference in H}^3\text{-thymidine uptake} = ((\text{c.p.m. untreated} - \text{c.p.m. treated}) / \text{c.p.m. untreated}) \times 100$$

Semiquantitative RT-PCR

Total RNA was extracted from cells by Trizol (Invitrogen) according to the manufacturer's protocol. One to two micrograms of the extracted RNA was used as template for RT-PCR reaction (Access quick RT-PCR kit, Promega, Madison, WI, USA). Sequence of the primers is available upon request.

Immunohistochemistry

BxPC3 Neo and MUC1 cells (1×10^6 cells per mouse) were implanted subcutaneously in nude mice, and 30 days later tumors were collected for immunohistochemical analysis and protein lysate as described



previously.²⁰ In brief, paraffin-embedded blocks of formalin-fixed tumor sections were made by the Histology Core at Mayo Clinic. Four-micron-thick sections were prepared for immunohistochemical staining. MRP1 expression in the tumor was determined using anti-MRP1 antibody (1:50 dilution, Santa Cruz) followed by appropriate secondary antibody (1:100 dilution, Dako).

Slides were examined under a light microscope and pictures were taken at $\times 20$.

Chromatin immunoprecipitation

Cells grown to near 80% confluence were cross-linked with formaldehyde (Sigma) at room temperature for 10 min. Cross-linked chromatin prepared with a commercial ChIP assay kit (EZ-Magna ChIP; Millipore) was immunoprecipitated with 20 μ g of normal Armenian hamster IgG (Santa Cruz Biotechnology, CA, USA) and 20 μ g of anti-MUC1 CT antibody (CT2). MUC1 CT binding site on the *ABCC1/Abcc1* promoter was amplified by PCR using the input DNA (1%) or DNA isolated from precipitated chromatin as templates and using primers flanking the promoter region 1000 bp upstream (ChIP region I) and 2000 bp upstream (ChIP region II) of *ABCC1/Abcc1* gene (Figure 6b). ChIP region II was used as a negative control for binding of MUC1 CT to the promoter region. Sequence of the primers is available upon request.

Statistical analysis

Statistical analysis was performed with GraphPad software, La Jolla, CA, USA.

CONFLICT OF INTEREST

The authors declare no conflict of interest.

ACKNOWLEDGEMENTS

We thank all the technicians in the animal facility and in the histology core facilities at The Mayo Clinic and UNCC. This study was supported by R01 CA118944. This work was supported by National Institute of Health R01 CA118944-01A1 and Irwin Belk Endowment Funds.

REFERENCES

- Bardeesy N, DePinto RA. Pancreatic cancer biology and genetics. *Nat Rev Cancer* 2002; **2**: 897–909.
- Strimpakos A, Saif MW, Strygos KN. Pancreatic cancer: from molecular pathogenesis to targeted therapy. *Cancer Metastasis Rev* 2008; **27**: 495–522.
- Konig J, Hartel M, Nies AT, Martignoni ME, Guo J, Büchler MW *et al*. Expression and localization of human multidrug resistance protein (ABCC) family members in pancreatic carcinoma. *Int J Cancer* 2005; **115**: 359–367.
- Sperti C, Pasquali C, Piccoli A, Pedrazzoli S. Recurrence after resection for ductal adenocarcinoma of the pancreas. *World J Surg* 1997; **21**: 195–200.
- Wang Z, Li Y, Ahmad A, Banerjee S, Azmi AS, Kong D *et al*. Pancreatic cancer: understanding and overcoming chemoresistance. *Nat Rev Gastroenterol Hepatol* 2011; **8**: 27–33.
- Jager w. Classical resistance mechanisms. *Int J Clin Pharmacol Ther* 2009; **47**: 46–48.
- Gottesman MM, Fojo T, Bates SE. Multidrug resistance in cancer: role of ATP-dependent transporters. *Nat Rev Cancer* 2002; **2**: 48–58.
- Misra S, Ghatak S, Toole BP. Regulation of MDR1 expression and drug resistance by a positive feedback loop involving hyaluronan, phosphoinositide 3-kinase, and ErbB2. *J Biol Chem* 2005; **280**: 20310–20315.
- Sharom FJ. ABC multidrug transporters: structure, function and role in chemoresistance. *Pharmacogenomics* 2008; **9**: 105–127.
- Lee Jr JT, Steelman LS, McCubrey JA. Phosphatidylinositol 3'-kinase activation leads to multidrug resistance protein-1 expression and subsequent chemoresistance in advanced prostate cancer cells. *Cancer Res* 2004; **64**: 8397–8404.

- Raina D, Kharbanda S, Kufe D. The MUC1 oncoprotein activates the anti-apoptotic phosphoinositide 3-kinase/Akt and Bcl-xL pathways in rat 3Y1 fibroblasts. *J Biol Chem* 2004; **279**: 20607–20612.
- Siragusa M, Zerilli M, Iovino F, Francipane MG, Lombardo Y, Ricci-Vitiani L *et al*. MUC1 oncoprotein promotes refractoriness to chemotherapy in thyroid cancer cells. *Cancer Res* 2007; **67**: 5522–5530.
- Hollingsworth MA, Swanson BJ. Mucins in cancer: protection and control of the cell surface. *Nat Rev Cancer* 2004; **4**: 45–60.
- Levi E, Klimstra DS, Andea A, Basturk O, Adsay NV. MUC1 and MUC2 in pancreatic neoplasia. *J Clin Pathol* 2004; **57**: 456–462.
- Chheng DC, Benson E, Eltoum I, Eloubeidi MA, Jhala N, Jhala D *et al*. MUC1 and MUC2 expression in pancreatic ductal carcinoma obtained by fine-needle aspiration. *Cancer* 2003; **99**: 365–371.
- Gendler SJ. MUC1, the renaissance molecule. *J Mammary Gland Biol Neoplasia* 2001; **6**: 339–353.
- Kufe DW. Mucins in cancer: function, prognosis and therapy. *Nat Rev Cancer* 2009; **9**: 874–885.
- Carson DD. The cytoplasmic tail of MUC1: a very busy place. *Sci Signal* 2008; **1**: pe35.
- Besmer DM, Curry JM, Roy LD, Tinder TL, Sahraei M, Schettini J *et al*. Pancreatic ductal adenocarcinoma mice lacking mucin 1 have a profound defect in tumor growth and metastasis. *Cancer Res* 2011; **71**: 4432–4442.
- Roy LD, Sahraei M, Subramani DB, Besmer D, Nath S, Tinder TL *et al*. MUC1 enhances invasiveness of pancreatic cancer cells by inducing epithelial to mesenchymal transition. *Oncogene* 2011; **30**: 1449–1459.
- Sahraei M, Roy LD, Curry JM, Teresa TL, Nath S, Besmer D *et al*. MUC1 regulates PDGFA expression during pancreatic cancer progression. *Oncogene* 2012; **31**: 4935–4945.
- Behrens ME, Grandgenett PM, Bailey JM, Singh PK, Yi CH, Yu F *et al*. The reactive tumor microenvironment: MUC1 signaling directly reprograms transcription of CTGF. *Oncogene* 2010; **29**: 5667–5677.
- Ren J, Agata N, Chen D, Li Y, Yu WH, Huang L *et al*. Human MUC1 carcinoma-associated protein confers resistance to genotoxic anticancer agents. *Cancer Cell* 2004; **5**: 163–175.
- Scotto KW. Transcriptional regulation of ABC drug transporters. *Oncogene* 2003; **22**: 7496–7511.
- Kurz EU, Cole SP, Deeley RG. Identification of DNA-protein interactions in the 5' flanking and 5' untranslated regions of the human multidrug resistance protein (MRP1) gene: evaluation of a putative antioxidant response element/AP-1 binding site. *Biochem Biophys Res Commun* 2001; **285**: 981–990.
- Thompson EJ, Shanmugam K, Hatrup CL, Kotlarczyk KL, Gutierrez A, Bradley JM *et al*. Tyrosines in the MUC1 cytoplasmic tail modulate transcription via the extracellular signal-regulated kinase 1/2 and nuclear factor-kappaB pathways. *Mol Cell Res* 2006; **4**: 489–497.
- Behrens ME, Grandgenett PM, Bailey JM, Singh PK, Yi CH, Yu F *et al*. The reactive tumor microenvironment: MUC1 signaling directly reprograms transcription of CTGF. *Oncogene* 2010; **29**: 5667–5677.
- Sahraei M, Roy LD, Curry JM, Teresa TL, Nath S, Besmer D *et al*. MUC1 regulates PDGFA expression during pancreatic cancer progression. *Oncogene* 2012; **31**: 4935–4945.
- Hingorani SR, Petricoin EF, Maitra A, Rajapakse V, King C, Jacobetz MA *et al*. Preinvasive and invasive ductal pancreatic cancer and its early detection in the mouse. *Cancer Cell* 2003; **4**: 437–450.
- Tinder TL, Subramani DB, Basu GD, Bradley JM, Schettini J, Million A *et al*. MUC1 enhances tumor progression and contributes toward immunosuppression in a mouse model of spontaneous pancreatic adenocarcinoma. *J Immunol* 2008; **181**: 3116–3125.



Oncogenesis is an open-access journal published by Nature Publishing Group. This work is licensed under a Creative Commons Attribution-NonCommercial-ShareAlike 3.0 Unported License. To view a copy of this license, visit <http://creativecommons.org/licenses/by-nc-sa/3.0/>

Supplementary Information accompanies this paper on the Oncogenesis website (<http://www.nature.com/oncsis>).

OPEN

Mucin 1 Regulates Cox-2 Gene in Pancreatic Cancer

Sritama Nath, PhD,* Lopamudra Das Roy, PhD,* Priyanka Grover, BSc,* Shanti Rao, BSc,† and Pinku Mukherjee, PhD*

Objective: Eighty percent of pancreatic ductal adenocarcinomas (PDAs) overexpress mucin 1 (MUC1), a transmembrane mucin glycoprotein. MUC1^{high} PDA patients also express high levels of cyclooxygenase 2 (COX-2) and show poor prognosis. The cytoplasmic tail of MUC1 (MUC1-CT) partakes in oncogenic signaling, resulting in accelerated cancer progression. Our aim was to understand the regulation of Cox-2 expression by MUC1.

Methods: Levels of COX-2 and MUC1 were determined in MUC1^{+/+}, MUC1^{low}, and MUC1^{high} PDA cells and tumors using reverse transcriptase-polymerase chain reaction, Western blot, and immunohistochemistry. Proliferative and invasive potential was assessed using MTT and Boyden chamber assays. Chromatin immunoprecipitation was performed to evaluate binding of MUC1-CT to the promoter of COX-2 gene.

Results: Significantly higher levels of COX-2 mRNA and protein were detected in MUC1^{high} versus MUC1^{low/mult} cells, which were recapitulated in vivo. In addition, deletion of MUC1 gene and transient knockdown of MUC1 led to decreased COX-2 level. Also, MUC1-CT associated with the COX-2 promoter at ~1000 base pairs upstream of the transcription start site, the same gene locus where nuclear factor κ B p65 associates with the COX-2 promoter.

Conclusions: Data supports a novel regulation of COX-2 gene by MUC1 in PDA, the intervention of which may lead to a better therapeutic targeting in PDA patients.

Key Words: pancreatic cancer, mucin 1 cytoplasmic tail, cyclooxygenase 2, NF- κ B p65

Abbreviations: MUC1, mucin 1, MUC1-CT, MUC1 cytoplasmic tail, PDA, pancreatic ductal adenocarcinoma, PC, pancreatic cancer, Cox-2, cyclooxygenase 2, PGE₂, prostaglandin E₂, UTR, untranslated region, CRE, cAMP response element, IHC, immunohistochemistry

(Pancreas 2015;44: 909-917)

Pancreatic ductal adenocarcinoma is a lethal disease and is the fourth leading cause of cancer-related deaths in the United States. Because of the absence of effective screening methods, efforts have been focused on developing new treatment modalities. However, most new clinical trials have shown limited survival benefit for the patients. Chronic inflammation is now considered

as 1 of the 7 hallmarks of cancer. Cyclooxygenase 2 (Cox-2) is an inducible proinflammatory enzyme that converts arachidonic acid to prostaglandins. In cancer, the major functional metabolite of Cox-2 is prostaglandin E₂ (PGE₂). Cyclooxygenase 2 and PGE₂ are frequently overexpressed in a vast majority of epithelial malignancies,^{1,2} including pancreatic ductal adenocarcinoma (PDA) (>60%),³ and is known to be associated with enhanced inflammation, metastasis, and immune suppression within the tumor microenvironment.⁴⁻⁷ Cyclooxygenase 2 inhibition has been successfully used as a chemopreventive agent against colon polyps.⁸ However, even in combination with chemotherapeutic agents, Cox-2 inhibition has not been useful in patients with PDA.⁹ This is possibly because regulation of Cox-2 is not well understood in PDA. Mucin 1 (MUC1), a heavily glycosylated membrane tethered glycoprotein normally expressed on glandular epithelial cells, becomes aberrantly hypoglycosylated and vastly overexpressed in malignant cells.¹⁰ The cytoplasmic tail of the tumor-induced form of MUC1 (MUC1-CT) associates with several oncogenic proteins including β -catenin and nuclear factor κ B (NF- κ B).¹¹ The complex then translocates to the nucleus and promotes transcription of tumor-promoting genes.^{12,13} Approximately 80% of human PDA overexpresses the tumor form of MUC1 (tMUC1)¹⁰ and is correlated with poor prognosis. We therefore sought to assess if tMUC1 may be involved in the regulation of Cox-2 in PDA. We have recently generated a mouse model of spontaneous PDA that expresses human MUC1 (PDA.MUC1 mice).^{14,15} PDA.MUC1 mice develop a spectrum of pre-malignant lesions called pancreatic intraepithelial neoplasias that progress to adenocarcinoma with 100% penetrance. In most instances, the tumors have a moderately differentiated ductal morphology with extensive stromal desmoplasia commonly observed in humans. Similar to human disease, these mice develop metastases primarily in the liver, peritoneum, and lungs. Along with overexpression of tMUC1, the tumors exhibit high levels of Cox-2 and PGE₂.¹⁴ PDA.MUC1 mice are highly resistant to gemcitabine and celecoxib (a specific Cox-2 inhibitor) when each drug is administered separately. However, when treated with a combination of MUC1 vaccine, celecoxib, and gemcitabine, the antitumor response is clinically significant.¹⁵ In addition, the PDA.MUC1 cells generated from these tumors exhibit increased multidrug resistance genes.^{13,15} Thus, it becomes imperative to understand the regulation of Cox-2 overexpression in PDA and design alternative therapeutics to block Cox-2 activation.

We demonstrate a novel regulation of Cox-2 gene expression by MUC1, suggesting MUC1 as an alternative target to prevent Cox-2 overexpression and associated aggressiveness in PDA.

MATERIALS AND METHODS

Mouse Model and Cell Lines

PDA.Muc1KO and PDA.MUC1 as described by Besmer et al¹⁶ are used. KCM and KCKO cell lines were generated from PDA.MUC1 and PDA.Muc1 KO mice, respectively.¹⁶

Human PDA cell lines Hs766T, Capan-2, HPAFII, HPAC and CFPAC, BxPC3, Capan-1, and MIA-PaCa-2 were obtained from ATCC (Manassas, Va). BxPC3 cells were stably transfected with

From the *Department of Biology, University of North Carolina at Charlotte, Charlotte; and †School of Medicine, University of North Carolina at Chapel Hill, Chapel Hill, NC.

Received for publication October 1, 2014; accepted March 25, 2015.

Reprints: Pinku Mukherjee, PhD, Department of Biological Sciences, University of North Carolina-Charlotte, 9201 University City Blvd, Charlotte, NC 28223 (e-mail: pmukherj@uncc.edu).

This study was supported by the National Institutes of Health (RO1 CA118944-01A1) and Irwin Belk Endowment Funds.

The authors declare no conflict of interest.

Supplemental digital contents are available for this article. Direct URL citations appear in the printed text and are provided in the HTML and PDF versions of this article on the journal's Web site (www.pancreasjournal.com).

Copyright © 2015 Wolters Kluwer Health, Inc. All rights reserved. This is an open-access article distributed under the terms of the Creative Commons Attribution-Non Commercial-No Derivatives License 4.0 (CCBY-NC-ND), where it is permissible to download and share the work provided it is properly cited. The work cannot be changed in any way or used commercially.

empty vector or vector containing full-length *MUC1* to generate BxPC3.Neo and BxPC3.MUC1 cells, respectively. Dr Michael Hollingsworth generously donated mouse Panc02.Neo and Panc02.MUC1 cell lines.

Transient Knockdown of Target Genes Using siRNA

Cells were plated in a 6-well plate in antibiotic-free complete media and upon reaching 30% confluence and were transfected with 100 to 200 nM of smart pool *MUC1* siRNA (DHARMACON; Thermo Fisher Scientific, Waltham, Mass), 200 nM of NF- κ B siRNA (Santa Cruz Biotechnology, Santa Cruz, Calif), or 100 to 200 nM of scramble control siRNA (Cell Signaling Technology, Danvers, Mass) using Lipofectamine 2000 (Invitrogen, Grand Island, NY) for 5 to 6 hours in serum-free Opti-MEM media (Invitrogen). Whole cell lysates prepared at 48, 72, and 96 hours post siRNA treatment were subjected to Western blotting to determine the efficiency of the knockdown.

Western Blots

Cell lysates were prepared using RIPA buffer, and 30 to 60 μ g of protein was subjected to denaturing sodium dodecyl sulfate–polyacrylamide gel electrophoresis (SDS-PAGE) and Western blot. The polyvinylidene fluoride membrane was probed with anti-MUC1 antibody CT2, anti-NF- κ B p65 (Cell Signaling Technology), anti-Cox-2, anti-lamin A/C, and anti- β -actin (Santa Cruz Biotechnology) antibodies. Appropriate secondary antibodies conjugated to horseradish peroxidase were used, and protein detected using the chemiluminescence kit. All antibodies were used according to manufacturer's recommendations.

Preparation of Nuclear Extract

Cells were grown in 10-cm plate and upon reaching 85% confluence were lysed using the EMD Millipore nuclear extraction kit to isolate the nuclear and the cytosolic fractions.

Serum PGE₂ Metabolite by Enzyme-Linked Immunosorbent Assay

Serum PGE₂ levels were determined using a specific enzyme-linked immunosorbent assay (ELISA) kit (Cayman Pharmaceuticals, Ann Arbor, Mich) that measures for the prostaglandin E₂ metabolite (PGEM) (13,14-dihydro 15-keto prostaglandin A₂). The protocol was followed as recommended by the manufacturer. Results were expressed in picograms per milliliter of PGE₂ or PGEM.

Human PDA Samples

Tissue sections of human pancreatic adenocarcinoma (PDA) and normal pancreas were obtained from the National Institutes of Health/National Cancer Institute tissue repository (<http://seer.cancer.gov/biospecimen>). The sera of patients with pancreatic cancer (PC) from different stages were also obtained from the National Cancer Institute.

Mouse PDA Samples

Two-month-old nude mice were injected with 5×10^6 BxPC3.Neo or BxPC3.MUC1 cells in the flank region, and the tumors were allowed to grow for 2 months. Tumors were harvested for immunohistochemistry (IHC) and tumor lysate. PDA.MUC1 and PDA.MUC1 knockout mice between 16 and 40 weeks of age were killed, and tumors were harvested. Paraffin-embedded blocks of formalin-fixed tumor sections were made by the Histology Core at Carolinas Medical Center. Four-micron-thick sections were prepared for IHC staining.

Immunohistochemistry

Standard IHC method was followed. Primary antibodies used were as follows: Armenian hamster anti-MUC1-CT antibody CT2 (1:50, gift from Dr Gendler) and goat anti-COX-2 (1:100; Santa Cruz Biotechnology). Secondary antibodies used were anti-hamster (1:250; Jackson Laboratory, Bar Harbor, Maine) and anti-goat (1:100; Dako, Carpinteria, Calif) IgGs conjugated to horseradish peroxidase. Immunopositivity was assessed using light microscopy, and images were taken at 200 \times magnification.

Chromatin Immunoprecipitation

Cells grown to near 80% confluence were cross-linked with formaldehyde (Sigma) at room temperature for 10 minutes. Cross-linked chromatin prepared with a commercial chromatin immunoprecipitation (ChIP) assay kit (EZ-Magna ChIP; Millipore) was immunoprecipitated with normal Armenian hamster IgG (1:20) (Santa Cruz Biotechnology), anti-MUC1-CT antibody (CT2) (1:15), and anti-NF- κ B p65 (1:20) antibody. IgG was used as a negative control for the immunoprecipitation step. Input DNA (2%) and DNA isolated from the precipitated chromatin were amplified by polymerase chain reaction (PCR) using mouse- or human-specific primers flanking the promoter region containing the NF- κ B-binding site (ChIP region I) or distant sites from the promoter region (ChIP region II). Chromatin immunoprecipitation region II was used as a negative control to evaluate specificity of association between MUC1-CT and NF- κ B p65 to the promoter region of *Ptgs2/PTGS2* gene. Sequence of the primers is available upon request.

Semiquantitative and Quantitative Reverse Transcriptase-PCR

TRIzol (Invitrogen) was used to extract total RNA according to the manufacturer's protocol; 1 to 2 μ g of the extracted RNA was used as template for semiquantitative reverse transcriptase (RT)-PCR reaction (Access quick RT-PCR kit; Promega, Madison, Wis) and real-time RT-PCR (KAPA SYBR Fast One-step qRT-PCR kit, Willmington, Mass). Sequence of the primers is available upon request.

Cell Growth by MTT Assay

Ten thousand cells plated in a 96-well plate were permitted to grow overnight. Cells were left untreated or treated with celecoxib (Pfizer, China) for 24 hours. Next, MTT (Biotium, Hayward, Calif) solution was added (10 μ L/well) to cells incubated for an additional 3 to 4 hours. In the final step, media was removed, formazan was dissolved in dimethyl sulfoxide (200 μ L/well), and the absorbance read using an ELISA plate reader.

Invasion Assay

Cells were grown in culture dishes and serum starved for 18 hours before plating for the invasion assay. In a 24-well plate, 50,000 cells in serum-free media with or without celecoxib were plated over Transwell inserts (BD Biosciences, San Jose, California) precoated with reduced growth factor Matrigel (BD Biosciences). Cells were allowed to invade through the matrix toward the serum-supplemented media contained in the bottom chamber over a period of 36 hours. Percent invasion was calculated as follows: (absorbance of samples / absorbance of controls) \times 100.

Confocal Microscope

Cells grown on chamber slides were fixed with formalin, permeabilized with 0.5% Tween, and incubated with CT2 conjugated with fluorescein isothiocyanate (Jackson Laboratory) and

anti-NF- κ B p65 (rabbit IgG) antibody (Santa Cruz Biotechnology) overnight. On the next day, the cells probed with anti-rabbit IgG antibody conjugated with Alexa fluor (Invitrogen) for 1 hour at room temperature and mounted with ProLong Gold antifade reagent with DAPI. Photographs were taken at 400 \times using the confocal microscope (Carl Zeiss International, Thornwood, NY).

Densitometric Analyses

The bands on Western blot and semiquantitative RT-PCR were quantified using image analysis software (Image J) from the National Institutes of Health (Bethesda, Md).

Statistical Analysis

Statistical analysis was performed with GraphPad software (La Jolla, Calif). Statistical significance was determined using 1-way analysis of variance (ANOVA), 2-way ANOVA, and *t* test.

RESULTS

Human Primary PDA Expresses High Levels of MUC1 and Cox-2 Protein

Human PDA sections ($n = 4$ patient tumors) showed high expression of both MUC1 and Cox-2 protein in comparison to the normal pancreas, as indicated by intense brown staining in PDA compared with the normal counterpart (Fig. 1A). In serum of patients with stages 2, 3, and 4 PDA, the PGEM levels increased from a normal level of 63.8 pg/mL (designated as stage 0) to 118 pg/mL in stage 2, 148.8 pg/mL in stage 3, and 210 pg/mL in stage 4 (Fig. 1B), suggesting a stage-dependent increase. There was a 4-fold increase in serum PGEM level of patients with stage 4 versus stage 0. Prostaglandin E₂ metabolite is a measure of Cox-2 enzymatic activity. The same serum samples analyzed for circulating MUC1 showed a similar stage-dependent increase in shed MUC1 level.¹⁷ The data indicated a positive correlation between MUC1 and Cox-2 expression and function in human PDA.

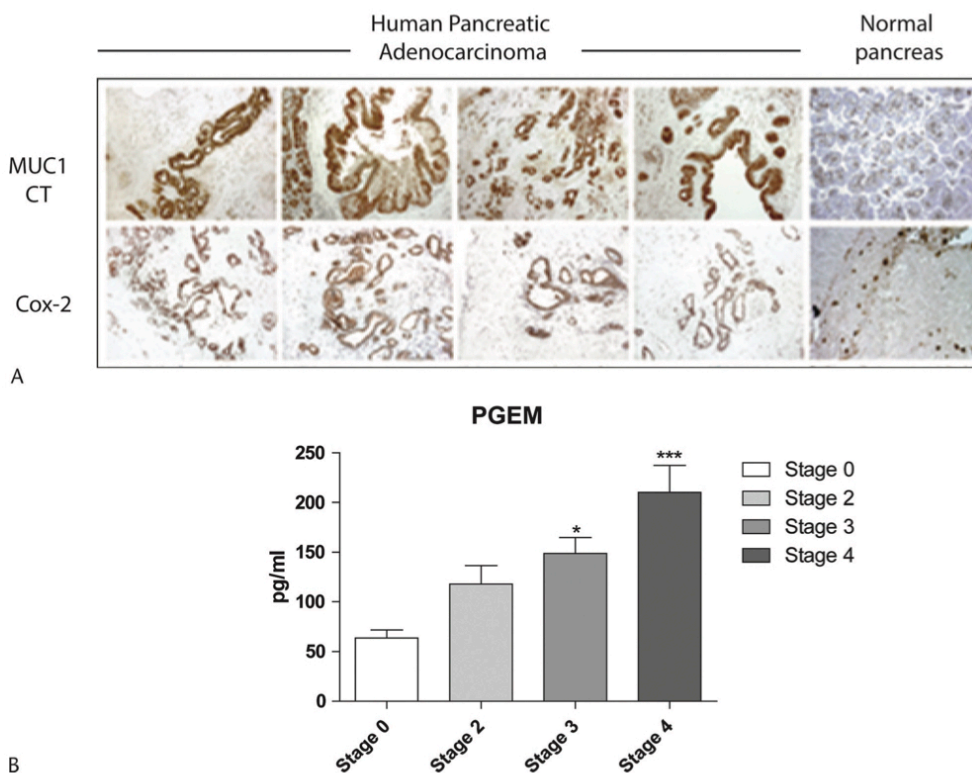


FIGURE 1. Expression of MUC1 and COX-2 in human PDA sections and levels of PGEM in the patient serum. A, Immunohistochemistry was performed to compare MUC1 and Cox-2 expression between the human PDA and adjacent normal pancreas tissue sections. Morphologically normal pancreas section shows low apical membranous MUC1 staining and lack of Cox-2 expression. Pancreatic ductal adenocarcinoma samples show strong membranous and cytoplasmic MUC1 staining and show abundant Cox-2 in tumor cells. B, Serum PGE₂ levels from patients with PDA were assessed by PGEM ELISA kit. An average of $n = 5$ patient samples are shown. One-way ANOVA was performed to determine the statistical significance between the samples (* $P = 0.05$, *** $P = 0.0005$).

Positive Correlation between MUC1 and Cox-2 Expression in Human PDA Cell Lines

A panel of human PDA cell lines expressing various levels of endogenous MUC1 was analyzed for basal MUC1 and Cox-2 protein levels by Western blot. HPAFII, HPAC, CFPAC, and Capan-1 PDA cells expressing high levels of endogenous MUC1 also expressed high Cox-2, whereas Hs766T, Capan-2, and MIA PaCa-2-expressing low levels of endogenous MUC1 expressed low Cox-2 (Fig. 2A). However, this was not the case with BxPC3 cell line that has low endogenous MUC1 but expresses high levels of Cox-2. This may be because BxPC3 cells have normal Kras protooncogene, whereas all other cell lines tested have mutated Kras.¹⁸ Nevertheless, when we overexpressed full-length MUC1 in BxPC3 cells, we did observe a significant increase in Cox-2 levels but no increase in Cox-2 message (Supplemental Figure 1, <http://links.lww.com/MPA/A375> and Supplemental Table 1,

<http://links.lww.com/MPA/A376>). Overall, the data validate the existence of a positive correlation between MUC1 and Cox-2 expression in Kras-driven PDA.

Overexpression of MUC1 Augments Cox-2 Expression and a Simultaneous Attenuation Upon MUC1 Down-regulation

Next, we manipulated the levels of MUC1 protein in PDA cells to determine the importance of MUC1 in the regulation of Cox-2 expression. Overexpression of MUC1 in normally low MUC1-expressing Panc02 cells (Panc02.MUC1) caused a 2.6-fold increase in Cox-2 protein level compared with its control counterpart (Panc02.Neo) (Fig. 2B, Supplemental Table 1, <http://links.lww.com/MPA/A376>, tabulating the densitometric analysis of the blots). Similarly, KCM (Muc1-hi) cells expressed 3.9-fold higher Cox-2 than KCKO (Muc1-null) cells (Fig. 2B,

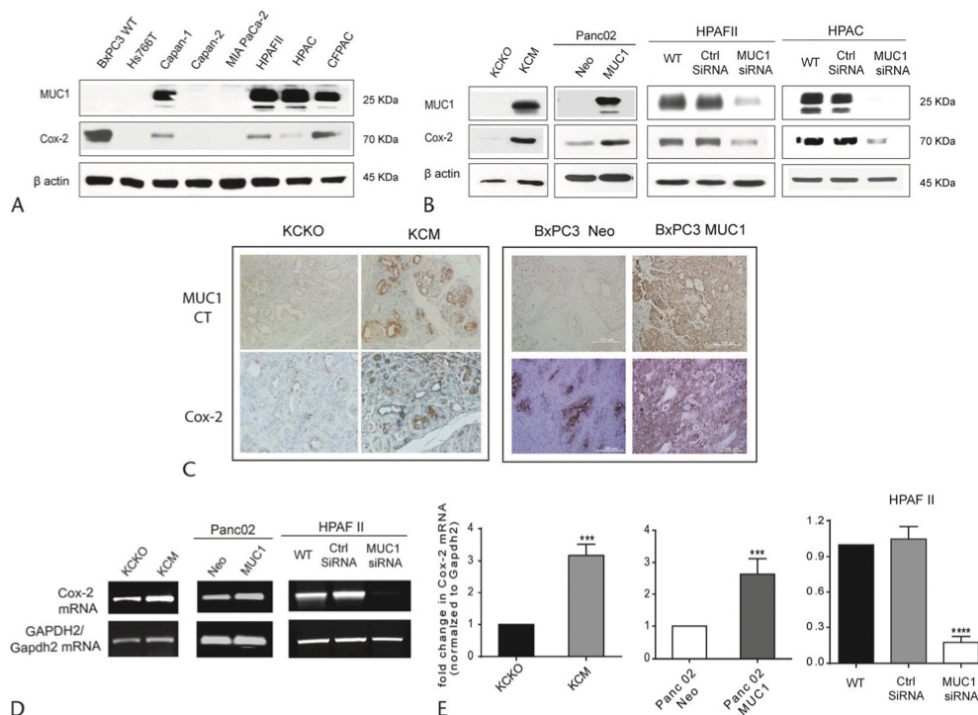


FIGURE 2. Positive correlation between MUC1 and Cox-2 expression in human PC cell lines (in vitro) and in mouse PDA sections. A, Endogenous levels of MUC1 and Cox-2 protein in a panel of human PDA cell lines were evaluated by Western blot using MUC1-CT-specific antibody CT2 and anti-Cox-2 antibody, respectively. Sixty micrograms of protein was loaded for SDS-PAGE. β-Actin was used as loading control. B, Levels of endogenous MUC1 and Cox-2 protein in mouse PDA cell lines, KCM and KCKO, as well as Panc02 cells that were stably infected to overexpress human MUC1. In addition, MUC1 was knockdown in HPAFII and HPAC human PDA cells using a smart pool of MUC1-specific siRNA. Seventy-two hours later, Cox-2 and MUC1 levels were analyzed by Western blot; 60 μg of protein was loaded for SDS-PAGE. C, Immunohistochemistry was performed to compare levels of MUC1 and Cox-2 expression between spontaneously occurring KCKO and KCM tumors at 24 weeks of age. BxPC3 Neo and BxPC3 MUC1 xenografted tumors were stained for MUC1 and Cox-2 expression. KCM and BxPC3.MUC1 tumors showed high levels of Cox-2 in comparison to MUC1-low KCKO and BxPC3 Neo tumors. D, Total mRNA from PDA cell lines were isolated using TRIzol, and the basal levels of Cox-2 mRNA were determined using semiquantitative 1-step RT-PCR kit. E, Graphical representation of fold increase in levels of Cox-2 mRNA normalized to Gapdh2 using real-time quantitative RT-PCR. Unpaired t test was performed to determine the statistical significance between KCKO and KCM, n = 3 (**P < 0.0004). Unpaired t test was performed to determine the statistical significance between Panc02Neo and Panc02MUC1, n = 3 (**P < 0.001). One-way ANOVA was performed to determine the statistical significance between HPAFII WT, control siRNA, and MUC1 siRNA-treated samples, n = 3 (****P < 0.0001).

Supplemental Table 1, <http://links.lww.com/MPA/A376>). Upon transient knockdown of MUC1, we observed a 3.5- and 5.8-fold decrease in Cox-2 expression in HPAFII and HPAC cells, respectively (Fig. 2B, Supplemental Table 1, <http://links.lww.com/MPA/A376>). Thus, manipulation of the MUC1 level altered Cox-2 expression in PDA cells, indicating that Cox-2 (*Ptgs2/PTGS2*) may be regulated by MUC1.

This was further confirmed in vivo in the PDA.MUC1 and PDA.Muc1KO tumors. Immunohistochemistry was performed to evaluate the coexpression of MUC1 and Cox-2 in situ. PDA.MUC1 tumors expressed higher levels of Cox-2 in comparison to the PDA.Muc1KO tumors, as indicated by the strong brown staining (Fig. 2C, left panel). A similar trend in MUC1 and Cox-2 expression was observed in xenografted human BxPC3.MUC1 and BxPC3.Neo tumors in nude mice. As was expected, BxPC3.MUC1 tumors showed higher Cox-2 expression than MUC1-low BxPC3.Neo tumors (Fig. 2C, right panel).

MUC1 High PDA Cells Express High Levels of Cox-2 mRNA

The level of Cox-2 mRNA in PDA cells expressing variable levels of MUC1 was analyzed by semiquantitative and quantitative RT-PCR. Significant increase and decrease in the Cox-2 transcript level were detected upon MUC1 overexpression or down-regulation, respectively (Fig. 2D, Supplemental Table 2, <http://links.lww.com/MPA/A376>) by semiquantitative RT-PCR. Furthermore, data obtained using quantitative RT-PCR revealed that the steady-state level of Cox-2 mRNA was 2.4- and 3-fold higher in MUC1-positive Panc02 MUC1 and KCM cells, respectively, compared with Panc02.Neo and KCKO cells (Fig. 2E). Conversely, a 3-fold decrease in Cox-2 mRNA level was observed upon transient knockdown of MUC1 in HPAFII cells (Fig. 2E), indicating that the Cox-2 gene may be regulated by MUC1 in PDA cells.

MUC1 and NF- κ B Colocalizes and Binds to the Promoter of the Cox-2 Gene (*Ptgs2/PTGS2* Gene)

We investigated the molecular mechanism of MUC1-induced Cox-2 gene expression in PDA cells. The 5' untranslated region (UTR) of human Cox-2 gene (*PTGS2/Ptgs2* gene) contains a TATA box and several potential transcriptional regulatory elements such as CRE (cAMP response element) (59/53), NF-IL6 (-132/-124), and NF- κ B (-233/-214 and -448/-439), whereas mouse Cox-2 gene contains CRE-2 (-438/-428), NF- κ B (-400/-392), C/EBP (-136/-128), and AP-1 (-67/-62) sites, which are essential for transcriptional regulation of Cox-2 gene expression. In colon cancer, NF- κ B p65 is an important transcriptional regulator of Cox-2 gene as indicated by attenuation of Cox-2 expression upon NF- κ B p65 down-regulation in colon cancer cells.^{19,20} To determine if NF- κ B p65 is also important for up-regulation of Cox-2 gene in PDA, we determined Cox-2 levels following the transient knockdown of NF- κ B p65 in KCKO and KCM cells. Upon down-regulation of NF- κ B p65 subunit, we observed significant attenuation of Cox-2 expression in KCM cells (Fig. 3A, Supplemental Table 3, <http://links.lww.com/MPA/A376>). In contrast, the level of Cox-2 was unaffected in KCKO cells suggesting that MUC1 cooperates with NF- κ B p65 to drive the overexpression of Cox-2 gene in PDA cells.

To further assess MUC1's role in driving Cox-2 gene expression, we performed Chip assay to test if MUC1-CT and NF- κ B p65 bind to the promoter region of Cox-2 gene (*PTGS2/Ptgs2* gene). Primers were designed to amplify the precipitated chromatin flanking -377/-175 base pairs (bp) upstream (ChIP region I) and +8320/+8550-bp downstream (ChIP region II) of transcription

start site of mouse Cox-2 (*Ptgs2*) gene (Fig. 3B, top panel). Corresponding human-specific primers were designed spanning -346/-118 bp upstream (ChIP region I) and -4053/3820 bp upstream (ChIP region II) of human Cox-2 (*PTGS2*) gene (Fig. 3B, bottom panel). In Panc02.MUC1, KCM, and HPAFII cells, we observed MUC1-CT and NF- κ B p65 binding to the mouse Cox-2 (*Ptgs2*) or human Cox-2 (*PTGS2*) promoter ChIP region I, respectively (Fig. 3C, left panel, Supplemental Table 4, <http://links.lww.com/MPA/A376>). This region contains the NF- κ B p65 response element (NF- κ B p65 RE). In contrast, Panc02.Neo and KCKO cells did not show strong binding of NF- κ B p65 to the same region (Fig. 3C, left panel, Supplemental Table 4, <http://links.lww.com/MPA/A376>). No significant interaction was observed between MUC1-CT and NF- κ B p65 with Cox-2 (*PTGS2/Ptgs2*) promoter in the control region (ChIP region II) (Fig. 3C, right panels, Supplemental Table 4, <http://links.lww.com/MPA/A376>) validating the specificity of binding.

To confirm that MUC1 and NF- κ B p65 translocate to the nucleus, we assessed the nuclear localization of MUC1 and NF- κ B p65 in PDA cell lines. Western blot on the nuclear fraction demonstrated the presence of MUC1-CT in the nucleus of Panc02.MUC1, KCM, HPAFII, and HPAC cells and absence in Panc02.Neo and KCKO cells (Fig. 3D, Supplemental Table 5, <http://links.lww.com/MPA/A376>). However, we did not observe any significant difference in the nuclear accumulation of NF- κ B p65 in the MUC1-null/low (KCKO and Panc02.Neo) versus MUC1-high (KCM and Panc02.MUC1) cells (Fig. 3D), indicating that the nuclear localization of NF- κ B p65 is not affected by the absence of MUC1 in these PDA cells. Confocal microscopy further confirmed the colocalization of MUC1 and NF- κ B p65 in the cytoplasm and in the nucleus of the KCM cells (Fig. 3E). Taken together, these data suggest that MUC1 binds to NF- κ B p65 subunit, translocates to the nucleus, and drives the transcription of Cox-2 (*Ptgs2/PTGS2*) gene.

Blocking Cox-2 Activity With a Specific Inhibitor, Celecoxib, Reduces Proliferation and Invasion in PDA Cells

We and others have demonstrated that overexpression of MUC1 increases the proliferative index and invasive potential of the PDA cells.^{12,21,22} Thus, we questioned if the aggressive phenotype of MUC1-positive PDA cells may be a manifestation of Cox-2 up-regulation in these cells. To test our hypothesis, we blocked Cox-2 activity with celecoxib and analyzed growth and invasive potential of the PDA cells.

A dose-dependent increase in percentage of cells undergoing growth arrest was observed in HPAFII and HPAC cells treated with 50, 75, and 100 μ M of celecoxib with 18.9%, 42.7%, and 56.4% for HPAFII (Fig. 4A, left panel) and 16%, 47.1%, and 59.6% for HPAC (Fig. 4A, middle panel). In KCKO and KCM cells, a similar dose-dependent increase in percentage of cells undergoing growth arrest was observed upon treatment with increasing dose of celecoxib (Fig. 4A, right panel); however, KCM cells were more resistant to the treatment than KCKO cells. Treatment with celecoxib caused a gradual decrease in the Cox-2 protein expression in all cell lines (Fig. 4B). However, there was no significant change in MUC1 expression upon Cox-2 inhibition (Fig. 4B). The data thus indicated that Cox-2 is under the regulation of MUC1, but MUC1 is not under Cox-2 regulation. Interestingly, in HPAC cells, we observed a moderate increase in MUC1 expression upon exposure to celecoxib (Fig. 4B, middle panel). Although down-regulation of Cox-2 expression upon celecoxib treatment was comparable in KCM and KCKO cell lines, KCM

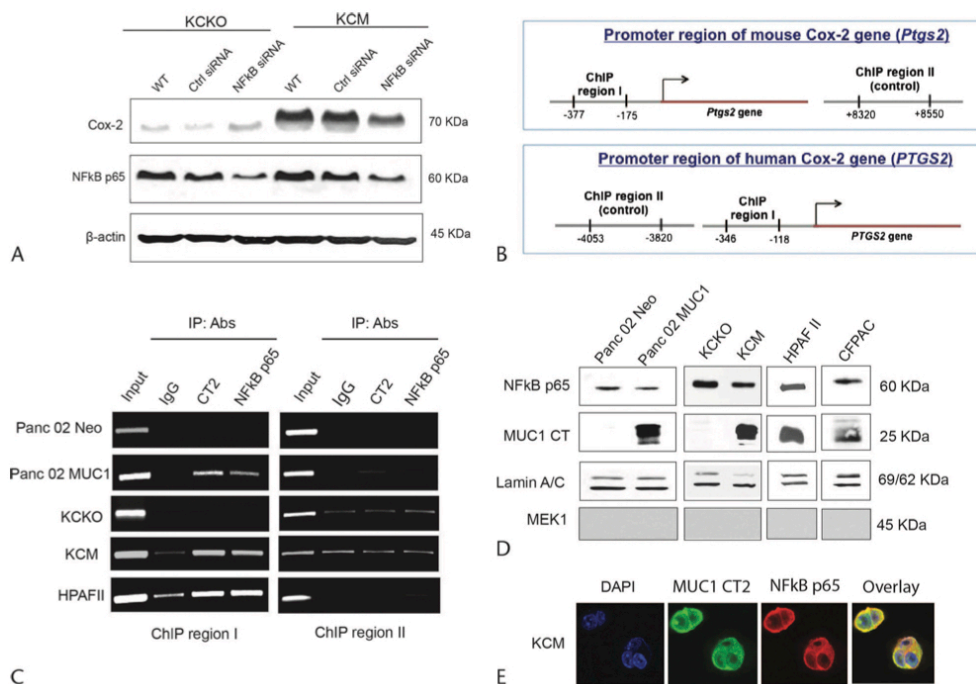


FIGURE 3. Mucin 1 and NF-κB p65 drive the expression of *Cox-2* (*Ptgs2*/*PTGS2*) gene. **A**, Nuclear factor κB p65 was transiently knockdown using NF-κB p65-specific siRNA; 72 hours later, *Cox-2* and NF-κB p65 levels were analyzed by Western blot; 35 μg of protein was loaded for SDS-PAGE. **B**, Schematic representation of the promoter region with its putative DNA-binding elements in mouse and human *Cox-2* (*Ptgs2*/*PTGS2*) gene. **C**, Sheared chromatin was immunoprecipitated using anti-MUC1-CT antibody CT2 and anti-NF-κB p65 antibody. The immunoprecipitated chromatin was PCR amplified. **D**, Nuclear lysates were immunoblotted to determine the constitutive nuclear localization of NF-κB p65, MUC1-CT. Lamin A/C was used as a loading control. MEK1 was used as control for cytoplasmic contaminants. **E**, KCM cells grown on chamber slides were fixed and double stained with anti-NF-κB p65 antibody (red) and anti-MUC1 antibody CT2 (green). Nuclei were stained and mounted with DAPI (blue). Yellow represents overlay of green and red fluorescence suggesting colocalization.

cells were more resistant to growth arrest in comparison to KCKO. This could be due to hyperactivation of the pro-survival pathway such as PI3K/Akt in KCM cells, which counteracts the growth inhibitory effect of celecoxib.¹³ The exact mechanisms for celecoxib's anticancer activities are still not clear, but they most likely involve both COX-2-dependent and COX-2-independent mechanisms, as growth arrest was observed regardless of *Cox-2* levels in the PDA cells.

We next evaluated the invasive potential of PDA cells upon blocking *Cox-2* activity. A 2-fold decrease in the invasive potential of CFPAC cells was observed upon treatment with 15 and 30 μM of celecoxib (Fig. 4C), indicating that *Cox-2* is important for the enhanced invasive potential of the MUC1-high PDA cells. Similarly, 1.6-fold (51.6%) and 4.3-fold (19.49%) decrease in the invasive potential of the KCM cells was observed upon treatment of the cells with 15 and 30 μM of celecoxib, respectively (Fig. 4D).

DISCUSSION

The data demonstrate that in PDA cells the proinflammatory-inducible enzyme, *Cox-2*, is under the regulation of tMUC1. The 2 proteins are abundantly coexpressed in the human and mouse

PDA tissues, and their expression increases with stage of the tumor (Fig. 1). Furthermore, overexpression of full-length *MUC1* in PDA cells increases *Cox-2* mRNA and protein expression, and conversely, knockdown of *MUC1* attenuated *Cox-2* mRNA and protein expression (Fig. 2). In most human cell lines tested, high *MUC1* levels correlated with high *Cox-2* levels except in BxPC3 cells. These cells displayed significantly high level of *Cox-2* despite low levels of *MUC1* (Fig. 2A). This difference may be due to the presence of normal *Kras* protooncogene in the BxPC3 cells.¹⁸ All other cell lines tested exhibit mutated *Kras*. Interestingly, there was no significant difference in the *Cox-2* mRNA levels between BxPC3.MUC1 and BxPC3.Neo cells, indicating a possible role of posttranscriptional regulation of *Cox-2* gene by *MUC1* in BxPC3 cells (Supplemental Figure 1, <http://links.lww.com/MPA/A375> and Supplemental Table 1, <http://links.lww.com/MPA/A376>). The 3' UTR of *Cox-2* mRNA contains the ARE elements that may regulate the stability of *Cox-2* mRNA at a posttranscriptional level in BxPC3 cells. The Erk1/2, p38 MAPK, and PI3K pathways have been reported to be instrumental in mediating posttranscriptional regulation of *Cox-2* gene.²³ Most of these core signaling pathways are overactivated in cancer cells that overexpress *MUC1*.^{13,16,24}

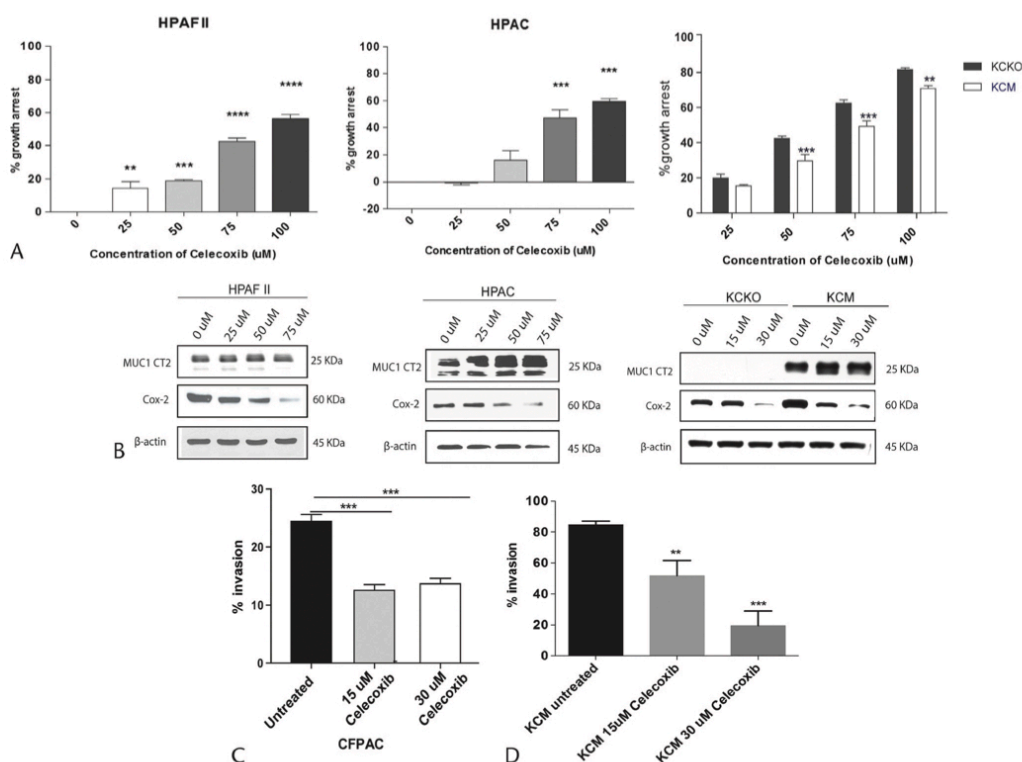


FIGURE 4. Selective inhibition of Cox-2 with celecoxib attenuates the growth and invasive potential of PDA cells. A, MTT assay was performed to determine the growth inhibition following celecoxib treatment. Significant growth arrest is noted in all cell lines tested in response to celecoxib. To determine the statistical significance between celecoxib-treated HPAFII and HPAC cells, 1-way ANOVA was performed, $n = 6$ (** $P < 0.001$, *** $P < 0.0001$). To determine the statistical significance between celecoxib-treated KCKO and KCM cells, 2-way ANOVA (right panel) was performed, $n = 5$ (** $P < 0.001$, *** $P < 0.01$). B, Cells grown overnight in a 6 well plate were left untreated or treated with indicated concentration of celecoxib for 24 hours. Cell lysates were prepared and were subjected to immunoblotting. The membrane was probed for MUC1 (CT2), Cox-2, and β -actin. No change in MUC1 levels was observed following treatment with celecoxib. C and D, Significant reduction in invasive potential was observed in CFPAC and KCM cells after treatment with celecoxib. One-way ANOVA was performed to determine the statistical significance between celecoxib-treated CFPAC ($n = 3$, $P = 0.0004$) and celecoxib-treated KCM cells ($n = 3$, $P = 0.0002$). Percentage of invasion was calculated as absorbance of samples / absorbance of controls $\times 100$.

Thus, a possibility of MUC1 increasing Cox-2 expression posttranscriptionally in PDA cells cannot be overruled. Recently, it was reported that down-regulation of miR-143 in PDA cells increases the stability of Cox-2 mRNA, leading to increased Cox-2 protein in PDA cells.²⁵ Mucin 1 has been shown to mediate posttranscriptional regulation of 1 of its target gene galectin 3 expression via miR-322.²⁶

To elucidate the mechanism by which MUC1 regulates Cox-2 expression, we assessed the (a) nuclear accumulation of MUC1 and NF- κ B p65 in MUC1-high and -low PDA cells and (b) occupancy of MUC1 and NF- κ B p65 on the promoter of *Cox-2* (*PTGS2/PTGS2*) gene by ChIP assay. There was no difference in the nuclear accumulation of NF- κ B p65 in MUC1-high and -low PDA cell lines, indicating that the nuclear localization of NF- κ B p65 is not affected by the presence or absence of MUC1 in the cells. This observation is in contrast to previous reports that showed decreased nuclear accumulation of NF- κ B p65 in ZR-75-1 breast cancer cells upon MUC1 down-regulation.²⁷ The contrast in

observation could arise from differences in tumor origin (breast vs pancreas). Nevertheless, we found that MUC1-CT and NF- κ B bind to ChIP region I (within 1000 bp upstream of transcription start site) of the 5' UTR region of both mouse and human *COX-2/Cox-2* gene. KCKO cells that are null for MUC1 did not show any binding of MUC1-CT and NF- κ B p65 to the 5' UTR of mouse *Ptgs2* gene (Fig. 3). These cells also display low Cox-2 mRNA levels, indicating that the loss of MUC1 attenuates binding of NF- κ B p65 to the promoter of *Cox-2* gene and thereby affects the transcription of *Ptgs2* gene. We postulate that during tumor progression, possibly due to hypoglycosylation of MUC1, the MUC1-CT cleaves, associates with NF- κ B p65 and translocates as a complex to the nucleus, and binds to the promoter of Cox-2 driving its transcription. The byproduct of Cox-2 enzymatic activity, PGE₂, interacts with its EP receptors and enhances cell survival, proliferation, and invasiveness (Fig. 5).

In colon, breast, PDA, and non-small cell lung cancer (NSCLC), Cox-2/PGE₂ signaling axis promotes proliferation,

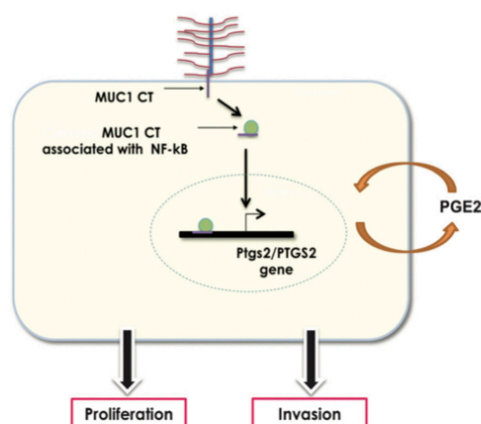


FIGURE 5. Schematic of a model representing the mechanism of Cox-2 regulation in PDA cells. The MUC1-CT undergoes cleavage, associates with NF-κB p65, and translocates as a complex to the nucleus. The transcription complex binds to the promoter of Cox-2 (*PTGS2/Pigs2*) gene driving its expression. The byproduct of Cox-2 enzymatic activity, PGE₂, promotes cell survival, proliferation, and invasiveness of cancer cells via engaging with the EP receptors.

survival, and invasion of cancer cells,^{28–30} either through decreased production of CD44, MMP-2, and EP4 receptors³¹ or by suppressing E-cadherin expression via transcriptional suppressor ZEB1.³² Thus, lastly, we determined the biological significance of Cox-2 in the MUC1-high PDA cells by blocking the Cox-2 activity. We observed a dose-dependent decrease in growth of HPAFII, HPAC, KCKO, and KCM cells upon treatment with celecoxib underscoring the importance of Cox-2 in proliferation of PDA cells (Fig. 4). Regardless of the levels of Cox-2 or MUC1, all cells responded to Cox-2 inhibition to some degree. Interestingly, KCKO cells that express low levels of Cox-2 as compared with KCM cells were more susceptible to growth inhibition by celecoxib compared with KCM. This may be due to the fact that celecoxib not only inhibits Cox-2 activity, but also modulates cell survival pathways and other cellular responses. A study showed that the antitumor effect of Cox-2 is not entirely contingent upon its ability to inhibit Cox-2 activity but rather to its ability to initiate ER stress.³³ It could be possible that celecoxib initiates ER stress in cells that is counteracted better in MUC1-positive KCM cells, making them more resistant to celecoxib.

Although Cox-2 is overexpressed in MUC1-high PDA cells, the biological effect of Cox-2 may not be the same in all MUC1-high cell lines. We found Cox-2 to be critical for proliferation of HPAFII, HPAC, KCKO, and KCM cells, but not for their invasive potential (data not shown). In contrast, Cox-2 was important for both invasion and proliferation of CFPAC and KCM cells. This variation in the biological effect of Cox-2 could be attributed to the difference in the expression profile of the EP receptors in these cell lines and the subsequent engagement of 1 or more of the signaling pathways downstream of Cox-2/PGE₂ signaling axis. Nonetheless, the significance of Cox-2 overexpression by the MUC1-high cells cannot be underrated, as Cox-2 affects not only tumor cells but also other cellular components in the tumor microenvironment such as immune responses against tumor by recruiting myeloid-derived suppressor cells in the tumor microenvironment. Moreover, Cox-2 is known to regulate vascular

endothelial growth factor expression and promote angiogenesis.^{34,35} Previously, others and we reported that MUC1 modulates expression of vascular endothelial growth factor in pancreatic and breast cancer cells.^{21,36}

Controlling Cox-2 overexpression in cancers remains a challenging task. Our study indicates that MUC1 may serve as an alternative target for blocking Cox-2 overexpression in PDA cells. GO-203, a small molecule inhibitor designed to block MUC-C dimerization and its nuclear translocation, has been shown to reverse MUC1-mediated proliferation in NSCLC and multiple myeloma cells.^{37,38} Thus, it might be worth investigating if GO-203 can similarly prevent MUC1 localization to the nucleus and block MUC1-mediated Cox-2 overexpression in PDA cells.

ACKNOWLEDGMENTS

The authors thank the graduate student Michael Shu-Wu at UNC-Charlotte for taking the confocal photographs.

REFERENCES

- Greenhough A, Smartt HJ, Moore AE, et al. The COX-2/PGE₂ pathway: key roles in the hallmarks of cancer and adaptation to the tumour microenvironment. *Carcinogenesis*. 2009;30:377–386.
- Koehne C, Dubois R. COX-2 inhibition and colorectal cancer. *Semin Oncol*. 2004;2:12–21.
- Yip-Schneider MT, Barnard DS, Billings SD, et al. Cyclooxygenase-2 expression in human pancreatic adenocarcinomas: treatment of pancreatic cancer. *Carcinogenesis*. 2000;21:139–146.
- Basu GD, Liang WS, Stephan DA, et al. A novel role for cyclooxygenase-2 in regulating vascular channel formation by human breast cancer cells. *Breast Cancer Res*. 2006;8:R69.
- Sinha P, Clements VK, Fulton AM, et al. Prostaglandin E₂ promotes tumor progression by inducing myeloid-derived suppressor cells. *Cancer Res*. 2007;67:4507–4513.
- Williams CS, Mann M, DuBois RN. The role of cyclooxygenases in inflammation, cancer, and development. *Oncogene*. 1999;18:7908–7916.
- Williams CS, Watson AJ, Sheng H, et al. Celecoxib prevents tumor growth in vivo without toxicity to normal gut: lack of correlation between in vitro and in vivo models. *Cancer Res*. 2000;60:6045–6051.
- Arber N, Eagle CJ, Spicak J, et al. Celecoxib for the prevention of colorectal adenomatous polyps. *N Engl J Med*. 2006;355:885–895.
- El-Rayes BF, Zalupski MM, Shields AF, et al. A phase II study of celecoxib, gemcitabine, and cisplatin in advanced pancreatic cancer. *Invest New Drugs*. 2005;23:583–590.
- Nath S, Mukherjee P. MUC1: a multifaceted oncoprotein with a key role in cancer progression. *Trends Mol Med*. 2014;20:332–342.
- Wen Y, Caffrey TC, Wheelock MJ, et al. Nuclear association of the cytoplasmic tail of MUC1 and beta-catenin. *J Biol Chem*. 2003;278:38029–38039.
- Sahraei M, Roy LD, Curry JM, et al. MUC1 regulates PDGFA expression during pancreatic cancer progression. *Oncogene*. 2012;31:4935–4945.
- Nath S, Daneshvar K, Roy LD, et al. MUC1 induces drug resistance in pancreatic cancer cells via upregulation of multidrug resistance genes. *Oncogenesis*. 2013;2:e51.
- Tinder TL, Subramani DB, Basu GD, et al. MUC1 enhances tumor progression and contributes toward immunosuppression in a mouse model of spontaneous pancreatic adenocarcinoma. *J Immunol*. 2008;181:3116–3125.
- Mukherjee P, Basu GD, Tinder TL, et al. Progression of pancreatic adenocarcinoma is significantly impeded with a combination of vaccine and COX-2 inhibition. *J Immunol*. 2009;182:216–224.

16. Besmer DM, Curry JM, Roy LD, et al. Pancreatic ductal adenocarcinoma mice lacking mucin 1 have a profound defect in tumor growth and metastasis. *Cancer Res.* 2011;71:4432–4442.
17. Curry JM, Thompson KJ, Rao SG, et al. The use of a novel MUC1 antibody to identify cancer stem cells and circulating MUC1 in mice and patients with pancreatic cancer. *J Surg Oncol.* 2013;107:713–722.
18. Ura H, Obara T, Nishino N, et al. Cytotoxicity of simvastatin to pancreatic adenocarcinoma cells containing mutant ras gene. *Jpn J Cancer Res.* 1994; 85:633–638.
19. Plummer S, Holloway K, Manson M, et al. Inhibition of cyclo-oxygenase 2 expression in colon cells by the chemopreventive agent curcumin involves inhibition of NF-kappaB activation via the NIK/IKK signalling complex. *Oncogene.* 1999;18:6013–6020.
20. Charalambous MP, Lightfoot T, Speirs V, et al. Expression of COX-2, NF-kappaB-p65, NF-kappaB-p50 and IKKalpha in malignant and adjacent normal human colorectal tissue. *Br J Cancer.* 2009;101:106–115.
21. Roy LD, Sahmei M, Subramani DB, et al. MUC1 enhances invasiveness of pancreatic cancer cells by inducing epithelial to mesenchymal transition. *Oncogene.* 2011;30:1449–1459.
22. Rajabi H, Alam M, Takahashi H, et al. MUC1-C oncoprotein activates ZEB1/miR-200c regulatory loop and epithelial-mesenchymal transition. *Oncogene.* 2014;33:1680–1689.
23. Dixon D. Dysregulated post-transcriptional control of COX-2 gene expression in cancer. *Curr Pharm Des.* 2004;10:635–646.
24. Hatstrup CL, Gendler SJ. MUC1 alters oncogenic events and transcription in human breast cancer cells. *Breast Cancer Res.* 2006;8:R37.
25. Pham H, Rodriguez CE, Donald GW, et al. miR-143 decreases COX-2 mRNA stability and expression in pancreatic cancer cells. *Biochem Biophys Res Commun.* 2013;439:6–11.
26. Ramasamy S, Duraisamy S, Barbashov S, et al. The MUC1 and galectin-3 oncoproteins function in a microRNA-dependent regulatory loop. *Mol Cell.* 2007;27:992–1004.
27. Ahmad R, Raina D, Joshi MD, et al. MUC1-C oncoprotein functions as a direct activator of the nuclear factor-kappaB p65 transcription factor. *Cancer Res.* 2009;69: 7013–7021.
28. Ding XZ, Hennig R, Adrian TE. Lipoxygenase and cyclooxygenase metabolism: new insights in treatment and chemoprevention of pancreatic cancer. *Mol Cancer.* 2003;2:10.
29. Howe LR. Inflammation and breast cancer. *Breast Cancer Res.* 2007;9:210.
30. Zhu M, Zhu Y, Lance P. TNF α -activated stromal COX-2 signalling promotes proliferative and invasive potential of colon cancer epithelial cells. *Cell Prolif.* 2013;46:374–381.
31. Dohadwala M, Batra RK, Luo J, et al. Autocrine/paracrine prostaglandin E₂ production by NSCLC cells regulates matrix metalloproteinase-2 and CD44 in cyclooxygenase-2-dependent invasion. *J Biol Chem.* 2002; 277:50828–50833.
32. Dohadwala M, Yang SC, Luo J, et al. Cyclooxygenase-2-dependent regulation of E-cadherin: prostaglandin E(2) induces transcriptional repressors ZEB1 and snail in non-small cell lung cancer. *Cancer Res.* 2006;66:5338–5345.
33. Chuang HC, Kardosh A, Gaffney KJ, et al. COX-2 inhibition is neither necessary nor sufficient for celecoxib to suppress tumor cell proliferation and focus formation in vitro. *Mol Cancer.* 2008;7:38.
34. Yoshida S, Amano H, Hayashi I, et al. COX-2/VEGF-dependent facilitation of tumor-associated angiogenesis and tumor growth in vivo. *Lab Invest.* 2003;83:1385–1394.
35. Liu H, Yang Y, Xiao J, et al. COX-2-mediated regulation of VEGF-C in association with lymphangiogenesis and lymph node metastasis in lung cancer. *Anat Rec.* 2010;293:1838–1846.
36. Woo JK, Choi Y, Oh SH, et al. Mucin 1 enhances the tumor angiogenic response by activation of the AKT signaling pathway. *Oncogene.* 2012;31: 2187–2198.
37. Raina D, Kosugi M, Ahmad R. Dependence on the MUC1-C oncoprotein in non-small cell lung cancer cells. *Mol Cancer Ther.* 2011;10:806–816.
38. Yin L, Ahmad R, Kosugi M, et al. Survival of human multiple myeloma cells is dependent on MUC1 C-terminal transmembrane subunit oncoprotein function. *Mol Pharmacol.* 2010;166–174.

ORIGINAL ARTICLE

A novel association of neuropilin-1 and MUC1 in pancreatic ductal adenocarcinoma: role in induction of VEGF signaling and angiogenesis

R Zhou¹, JM Curry¹, LD Roy¹, P Grover¹, J Haider², LJ Moore¹, S-t Wu¹, A Kamesh¹, M Yazdanifar¹, WA Ahrens³, T Leung² and P Mukherjee¹

We report that Mucin1 (MUC1), a transmembrane glycoprotein that is overexpressed in >80% of pancreatic ductal adenocarcinoma (PDA), induced a pro-angiogenic tumor microenvironment by increasing the levels of neuropilin-1 (NRP1, a co-receptor of vascular endothelial growth factor (VEGF) and its ligand VEGF. Expression of tumor-associated MUC1 (tMUC1) positively correlated with NRP1 levels in human and mouse PDA. Further, tMUC1^{hi} PDA cells secreted high levels of VEGF and expressed high levels of VEGF receptor 2 (VEGFR2) and its phosphorylated forms as compared with tMUC1^{low/nu} PDA. This enabled the tMUC1^{hi}/NRP1^{hi} PDA cells to (a) induce endothelial cell tube formation, (b) generate long ectopic blood vessels and (c) enhance distant metastasis in a zebrafish xenograft model. Concurrently, the proteins associated with epithelial-to-mesenchymal transition, N-cadherin and Vimentin, were highly induced in these tMUC1^{hi}/NRP1^{hi} PDA cells. Hence, blocking signaling via the NRP1–VEGF axis significantly reduced tube formation, new vessel generation and metastasis induced by tMUC1^{hi} PDA cells. Finally, we show that blocking the interaction between VEGF₁₆₅ and NRP1 with a NRP1 antagonist significantly reduced VEGFR signaling and PDA tumor growth *in vivo*. Taken together, our data suggest a novel molecular mechanism by which tMUC1 may modulate NRP1-dependent VEGFR signaling in PDA cells.

Oncogene (2016) 35, 5608–5618; doi:10.1038/onc.2015.516; published online 25 January 2016

INTRODUCTION

Angiogenesis is a complex process of new blood vessel formation from pre-existing vascular networks by capillary sprouting. Full execution of angiogenesis requires complex signaling via vascular endothelial growth factor (VEGF) and its receptors (VEGFRs).¹ VEGF-A is one of the major stimulators of angiogenesis induced by hypoxia during oncogenic process. Within the VEGF-A family of growth factors, VEGF₁₆₅ is well characterized and mediates angiogenic sprouting and endothelial cell organization *in vitro* and *in vivo*.^{2,3}

Three structurally homologous tyrosine kinase VEGFRs are VEGFR1 (Flt-1), VEGFR2 (KDR/Flk-1) and VEGFR3 (Flt-4). The majority of the endothelial cell responses to VEGF including differentiation, proliferation, migration and formation of the vascular tubes are mediated through VEGFR2.^{4–7} VEGFR1 is speculated as a decoy receptor, sequestering VEGF signaling through VEGFR2.^{4,5} VEGFR3 expression is restricted mainly to the lymphatic endothelium of adult tissues. It binds VEGF-C and VEGF-D, but not VEGF-A, and is thought to control lymphangiogenesis.^{8,9}

Neuropilins (NRPs) are transmembrane receptors without a tyrosine kinase domain and can act as co-receptors for VEGF family of pro-angiogenic cytokines¹⁰ and for the class 3 semaphorin (Sema3) family of axon guidance molecules.¹¹ NRPs are gaining much attention as multifunctional proteins involved in normal development, immunity and tumor progression as reviewed by Prud'homme and Glinka.¹² NRP1 is expressed by

endothelial cells, dendritic cells, regulatory T cells, several other normal cell types and tumor cells as well.^{13–15} It is a co-receptor for VEGFR2, with VEGF₁₆₅ binding to both NRP1 and VEGFR2 simultaneously.¹⁰ It has been proposed that NRP1 may enhance VEGF₁₆₅ binding and bioactivity by forming a bridge between NRP1 and VEGFR2, bringing these receptors into close proximity and promoting angiogenesis.¹⁶ Neutralizing NRP1 is additive to VEGF neutralization in suppressing vascular remodeling and tumor growth.¹⁷ Importantly, NRP1 is predominantly expressed in carcinomas (in particular those of epithelial cell origin), including carcinomas of the lung, breast, prostate, pancreas and colon.^{18,19} Overexpression of NRPs correlates with disease progression, metastatic potential and poor prognosis.^{10,19,20}

Therefore, NRP1 is an attractive therapeutic target. A number of strategies have been evaluated by using NRP1 ectodomains or soluble NRP1 as VEGF Trap, anti-NRP1 antibodies, knockdown by small interfering RNA (siRNA), or by using a small peptide-mimetic of VEGF to selectively block VEGF binding to NRP1.¹⁵ A heptapeptide ATWLPPR (A7R) is identified by screening a phage-displayed peptide library against an anti-VEGF antibody that blocks VEGF₁₆₅-dependent endothelial cell proliferation.²¹ A7R inhibits VEGF₁₆₅ binding to NRP1 but not to VEGFR1, VEGFR2 or heparin. *In vivo* treatment with A7R reduces blood vessel density and endothelial cell area, and suppresses the growth of MDA-MB-231 xenografts in nude mice.²²

Pancreatic ductal adenocarcinoma (PDA) is the fourth leading cause of cancer-related death in the United States.²³

¹Department of Biological Sciences, University of North Carolina at Charlotte, Charlotte, NC, USA; ²Julius L. Chambers Biomedical Biotechnology Research Institute, North Carolina Central University, Kannapolis, NC, USA and ³Section of Hepatobiliary and Pancreas Surgery, Department of Surgery, Carolinas Medical Center, Charlotte, NC, USA. Correspondence: Professor P Mukherjee, Department of Biological Sciences, University of North Carolina at Charlotte, 9201 University City Boulevard, Charlotte, NC 28223, USA. E-mail: pmukherj@uncc.edu.

Received 27 May 2015; revised 3 November 2015; accepted 27 November 2015; published online 25 January 2016

The transmembrane glycoprotein Mucin1 (MUC1) is overexpressed and aberrantly glycosylated in > 80% of metastatic PDA and is associated with poor prognosis.²⁴ We and others have shown that this tumor-associated form of MUC1 (tMUC1) enhances invasiveness of pancreatic cancer cells by inducing epithelial-to-mesenchymal transition (EMT), and that these tumors express high levels of VEGF, cyclooxygenase-2, prostaglandin E2 and platelet-derived growth factor.^{25,26} Lack of tMUC1 in PDA mice prevents tumor progression and metastasis, and has lower levels of VEGF.^{25,27} In addition, MUC1 overexpression has been demonstrated to promote VEGF production through insulin-like growth factor-1 receptor/Akt cascades, leading to the enhanced tumor growth and angiogenesis in human breast carcinoma.²⁸ Thus, in this study we assess whether tMUC1 induces a pro-angiogenic microenvironment in PDA and begin to elucidate the mechanism. We show for the first time that PDA cells and tumors that express high levels of tMUC1 have increased levels of NRP1 as compared with PDA with no or low levels of tMUC1. NRP1 potentiates VEGFR signaling and pro-angiogenic activities, thus indicative of enhanced intra-tumoral angiogenesis and disease progression. Finally, we show that blocking the interaction between VEGF₁₆₅ and NRP1 within the tumor microenvironment leads to disruption of VEGF signaling and therapeutic benefit in mouse models.

RESULTS

Level of NRP1 expression correlates with expression of tMUC1 in human PDA

We and others have shown that tMUC1 is overexpressed in PDA and is associated with enhanced metastasis and poor diagnosis.^{24,25,27,29} Parikh *et al.*³⁰ first reported NRP1 expression in the PDA. Here we first showed that tMUC1 and NRP1 were expressed in primary human PDA, but minimally in the normal pancreas (Figure 1a). The staining in the tumor was mainly restricted to the ductal epithelia. To determine whether a correlation existed between tMUC1 and NRP1, we examined a panel of human PDA cell lines that endogenously express high, medium or low tMUC1 by western blotting using an antibody against the extracellular tandem repeat of MUC1 (TAB004). Cells expressing high endogenous tMUC1 such as CFPAC, HPAC and HPAC also displayed high NRP1, whereas cells with low endogenous tMUC1 displayed low NRP1 with the exception of Panc1 cells (Figure 1b; quantification data shown as Supplementary Figure S1a). As NRP1 is a co-receptor of VEGF and signaling through VEGFR2 is critical for the angiogenic signaling to occur,¹⁰ we examined the levels of VEGFR2 in the same cell lines. However, the correlation between tMUC1 and VEGFR2 levels were not consistent among the cell lines (Figure 1b).

Thus, we determined whether MUC1 regulated the expression of NRP1 by conducting gain- and loss-of-function studies. The full-length human MUC1 was stably transfected into two tMUC1^{low} cells, a human pancreatic cell line BxPC3 and a mouse pancreatic cell line Panc02. The overexpression of tMUC1 was confirmed by flow cytometry (Figure 1c left panel) and by western blotting (Figure 1c right panels). In BxPC3.MUC1 and Panc02.MUC1 cells, tMUC1 overexpression induced significantly higher expression of NRP1 than their control counterparts carrying the empty vector (BxPC3.Neo and Panc02.Neo) (Figure 1c right panels and Supplementary Figure S1b). On the other hand, three tMUC1^{hi} cell lines (HPAC, CFPAC and HPAC) treated with MUC1-specific siRNA showed dramatically reduced MUC1 and moderately decreased NRP1 expression, although not statistically significant (Figures 1d and e). Protein expression of tMUC1 and NRP1 relative to β -actin was shown in Figure 1e. Whether this regulation was direct or indirect was yet to be delineated.

Increased expression of NRP1, VEGFR and VEGF in tumor cells derived from spontaneous Muc1⁺ PDA mouse

We have established two mouse PDA cell lines, KC and KCKO, from spontaneously arising PDA tumors in wild-type (Muc1 intact) and in Muc1-null mice, respectively.²⁷ A gene microarray was conducted in these two cells and in BxPC3.MUC1 and BxPC3.Neo cells as well. Among those altered genes, KC and BxPC3.MUC1 cells showed higher NRP1 levels than those in KCKO and BxPC3.Neo cells (data not shown). Thus, we confirmed expression of Muc1 and NRP1 in KC cells by flow cytometry (Figure 2a) and western blotting (Figure 2b and Supplementary Figure S2). Compared with KCKO, KC cells displayed higher levels of Muc1 (Figure 2a left panel and Figure 2b) and moderately higher level of NRP1 (Figure 2a right panel and Figure 2b). In addition, Muc1^{hi} KC cells expressed higher levels of VEGFR2 than the Muc1-null KCKO cells (Figure 2b).

Further, KC cells secreted significantly higher levels of VEGF than KCKO cells (Figure 2c), which could be partially inhibited by NRP1 antagonist A7R (Figure 2d) without affecting cell numbers (Figure 2e). These data may suggest that the NRP1-VEGFR2 signaling may positively regulate VEGF secretion and this may be partially dependent on Muc1 expression in PDA cells.

Muc1-expressing PDA cells promote endothelial cell tube formation through VEGF signaling

As endothelial tube formation assay is used as a surrogate for angiogenesis, we studied the influence of conditioned medium from tumor cells on endothelial cell tube formation and whether signaling via NRP1 was required. As shown in Figure 3a, murine endothelial 2H11 cells endogenously expressed high levels of NRP1 and VEGFR2. Functionally, capillary-like structure formation is one of the most important morphological changes during angiogenesis and can be quantified by counting the sprouting and branching of endothelial cells.³¹ As compared with conditioned medium from KCKO cells, the medium from KC cells induced enhanced tube formation in 2H11 cells (5 h post incubation) (Figure 3b). Tube formation was partially suppressed by blocking NRP1 activity with A7R or by neutralizing VEGF (Figure 3d). Combination of A7R with anti-VEGF antibody had additive effect in significantly inhibiting the tubular structure formation on the matrigel basement (Figure 3d). The quantitative results were shown in Figures 3c and e. In addition, direct pretreatment of KC cells with A7R effectively decreased VEGF secretion in the supernatant (Supplementary Figure S3a). Further, the supernatant from A7R-pretreated KC cells induced significantly less tube formation (Supplementary Figures S3b and c).

NRP1 has a critical role in promoting ectopic blood vessel formation and enhancing metastatic spread in a zebrafish embryo xenograft model

As MUC1/VEGF signaling increased the *in vitro* endothelial cell tube formation (Figure 3), we evaluated the role *in vivo*. The zebrafish/tumor xenotransplantation has been characterized as a whole-animal model to study tumor angiogenesis *in vivo*.³² In this zebrafish model, we studied whether the xenograft of tMUC1^{hi}/NRP1^{hi} cells affected formation of ectopic blood vessel (number and length) 1 day post tumor cell injection. We showed for the first time that human PDA cell line, BxPC3.MUC1 promoted a significant increase in the number and length of ectopic vessels than its BxPC3.Neo counterpart (Figures 4a and b, see arrows). Furthermore, compared with BxPC3.Neo cells, BxPC3.MUC1 cells exhibited significantly more metastasis by showing their migration away from the site of injection (Figures 4c and d). To elucidate the role of NRP1 in the tumor-induced angiogenesis and metastasis, BxPC3.MUC1 cells with or without A7R treatment were injected into the zebrafish embryo. A known angiogenesis

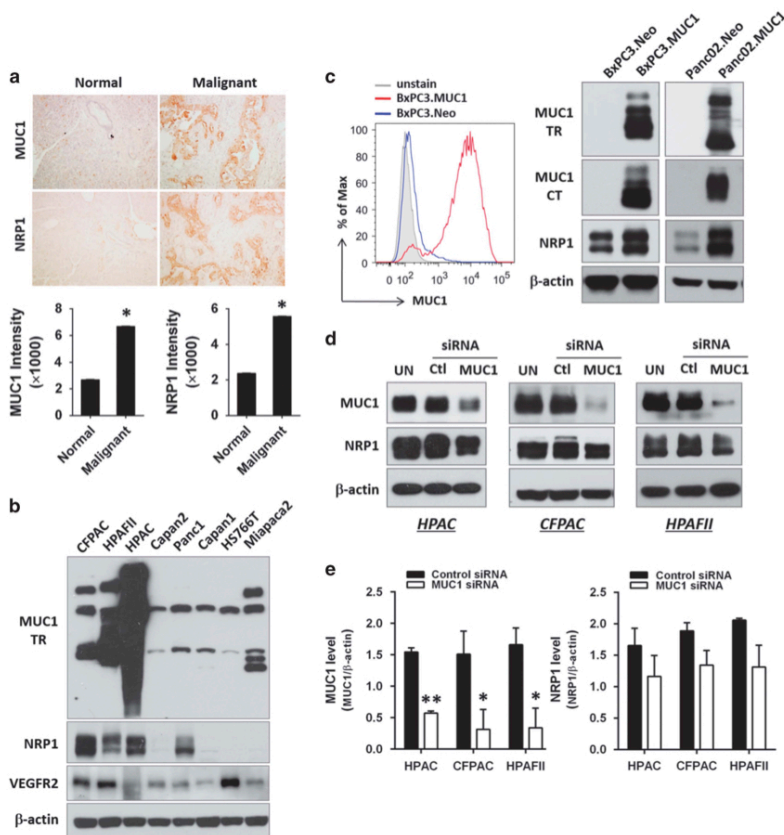


Figure 1. In PDA, tMUC1 may regulate NRP1 protein expression. **(a)** IHC staining in human pancreas tissues. The top panels show representative images and the bottom panels show the intensity quantification for protein expression. **(b)** Western blotting of total cell lysates from a panel of human pancreatic cell lines. β -actin was included as control for equal loading of protein. **(c)** Gain of function. BxPC3 (human) and Panc02 (murine) PDA cell lines were stably transfected with full-length human MUC1. Left panel, tMUC1 expression in BxPC3 cells analyzed by flow cytometry. Cells were left unstained or stained with tMUC1-specific TAB004 antibody. Right panel, tMUC1 and NRP1 expression analyzed by western blotting. CT, cytoplasmic tail; TR, tandem repeat. **(d)** Loss of function. Western blotting of cell lysates from tMUC1^{hi} cells treated with control small interfering RNA (siRNA; Ctl), MUC1-specific siRNA (MUC1) or left untreated (UN) for 48 h (in HPAFII) or 72 h (in HPAC and CFPAC). **(e)** The quantification of repeated experiments for **d** with ImageJ software. * $P < 0.05$ and ** $P < 0.01$.

inhibitor, PTK787 was used as a positive control that blocks all known VEGFR tyrosine kinases.^{33,34} We observed moderately reduced growth of ectopic vessels and tumor cell metastasis in the embryos treated with PTK787. However, A7R treatment significantly blocked ectopic vessel formation and metastatic spread, implicating a critical involvement of NRP1 (Figure 4e).

Muc1 upregulates NRP1 and creates a pro-angiogenic niche *in vivo*
To further demonstrate that high expression of Muc1 may create a pro-angiogenic niche *in vivo*, spontaneously arising tumors from PDA mice were assessed for the expression of angiogenesis-related proteins by immunohistochemistry (IHC) staining. Expression of NRP1, VEGF, CD31 and proliferating cell nuclear antigen (PCNA) was higher in the spontaneously arising KC than KCKO tumors (Figure 5a). It was noted that the NRP1 and PCNA

expressions were mainly localized to the epithelial layer of ductal region.

To understand the mechanism of NRP1-associated VEGF signaling, lysates from KC and KCKO tumors were analyzed for the VEGFR2 phosphorylation and proteins of other angiogenesis-related pathways. Western blotting data were summarized in Figure 5b and quantified (Supplementary Figure S4). Interestingly, not only were the levels of NRP1 and VEGFR2 significantly lower in the KCKO tumors, the phosphorylation of VEGFR2 at tyrosine sites of 1175 and 996 were also lower as well (Figure 5b), which was likely due to the lower level of receptor itself. Tyrosine1175 is essential for VEGF-induced kinase activation, including PLC- γ and mitogen-activated protein kinase, and for VEGF-induced proliferation of endothelial cells.³⁵ Other sites of tyrosine autophosphorylation include Tyr996 along with Tyr951, 1054 and

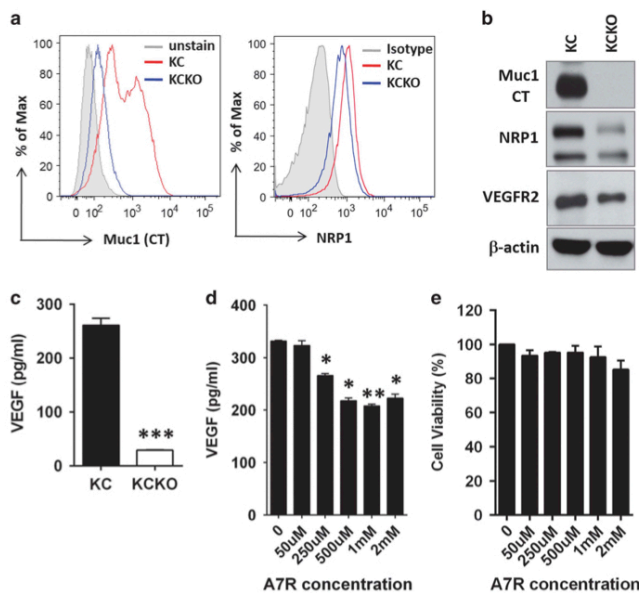


Figure 2. Muc1-expressing spontaneous mouse PDA cells have increased NRP1 expression and VEGF production. (a) KC cells were positive for Muc1 and expressed higher NRP1 than KCKO cells by flow cytometry analysis. (b) The expression of Muc1, NRP1 and VEGFR2 were assessed in cell lysates by western blotting. (c) KC cells produced more VEGF determined by enzyme-linked immunosorbent assay (ELISA). *** $P < 0.001$. (d) NRP1 antagonist A7R suppressed VEGF production in KC cells. * $P < 0.05$ and ** $P < 0.01$. (e) No significant effect of A7R on KC cell viability determined by MTT (3-(4,5-dimethylthiazol-2-yl)-2,5-diphenyltetrazolium bromide) assay.

1059.^{36,37} Moreover, levels of N-Cadherin and Vimentin were higher, while E-Cadherin was lower in KC versus KCKO tumors (Figure 5b), suggestive of EMT transition. Together, the data suggested that lack of Muc1 impaired the expression of NRP1 and VEGFR2, and thereby downregulated the angiogenic and EMT signaling, which are potential pre-requisites for metastasis.

Blockade of NRP1 signaling attenuates tMUC1^{hi} tumor growth *in vivo*

Based on the above findings, we lastly validated the activity of NRP1 antagonist A7R in tumor-bearing mice. In the immunocompetent C57BL/6 mice, the growth of KC tumor was significantly reduced over time by subcutaneous injection of A7R (Figure 6a). Nude mice bearing BxPC3.MUC1 tumors also responded to the monotherapy with A7R, displaying significantly lower tumor burden and with four out of seven mice showing a complete response (Figure 6b). Western blotting data from A7R-treated KC tumors further confirmed that the *in vivo* inhibition of NRP1 activity by A7R led to the reduction of VEGFR2 activation, as evidenced by decreased phosphorylation at Tyr1175 (Figure 6c and Supplementary Figure S5). In addition, interestingly, the protein level of NRP1 was clearly reduced by suppressing its own activity, suggesting a possible autocrine regulation of NRP1 expression via the VEGFR2 signaling.

Primary human PDA tumors express varying levels of NRP1

The tumors from pancreatic cancer patients expressed tMUC1 and NRP1 as shown in Figure 1a. In addition, the IHC staining verified the presence of pro-angiogenic factors including VEGF, CD31 and PCNA in the tumors (Figure 7a). Using a pancreatic cancer tissue

array, tMUC1 expression was detected in all PDA tissues restricted to the ductal epithelia, but the intensity of expression varied (Supplementary Figure S6a). Normal adjacent pancreas tissue also showed MUC1 staining but was restricted to the acinar secretions and absent in the ductal epithelial cells (data not shown). Similarly, NRP1 was expressed at varying levels in the tumors from the same 40 PDA patients. Closely but not exactly, we found the higher the tMUC1 expression in PDA, the stronger the NRP1 expression (Figures 7b and c, and Supplementary Figure S6). A nonparametric Spearman's correlation of 0.70 was achieved with $n = 65$ tissue cores, which was highly significant ($P < 0.0001$) and indicated a positive association between the MUC1 and NRP1 in human PDA.

DISCUSSION

To the best of our knowledge, we are the first to demonstrate that tMUC1 in PDA may have a role in VEGF signaling through the upregulation of VEGF co-receptor NRP1 (Figures 1 and 2), and that blocking the interaction between VEGF₁₆₅ and NRP1 within the tumor microenvironment has therapeutic benefit *in vivo* (Figure 6). Positive staining for NRP1 in $n = 41$ patient PDA sections (Figure 7) substantiates the clinical relevance of this protein as a potential therapeutic target.

Our previous study has shown that the spontaneously arising Muc1/MUC1-expressing PDA mice developed aggressive tumors and had poor survival than PDA mice null for Muc1/MUC1.²⁷ tMUC1 enhances the molecular process of EMT, promotes the expression of pro-angiogenic and pro-metastatic proteins in PDA,²⁵ and make tumors more drug resistant.^{26,38} In this study, we found a positive correlation between tMUC1 expression and NRP1 level in PDA cell lines and tumors (Figures 1 and 2), which

5612

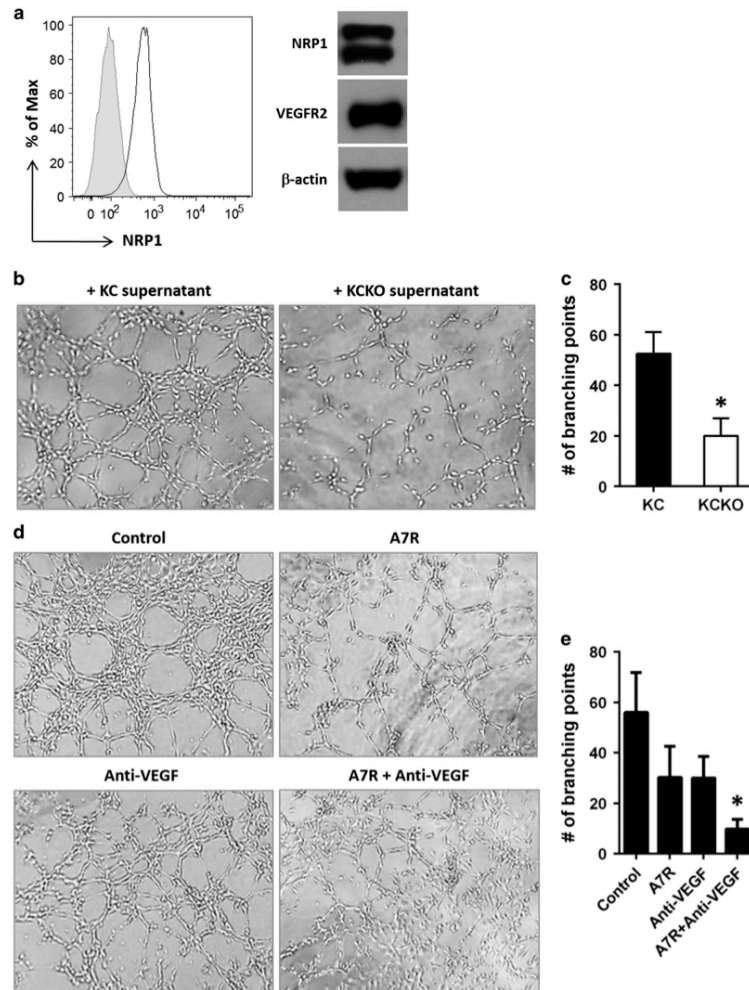


Figure 3. KC cell conditioned medium induces stronger tube formations in 2H11 endothelial cells, which can be reversed by blocking VEGF signaling. **(a)** 2H11 cells expressed NRP1 and VEGFR2, determined by flow cytometry (left panel) and western blotting (right panel). Gray-shaded histogram, isotype staining; open white histogram, anti-NRP1 staining. **(b)** KC (Muc1^{hi}) cell conditioned medium induced more capillary-like structure in 2H11 cells. **(c)** Quantification of tube formation in **b** with ImageJ. * $P < 0.05$. **(d)** Reversal of tube formation by NRP1 blockade and VEGF neutralization. KC cell conditioned medium was pre-incubated with 500 μ M of A7R and/or 2 μ g/ml of anti-VEGF antibody for 2 h before adding to 2H11 cells on Matrigel. **(e)** Quantification of tube formation in **d**.

may suggest the contribution of NRP1 to the malignant progression of tMUC1^{hi} tumor.

It has been proposed that VEGF can signal through NRP1 in tumor and endothelial cells by (1) autocrine signaling in tumor cells to inhibit tumor cell apoptosis, (2) paracrine signaling from tumor cells to endothelial cells for angiogenesis induction, or (3) juxtacrine signaling in both cells in which VEGF may bind to NRP1 on tumor cells and bind to VEGFR2 on endothelial cells simultaneously for NRP1 induction of angiogenesis and tumor

growth.^{16,39} We found that although blockade of NRP1 activity inhibited VEGF-induced extracellular signal-regulated kinase and Akt activation in KC cells (data not shown), the cell proliferation and survival were not affected (data not shown), indicating that the NRP1-dependent extracellular signal-regulated kinase and Akt activation may have roles in other aspects of tumor growth. We further found that NRP1 was involved in VEGF production probably by VEGF self-regulation through VEGFR–NRP1 signaling. The partial reduction of VEGF by NRP1 antagonism in tMUC1^{hi}

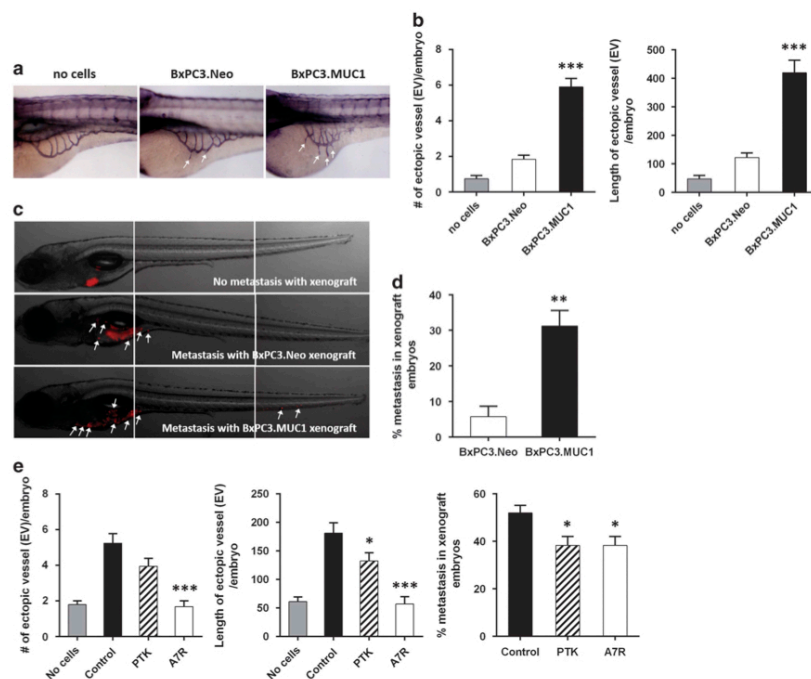


Figure 4. NRP1 is essential in promoting ectopic blood vessel formation and enhancing tumor cell metastasis in a zebrafish embryo xenograft model. **(a)** Representative images of zebrafish embryo with formation of new ectopic blood vessels, as pointed with white arrows. **(b)** Quantitative measurement of number and length of ectopic vessels formed in the embryo. $***P < 0.001$ between BxPC3.Neo group and BxPC3.MUC1 group. **(c)** Representative images of zebrafish embryo with metastatic lesions. The metastatic spread of tumor cells from the site of injection was pointed with white arrows. **(d)** The percentage of metastasis in the embryo. $**P < 0.01$ between BxPC3.Neo group and BxPC3.MUC1 group. **(e)** Suppression of ectopic vessel formation (length and number) and metastatic spread in embryo by VEGFR or NRP1 antagonists. Statistics was performed between control and treatment groups. $*P < 0.05$ and $***P < 0.001$.

cells might emphasize its role as a co-receptor for VEGFR2, but also suggested the involvement of other signaling cascades. Woo *et al.*²⁸ has reported the MUC1 overexpression/insulin-like growth factor-1–insulin-like growth factor-1 receptor/Akt/VEGF signaling in the human breast carcinoma models, which could be one of the possibilities involved in our models. Although we did not prove the juxtacrine signaling between tumor cells and endothelial cells here, it was obvious from Figure 3c that PDA cells could directly promote the formation of capillary structure in endothelial cells through soluble factors. VEGF was not the only soluble contributor for tube formation, as neutralization of VEGF only partially suppressed the tube induction. However, combination of A7R treatment with VEGF neutralization displayed additive benefit in suppressing endothelial tube formation (Figure 3e). As blocking NRP1 on either tumor cell (Supplementary Figure S3) or endothelial cell (Figures 3d and e) effectively decreased the tube formation, it shed light on the NRP1 as a promising target for tumor-associated angiogenesis.

Furthermore, BxPC3 cells with high tMUC1/NRP1 could enhance new vessel formation in the zebrafish embryo xenotransplantation model (Figures 4a and b) and they were also highly migratory (Figures 4c and d). These activities were largely dependent on NRP1 as demonstrated by its blockade (Figure 4e). Together, our data strongly suggested that tMUC1 increased NRP1 level, which was essential for tumor-associated angiogenesis and metastasis.

Despite the advantages and simplicity of the zebrafish model, the spontaneously arising PDA mouse model resembles more closely the human disease. We found minimal expression of pro-angiogenic proteins (VEGF, NRP1, CD31 and PCNA) in tumors from Muc1^{null} KCKO mice when compared with tumors from Muc1^{hi} KC mice (Figure 5a). In addition, the NRP1, VEGFR2 and its activation forms of Tyr1175 and Tyr996 were significantly higher in the KC versus KCKO tumors (Figure 5b). These data strongly indicate that increased NRP1/VEGF signaling in tMUC1^{hi} tumors correlates with enhanced angiogenesis *in vivo*. However, as both tumor cells and endothelial cells express NRP1 and other VEGF signaling molecules (Figures 2 and 3), the contribution of intratumoral endothelial cells for their expression and activation could not be excluded. In addition, there was also biased expression of EMT markers in KC tumors versus KCKO tumors, which may favor the KC cell invasion and metastasis. In our early publication, we found that the cytoplasmic tail of MUC1 translocates to the nucleus in association with β -catenin, represses E-Cadherin expression and upregulates the level of the EMT inducers Snail, Slug, Vimentin and Twist.²⁵ VEGF and NRP1 have been found to directly promote EMT.⁴⁰ Besides, it has been proposed that NRP1 enhances signaling in three major pathways that are linked to EMT, that is, transforming growth factor β 1, Hedgehog and hepatocyte growth factor and its receptor (cMet).¹² Together, we speculate that in the presence of high tMUC1, the increased NRP1

5614

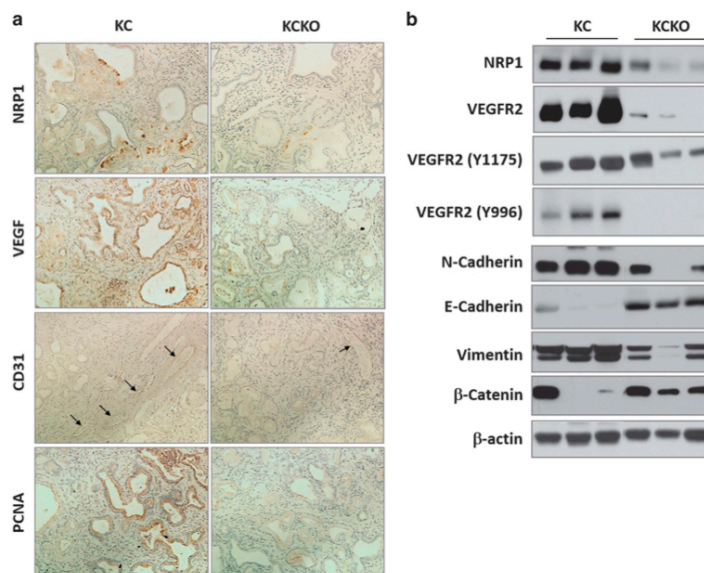


Figure 5. tMUC1 enhances proteins associated with angiogenesis and EMT. (a) Higher expression of angiogenesis-associated proteins in spontaneously developed KC tumor compared with KCKO tumor. (b) Higher VEGF signaling and EMT switch in Muc1-expressing KC tumor. KC and KCKO cells were subcutaneously injected into C57BL/6 mice. After 26 days, tumors were subcutaneously collected and lysates were analyzed by western blotting. Data from three mice out of six to eight mice were shown.

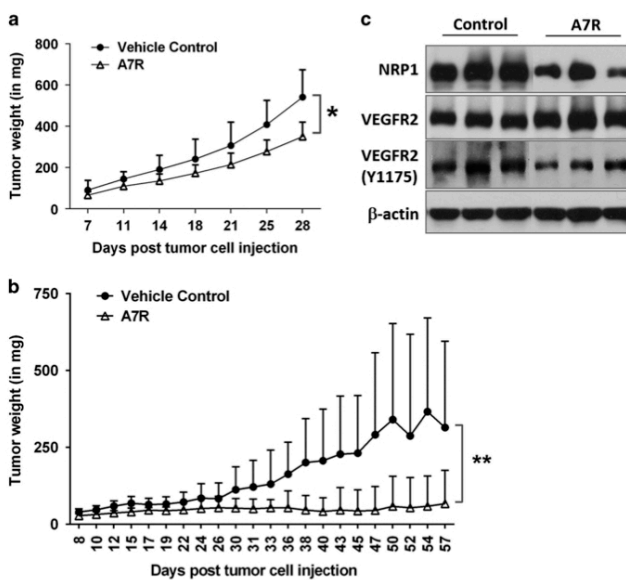


Figure 6. NRP1 antagonist A7R retards tumor growth *in vivo*. (a) Treatment with A7R attenuated KC tumor growth in C57BL/6 mice. $*P < 0.05$. (b) Treatment with A7R attenuated BxPC3.MUC1 tumor growth in nude mice. $**P < 0.01$. (c) A7R treatment *in vivo* reduced NRP1 level as well as VEGFR2 phosphorylation at Tyr1175. Data from three mice out of seven mice were shown.

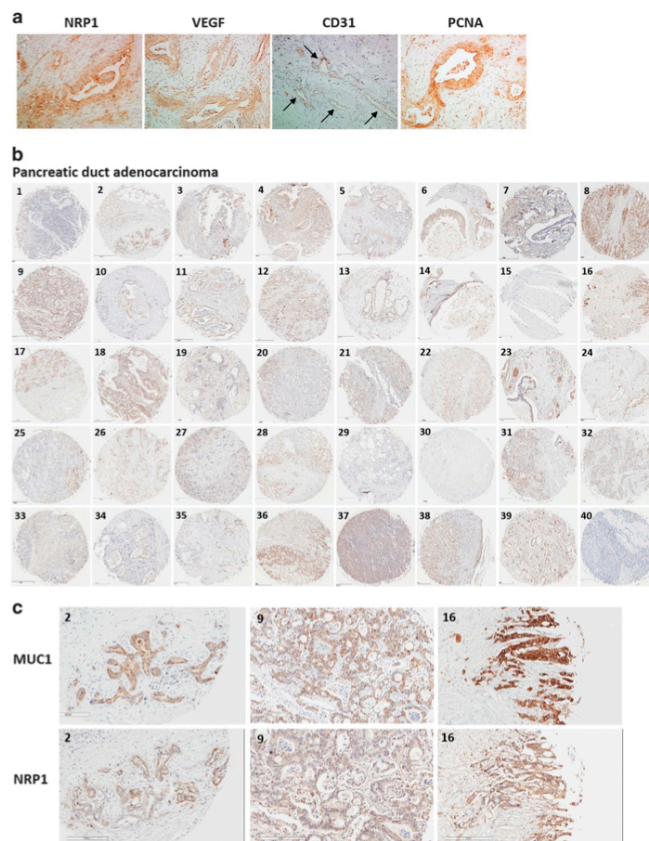


Figure 7. Primary human PDA tumors express NRP1 and other angiogenesis-associated proteins. **(a)** High expression of angiogenesis-associated proteins in primary human PDA tissue. The CD31⁺ vessels were pointed by black arrows. **(b)** Pancreas tissue microarray for NRP1 expression. Representative images of $n=40$ PDA cores were shown at $\times 40$ magnification. The pathologic/diagnostic information was provided in Supplementary Table S1. **(c)** MUC1 and NRP1 staining in PDA tissues from the same patients: images from cores 2, 9 and 16 were shown at higher magnification. Using 65 such cores, a nonparametric Spearman's correlation of 0.70 was achieved, which was highly significant ($P < 0.0001$) and indicated a positive association between the two biomarkers (Supplementary Figure S6).

may have dual roles in both VEGFR2-associated angiogenesis and EMT-led metastasis, resulting in the aggressive tumor growth.

Finally, targeting NRP1 activity with a 7-mer peptide, A7R, inhibited the tMUC1^{hi} tumor growth of both mouse and human origin but had little effect on tMUC1-low cells (data not shown). A7R competes with VEGF₁₆₅ for binding to NRP1 without affecting its binding to VEGFR2.²² As a result, it partially prevented VEGFR2 activation *in vivo* (Figure 6c), decreased NRP1 protein level and in turn led to retardation of tumor growth (Figures 6a and b). Furthermore, we observed high expression of these pro-angiogenic factors including NRP1, VEGF and CD31 in spontaneous mouse PDA tumors and in the primary human PDA tissues, signifying the clinical relevance of this study. It may thus be promising to target NRP1 along with other standard therapies for treatment of tMUC1^{hi} PDA. As recently discovered, NRP1 and NRP2 actually have much broader activities. They bind transforming growth factor β 1 and its receptors, hepatocyte growth factor/

cMet, platelet-derived growth factor and its receptors, fibroblast growth factors and integrins. They also promote Hedgehog signaling. These ligands and pathways are all relevant to angiogenesis and wound healing. In the immune system, the NRPs are expressed primarily on dendritic cells and regulatory T cells, and exert mainly inhibitory effects. They promote EMT, and the survival and self-renewal of cancer stem cells.^{41–43} These important functions of NRP1 are extremely relevant to this study, as tMUC1 is expressed on pancreatic cancer stem cells⁴⁴ and is associated with platelet-derived growth factor signaling, EMT and drug resistance^{25,26,38} in pancreatic cancer. Further, tumors with high tMUC1 shows higher prevalence of T-regulatory cells and myeloid-derived suppressor cell population in the tumor draining lymph nodes and tumor-infiltrating lymphocytes.⁴⁵ Thus, the precise mechanism for tumor inhibition by A7R will need to be further demonstrated.

In conclusion, despite the complex role of NRP1 in endothelial and tumor cells, and in tumor progression, NRP1 may be an excellent target for treating tMUC1^{hi} PDA. Our current study lays the ground for combinational therapy of NRP1 antagonist with standard-of-care drugs. We recognize that previous trials with drugs targeting angiogenesis have produced serious side effects, including hypertension, thrombotic events and allergic reactions. Several phase I studies of the human monoclonal anti-NRP1 antibody MNRP1685A in patients with solid tumors have shown its inhibition of the VEGF pathway, either alone or in combination with VEGF blockade.^{46–48} It is well accepted that drug delivery into the pancreas is difficult, as PDA is highly desmoplastic with dense stroma. Thus, compared with the anti-NRP1 antibody therapy, a small peptide antagonist against NRP1 is probably more effective to get into tumor. In the next study we propose targeted drug delivery by conjugating NRP1 inhibitors to a tMUC1-specific antibody and combine this with other standard chemotherapy, which might be highly efficacious for treatment of tMUC1^{hi} PDA.

MATERIALS AND METHODS

Spontaneous mouse models and tissue culture

KC mice were generated in our laboratory on C57BL/6 background by mating the P48-Cre with the LSL-KRAS (G12D) mice.⁴⁹ They were further mated with the Muc1 knockout mice to generate KCKO mice.⁵⁰ The respective KC and KCKO cell lines were generated and maintained as described previously.²⁷ The animal study protocol was approved by the Institutional Animal Care and Use Committee of the University of North Carolina at Charlotte. Animal care and use were in compliance with institutional guidelines.

Cell culture

Selected human pancreatic cancer cell lines (CFPAC, HPAC, Capan1, Capan2, Panc1, HS766T and Miapaca2) were obtained from American Type Culture Collection and cultured as instructed. BxPC3.Neo and BxPC3.MUC1 were generated as described previously.²⁵ Panc02.Neo and Panc02.MUC1 cells were originally gifted by Dr Hollingsworth (University of Nebraska) and maintained in medium with Geneticin (G418; Invitrogen, Carlsbad, CA, USA). Murine endothelial 2H11 cell line was kindly provided by Dr Didier Dreau (Department of Biological Sciences, University of North Carolina at Charlotte).

NRP1 antagonist A7R

The A7R peptide (ATWLPPR) was synthesized by Selleck Chemicals (Houston TX, USA) and also by Shengnuo Peptide USA (Menlo Park, CA, USA). A7R was dissolved in phosphate-buffered saline (PBS) and sterilized by filtration.

siRNA transfection

HPAC, CFPAC and HPACII cells were plated at 3 000 000 cells/well in six-well plates and grown to 50% confluence. Cells were transfected with human MUC1-specific siRNA (Dharmacon, Lafayette, CO, USA) or control siRNA (Cell Signaling Technologies, Danvers, MA, USA) in Lipofectamine 2000 transfection reagent (Invitrogen), in accordance with the manufacturer's instructions. MUC1 and NRP1 protein levels were determined after transfection.

Flow cytometry

Cells were stained for human MUC1 with TAB004 (OncoTab Inc., Charlotte, NC, USA⁴⁴) conjugated with Cy5.5 (Abcam, Cambridge, MA, USA) and for mouse NRP1 with CD304-APC (Biolegend, San Diego, CA, USA). For mouse Muc1, cells were fixed in 4% paraformaldehyde (Sigma-Aldrich, St Louis, MO, USA) and permeabilized with Triton X-100 (Fisher Scientific, Waltham, MA, USA), stained with CT2 antibody (kind gift from Dr Gendler at Mayo Clinic Arizona⁵¹), followed by Phycoerythrin (PE)-conjugated anti-Armenian hamster antibody (BD Biosciences, San Jose, CA, USA). Data were acquired on BD LSRFortessa flow cytometer (BD Biosciences) and analyzed with FlowJo software (version 8.8.7; FLOWJO, Ashland, OR, USA).

Ezyme-linked immunosorbent assay

KC and KCKO cells were plated overnight, followed by serum starvation for 24 h. Cell conditioned medium (culture supernatant) was collected and frozen at -80°C . For A7R treatment, various concentrations of A7R were added into serum-free cell culture for 24 h. The VEGF concentration was determined by enzyme-linked immunosorbent assay (R&D Systems, Minneapolis, MN, USA).

MTT (3-(4,5-dimethylthiazol-2-yl)-2,5-diphenyltetrazolium bromide) assay

KC cells were plated as triplicate overnight and treated with various concentrations of A7R in serum-free medium for 24 h. The cell viability was determined by Vybrant MTT Cell Proliferation Assay Kit (Life Technologies, Grand Island, NY, USA).

Tube formation assay

A 96-well tissue culture plate was coated with 50 μl /well of growth factor-reduced Matrigel (BD Biosciences), which was allowed to solidify at 37°C for 30 min. 2H11 murine endothelial cells (4×10^4 cells/50 μl /well) was added to the Matrigel in the presence of different treatments and incubated at 37°C for varying times. Cells were photographed using a phase contrast microscope (Nikon USA, Garden City, NY, USA). Tube formation was quantified by counting the average number of branching points in four randomly selected fields, using $\times 40$ magnification.

Western blotting

Western blotting was performed as previously described.²⁵ CT2 and TAB004 antibodies were used. NRP1 antibody was purchased from Abcam and β -actin antibody from Santa Cruz Biotechnology (Dallas, Texas, USA). Other antibodies were purchased from Cell Signaling Technologies. The density of signal was quantified by ImageJ (version 1.49e; National Institutes of Health, Bethesda, MD, USA) and summarized as Supplementary Data.

IHC staining

Tissues were fixed in 10% neutral-buffered formalin. Paraffin-embedded blocks were prepared by the Histology Core at the Carolina Medical Center and 4- μm -thick sections were cut for staining. IHC was performed as described previously.²⁵ Representative images were taken at $\times 100$ or $\times 200$ magnification and quantified by CaresBio Laboratory (Shelton, CT, USA). Antibodies for NRP1 and CD31 were from Abcam, and antibodies for VEGF and PCNA were from Santa Cruz. Horseradish peroxidase-conjugated TAB004 was used for tMUC1 staining at 1:750 dilution. The normal and malignant patient pancreas tissues were kindly provided by National Cancer Institute. The tissue microarray slides were purchased from US Biomax (Rockville, MD, USA). The staining procedure for NRP1 was adapted from literature published previously.⁵² The tissue microarray slides were deparaffinized in xylene, rehydrated in a series of ethanol (100, 95 and 70%) followed by tap water and PBS, and then subjected to antigen retrieval in 99°C water bath for 40 min. The activity of endogenous peroxidases was blocked by 2% hydrogen peroxide for 15 min. The slides were washed twice in PBS, followed by PBS containing 0.05% Triton X-100, for 5 min each wash. The slides were blocked with 5% normal goat serum for 1 h at room temperature and then incubated with diluted NRP1 antibody (1:200) overnight at 4°C . The tissues were washed twice in PBS and incubated with secondary goat anti-rabbit antibody (1:100). The signal was enhanced by one-step incubation with Vectastain Elite ABC reagent (Vector Laboratories, Burlingame, CA, USA) for 30 min at room temperature. The substrate 3,3'-diaminobenzidine was added for 5 min, followed by counterstaining with Mayer's hematoxylin solution. The tissue microarray tissues were then dehydrated in a series of ethanol, immersed into xylene and mounted using Permount (Fisher Scientific).

Zebrafish/tumor xenograft model

The transplantation of tumor cells into zebrafish embryos is described in details by Moshal et al.⁵³ In brief, tumor cells were stained with chloromethylbenzamide-Dil (showing red fluorescence, Invitrogen) and injected at the superficial location of the yolk near the perivitelline space of the 2-day-old zebrafish embryos. Six days later, the metastatic spread of the chloromethylbenzamide-Dil-labeled tumor cells from the site of injection represented metastasis. Imaging was performed using an

Olympus MVX10 MacroView Fluorescence Microscope (Olympus, Center Valley, PA, USA) with Hamamatsu C9300-221 high-speed digital charge-coupled device camera (Hamamatsu City, Japan).

The tumor-induced angiogenic response was evaluated on the new vasculature sprouting from the developing subintestinal vessels by using whole-mount alkaline phosphatase staining. One day after transplantation, the zebrafish embryos were fixed in 4% paraformaldehyde and stained for endogenous alkaline phosphatase activity using nitroblue tetrazolium and 5-bromo-4-chloro-3-indolyl phosphate (Roche Applied Science, Indianapolis, IN, USA). Images were taken by using Nikon SMZ1500 fluorescent stereomicroscope with digital color camera DXM1200c (Nikon Instruments, Lewisville, TX, USA). The number and length of the newly formed ectopic blood vessels were quantified by using NIS-Element AR software (Nikon Instruments) for analysis; $N = 100$ embryos/each group.

Where appropriate, A7R at 1 mm was mixed with tumor cell suspension right before cell injection. PTK787 (Santa Cruz Biotechnology) at 0.1 μM was added into the embryo culture medium right after tumor cell injection; $N = 33$ embryos/each group.

In vivo tumor growth

Eight- to 10-week-old C57BL/6 mice were subcutaneously injected with KC cells at 4×10^6 cells/mouse (in 100 μl PBS) into the flank. Nude mice (JNU) were subcutaneously injected with BxPC3.MUC1 cells at 4×10^6 cells/mouse (in 100 μl PBS) into the flank. When tumor reached $\sim 30\text{--}60$ mm³, the mice were treated subcutaneously with A7R at 100 mg/kg (for KC tumor) or 20 mg/kg (for BxPC3.MUC1 tumor) in 100 μl PBS, close to tumor, three times a week. Caliper measurements were taken by investigator and tumor weight was calculated according to the formula: weight (mg) = (length in mm \times (width in mm)²)/2.²⁷ On killing, the tumors were weighed, prepared for tissue lysates and fixed for IHC. Mice were from Jackson Laboratory (Bar Harbor, ME, USA) and randomly assigned as seven mice/group.

Statistical analysis

Data were analyzed with GraphPad Prism 6 software (GraphPad Software, La Jolla, CA, USA). Results were expressed as mean \pm s.d. where indicated and were representative of two or more independent experiments. Significance was determined by unpaired Student's *t*-test or two-way analysis of variance ($*P < 0.05$, $**P < 0.01$ and $***P < 0.001$). A nonparametric Spearman's correlation (SAS program; SAS Institute, Cary, NC, USA) was used to determine the association between MUC1 and NRP1 in patient samples.

ABBREVIATIONS

EMT, epithelial-to-mesenchymal transition; IHC, immunohistochemistry; NRP1, neuropilin-1; PCNA, proliferating cell nuclear antigen; PDA, pancreatic ductal adenocarcinoma; siRNA, small interfering RNA; tMUC1, tumor-associated MUC1

CONFLICT OF INTEREST

Dr Pinku Mukherjee is a board member in OncoTab. Dr Lopamudra Das Roy is an employee of OncoTab. The other authors declare no conflict of interest.

ACKNOWLEDGEMENTS

This study was supported by NIH CA118944-01A1 and NIH CA173668-01. This work was also supported by the Office of the Assistant Secretary of Defense for Health Affairs through the Pancreatic Cancer Research Program under Award No. W81XWH-12-1-0220. Opinions, interpretations, conclusions, and recommendations are those of the author and are not necessarily endorsed by the Department of Defense. We thank Dr Tim D Eubank (Department of Internal Medicine, The Ohio State University, Columbus, Ohio, USA) for the valuable support with angiogenesis study. We thank Dr Lloye Dillon (OncoTAB, Inc., Charlotte, NC, USA) for the critical review of the manuscript. We thank all the technicians in the animal facility for their assistance in maintaining our colonies.

REFERENCES

- Roskoski R Jr. Vascular endothelial growth factor (VEGF) signaling in tumor progression. *Crit Rev Oncol Hematol* 2007; **62**: 179–213.
- Ferrara N, Davis-Smyth T. The biology of vascular endothelial growth factor. *Endocr Rev* 1997; **18**: 4–25.

- Whittle C, Gillespie K, Harrison R, Mathieson PW, Harper SJ. Heterogeneous vascular endothelial growth factor (VEGF) isoform mRNA and receptor mRNA expression in human glomeruli, and the identification of VEGF148 mRNA, a novel truncated splice variant. *Clin Sci (Lond)* 1999; **97**: 303–312.
- Robinson CJ, Stringer SE. The splice variants of vascular endothelial growth factor (VEGF) and their receptors. *J Cell Sci* 2001; **114**: 853–865.
- Park JE, Chen HH, Winer J, Houck KA, Ferrara N. Placenta growth factor. Potentiation of vascular endothelial growth factor bioactivity, *in vitro* and *in vivo*, and high affinity binding to Flt-1 but not to Flk-1/KDR. *J Biol Chem* 1994; **269**: 25646–25654.
- Waltenberger J, Claesson-Welsh L, Siegbahn A, Shibuya M, Heldin CH. Different signal transduction properties of KDR and Flt1, two receptors for vascular endothelial growth factor. *J Biol Chem* 1994; **269**: 26988–26995.
- Seetharam L, Gotoh N, Maru Y, Neufeld G, Yamaguchi S, Shibuya M. A unique signal transduction from FLT tyrosine kinase, a receptor for vascular endothelial growth factor VEGF. *Oncogene* 1995; **10**: 135–147.
- Pajusola K, Aprelikova O, Korhonen J, Kaipainen A, Pertovaara L, Alitalo R et al. FLT4 receptor tyrosine kinase contains seven immunoglobulin-like loops and is expressed in multiple human tissues and cell lines. *Cancer Res* 1992; **52**: 5738–5743.
- Kaipainen A, Korhonen J, Mustonen T, van Hinsbergh VW, Fang GH, Dumont D et al. Expression of the fms-like tyrosine kinase 4 gene becomes restricted to lymphatic endothelium during development. *Proc Natl Acad Sci USA* 1995; **92**: 3566–3570.
- Wild JR, Staton CA, Chapple K, Corfe BM. Neuropilins: expression and roles in the epithelium. *Int J Exp Pathol* 2012; **93**: 81–103.
- He Z, Tessier-Lavigne M. Neuropilin is a receptor for the axonal chemorepellent Semaphorin III. *Cell* 1997; **90**: 739–751.
- Prud'homme GJ, Glinka Y. Neuropilins are multifunctional coreceptors involved in tumor initiation, growth, metastasis and immunity. *Oncotarget* 2012; **3**: 921–939.
- Tordjman R, Lepelletier Y, Lemarchandel V, Cambot M, Gaulard P, Hermine O et al. A neuronal receptor, neuropilin-1, is essential for the initiation of the primary immune response. *Nat Immunol* 2002; **3**: 477–482.
- Bruder D, Probst-Kepper M, Westendorp AM, Geffers R, Beissert S, Loser K et al. Neuropilin-1: a surface marker of regulatory T cells. *Eur J Immunol* 2004; **34**: 623–630.
- Bagri A, Tessier-Lavigne M, Watts RJ. Neuropilins in tumor biology. *Clin Cancer Res* 2009; **15**: 1860–1864.
- Staton CA, Kumar I, Reed MW, Brown NJ. Neuropilins in physiological and pathological angiogenesis. *J Pathol* 2007; **212**: 237–248.
- Pan Q, Chantry Y, Liang WC, Stawicki S, Mak J, Rathore N et al. Blocking neuropilin-1 function has an additive effect with anti-VEGF to inhibit tumor growth. *Cancer Cell* 2007; **11**: 53–67.
- Pellet-Many C, Frankel P, Jia H, Zachary I. Neuropilins: structure, function and role in disease. *Biochem J* 2008; **411**: 211–226.
- Bielenberg DR, Pettaway CA, Takashima S, Klagsbrun M. Neuropilins in neoplasms: expression, regulation, and function. *Exp Cell Res* 2006; **312**: 584–593.
- Latil A, Bieche I, Pesche S, Valeri A, Fournier G, Cussenot O et al. VEGF overexpression in clinically localized prostate tumors and neuropilin-1 overexpression in metastatic foci. *Int J Cancer* 2000; **89**: 167–171.
- Binetruy-Tournaire R, Demangel C, Malavaud B, Vassy R, Rouyre S, Kraemer M et al. Identification of a peptide blocking vascular endothelial growth factor (VEGF)-mediated angiogenesis. *EMBO J* 2000; **19**: 1525–1533.
- Starzec A, Vassy R, Martin A, Lecouvey M, Di Benedetto M, Crepin M et al. Antiangiogenic and antitumor activities of peptide inhibiting the vascular endothelial growth factor binding to neuropilin-1. *Life Sci* 2006; **79**: 2370–2381.
- Chang BW, Siccion E, Saif MW. Updates in locally advanced pancreatic cancer. Highlights from the "2010 ASCO Annual Meeting". Chicago, IL, USA. June 4–8, 2010. *JOP* 2010; **11**: 313–316.
- Lan MS, Batra SK, Qi WN, Metzgar RS, Hollingsworth MA. Cloning and sequencing of a human pancreatic tumor mucin cDNA. *J Biol Chem* 1990; **265**: 15294–15299.
- Roy LD, Sahraei M, Subramani DB, Besmer D, Nath S, Tindler TL et al. MUC1 enhances invasiveness of pancreatic cancer cells by inducing epithelial to mesenchymal transition. *Oncogene* 2011; **30**: 1449–1459.
- Sahraei M, Roy LD, Curry JM, Teresa TL, Nath S, Besmer D et al. MUC1 regulates PDGFA expression during pancreatic cancer progression. *Oncogene* 2012; **31**: 4935–4945.
- Besmer DM, Curry JM, Roy LD, Tindler TL, Sahraei M, Schettini J et al. Pancreatic ductal adenocarcinoma mice lacking mucin 1 have a profound defect in tumor growth and metastasis. *Cancer Res* 2011; **71**: 4432–4442.
- Woo JK, Choi Y, Oh SH, Jeong JH, Choi DH, Seo HS et al. Mucin 1 enhances the tumor angiogenic response by activation of the AKT signaling pathway. *Oncogene* 2012; **31**: 2187–2198.

- 29 Lau SK, Weiss LM, Chu PG. Differential expression of MUC1, MUC2, and MUC5AC in carcinomas of various sites: an immunohistochemical study. *Am J Clin Pathol* 2004; **122**: 61–69.
- 30 Parikh AA, Liu WB, Fan F, Stoeltzing O, Reinmuth N, Bruns CJ *et al*. Expression and regulation of the novel vascular endothelial growth factor receptor neuropilin-1 by epidermal growth factor in human pancreatic carcinoma. *Cancer* 2003; **98**: 720–729.
- 31 Guidolin D, Vacca A, Nussdorfer GG, Ribatti D. A new image analysis method based on topological and fractal parameters to evaluate the angiostatic activity of docetaxel by using the Matrigel assay in vitro. *Microvasc Res* 2004; **67**: 117–124.
- 32 Moshal KS, Ferri-Lagneau KF, Leung T. Zebrafish model: worth considering in defining tumor angiogenesis. *Trends Cardiovasc Med* 2010; **20**: 114–119.
- 33 Hess-Stump H, Haberey M, Thierauch KH. PTK 787/ZK 222584, a tyrosine kinase inhibitor of all known VEGF receptors, represses tumor growth with high efficacy. *Chembiochem* 2005; **6**: 550–557.
- 34 Solorzano CC, Baker CH, Bruns CJ, Killion JJ, Ellis LM, Wood J *et al*. Inhibition of growth and metastasis of human pancreatic cancer growing in nude mice by PTK 787/ZK222584, an inhibitor of the vascular endothelial growth factor receptor tyrosine kinases. *Cancer Biother Radiopharm* 2001; **16**: 359–370.
- 35 Takahashi T, Yamaguchi S, Chida K, Shibuya M. A single autophosphorylation site on KDR/Flk-1 is essential for VEGF-A-dependent activation of PLC-gamma and DNA synthesis in vascular endothelial cells. *EMBO J* 2001; **20**: 2768–2778.
- 36 Bernatchez PN, Soker S, Sirois MG. Vascular endothelial growth factor effect on endothelial cell proliferation, migration, and platelet-activating factor synthesis is Flk-1-dependent. *J Biol Chem* 1999; **274**: 31047–31054.
- 37 Shibuya M, Claesson-Welsh L. Signal transduction by VEGF receptors in regulation of angiogenesis and lymphangiogenesis. *Exp Cell Res* 2006; **312**: 549–560.
- 38 Nath S, Daneshvar K, Roy LD, Grover P, Kidyoor A, Mosley L *et al*. MUC1 induces drug resistance in pancreatic cancer cells via upregulation of multidrug resistance genes. *Oncogenesis* 2013; **2**: e51.
- 39 Miao HQ, Lee P, Lin H, Soker S, Klagsbrun M. Neuropilin-1 expression by tumor cells promotes tumor angiogenesis and progression. *FASEB J* 2000; **14**: 2532–2539.
- 40 Mak P, Leav I, Pursell B, Bae D, Yang X, Taglienti CA *et al*. ERbeta impedes prostate cancer EMT by destabilizing HIF-1alpha and inhibiting VEGF-mediated snail nuclear localization: implications for Gleason grading. *Cancer Cell* 2010; **17**: 319–332.
- 41 Prud'homme GJ. Cancer stem cells and novel targets for antitumor strategies. *Curr Pharm Des* 2012; **18**: 2838–2849.
- 42 Beck B, Driessens G, Goossens S, Youssef KK, Kuchnio A, Cauwe A *et al*. A vascular niche and a VEGF-Nrp1 loop regulate the initiation and stemness of skin tumours. *Nature* 2011; **478**: 399–403.
- 43 Hamerlik P, Lathia JD, Rasmussen R, Wu Q, Bartkova J, Lee M *et al*. Autocrine VEGF-VEGFR2-Neuropilin-1 signaling promotes glioma stem-like cell viability and tumor growth. *J Exp Med* 2012; **209**: 507–520.
- 44 Curry JM, Thompson KJ, Rao SG, Besmer DM, Murphy AM, Grdzlishvili VZ *et al*. The use of a novel MUC1 antibody to identify cancer stem cells and circulating MUC1 in mice and patients with pancreatic cancer. *J Surg Oncol* 2013; **107**: 713–722.
- 45 Tinder TL, Subramani DB, Basu GD, Bradley JM, Schettini J, Million A *et al*. MUC1 enhances tumor progression and contributes toward immunosuppression in a mouse model of spontaneous pancreatic adenocarcinoma. *J Immunol* 2008; **181**: 3116–3125.
- 46 Xin Y, Li J, Wu J, Kinard R, Weekes CD, Patnaik A *et al*. Pharmacokinetic and pharmacodynamic analysis of circulating biomarkers of anti-NRP1, a novel antiangiogenesis agent, in two phase I trials in patients with advanced solid tumors. *Clin Cancer Res* 2012; **18**: 6040–6048.
- 47 Weekes CD, Beeram M, Tolcher AW, Papadopoulos KP, Gore L, Hegde P *et al*. A phase I study of the human monoclonal anti-NRP1 antibody MNRP1685A in patients with advanced solid tumors. *Invest New Drugs* 2014; **32**: 653–660.
- 48 Patnaik A, LoRusso PM, Messersmith WA, Papadopoulos KP, Gore L, Beeram M *et al*. A Phase Ib study evaluating MNRP1685A, a fully human anti-NRP1 monoclonal antibody, in combination with bevacizumab and paclitaxel in patients with advanced solid tumors. *Cancer Chemother Pharmacol* 2014; **73**: 951–960.
- 49 Hingorani SR, Petricoin EF, Maitra A, Rajapakse V, King C, Jacobetz MA *et al*. Preinvasive and invasive ductal pancreatic cancer and its early detection in the mouse. *Cancer Cell* 2003; **4**: 437–450.
- 50 Spicer AP, Rowse GJ, Lidner TK, Gendler SJ. Delayed mammary tumor progression in Muc-1 null mice. *J Biol Chem* 1995; **270**: 30093–30101.
- 51 Schroeder JA, Thompson MC, Gardner MM, Gendler SJ. Transgenic MUC1 interacts with epidermal growth factor receptor and correlates with mitogen-activated protein kinase activation in the mouse mammary gland. *J Biol Chem* 2001; **276**: 13057–13064.
- 52 Adham SA, Al Harrasi I, Al Haddabi I, Al Rashdi A, Al Sinawi S, Al Maniri A *et al*. Immunohistological insight into the correlation between neuropilin-1 and epithelial-mesenchymal transition markers in epithelial ovarian cancer. *J Histochem Cytochem* 2014; **62**: 619–631.
- 53 Moshal KS, Ferri-Lagneau KF, Haider J, Pardhanani P, Leung T. Discriminating different cancer cells using a zebrafish in vivo assay. *Cancers (Basel)* 2011; **3**: 4102–4113.

Supplementary Information accompanies this paper on the Oncogene website (<http://www.nature.com/onc>)

Antibody-Guided *In Vivo* Imaging for Early Detection of Mammary Gland Tumors^{1,2}



Laura Jeffords Moore^{*}, Lopamudra Das Roy^{*,†},
Ru Zhou^{*}, Priyanka Grover^{*}, Shu-ta Wu^{*},
Jennifer M. Curry^{*}, Lloye M. Dillon^{*,†},
Priya M. Puri^{*}, Mahboubeh Yazdanifar^{*},
Rahul Puri[†], Pinku Mukherjee^{*,†} and Didier Dréau^{*}

^{*}Department of Biological Sciences, University of North Carolina at Charlotte, 9201 University City Blvd., Charlotte, NC 28223 USA; [†]OncoTAB, Inc., 243 Bioinformatics, 9201 University City Blvd., Charlotte, NC 28223, USA

Abstract

BACKGROUND: Earlier detection of transformed cells using target-specific imaging techniques holds great promise. We have developed TAB 004, a monoclonal antibody highly specific to a protein sequence accessible in the tumor form of MUC1 (tMUC1). We present data assessing both the specificity and sensitivity of TAB 004 *in vitro* and in genetically engineered mice *in vivo*. **METHODS:** Polyoma Middle T Antigen mice were crossed to the human MUC1.Tg mice to generate MMT mice. In MMT mice, mammary gland hyperplasia is observed between 6 and 10 weeks of age that progresses to ductal carcinoma *in situ* by 12 to 14 weeks and adenocarcinoma by 18 to 24 weeks. Approximately 40% of these mice develop metastasis to the lung and other organs with a tumor evolution that closely mimics human breast cancer progression. Tumor progression was monitored in MMT mice (from ages 8 to 22 weeks) by *in vivo* imaging following retro-orbital injections of the TAB 004 conjugated to indocyanine green (TAB-ICG). At euthanasia, mammary gland tumors and normal epithelial tissues were collected for further analyses. **RESULTS:** *In vivo* imaging following TAB-ICG injection permitted significantly earlier detection of tumors compared with physical examination. Furthermore, TAB-ICG administration in MMT mice enabled the detection of lung metastases while sparing recognition of normal epithelia. **CONCLUSIONS:** The data highlight the specificity and the sensitivity of the TAB 004 antibody in differentiating normal versus tumor form of MUC1 and its utility as a targeted imaging agent for early detection, tumor monitoring response, as well as potential clinical use for targeted drug delivery.

Translational Oncology (2016) 9, 295–305

Introduction

In the past decade, survival of patients with breast cancer has improved [1–3]. Routine mammograms and other screening approaches have been associated with early detection of breast cancers [4,5]. However, the repeated use of mammograms is not without risk [4], and clinical guidelines remain highly debated [4]. Chiefly, mammograms overall miss 25% of tumors and up to 50% of the tumors in late-stage diagnosis of women with extremely dense breasts [4,6–8], resulting in late stage diagnosis. It is becoming clear that cancer cells undergo specific molecular transformations long before there is a detectable change in tumor morphology. The ability to detect at these earliest stages of molecular dysregulation, before any

Address all correspondence to: Didier Dréau, PhD, Department of Biological Sciences and Center for Engineering and Biological Sciences, University of North Carolina at Charlotte, 9201 University City Blvd., Charlotte, NC 28223 USA.

E-mail: ddreau@uncc.edu

¹Funding: Supported in part through a grant from the North Carolina Biotechnology Center. The funding sources had no involvement in study design; in the collection, analysis, and interpretation of data; in the writing of the report; or in the decision to submit the article for publication.

²Conflict of interest: Drs. Rahul Puri, Pinku Mukherjee, Lopamudra das Roy, and Lloye Dillon are, respectively, CEO, CSO, and employees of OncoTAB Inc., a startup company that own patents and rights to the TAB 004 antibody. Other authors declare no conflict of interest. Received 26 February 2016; Revised 28 April 2016; Accepted 2 May 2016

© 2016 The Authors. Published by Elsevier Inc. on behalf of Neoplasia Press, Inc. This is an open access article under the CC BY-NC-ND license (<http://creativecommons.org/licenses/by-nc-nd/4.0/>). 1936-5233/16

<http://dx.doi.org/10.1016/j.tranon.2016.05.001>

obvious symptoms have developed, would permit better therapeutic intervention. Thus, the concept of molecularly targeted diagnostic approaches would be very valuable.

MUC1 is a conserved transmembrane protein with an extensive extracellular domain composed of repeated glycosylated peptide motifs [9,10]. In tumor cells including breast tumors, these motifs are hypoglycosylated and the MUC1 distribution is altered [11–13]. In addition, as early as hyperplasia stages, the distribution and glycosylation of MUC1 are altered and the cell-cell organization disrupted [12,14]. As such, MUC1 is viewed as a key therapeutic target in patients with breast cancer [15,16]. In breast cancers, presence of circulatory MUC1 is associated with cancer progression and can be monitored through detection of MUC1 (CA-15-3 antigen) circulatory concentrations [17–19]. However, CA-15-3 tests rely mostly on the tumor burden and shed MUC1 and lack the specificity to identify hypoglycosylated MUC1, a hallmark of breast cancer progression. We have developed a new antibody that specifically detects altered hypoglycosylated form of MUC1 (tMUC1): TAB 004 (OncoTAB, Inc., Charlotte, NC) [20].

Breast cancer progression is uniquely modeled in the immune-competent spontaneous murine MMT model [10,21]. Derived from the PyMT model of spontaneous breast cancer and genetically engineered to express the human form of hypoglycosylated mucin-1 (tMUC1), the MMT mice develop spontaneous mammary gland tumors expressing the human form of tMUC1 [10]. In those mice, as in the parental PyMT mice, mammary gland hyperplasia is observed between 6 and 10 weeks of age that progresses to ductal carcinoma *in situ* by 12 to 14 weeks and adenocarcinoma by 18 to 24 weeks, and approximately 40% of the mice develop metastasis to the lung and other organs [10]. In MMT mice, mammary tumor evolution closely mimics human breast cancer progression. The tumors are basal in cell origin and Her-2+ subtype [10].

Here we investigated the specificity and sensitivity of TAB 004 for the early detection and monitoring of mammary tumor progression in the MMT mice. Results indicate that TAB 004 specifically immunoreacts with human tMUC1 and, when conjugated to an imaging agent, indocyanine green (ICG), allows the early detection and monitoring of mammary tumor progression and metastases by *in vivo* imaging systems.

Material and Methods

Chemical and Reagents

TAB 004 was graciously provided for the study by OncoTAB Inc. Conjugation kits to derive biotin-conjugated, horseradish peroxidase (HRP)-conjugated, and ICG-conjugated TAB 004 were obtained from Dojindo Molecular Technologies, Inc. (Rockville, MD) and used according to manufacturers' recommendations.

Generation of TAB 004 Antibody

Briefly, TAB 004 antibody (patent #US-2011-0123442, PCT/US2011/037972) is a mouse IgG1 monoclonal antibody obtained through the hybridoma approach and selected for its specific binding to extracellular repeated sequences of tumor associated MUC1 altered, i.e., hypoglycosylated MUC1 protein specifically the TAPPA sequence and the specific epitope (STAPPVHNV) [20]. The production of TAB 004 is currently conducted in batches of antibody rigorously assayed for consistent binding, stability, and purity (Supplemental Figure 1S, A–C; LakePharma Inc., Belmont, CA).

Cells and In Vitro Cultures

Murine cells PyMT and MMT were derived as described previously [10]. The PyMT cell line was derived from PyMT tumor, and the MMT cell line was obtained by stably expressing full-length MUC1 in PyMT cells. Both cell lines were derived in Dr. Mukherjee's laboratory originally in 1998 and stored in multiple vials in liquid nitrogen. Cells were authenticated by polymerase chain reaction for specific DNA signatures for the polyoma middle T antigen; the MMTV promoter; and, for MMT cells, the human MUC1 gene. Additionally, in MMT cells, the cell surface expression of human MUC1 was also assessed by Western blot (WB) and flow cytometry. For this study, the PyMT and MMT cells used were authenticated using the characterization methods described above within 6 to 12 months of their use. All cells used either to generate lysates or for cytometry investigations were cultured in sterile conditions in Dulbecco's modified Eagle's medium in the presence of antibiotics and antifungals supplemented with FBS and incubated at 37°C, >90% humidity, and 5% CO₂ conditions.

Orthotopic Mammary Tumor Model

MMT cells were implanted in the mammary pad of C57bl/6 6- to 8-week-old female mice, and the tumor growth was monitored using both physical examination including caliper to measure tumor growth and fluorescent monitoring as described for MMT spontaneous tumor model (see below). Controls included mice similarly implanted with PyMT cells. Furthermore, the route of injection of TAB 004 was assessed in the orthotopic model. Briefly, C57bl/6 mice implanted orthotopically with MMT tumor cells were injected 2 to 3 weeks post-tumor implantation with either saline (vehicle control) or intratumorally, intravenously, or intraperitoneally with TAB 004 conjugated with biotin, and tissues including tumor, spleen, kidneys, liver, and lungs were collected 24 hours later. Tissues were fixed and embedded in paraffin, and the presence of biotin-conjugated TAB 004 in the different tissues was assessed following incubation with streptavidin-HRP and 3,3'-diaminobenzidine (DAB). As shown in Figure 2S, in the absence of antibody, no HRP activity was detected. HRP activity associated with the HRP-conjugated TAB 004 antibody was faintly, highly, and strongly detected in tumor following intratumoral, intravenous, and intraperitoneal injections, respectively. With the exception of the spleen, in animals administered biotin-conjugated TAB 004 intravenously, no other organ exhibited an HRP activity associated with the HRP-conjugated TAB 004 antibody.

Specificity and Sensitivity of TAB 004 Antibody

The presence of altered MUC-1 was also determined by flow cytometry and WB on PyMT and MMT murine cells using TAB 004. Briefly, for flow cytometry analyses, cells were grown in culture conditions described above; detached from vessels; and, following a blocking step incubated with TAB 004 antibody (30 minutes) and after a secondary antibody stain (15 minutes), run on a Fortessa flow cytometer (BD-Biosciences, San Jose, CA). Raw data were further analyzed using FlowJo Software (Ashland, OR). Data are presented as histogram with information on mean fluorescence intensity and percentage of positive cells along with controls. Additionally, PyMT and MMT cell lysates and MMT tumor mass lysates were assessed by WBs. Briefly, lysates were obtained from cell cultured as described above and from MMT tumors through incubation with lysis buffer as described previously [22,23]. Cell lysates were stored at –80°C until use. Following electrophoresis in reducing conditions and transfer to

polyvinylidene difluoride membranes, the presence of altered tMUC1 was determined using TAB 004 antibody (overnight, 4°C) and revealed using ECL reagent (ThermoFisher Scientific, Waltham, MA). β -Actin was used as the loading control.

Monitoring Mammary Tumor Growth in the MMT Spontaneous Murine Model

All mice were monitored and followed in accordance with the University of North Carolina at Charlotte Institutional Animal Care and Use Committee–approved protocol. MMT mice were genetically derived from PyMT mice (C57BL/6 background) that spontaneously develop mammary tumors and specifically express MUC1 [10]. Spontaneous tumor progression follows a similar time line in PyMT and MMT female mice. From puberty (6–8 weeks old) onward, mammary tissues expressing the polyoma middle T antigen driven by the MMTV promoter mimic all the steps of breast cancer progression in humans including hyperplasia, ductal carcinoma *in situ*, invasive carcinoma, and metastasis [10] at any given time from 8 up to 22 to 24 weeks of age. Furthermore, multiple tumor masses at different stages are present in this spontaneous model of breast cancer progression. This murine model is aggressive as most animals (>95%) develop multiple mammary tumor lesions which are usually palpable by 14 to 16 weeks of age [10]. The main difference in tumor progression between PyMT and MMT mice is the expression of murine and human MUC1 glycoprotein, respectively [10].

Here, MMT mice were monitored *in vivo* for tumor progression using the *in vivo* imaging system (IVIS; Perkin Elmer, Waltham, MA). Both C57BL/6 and PyMT mice were used as controls. *In vivo* monitoring was conducted according to manufacturer's recommendations, following injections of TAB 004 conjugated with the fluorophore indocyanine green (TAB-ICG). ICG has been shown to have no significant side effects and is currently FDA-approved for multiple procedures including angiography [24]. Before each imaging sequence, TAB-ICG in sterile saline was administered retro-orbitally or intraperitoneally to mice, and imaging was conducted 0.5, 4, 24, and 48 hours postinjection. Animals were injected and imaged every 2 weeks for tumor progression. Tumor fluorescence was analyzed using the Life Science Software Suite (Perkin Elmer), and region of interest was defined at tumor location. In parallel, the presence of tumor masses was assessed by palpation and recorded. Additionally, after mouse euthanasia, further analyses of tumors (T) and specific organs including mammary pads (MP), liver (Li), lungs (Lu), spleen (S), and kidneys (K) were conducted *ex vivo* using the IVIS system and by histology and immunohistochemistry (IHC; see below).

MMT spontaneous mammary tumor growth was also monitored over time for gross pathology, cellular morphology, and the presence of specific markers including tMUC1 using IHC with TAB 004 antibody (see below).

Monitoring Mammary Tumor Lung Metastases in the MMT Spontaneous Murine Model

In the PyMT and MMT mouse models, early metastases, which occur in the lungs, is masked *in vivo* by the fluorescence emitted by larger tumors. Therefore, *ex vivo* analyses of organs isolated post-euthanasia were conducted using the IVIS system. The fluorescence signal (expressed as fluorescence units) was normalized to the background fluorescence generated by each organ specifically the lung, liver, spleen, and brain from control MMT mice (i.e., MMT mice not injected with TAB-ICG). Additionally, the presence of lung metastases was determined following fixation, embedding,

and sectioning of the lungs of MMT mice. Briefly, lungs from animals 16 weeks or older were collected 24 hours postinjections and embedded in paraffin. Five- to six-micrometer-thick sections were obtained, stained with hematoxylin and eosin (H&E), and examined for the presence of metastases.

Detection of tMUC1 by IHC

The expression of human altered MUC1 (tMUC1) was determined in murine tumors using TAB 004. Murine tumors from PyMT and MMT mice and normal mammary gland from C57bl/6 mice were collected. Samples were fixed in buffered formalin and embedded in paraffin, and 5- to 6- μ m-thick sections were obtained. In addition to H&E staining, murine samples were assessed for expression of tMUC1 using TAB 004 antibody. Briefly, either unconjugated TAB 004 antibody followed with a second step detection with an anti-mouse HRP-conjugated secondary antibody or the TAB 004-HRP conjugated was used. The staining procedure includes a blocking step, incubation with primary antibody (overnight, 4°C) and secondary antibody (1 hour), or incubation with primary antibody conjugated with HRP (overnight, 4°C). In both approaches, the presence of TAB 004 antibody was revealed using DAB with a hematoxylin counterstain followed by mounting the tissue slides. Tissue slides were then assessed by light microscopy, and microphotographs were taken using a DP70 camera and the Olympus Software Suite (Olympus, Waltham, MA).

Statistical Analyses

The linearity associating TAB 004 dose with the detection of tMUC1 was assessed by linear regression. The difference between methods in early detection time was determined by unpaired *t* test. The detection of lung metastases was assessed by one-way ANOVA followed with *post hoc* tests with *a priori* significance sets at $P < .05$.

Results

The MMT Murine Model Mimics Human Breast Cancer Progression

The MMT mouse model has been described previously [10]. Briefly, as schematized in Figure 1A, this spontaneous model of mammary tumor progression was developed through the generation of double transgenic mice by crossing of mice expressing human MUC1 gene [25] and mice expressing the polyoma middle T antigen under the MMTV promoter [26]. PyMT and MMT tumor cell lines were also developed (Figure 1A). Over time, MMT tumors mimic the stages and cellular morphology of human breast cancer progression (Figure 1B). Furthermore, the biomarker tumor profiles indicate a decrease in both estrogen receptors (ERs) and progesterone receptors (PRs), increase in Neu and Cyclin D1, and decrease in integrin β as tumor progresses mimicking the ER⁺PR⁻Neu⁺ human disease [27]. In addition, tMUC1 expression detected by TAB 004 increases as tumors progress (Figure 1B), which makes this model ideal for our studies. Importantly, TAB 004 does not recognize normal mammary epithelial tissue from non-tumor-bearing control mice (Figure 1B). The monoclonal antibody TAB 004 recognizes the hypoglycosylated tandem repeat epitope within the STAPPVHNV sequence of human MUC1 [20].

TAB 004 Specifically Recognizes tMUC1 In Situ by IHC, In Vitro by Flow Cytometry, and In Vivo Following Orthotopic Implantation of MMT Cells

PyMT and MMT cell lines were tested for tMUC1 expression *in vitro* and *in vivo*. Compared with PyMT cells, MMT cells expressed

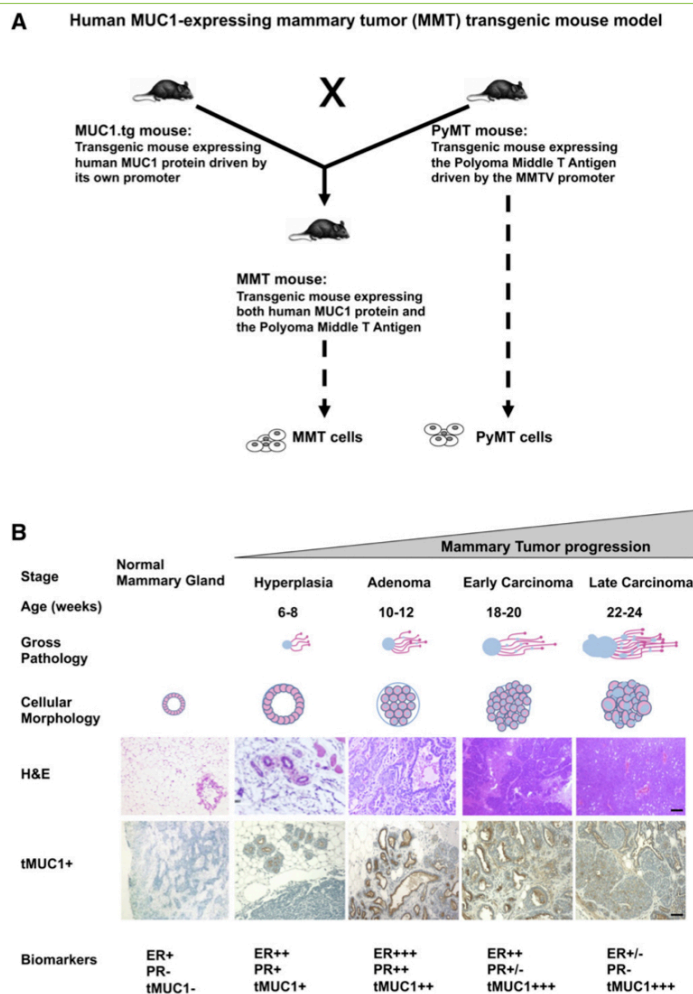


Figure 1. (A) Human MUC1-expressing mammary tumor (MMT) transgenic mouse model and associated PyMT and MMT tumor cells. Briefly, the spontaneous MMT mammary tumor model was generated through the cross of MUC1.tg mice [C57BL/6-Tg(MUC1)79.24Gend/J mice] [25] with PyMT mice [FVB/N-Tg(MMTV-PyMT)634Mul/J mice] [26]. The resulting dual transgenic female mice spontaneously develop mammary tumors that express human MUC1. Additionally, associated PyMT and MMT cell lines have been developed that are transgenic for the polyoma middle T antigen and for both the polyoma middle T antigen and human MUC1, respectively. (B) Mammary tumor growth in the MMT transgenic mouse model mimics human breast cancer progression. Briefly, in the spontaneous MMT mammary tumor model, the stages of hyperplasia, adenoma, and early and late carcinoma are identified at 6 to 8, 10 to 12, 18 to 20, and 22 to 24 weeks of age, respectively. Each stage is associated with gross pathology and cellular morphology similar to those observed in human breast cancer progression as indicated by visual observation and H&E staining. Moreover, expressions of biomarkers including ERs and PRs decreased, whereas tMUC1 expression (detected using TAB 004) increased, with mammary tumor progression as determined using specific antibodies and IHC techniques (scale bar = 200 μ m). Normal C57BL/6 mammary gland is also displayed (left) and shows no staining with TAB 004.

significantly higher levels of tMUC1 as determined by TAB 004-Cy7 staining and flow cytometry (Figure 2, A and B). Additionally, IHC staining with TAB 004-HRP confirmed that TAB 004 only binds to

the MMT tumors but not to the PyMT tumors, further indicating specificity to the human form of tMUC1 (Figure 2, C and D). To determine if TAB 004 specifically localizes to the MMT tumor when

injected *in vivo*, TAB-ICG was injected (retro-orbitally) into PyMT and MMT tumor-bearing mice, and tumor progression was successfully imaged in MMT mice over time using the IVIS system (Figure 2, E and F). Tumor volume was monitored by caliper measurements (Figure 2, G and H). Although both tumors grew at a similar rate, TAB-ICG only localized to the MMT but not in the PyMT tumors, and accumulation of TAB-ICG increased with tumor size (Figure 2, E and F).

Next, we determined the expression of tMUC1 in the spontaneously arising tumors dissected from the PyMT and MMT mice. By WB analysis, TAB 004 showed immunoreactivity with the tumor lysates from MMT but not from PyMT tumors (Figure 2I). Lysate from the MMT cell line was used as the positive control, and β -actin served as the loading control. By IHC, TAB 004 stained the MMT tumors but did not stain normal mammary epithelia or PyMT tumors (Figure 2J). Taken together, TAB 004 showed high specificity to human tMUC1 and did not bind to normal or mouse Muc1.

Monitoring of Mammary Tumor Progression Is Dependent on the Dose of TAB 004 Administered in the MMT Mice

The dose of TAB-ICG injected to monitor the presence of tumor mass within the MMT spontaneous mammary tumor model was assessed for doses ranging from 12.5 to 100 μ g (Figure 3). As expected, regardless of the dose, the tumor fluorescent signal peaked at ~24 hours and decreased thereafter, as shown in the representative IVIS images taken over time (Figure 3A). When compared with the number of palpable tumors, the number of fluorescent tumors in MMT mice (8-22 weeks old) with at least one tumor mass 24 hours postinjection of TAB-ICG varied depending on the dose of TAB-ICG administered (Figure 3B). Indeed, whereas detection following injections of 12.5 μ g or 25 μ g of TAB-ICG was high, injections of 50 μ g or 100 μ g of TAB-ICG were associated with lower tumor mass detection (Figure 3B). Furthermore, analyses limited to mice with two or more tumors (11-22 weeks old) demonstrated that the fluorescent detection was correlated with the amount of

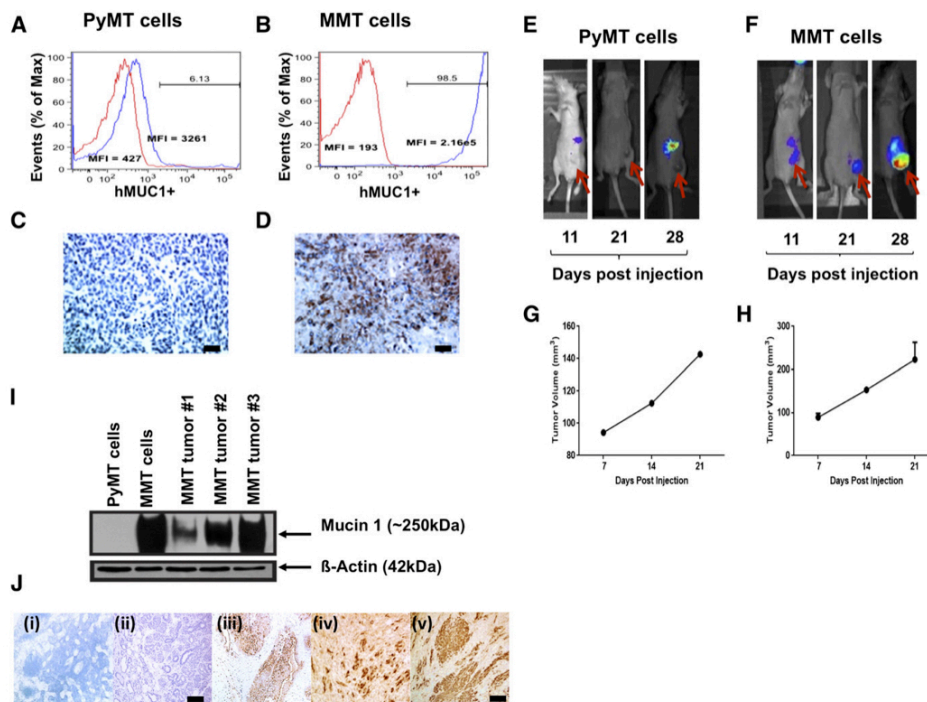


Figure 2. TAB 004 detects tMUC1 in MMT cells and allows the monitoring over time of MMT orthotopic tumor growth *in vivo*. TAB 004 detected tMUC1 in MMT cells (B) but not in PyMT cells (A) by flow cytometry and IHC (C and D), respectively (scale bar = 100 μ m). When orthotopically implanted in C57Bl/6 mice, PyMT and MMT tumors grew over time (as determined by caliper measurements) (G and H) and could be monitored using ICG-conjugated TAB 004 but only for MMT tumors (E and F). By WB, HRP-conjugated TAB 004 detected human tMUC1 in lysates from MMT cells as well as in lysates from tumors collected following orthotopic implantation of MMT tumor cells but not in lysates from PyMT cells (I). Furthermore, IHC analyses (J) of normal mammary gland [C57Bl/6 (i)], PyMT (ii) and MMT (iii, iv, v) using HRP-conjugated TAB 004 detected human tMUC1 (brown stain) only in MMT tumors (scale bar = 150 μ m).

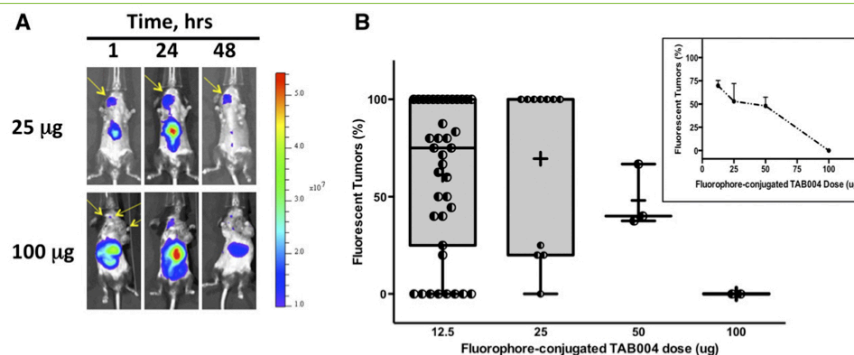


Figure 3. *In vivo* detection of mammary tumor masses in the MMT mice following TAB-ICG injection is dose-dependent. MMT mice (8-22 weeks old) with palpable tumors were repeatedly injected with ICG-conjugated TAB 004 (12.5, 25, 50, or 100 μ g in sterile saline) and monitored for fluorescence using the IVIS system. (A) Representative IVIS imaging of MMT mice injected with 25 μ g (top) and 100 μ g (bottom) of ICG-conjugated TAB 004 taken 1, 24, and 48 hours postinjection. The fluorescent scale [from low (blue) to high (red)] indicates the presence of fluorescence with varying intensity at different location with the mice monitored. (B) Tumor mass fluorescent detection (% of palpable tumors) in MMT mice with at least one tumor mass 24 hours postinjection of ICG-conjugated TAB 004. As shown, the injection of 12.5 and 25 μ g of ICG-conjugated TAB 004 was associated with improved tumor detection compared with 50 and 100 μ g. Furthermore, when only mice with two or more tumors were analyzed (B, inset), the detection increased with decreasing amount of ICG-conjugated TAB 004 injected: from 0% to 75% for 100 and 12.5 μ g, respectively ($r^2 = 0.96$, $P = .019$).

TAB-ICG injected (Figure 3B, insert). When the amount of TAB-ICG injected decreased, the detection using fluorescence increased: from 0% to 75% for 100 μ g and 12.5 μ g, respectively ($r^2 = 0.96$, $P = .019$). Thus, all subsequent studies were conducted with 12.5 μ g of TAB-ICG.

Administration of TAB-ICG Enables Specific and Overtime Monitoring of tMUC1-Positive Tumors in the MMT Mice

The MMT mouse model uniquely permits the investigation of spontaneous tumor progression in an immunocompetent mouse model [10]. In this model, tumor progression leads to multiple tumor masses heterogeneous for both size and stages [10]. Nevertheless, the MMT model closely mimics human breast cancer progression [10,27]. Here, MMT and PyMT mice at 16 weeks of age bearing multiple palpable tumors were injected with TAB-ICG. The presence of TAB-ICG was monitored *in vivo* by IVIS. As shown in Figure 4A, TAB-ICG detected multiple palpable tumor masses in MMT mice but did not accumulate in any of the PyMT tumors (Figure 4A). The nonspecific fluorescence around the liver of the mice was attributed to tissue autofluorescence.

Injections of 12.5 μ g of TAB-ICG allowed the overtime monitoring of mammary tumor progression in MMT mice (10, 14, 17, and 21 weeks of age) as indicated by representative IVIS images shown in Figure 4B. As indicated by the yellow asterisk in the 10-week-old MMT mice, we detected the tumor by fluorescence, but there were no palpable tumors at that time. As mice aged to 14 weeks, several of those tumors that were nonpalpable became palpable as indicated by the yellow arrows. At later ages (weeks 17 and 21), the yellow arrows indicate palpable tumors with accumulation of the TAB-ICG. Whereas tumor detection by palpation and fluorescence was similar in 13-week-old and older MMT mice, tumor detection following injection of TAB-ICG was significantly increased compared with palpation in MMT mice 12 weeks of age or younger

(Figure 4C). Moreover, comparison of physical examination (i.e., palpation) and TAB 004 fluorescence indicates that primary tumors were detected significantly earlier (-3.4 weeks earlier) by fluorescence monitoring than by physical examination (9.4 ± 0.7 weeks of age vs 12.8 ± 0.4 weeks of age, $n = 9$, $P = .0016$, Figure 4D). Thus, TAB-ICG has the ability to detect early stages when normal MUC1 is undergoing the molecular transformation to tMUC1 much before any obvious palpable tumors appear.

Administration of TAB-ICG Enables Monitoring of tMUC1-Positive Tumors Demonstrated by Ex Vivo Assessment of Tumors Dissected from MMT Mice

To further ascertain the potential of TAB-ICG for detection of mammary tumor masses at early onset, *ex vivo* analyses were conducted. An 18-week-old MMT mouse was injected with TAB-ICG and imaged. Figure 5A shows high fluorescent signal corresponding to a large tumor. When dissected and imaged *ex vivo*, as expected, a very strong fluorescent signal was seen corresponding to the largest tumor mass, but weak fluorescent signal was also noted in the rest of the mammary fat pads (Figure 5B), indicating that these mammary glands were not normal but had transformed to express low levels of tMUC1. Thus, when mammary fat pads from 8- to 10-week-old MMT mice were assessed following TAB-ICG injection, we once again detected low fluorescent signal in some of the mammary fat pads (Figure 5C) indicating the presence of tMUC1 at very early stages of cancer progression. H&E staining confirmed and highlighted the presence of hyperplasia in those fluorescing mammary fat pads (Figure 5E (ii)), whereas the nonfluorescing mammary fat pad was composed mostly of normal tissue (Figure 5E (i)). *Ex vivo* imaging following TAB-ICG administration of tumors and mammary fat pad dissected from 18-week-old MMT mice bearing multiple tumors revealed that the amount of fluorescent signal distinguishes between tumor masses and hyperplastic

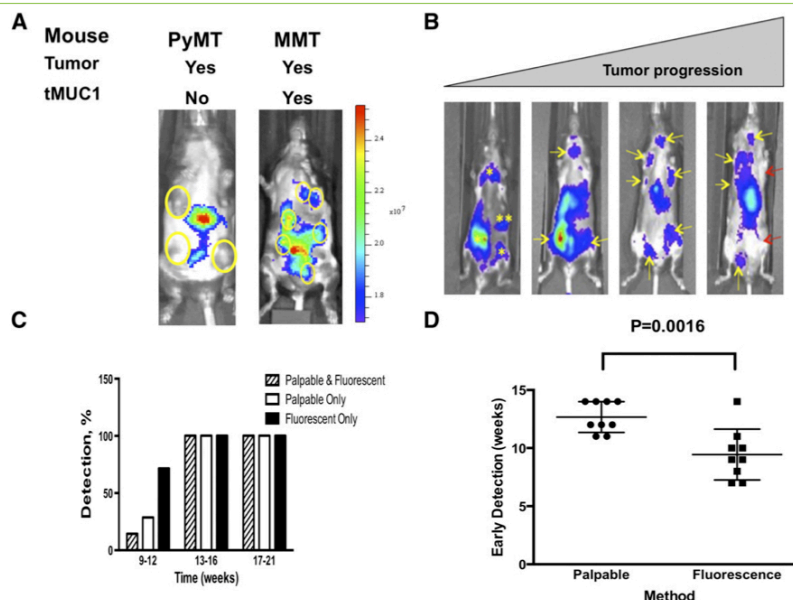


Figure 4. Early detection of primary mammary tumors in the MMT mice following TBA-ICG injection. (A) ICG-conjugated TAB 004 detected tMUC1+ tumors in MMT mice only but not in PyMT mice, where tumors were not fluorescent (only nonspecific liver fluorescence was observed). (B) Representative IVIS images of tumor masses detected in MMT mice 10, 14, 17, and 21 weeks of age. The presence of tumor mass was monitored over time in MMT mice aged 9 to 23 weeks. Both physical examination (palpation) and fluorescence monitoring using the IVIS system 24 hours postinjection of ICG-TAB 004 were collected over time. Yellow asterisks and yellow arrows indicate the presence of nonpalpable and palpable tumors, respectively, whereas red arrows note the presence of nonfluorescent palpable tumor mass essentially in older mice. (C) Whereas tumor detection by palpation and fluorescence was similar in 13-week-old and older MMT mice, tumor detection following injection of ICG-conjugated TAB 004 associated with IVIS system was increased compared with palpation in MMT mice 12 weeks old and younger. (D) Early detection indicates that primary tumors are detected significantly earlier by fluorescence monitoring than by physical examination (9.4 ± 0.7 weeks of age vs 12.8 ± 0.4 weeks of age, $n = 9$, $P = .0016$).

mammary fat pads (Figure 5D). H&E staining confirmed the extensive presence of tumor in the strongly fluorescing tumor in the 18-week-old MMT mice (Figure 5F).

Administration of TAB-ICG Allows Monitoring of tMUC1-Positive Lung Metastases Demonstrated by Ex Vivo Assessment of Fluorescent Signal in the Lungs of MMT Mice

Whether TAB 004 could detect the presence of metastases in the MMT mice was assessed *ex vivo* following *in vivo* administration of TAB-ICG. The fluorescent signal in several organs dissected from MMT mice at various ages (<16, 16-20, and >20 weeks of age) was determined using the IVIS system. No increase in fluorescence was observed in the liver, spleens, and brain of MMT mice versus normal C57BL/6 organs (data not shown). However, fluorescent signal in the lungs was significantly higher than control mouse lung, and the signal exponentially increased with the age of MMT mice (Figure 6A) [$1.71 \times 10^6 \pm 0.11 \times 10^6$, $2.21 \times 10^6 \pm 0.08 \times 10^6$, and $2.10 \times 10^6 \pm 0.05 \times 10^6$ for 8- to 11- ($n = 7$), 16- to 18- ($n = 6$), and 19- to 22- ($n = 7$) week-old MMT mice, respectively, $P < .05$]. This increase in fluorescent signal with age suggests micrometastasis in the lungs. Indeed, as in

the PyMT model, MMT mice develop metastases mainly in the lungs [10]. The presence of micrometastases was confirmed in these MMT mice following H&E staining of the lung (Figure 6B). Representative H&E shows clear lesion in the MMT lung [Figure 6B (ii)] versus no lesion in the control lung [Figure 6B (i)].

Discussion

We have demonstrated the specificity and sensitivity of TAB 004, an antibody against the hypoglycosylated form of human MUC1 (tMUC1). TAB 004 conjugated to indocyanine green (TAB-ICG) enables the *in vivo* monitoring of primary mammary tumor progression and metastasis in the MMT mice. The results highlight the early detection of neoplastic transformation as well as detect micrometastases in the lungs.

In contrast to PyMT mice, MMT mice have been genetically engineered to express human tMUC1, whereas the former express the murine form of hypoglycosylated Muc1 [10]. Those models, although significantly more aggressive than generally observed in human breast cancer progression, appropriately mimic the cancer progression from hyperplasia to adenocarcinoma and metastasis in an

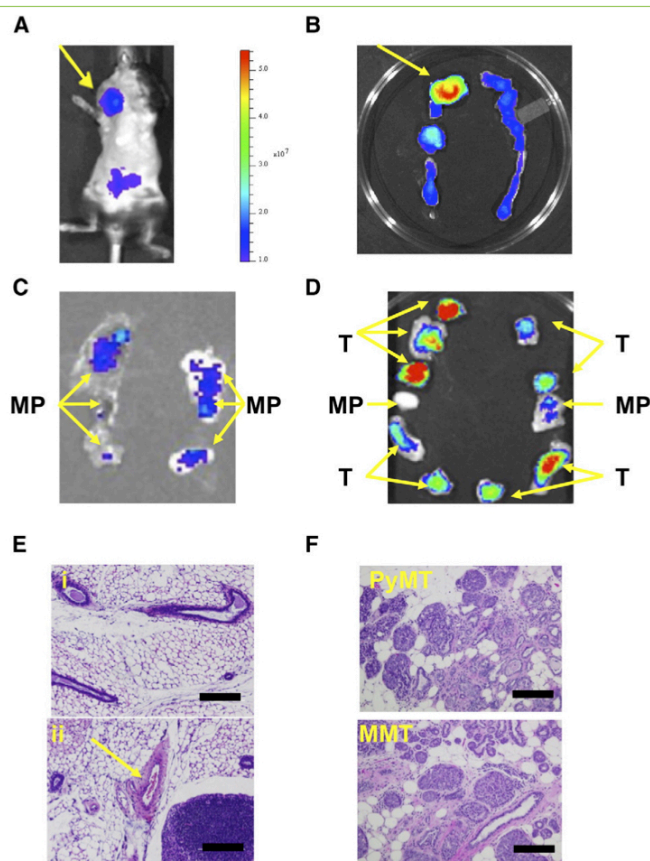


Figure 5. *Ex vivo* assessment of mammary gland tumors from MMT mice post TAB-ICG injection. Representative mouse assessed for fluorescence using IVIS system following injection of 12.5 μ g of TAB 004 conjugated with ICG *in vivo* (A) and the corresponding *ex vivo* post-euthanasia mammary fat pads assessed using the same system (B). Entire mammary ridges (left and right) isolated from a 10-week-old (C) and an 18-week-old (D) MMT mouse are displayed, and the presence within the mammary pad (MP) of tumor mass (T) is noted. Furthermore, when assessed following H&E staining (scale bar = 100 μ m), MP from the 10-week-old mouse presented mostly normal mammary tissues [E (i)]. However, even that early, hyperplasia was observed in a few areas of the MP [arrow, E (ii)]. In older mice (~18 weeks old), whether PyMT or MMT, the presence of tumor was extensive (F).

immunocompetent environment [10] and thus are appropriate models to investigate *in vivo* tumor detection.

TAB 004 specifically targets the transformed MUC1 protein with minimal immunoreactivity with the normal MUC1. This increased specificity of TAB 004 to tMUC1 expressed in the spontaneously arising mammary gland tumors in MMT mice is a novel finding and may allow earlier diagnosis of breast tumors. The specificity of TAB 004 was further demonstrated in MMT cell lines by IHC, WB, and flow cytometry. Extensive clinical research indicates that there are several molecular classifications of breast tumors based upon the expression of specific receptors (ER, PR, Her2/neu) and the cell origin (basal versus luminal). These subtypes are associated with

significant differences in patients' survival [28–30]. For instance, triple-negative breast cancers are more aggressive and difficult to treat. Those observations led to the generation of multiparameter tests (e.g., Oncotype DX, 21-gene recurrence score) to support therapeutic decision [31,32]. Although those tests have proven beneficial especially in determining specific treatment courses for a given tumor type [33,34], the tests are not useful for early diagnosis. The clinical use of TAB 004 may be in the space of aiding diagnosis early and accurately especially given that mammograms fail in women with dense breast 50% of the time and overall misses 25% of the tumors. Furthermore, mammograms have high false-positive rates as >80% of biopsies post suspicious mammograms turn out to be benign. Indeed,

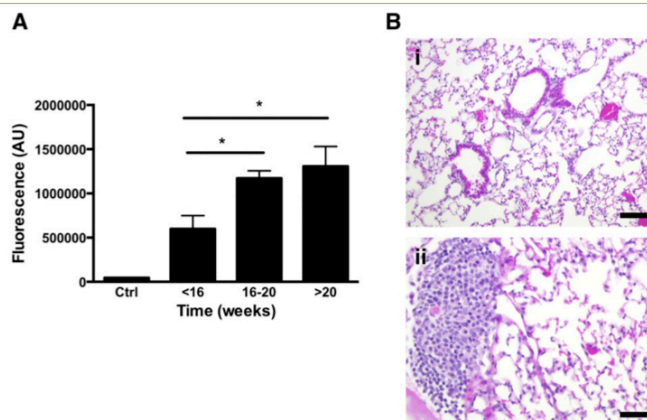


Figure 6. Detection of lung metastases in the MMT mice post TAB-ICG injection. (A) The presence of fluorescence [expressed as arbitrary unit (AU)] associated with the injection of ICG-conjugated TAB 004 was measured *ex vivo* on isolated lungs post-euthanasia using the IVIS system. Compared to control (Ctrl) lungs (lungs isolated from a noninjected MMT mouse), detected fluorescence increased with age in MMT mice [$5.99 \times 10^6 \pm 1.5 \times 10^6$, $11.73 \times 10^6 \pm 0.8 \times 10^6$, and $13.1 \times 10^6 \pm 2.23 \times 10^6$ for MMT mice <16 ($n = 7$), 16-20 ($n = 6$), and >20 ($n = 7$) weeks old, respectively; * $P < .05$]. (B) Normal lung (i) and micrometastasis (ii) in the lungs of a 16- to 17-week-old MMT female mouse stained with H&E (scale bar = 100 μ m).

using a panel of 440 patient breast cancer tissue arrays, we determined that 95% of BCs express tMUC1, as detected by TAB 004 staining and IHC, regardless of the tumor subtype and density of the breast tissue (manuscript in preparation).

Although most approaches (physical, imaging, blood tests, and combination thereof) diagnose with significant accuracy the presence of advanced breast cancer, the earlier stages remain much more difficult to detect reliably [4,7,35,36]. Indeed, for those early stages including atypical hyperplasia and ductal carcinoma *in situ*, mammographic examination is associated with a high false-positive rate [6]. Similarly, the determination of circulatory CEA and or CA-15-3 antigen lacks the specificity and sensitivity in individuals with early disease, although they may be of benefit in monitoring metastasis and disease recurrence [37]. Multiple studies have demonstrated improved detection when using ultrasounds and magnetic resonance imaging (MRI) [7,38], although those approaches are mostly used to further assess suspicious mass abnormalities detected during mammography [4,38] as opposed to screening. The numbers of false-positive and to a lesser extent of false-negative cases highlight the potential of molecularly targeted imaging, especially to detect early stages of the disease and possibly micrometastasis.

Moreover, as tMUC1 is present in multiple epithelial cancers including colon carcinoma, ovarian cancer, and pancreatic cancer, TAB 004 may serve as a detecting and monitoring tool for multiple cancers. Already, preclinical and clinical observations have demonstrated the specificity of TAB 004 antibody toward tMUC1 antigen in pancreatic cancer [20].

In vivo, TAB-ICG detected primary tumors generally before they were palpable in the MMT model. The early detection of nonpalpable tumors by TAB-ICG including hyperplasia forms proof of principle of the potential use of this antibody in the clinic in conjunction with other imaging modalities. For example,

conjugated with radioactive imaging agents, TAB 004 could greatly improve the reliability of early breast cancer diagnosis when used in conjunction with computed tomography or MRI [39–43].

Interestingly, *ex vivo* imaging and H&E staining provide evidence that TAB-ICG enabled detection of lung metastases as early as 16 weeks of age in MMT mice (Figure 6). Thus, we suggest that TAB 004 conjugated to radioactive material such as technetium (99m) along with MRI and computed tomography scan may provide improved monitoring of the development of distant metastases in patients with breast cancer.

Clinically, although early detection is the key in breast cancer treatment, standard mammography generates a high number of false negatives, especially in women with dense breasts [4,6,7,44–46]. For those patients, additional examinations and imaging such as ultrasounds and MRI may be conducted. Mammography also generates false positive and biopsies, which in many cases are unwarranted [4,47]. Overall, two-dimensional mammograms have been deemed of limited use in individuals with dense breast tissues (40% of the women) [6–8] because for those patients, the mammograms are often difficult to interpret [44,48].

In summary, our investigations demonstrate the specificity of TAB 004 antibody against hypoglycosylated human MUC1 and its potential in early detection of transformed mammary epithelial cells and micrometastasis. Based on this proof of principle, we suggest that TAB 004 conjugated with contrasting agents or radioisotopes used in current clinical imaging protocols will allow both early and accurate detection and monitoring of breast cancer, even in women with dense breast tissue. We further propose that because tMUC1 is present in most epithelium-derived cancers, TAB 004 likely may be beneficial in the detection and monitoring of multiple cancers.

Supplementary data to this article can be found online at <http://dx.doi.org/10.1016/j.tranon.2016.05.001>.

Acknowledgements

The authors acknowledge the support of the Vivarium staff and Dr. C. Williams, DVM, for the excellent animal care and imaging expertise provided. The authors also acknowledge Mallory B. Korman (Research Histology Confocal Core Lab) at Carolinas Medical Center for the histological embedding and sectioning of murine samples.

References

- Campono M, Valo I, Jezequel P, Moreau M, Boissard A, Campion L, Loussouarn D, Verrielle V, Coqueret O, and Guette C (2015). Prediction of recurrence and survival for triple-negative breast cancer by a protein signature in tissue samples. *Mol Cell Proteomics* **14**, 2936–2946.
- Ward EM, DeSantis CE, Lin CC, Kramer JL, Jemal A, Kohler B, Brawley OW, and Gansler T (2015). Cancer statistics: breast cancer in situ. *CA Cancer J Clin* **65**, 481–495.
- DeSantis C, Ma J, Bryan L, and Jemal A (2014). Breast cancer statistics, 2013. *CA Cancer J Clin* **64**, 52–62.
- Oeffinger KC, Fontham ET, Etzioni R, Herzig A, Michaelson JS, Shih YT, Walter LC, Church TR, Flowers CR, and LaMonte SJ, et al (2015). Breast cancer screening for women at average risk: 2015 guideline update from the American Cancer Society. *JAMA* **314**, 1599–1614.
- Gilbert FJ, Tucker L, Gillan MG, Willsher P, Cooke J, Duncan KA, Michell MJ, Dobson HM, Lim YY, and Purushothaman H, et al (2015). The TOMMY trial: a comparison of TOMosynthesis with digital Mammography in the UK NHS Breast Screening Programme—a multicentre retrospective reading study comparing the diagnostic performance of digital breast tomosynthesis and digital mammography with digital mammography alone. *Health Technol Assess* **19**, 1–136 [i-xxv].
- Kerlikowske K, Zhu W, Testostes AN, Sprague BL, Tice JA, Lehman CD, and Miglioretti DL (2015). Identifying women with dense breasts at high risk for interval cancer: a cohort study. *Ann Intern Med* **162**, 673–681.
- Scheel JR, Lee JM, Sprague BL, Lee CI, and Lehman CD (2015). Screening ultrasound as an adjunct to mammography in women with mammographically dense breasts. *Am J Obstet Gynecol* **212**, 9–17.
- Moshina N, Ursin G, Hoff SR, Akslen LA, Roman M, Sebuodegard S, and Hofvind S (2015). Mammographic density and histopathologic characteristics of screen-detected tumors in the Norwegian Breast Cancer Screening Program. *Acta Radiol Open* **4**. <http://dx.doi.org/10.1177/2058460115604340>.
- Beaton RE, Taylor-Papadimitriou J, and Burchell JM (2010). MUC1 immunotherapy. *Immunotherapy* **2**, 305–327.
- Mukherjee P, Madsen CS, Ginardi AR, Tindler TL, Jacobs F, Parker J, Agrawal B, Longenecker BM, and Gendler SJ (2003). Mucin 1-specific immunotherapy in a mouse model of spontaneous breast cancer. *J Immunother* **26**, 47–62.
- Ideo H, Hinoda Y, Sakai K, Hoshi I, Yamamoto S, Oka M, Maeda K, Maeda N, Hazama S, and Amano J, et al (2015). Expression of mucin 1 possessing a 3'-sulfated core1 in recurrent and metastatic breast cancer. *Int J Cancer* **137**, 1652–1660.
- Siroy A, Abdul-Karim FW, Miedler J, Fong N, Fu P, Gilmore H, and Baar J (2013). MUC1 is expressed at high frequency in early-stage basal-like triple-negative breast cancer. *Hum Pathol* **44**, 2159–2166.
- Lavrsen K, Madsen CB, Rasch MG, Woetmann A, Odum N, Mandel U, Clausen H, Pedersen AE, and Wandall HH (2013). Aberrantly glycosylated MUC1 is expressed on the surface of breast cancer cells and a target for antibody-dependent cell-mediated cytotoxicity. *Glycoconj J* **30**, 227–236.
- Mommers EC, Leonhart AM, von Mensdorff-Pouilly S, Schol DJ, Hilgers J, Meijer CJ, Baak JP, and van Diest PJ (1999). Aberrant expression of MUC1 mucin in ductal hyperplasia and ductal carcinoma in situ of the breast. *Int J Cancer* **84**, 466–469.
- Alam M, Rajabi H, Ahmad R, Jin C, and Kufe D (2014). Targeting the MUC1-C oncoprotein inhibits self-renewal capacity of breast cancer cells. *Oncotarget* **5**, 2622–2634.
- Raina D, Agarwal P, Lee J, Bharti A, McKnight CJ, Sharma P, Kharbanda S, and Kufe D (2015). Characterization of the MUC1-C cytoplasmic domain as a cancer target. *PLoS One* **10**, e0135156. <http://dx.doi.org/10.1371/journal.pone.0135156>.
- Di Gioia D, Dresse M, Mayr D, Nagel D, Heinemann V, and Stieber P (2015). Serum HER2 in combination with CA 15-3 as a parameter for prognosis in patients with early breast cancer. *Clin Chim Acta* **440**, 16–22.
- Incoronato M, Mirabelli P, Catalano O, Aiello M, Parente C, Soricelli A, and Nicolai E (2014). CA15-3 is a useful serum tumor marker for diagnostic integration of hybrid positron emission tomography with integrated computed tomography during follow-up of breast cancer patients. *BMC Cancer* **14**, 356. <http://dx.doi.org/10.1186/1471-2407-14-356>.
- Grzywa R, Lupicka-Slowik A, Walczak M, Idzi M, Bobrek K, Boivin S, Gawel A, Stefaniak T, Oleksyszyn J, and Sienczyk M (2014). Highly sensitive detection of cancer antigen 15-3 using novel avian IgY antibodies. *ALTEX* **31**, 43–52.
- Curry JM, Thompson KJ, Rao SG, Besmer DM, Murphy AM, Gidzelshvili VZ, Ahrens WA, McKillop IH, Sindram D, and Ianniti DA, et al (2013). The use of a novel MUC1 antibody to identify cancer stem cells and circulating MUC1 in mice and patients with pancreatic cancer. *J Surg Oncol* **107**, 713–722.
- Chen D, Xia J, Tanaka Y, Chen H, Koido S, Wernet O, Mukherjee P, Gendler SJ, Kufe D, and Gong J (2003). Immunotherapy of spontaneous mammary carcinoma with fusions of dendritic cells and mucin 1-positive carcinoma cells. *Immunology* **109**, 300–307.
- Roy LD, Sahraei M, Subramani DB, Besmer D, Nath S, Tindler TL, Bajaj E, Shanmugam K, Lee YY, and Hwang SI, et al (2011). MUC1 enhances invasiveness of pancreatic cancer cells by inducing epithelial to mesenchymal transition. *Oncogene* **30**, 1449–1459.
- Nath S, Roy LD, Grover P, Rao S, and Mukherjee P (2015). Mucin 1 regulates Cox-2 gene in pancreatic cancer. *Pancreas* **44**, 909–917.
- Hardesy DA, Thind H, Zabramski JM, Spletzer RF, and Nakajji P (2014). Safety, efficacy, and cost of intraoperative indocyanine green angiography compared to intraoperative catheter angiography in cerebral aneurysm surgery. *J Clin Neurosci* **21**, 1377–1382.
- Rowse GJ, Ritland SR, and Gendler SJ (1998). Genetic modulation of neoplastic growth by proto-oncogene-induced mammary tumorigenesis. *Cancer Res* **58**, 2675–2679.
- Guy CT, Cardiff RD, and Muller WJ (1992). Induction of mammary tumors by expression of polyomavirus middle T oncogene: a transgenic mouse model for metastatic disease. *Mol Cell Biol* **12**, 954–961.
- Flick MM and Schaffhausen BS (2009). Lessons in signaling and tumorigenesis from polyomavirus middle T antigen. *Microbiol Mol Biol Rev* **73**, 542–563.
- Perou CM, Sorlie T, Eisen MB, van de Rijn M, Jeffrey SS, Rees CA, Pollack JR, Ross DT, Johnsen H, and Akslen LA, et al (2000). Molecular portraits of human breast tumours. *Nature* **406**, 747–752.
- Sorlie T (2007). Molecular classification of breast tumors: toward improved diagnostics and treatments. *Methods Mol Biol* **360**, 91–114.
- Norum JH, Andersen K, and Sorlie T (2014). Lessons learned from the intrinsic subtypes of breast cancer in the quest for precision therapy. *Br J Surg* **101**, 925–938.
- Rutter CE, Yao X, Mancini BR, Aminawung JA, Chaggar AB, Saglam O, Hofstatter EW, Abu-Khalaf M, Gross CP, and Evans SB (2016). Influence of a 21-gene recurrence score assay on chemotherapy delivery in breast cancer. *Clin Breast Cancer* **16**, 59–62.
- Stemmer SM, Klang SH, Ben-Baruch N, Gefen DB, Steiner M, Soussan-Gutman L, Merling S, Svedman C, Rizel S, and Lieberman N (2013). The impact of the 21-gene Recurrence Score assay on clinical decision-making in node-positive (up to 3 positive nodes) estrogen receptor-positive breast cancer patients. *Breast Cancer Res Treat* **140**, 83–92.
- Cobain EF and Hayes DF (2015). Indications for prognostic gene expression profiling in early breast cancer. *Curr Treat Options Oncol* **16**, 23. <http://dx.doi.org/10.1007/s11864-015-0340-x>.
- McVeigh TP, Hughes LM, Miller N, Sheehan M, Keane M, Sweeney KJ, and Kerin MJ (2014). The impact of Oncotype DX testing on breast cancer management and chemotherapy prescribing patterns in a tertiary referral centre. *Eur J Cancer* **50**, 2763–2770.
- Retsky M, Demicheli R, and Hrushesky W (2003). Breast cancer screening: controversies and future directions. *Curr Opin Obstet Gynecol* **15**, 1–8.
- Nicolini A, Carpi A, and Tarro G (2006). Biomolecular markers of breast cancer. *Front Biosci* **11**, 1818–1843.
- Stieber P, Nagel D, Blankenburg I, Heinemann V, Untch M, Bauerfeind I, and Di Gioia D (2015). Diagnostic efficacy of CA 15-3 and CEA in the early detection of metastatic breast cancer—a retrospective analysis of kinetics on 743 breast cancer patients. *Clin Chim Acta* **448**, 228–231.
- Debald M, Abramian A, Nemes L, Doblner M, Kaiser C, Keyver-Paik MD, Leutner C, Holler T, Braun M, and Kuhl C, et al (2015). Who may benefit from preoperative breast MRI? A single-center analysis of 1102 consecutive patients with primary breast cancer. *Breast Cancer Res Treat* **153**, 531–537.
- Goldenberg DM and Nabi HA (1999). Breast cancer imaging with radiolabeled antibodies. *Semin Nucl Med* **29**, 41–48.
- Sampath L, Kwon S, Ke S, Wang W, Schiff R, Mawad ME, and Sevick-Muraca EM (2007). Dual-labeled trastuzumab-based imaging agent for the detection of

- human epidermal growth factor receptor 2 overexpression in breast cancer. *J Nucl Med* **48**, 1501–1510.
- [41] Lutje S, Rijpkema M, Franssen GM, Fracasso G, Helfrich W, Eek A, Oyen WJ, Colombatti M, and Boerman OC (2014). Dual-modality image-guided surgery of prostate cancer with a radiolabeled fluorescent anti-PSMA monoclonal antibody. *J Nucl Med* **55**, 995–1001.
- [42] Charalac KL, Veldhoven-Zweistra J, Bolkestein M, Hoeben S, Koning GA, Boerman OC, de Jong M, and van Weerden WM (2015). A novel (1)(1)In-labeled anti-prostate-specific membrane antigen nanobody for targeted SPECT/CT imaging of prostate cancer. *J Nucl Med* **56**, 1094–1099.
- [43] Signore A, Capriotti G, Chianelli M, Bonanno E, Galli F, Catalano C, Quintero AM, De Toma G, Manfredi S, and Pozzilli P (2015). Detection of insulinitis by pancreatic scintigraphy with ^{99m}Tc-labeled IL-2 and MRI in patients with LADA (Action LADA 10). *Diabetes Care* **38**, 652–658.
- [44] Chetlen A, Mack J, and Chan T (2016). Breast cancer screening controversies: who, when, why, and how? *Clin Imaging* **40**, 279–282.
- [45] Rosso A, Lang K, Petersson IF, and Zackrisson S (2015). Factors affecting recall rate and false positive fraction in breast cancer screening with breast tomosynthesis—a statistical approach. *Breast* **24**, 680–686.
- [46] Rhodes DJ, Radecki Breitkopf C, Ziegenfuss JY, Jenkins SM, and Vachon CM (2015). Awareness of breast density and its impact on breast cancer detection and risk. *J Clin Oncol* **33**, 1143–1150.
- [47] Kemp Jacobsen K, O'Meara ES, Key D, D S M Buist D, Kerlikowske K, Vejborg I, Sprague BL, Lyng E, and von Euler-Chelpin M (2015). Comparing sensitivity and specificity of screening mammography in the United States and Denmark. *Int J Cancer* **137**, 2198–2207.
- [48] Slanetz PJ, Freer PE, and Birdwell RL (2015). Breast-density legislation—practical considerations. *N Engl J Med* **372**, 593–595.

Research Paper

SMAD4-independent activation of TGF- β signaling by MUC1 in a human pancreatic cancer cell line**Priyanka Grover^{1,*}, Sritama Nath^{1,*}, Monica D. Nye¹, Ru Zhou¹, Mohammad Ahmad¹ and Pinku Mukherjee¹**¹Department of Biological Sciences, University of North Carolina at Charlotte, Charlotte, North Carolina 28223-0001, USA

*These authors have contributed equally to this work

Correspondence to: Pinku Mukherjee, email: pmukherj@uncc.edu

Keywords: apoptosis; epithelial-mesenchymal transition (EMT); transforming growth factor beta (TGF- β); pancreatic cancer; mucin 1 (MUC1)**Received:** January 20, 2017**Accepted:** December 18, 2017**Published:** January 05, 2018**Copyright:** Grover et al. This is an open-access article distributed under the terms of the Creative Commons Attribution License 3.0 (CC BY 3.0), which permits unrestricted use, distribution, and reproduction in any medium, provided the original author and source are credited.**ABSTRACT**

Pancreatic Ductal Adenocarcinoma (PDA) has a mortality rate that nearly matches its incidence rate. Transforming Growth Factor Beta (TGF- β) is a cytokine with a dual role in tumor development switching from a tumor suppressor to a tumor promoter. There is limited knowledge of how TGF- β function switches during tumorigenesis. Mucin 1 (MUC1) is an aberrantly glycosylated, membrane-bound, glycoprotein that is overexpressed in >80% of PDA cases and is associated with poor prognosis. In PDA, MUC1 promotes tumor progression and metastasis via signaling through its cytoplasmic tail (MUC1-CT) and interacting with other oncogenic signaling molecules. We hypothesize that high levels of MUC1 in PDA may be partly responsible for the TGF- β functional switch during oncogenesis. We report that overexpression of MUC1 in BxPC3 human PDA cells (BxPC3.MUC1) enhances the induction of epithelial to mesenchymal transition leading to increased invasiveness in response to exogenous TGF- β 1. Simultaneously, these cells resist TGF- β induced apoptosis by downregulating levels of cleaved caspases. We show that mutating the tyrosines in MUC1-CT to phenylalanine reverses the TGF- β induced invasiveness. This suggests that the tyrosine residues in MUC1-CT are required for TGF- β induced invasion. Some of these tyrosines are phosphorylated by the tyrosine kinase c-Src. Thus, treatment of BxPC3.MUC1 cells with a c-Src inhibitor (PP2) significantly reduces TGF- β induced invasiveness. Similar observations were confirmed in the Chinese hamster ovarian (CHO) cell line. Data strongly suggests that MUC1 may regulate TGF- β function in PDA cells and thus have potential clinical relevance in the use of TGF- β inhibitors in clinical trials.

INTRODUCTION

Pancreatic Ductal Adenocarcinoma (PDA) is the fourth leading cause of cancer related deaths in the United States with a median survival rate of less than six months and a 5-year survival rate of a dismal 7% [1, 2]. By 2030, PDA is predicted to be the second leading cause of

cancer-related deaths in the United States [3]. Its mortality rate nearly matches its incidence rate [4].

Transforming Growth Factor Beta (TGF- β) is a cytokine with a dichotomous role in oncogenesis. In normal tissue development and early oncogenesis, the TGF- β signaling complex is a cell cycle regulator and induces apoptosis. The canonical pathway of TGF- β

signaling starts with binding of two TGF- β Receptor type II (TGF- β RII) to two TGF- β Receptor type I (TGF- β RI) to activate the SMAD pathway [5, 6]. The receptors dimerize, when the ligand binds, triggering the activation of TGF- β RI kinase activity and switching it to a docking site for SMAD proteins [7]. SMAD 2 and SMAD 3 are activated by the TGF- β RI [8]. Once phosphorylated by TGF- β RI, SMAD 2 and 3 dimerize forming the SMAD 2/3 complex [9]. The SMAD 2/3 dimer joins with SMAD 4, creating a heterohexameric complex [9]. The newly created complex translocates to the nucleus, allowing for the transcriptional regulation of target genes which regulate cellular processes, such as induction of apoptosis [10]. However, it has been shown that in a SMAD 4 null cell line SMAD2 and SMAD3 are still able to translocate to the nucleus [11]. SMAD 4 is often mutated or deleted in about 55% of PDA cases showcasing the importance of studying SMAD4 independent mechanisms of PDA development [12]. Loss of functional SMAD 4 in PDA interferes with the TGF- β /SMAD pathway leading to decreased growth inhibition [13].

In later stages of cancer, a switch occurs and the TGF- β signaling pathway becomes a tumor promoter, inducing invasion and metastasis. TGF- β 1 stimulates Epithelial-to-Mesenchymal Transition (EMT) through the activation of the ERK pathway [14]. As reviewed in Kalluri et al, EMT is a biological process that transforms an epithelial cell to a mesenchymal cell phenotype, which can lead to resistance to apoptosis [15]. Increased migration and invasion of cancer cells has also been associated with EMT [16]. The TGF- β switch in function from a tumor suppressor, via apoptosis, to a tumor promoter, via EMT, is elusive but holds high importance in treatment refractory cancers like PDA [17]. The TGF- β ligand family consists of three different, highly homologous isoforms: TGF- β 1, TGF- β 2, and TGF- β 3 [18–20]. The most abundant isoform is TGF- β 1 [9]. TGF- β is considered an important target for cancer therapy, and there are multiple anti-TGF- β compounds in clinical trials [21].

Mucin-1 (MUC1), a transmembrane glycoprotein that plays a critical role in tumor progression and metastasis in PDA [22]. In normal epithelial cells lining the ducts, MUC1 is localized on the apical surface and provides a protective barrier. However, when normal cells transform to malignant cells and lose their polarity, MUC1 is no longer restricted to the apical surface; it becomes hypo glycosylated, and comes in close proximity to several growth factor receptors including TGF- β receptors [23]. The tumor-associated form of MUC1 plays an important role in oncogenic signaling [24–27]. Studies have linked overexpression of MUC1 in tumors with enhanced EMT leading to increased invasiveness, metastasis, and drug resistance [22, 28, 29]. MUC1 induces increased production of prostaglandin (Cox-2) and growth factors (PDGF and VEGF), which leads to

enhanced invasiveness of cells mainly through induction of EMT related genes [24, 27, 30, 31]. Importantly, MUC1 is overexpressed and aberrantly glycosylated in over 80% of PDA cases [22, 24, 30, 32, 33]. It is well established that the oncogenic signal transduction occurs through the cytoplasmic tail of MUC1 (MUC1-CT) [34, 35]. Once the MUC1-CT is phosphorylated, it associates with β -catenin and other transcription factors, and becomes released from the N-terminus of MUC1, leading it to translocate to the nucleus and subsequently activate downstream signaling pathways [25, 26, 36]. MUC1-CT is 72 amino acids long and is highly conserved with seven tyrosine residues that are phosphorylated by intracellular kinases. The phosphotyrosine residues act as a binding sites for molecules, such as c-Src, a proto-oncogene linked to cancer progression [22, 37].

In this study, we show that overexpression of MUC1 in human SMAD4 deleted PDA cell line BxPC3, plays an important role in the switch of TGF- β from a tumor suppressor to a tumor promoter, via a SMAD4 independent mechanism. Similar data is also reported in CHO cells. This study is the first to show that overexpression of MUC1 directly reduces TGF- β induced apoptosis and increases invasive potential in BxPC3 and CHO cells via signaling through the tyrosines in MUC1 CT.

RESULTS

Overexpression of MUC1 in BxPC3 and CHO cells significantly increases the amount of TGF- β 1 produced without altering levels of the TGF- β receptors or SMAD2/3

For this study, we selected Chinese hamster ovarian cell line (CHO) that is null for human MUC1 and a human PDA cell line BxPC3 that express low levels of endogenous human MUC1 and has SMAD4 independent TGF- β signaling, CHO cells have intact canonical TGF- β signaling pathway and were selected as a control cell line to investigate the effects of MUC1 on TGF- β signaling and phenotypic outcomes. Using a retroviral gene delivery system, we overexpressed the full-length human MUC1 transgene in BxPC3 and CHO cells creating two MUC1 high cell lines: BxPC3.MUC1 and CHO.MUC1. An empty vector, which does not carry the human MUC1 gene, was used to create the control cell lines BxPC3.Neo and CHO.Neo. Western blotting was performed to confirm the expression of human MUC1 in these cell lines. Cell lysates probed with CT2 antibody that recognizes the last 17 amino acids (SSLSYNTPAVAATSANL) of the cytoplasmic tail (CT) [38] revealed that BxPC3.MUC1 and CHO.MUC1 cells expressed high levels of human MUC1, while BxPC3.Neo and CHO.Neo did not (Figure 1A and 1B). Next, we tested expression of the key signaling

components of the canonical TGF- β pathway, TGF- β RI, TGF- β RII, SMAD 2/3, and SMAD4 (expressed in CHO cells) [39]. We found that the levels of these signaling proteins were not significantly altered in the BxPC3.MUC1 compared to BxPC3.Neo (Figure 1B) or in CHO.MUC1 compared to CHO.Neo (Figure 1A). Densitometric arbitrary units are shown in Figure 1A and 1B representing the levels of protein normalized to their β -actin loading control.

To investigate if overexpression of MUC1 alters SMAD4 independent TGF- β signaling, we first looked for differences in TGF- β 1 secretion by these cells. Specific ELISA was used to determine the TGF- β 1 concentration in the supernatant of these cells. Our data showed significantly higher levels of TGF- β 1 in the supernatants of CHO.MUC1 at 48 hours and BxPC3.MUC1 at 6, 12, and 24 hours when compared to the control cell lines that expressed low levels of endogenous MUC1 (Figure 1C, $p < 0.01$ and 1D, $p < 0.001$), suggesting that MUC1 is a major contributor to the abundant release of TGF- β 1. (Note: Only 48h time point is shown for CHO cells as earlier time points had very low undetectable levels of TGF- β 1 release). Thus, we concluded that MUC1 overexpression increases TGF- β 1 released but does not affect the expression of the receptors or the downstream signaling component.

Overexpression of MUC1 protects PDA cells from TGF- β 1-mediated apoptosis

We determined the effect of exogenous TGF- β 1 on induction of apoptosis in CHO and BxPC3 cells in context of MUC1 expression. Apoptosis was measured by performing Annexin V/7AAD staining followed by flow cytometry. Treatment with TGF- β 1 induced a 2-fold induction of apoptosis in the CHO.Neo cells compared to 0.5-fold induction of apoptosis in CHO.MUC1 cells (Figure 2A, $p < 0.05$). Similarly, BxPC3.MUC1 cells were completely protected from TGF- β 1 induced apoptosis compared to 5-fold induction of apoptosis in BxPC3.Neo cells (Figure 2B, $p < 0.05$). Furthermore, we found that TGF- β 1 treatment activated cleavage of Caspase 3 more in the BxPC3.Neo cells than in the BxPC3.MUC1 cells (Figure 2C and 2D, $p < 0.0001$) even though total Caspase 3 was significantly higher in the BxPC3.MUC1 versus the Neo cells (Figure 2C and 2E, $p < 0.001$). Caspase 3 is a death protease commonly associated with changes in cell morphology, and induction of apoptosis [40]. MUC1 expression has been shown to reduce stress induced apoptosis by blocking activation of Caspase 8, which is known to interact and activate Caspase 3 [41]. It has also been shown to inhibit apoptosis under genotoxic stress via JNK1 activation [29, 42]. Upon comparing overall

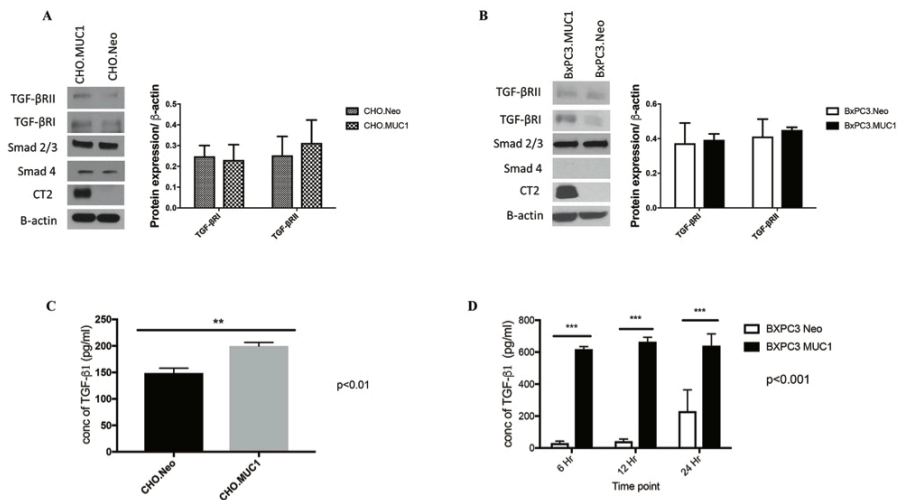


Figure 1: MUC1 overexpressing cells release significantly higher amounts of active TGF- β 1 when compared to MUC1-low expressing cells. (A and B) Western blotting detecting expression of MUC1-CT, TGF- β RI, TGF- β RII, SMAD 2/3, and SMAD4 in CHO and BxPC3 cells. Corresponding densitometric analysis for the TGF- β receptors. **(C and D)** TGF- β specific ELISA of supernatants from CHO and BxPC3 cells cultured in serum free medium for the indicated times. Results are presented as means \pm SEM of $n=3$. ** $p < 0.01$, *** $p < 0.001$.

Caspase 3 activation, we observed that BxPC3.Neo has a statistically significant increase when compared to BxPC3.MUC1 in the presence of TGF- β 1 (Figure 2C and 2F, $p < 0.0001$). We did not observe any significant difference in cleaved Caspase 7 in the MUC1-overexpressing cells in response to TGF- β 1 treatment (Figure 2C and 2G). However, when we compared the ratio of cleaved Caspase 7 versus total Caspase 7, a significant decrease in cleaved Caspase 7 in the MUC1-overexpressing cells was noted when exposed to TGF- β 1 (Figure 2I, $p < 0.01$). As with Caspase 3, Caspase 7 levels were significantly higher in BxPC3.MUC1 when compared to BxPC3.Neo cells (Figure 2C and 2H, $p < 0.05$). Etoposide was used as the positive control for inducing Caspase 3 and 7 cleavage and activation. However, we did not observe any significant difference in Caspase 3 and 7 cleavages, because both BxPC3.MUC1 and BxPC3.Neo cells were equally sensitive to high concentration (100uM) of etoposide. Therefore, we suggest that cleaved caspases may regulate TGF- β induced apoptosis in the absence of MUC1. The densitometric arbitrary unit shown in Figures 2D, 2E, 2G, and 2H represent levels of protein normalized to their β -actin loading control while F and I represent levels of cleaved caspase/total caspase.

Treatment with TGF- β 1 increases invasive properties of MUC1-overexpressing cells as compared to their Neo counterparts

We hypothesized that TGF- β 1 may induce invasiveness in MUC1-high but not MUC1-low cells by activating EMT. To test this hypothesis, we determined the invasive properties of BxPC3.MUC1 and CHO.MUC1 versus BxPC3.Neo and CHO.Neo cells in response to TGF- β 1. Results show 20-fold higher levels of invasion in CHO.MUC1 when compared to CHO.Neo (Figure 3A, $p < 0.0001$) and 1.5-fold higher in BxPC3.MUC1 when compared to BxPC3.Neo (Figure 3B, $p < 0.05$). We recognize that CHO cells that are SMAD4 positive respond better to TGF- β . However, to further explore whether SMAD4 deletion plays a role, we also tested the invasive potential of Wild Type SMAD4 PDA cell lines HPAF-II and MIA PaCa-2 (Supplementary Figure 4). HPAF-II, an endogenously high MUC1 line significantly increases its invasive potential when exposed to TGF- β 1. Following the trends established, MIA PaCa-2, an endogenously low MUC1 line, significantly decreases its invasive potential in the presence of TGF- β 1. These cell lines, in relation to

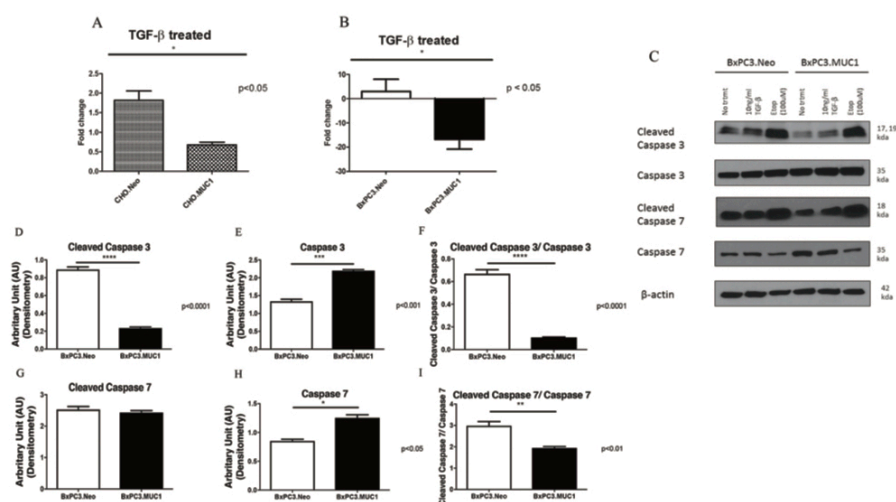


Figure 2: MUC1 overexpressing cells resist apoptosis in response to treatment with TGF- β 1 with corresponding decrease in cleaved caspase 3 when compared to MUC1 low expressing cells. (A and B) Apoptosis was determined at 48 hours post treatment with TGF- β 1 by Annexin V+/7AAD staining and flow cytometry. Data is presented as fold change in apoptosis from untreated cells. (C) Western blotting of apoptotic markers (cleaved Caspase 3 and 7) in BxPC3 cells 48 hours post TGF- β 1 treatment. (D-I) Corresponding densitometric analysis of C is presented. (D and G) Arbitrary densitometric unit of cleaved caspase 3 and cleaved caspase 7 normalized to β -actin respectively; (E and H) Arbitrary densitometric unit of total caspase 3 and caspase 7 normalized to β -actin; 2F: Ratio of cleaved caspase 3 and 7 normalized to total caspase 3 and 7. Results are presented as means \pm SEM of $n=3$. * $p < 0.05$, ** $p < 0.01$, *** $p < 0.001$, **** $p < 0.0001$.

their endogenous MUC1 levels, will be further studied. Overall, the results suggest that there is synergistic interaction between MUC1 and TGF- β signaling resulting in increased motility and invasiveness. Next, we assessed the levels of EMT associated proteins by western blotting in TGF- β 1 treated versus untreated cells. Forty-eight hours post TGF- β 1 treatment, levels of Snail, Slug, Vimentin, and N-Cadherin was determined. The percent change in density of the bands due to TGF- β 1 treatment is significantly higher in the BxPC3.MUC1 compared to BxPC3.Neo for all the EMT associated proteins except for Snail (Figure 3C-3G). Percent change was determined by formula (TGF- β treated – No treatment/No treatment) * 100. If the final answer was negative, this was percentage decrease (suggesting that the protein level remained unchanged with treatment). We observed no difference in the activation of the ERK pathway when examining levels of phospho-ERK between MUC1 and Neo cells. Presently, we do not know why that is, however we suspect that in the absence of SMAD4 in the MUC1 overexpressing BxPC3 cell line that the ERK pathway may not be activated [43].

TGF- β mediated functions require signaling through the tyrosines present in MUC1-CT

We next investigated if the functional differences of TGF- β were manifestations of signaling crosstalk between the TGF- β signaling components and MUC1-CT. MUC1 associated non-canonical regulation of TGF- β signaling in a SMAD4 independent mechanism is responsible for the activation of other transcription factors via their interaction with the cytoplasmic tail of MUC1 [44]. Therefore, we hypothesized that the interaction of MUC1-CT with the TGF- β signaling pathway regulates the differences in apoptosis and induction of EMT independently of SMAD4. To test this hypothesis we generated a phosphomutant form of MUC1 (CHO.Y0 and BxPC3.Y0), where all seven tyrosines of MUC1-CT were mutated to phenylalanine. The MUC1 Y0 mutant is considered 'a non-functional form' of MUC1 CT as it lacks the tyrosines for phosphorylation, a precursor for downstream signal transduction (Figure 4A). Western blots show the expression levels of MUC1-CT in Neo, MUC1, and Y0 cells (Figure 4B and 4C). As previously observed, TGF- β 1 treatment increases invasiveness in

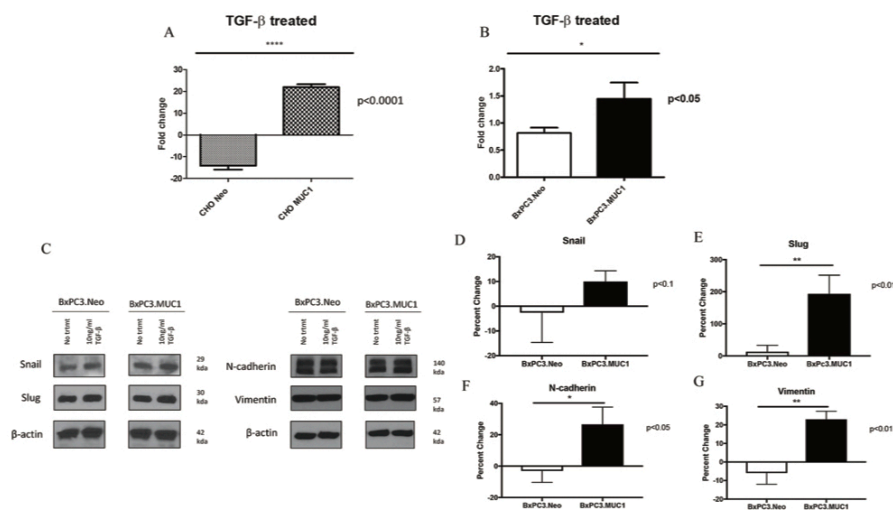


Figure 3: MUC1 overexpressing cells undergo significantly higher levels of invasion in response to TGF- β 1 treatment. (A and B) Invasion was determined by standard transwell assay at 48h time point. Results are presented as fold change from untreated. (C) Western blots to detect EMT markers 48 hours post TGF- β 1 treatment. (D-G) Corresponding densitometric analysis of C is presented. Percent change from untreated is presented. All values are first normalized to its corresponding β -actin levels. Results are presented as means \pm SEM of $n=3$. * $p < 0.05$, ** $p < 0.01$, **** $p < 0.0001$. D-G calculation: First the density value of each protein was normalized to their respective β -actin density value. Next the percent change was calculated by the formula: (TGF- β treated – No treatment/No treatment) * 100. If the final answer was negative, this was percentage decreased.

the MUC1-overexpressing cells when compared to the Neo cells. However, when comparing phosphomutant BxPC3.Y0 or CHO.Y0 cells to the full-length MUC1-overexpressing cells, we observed a complete reversal of the enhanced invasion when exposed to TGF- β 1 (Figure 4D and 4E). Since the only difference between the full length MUC1 and MUC1.Y0 expressing cells is the ability to signal through the tyrosine residues of MUC1-CT. We postulate that the tyrosine residues of MUC1-CT are critical for the synergistic cross talk between MUC1 and TGF- β signaling that results in the TGF- β associated apoptosis and invasion. To our surprise we observed an increase in Vimentin in the BxPC3.Y0 cells post TGF- β 1 treatment (Supplementary Figure 1A); however, it was striking to note that there were no cleaved caspases 3 or 7 in these cells post TGF- β 1 treatment suggesting that the tyrosines play a major role in the TGF- β induced apoptotic pathway (Supplementary Figure 1B). To confirm that treatment itself did not cause any changes in the MUC1 levels, we conducted western blotting for MUC1

extracellular domain expression pre and post-TGF- β 1 or etoposide treatment in BxPC3.Neo, MUC1, and Y0 cells (Supplementary Figure 2). Treatment did not result in any change in the expression levels of MUC1 in the cells. Due to the changes in tyrosine to phenylalanine, the Y0 cells always run smaller in size and has been published extensively [45].

C-Src inhibition negates TGF- β mediated invasion in MUC1-overexpressing cells

It has been shown that when Dasatinib, a Src inhibitor, was used on PDA cell lines PANC-1 and Colo-357, it inhibited TGF- β 1 induced SMAD phosphorylation, migration, and invasion, therefore it is a tyrosine to consider [46]. c-Src is also associated with MUC1-CT and plays a vital role in MUC1 induced tumor metastasis [22, 37, 47]. Therefore, when BxPC3.MUC1 cells were treated with PP2, a c-Src inhibitor, the invasiveness of the cells in response to TGF- β 1 was decreased (Figure

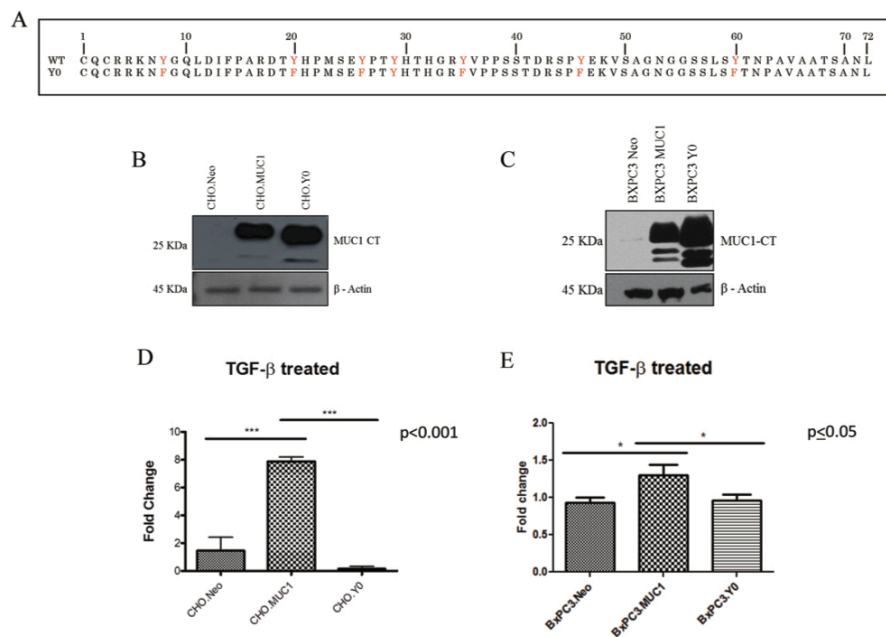


Figure 4: TGF- β 1 mediated invasiveness is dependent upon signaling through the tyrosines in MUC1-CT. (A) Amino Acid sequence of MUC1 CT WT and MUC1 CT Y0 where tyrosines are mutated to phenylalanine. (B and C) Western blots to detect MUC1 using the MUC1-CT antibody in CHO.Neo, MUC1, and Y0 cells as well as BxPC3.Neo, MUC1, and Y0 cells. (D and E) 48 hour invasion in response to TGF- β 1 treatment presented as fold change from untreated cells. Results are presented as means \pm SEM of n=3. * p<0.05, *** p<0.001.

5B and 5D, $p < 0.05$). However, PP2 treatment did not affect the invasive potential of BxPC3.Neo cells (Figure 5B and 5C). Although the BxPC3.Y0 cells had lower percent invasion than BxPC3.MUC1 and BxPC3.Neo cells, it is interesting that PP2 treatment further decreased invasiveness in BxPC3.Y0 cells (Figure 5B and 5E, $p < 0.001$, $p < 0.05$). The fact that PP2 inhibition affected the Y0 cells may be because PP2 is non-selective and is known to weakly inhibit EGFR and many other kinases with similar affinities [48, 49]. Overall, the results suggest that overexpression of MUC1 in these cell lines drive the anti-apoptotic oncogenic functions of TGF- β in a SMAD4 independent manner, and that this is partially via signaling interaction of c-Src with MUC1-CT. Further investigations need to be conducted to better understand the mechanisms and importance of MUC1-CT tyrosines and the interaction with other oncogenic signaling pathways. In a pilot study, we established the MUC1 CT expression levels and the natural invasive potential of a variety of MUC1-CT mutated BxPC3 cells (Supplementary Figure 3A and 3B). In BxPC3.Y2 and 5; BxPC3.Y6; BxPC3.Y7; and BxPC3.

Y3, 6 and 7 cell lines where either single or multiple tyrosines are mutated to phenylalanine, the results show that these cells behave similarly to BxPC3.Y0. These results further establish the critical oncogenic role of MUC1 CT as reviewed in [44].

It must be noted that the levels that we report for the endogenous TGF- β 1 production is in picograms/ml and what we add exogenously is in ngs/ml. In the CHO.MUC1 cells, the level is only 0.1ngs and in BxPC3.MUC1, it is 0.6ngs (Figure 1). Therefore, the functional differences we report in Figures 2-5 is due predominantly through the exogenous addition of TGF- β (10ngs).

DISCUSSION

In a noncancerous pancreas, MUC1 is expressed in low levels on the luminal surface of the ductal epithelial cells. Yet, an exponential increase in MUC1 expression occurs during early stages of pancreatic cancer development. Even in early stage pancreatic intraepithelial neoplasia (PanIN) lesions, there is an observed increase

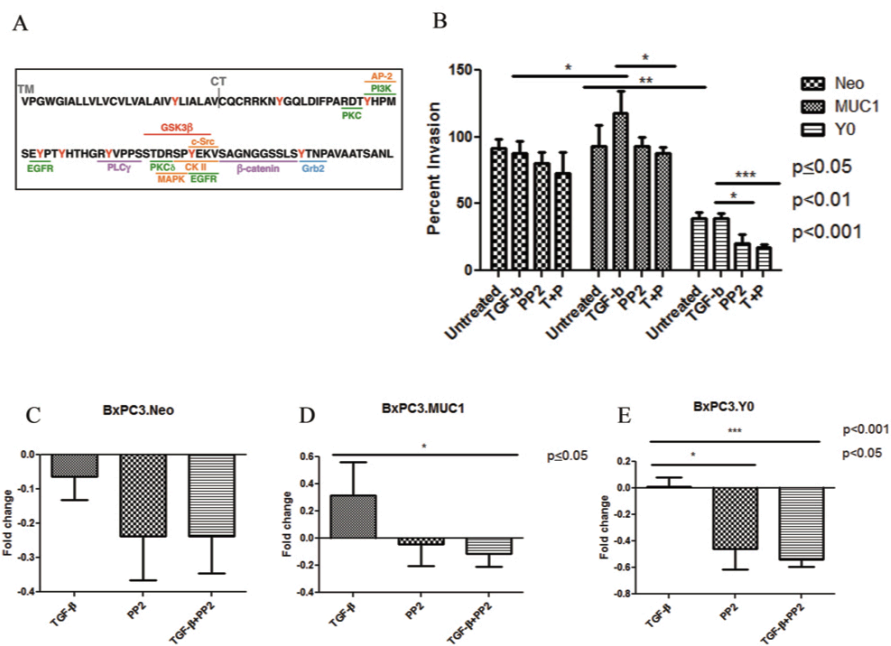


Figure 5: C-Src inhibition negates the aggressiveness of TGF- β mediated invasion in MUC1 expressing cells. (A) Schematic of MUC-CT amino acid sequence and the potential kinase binding sites. **(B)** Percent invasion was determined by standard transwell assay at 48 hours post treatment with TGF- β 1 \pm PP2 as indicated in the figure. **(C-E)** Each treatment is compared to the untreated within each individual cell line. Results of the invasion assay are presented as means \pm SEM of n=3. * $p < 0.05$, *** $p < 0.001$.

in MUC1 expression [27, 50, 51]. It is also shown that TGF- β mediated response changes from apoptotic and cell growth regulatory to increasing invasiveness and migration in cancer [9]. The data presented herein suggests that MUC1's interaction with components of the TGF- β signaling pathway, in a SMAD4 independent mechanism, increases the oncogenic features of anti-apoptosis, increased EMT signaling, and more invasion. This has important clinical relevance, because MUC1 may be a biomarker for anti-TGF- β therapies in PDA cells. Tumors with high MUC1 expression can now be considered for TGF- β neutralizing strategies, while MUC1 low expressing tumors should not be considered for the same.

Using a SMAD4 independent PDA cell model, we demonstrate that MUC1 increases TGF- β 1 secretion, without affecting expression of the key components of the TGF- β signaling in a SMAD-4 deleted cell line (Figure 1). We believe that the increase in TGF- β 1 secretion in the MUC1 overexpressing cells (Figure 1) may be due to the 3-fold increase in latent TGF-beta binding protein 1 (LTBP-1) gene expression in the BxPC3.MUC1 when compared to the Neo cells (from our microarray data¹ (data not shown)). LTBP-1 activates TGF- β secretion. This targets latent complexes of TGF- β to the extracellular matrix, where the latent cytokine is subsequently activated by various mechanisms. It has been previously shown that MUC1 expression increased TGF- β 1 expression at the mRNA and protein levels in human hepatocellular carcinoma cells [52]. In dry eye disease, it has also been shown that MUC1 increases basal TGF- β expression [53]. Recently, it has been shown that TGF- β signaling and deletion of SMAD 4 can alter AGR2 expression, which in turn positively correlates with MUC1 expression [54]. These studies support our findings that in a MUC1-overexpressing SMAD 4 deleted PDA cell line model, MUC1 increases TGF- β 1 expression and release. The mechanisms for upregulation of TGF- β 1 are unknown. However, once malignant cells lose their growth inhibitory response to TGF- β 1 and produce high levels of these protein, the increased expression of TGF- β 1 provides a selective advantage for tumor cell survival as TGF- β 1 are also angiogenic and have potent immunosuppressive effects [39].

During the early phases of tumorigenesis, TGF- β inhibits primary tumor development and growth by inducing cell cycle arrest and apoptosis [55, 56]. Apoptosis is characterized by morphological and biochemical changes [57]. When the role of TGF- β changes from tumor suppressor to tumor promoter, as reviewed in Lebrun 2012, the tumor promoting effects of TGF- β includes induction of EMT, resistance to apoptosis, migration, invasion, and tumor metastasis [58]. It has been shown that SMAD-4 deleted WT BxPC3 cells constitutively activates ERK, has an increased anti-apoptotic response but does not promote invasiveness [43, 59]. Finally, it has also been shown that MUC1

expression can confer resistance of epithelial cancer cells to cell death via anoikis [60]. Data from our study indicates that MUC1-overexpressing cells are resistant to TGF- β mediated apoptosis, (Figure 2) and become highly invasive in a SMAD4-independent manner (Figure 3). We have also shown similar results in an endogenously MUC1 high Wild Type SMAD4 PDA cell line (Supplementary Figure 4). Another study reported that inhibiting TGF- β downstream signaling reduces invasiveness in PANC-1 PDA cell line that is known to express MUC1 [61]. Thus, our data correlates with that study, showing that the MUC1-over expressing cell lines, BxPC3.MUC1 and CHO.MUC1, have significantly reduced TGF- β -induced invasiveness when downstream signaling is blocked in the MUC1 phosphomutant Y0 cells or in PP2 treated cells (Figures 4 and 5). The blocking of MUC1-CT downstream signaling in SMAD4 - negative pancreatic cancer cell line reduces the effects previously seen in the MUC1-high expressing cells, establishing the importance of MUC1-CT. This is significant for the 55% of PDA cases where SMAD4 is deleted. It is important to note that MUC1 expression level does not change with TGF- β 1 treatment or in cells with MUC1 CT tyrosines mutated to phenylalanine (Supplementary Figure 2). Therefore, the effects are not a reflection of differences in MUC1 expression levels. Although MUC1 is known to confer resistance to apoptosis in response to several genotoxic drugs in PDA and other cancer cells [29, 41, 42], this is the first study that shows MUC1 blocks TGF- β induced apoptosis. Signaling through the CT of MUC1 is critical for cleavage of caspases and apoptosis (Supplementary Figure 1B).

Previous studies have shown that the clinical efficiency of inhibition of c-Src in PDA cells is due to inhibition of tumor-promoting TGF- β signaling [46]. Our data supports this interaction by providing evidence that in BxPC3.MUC1 cells treated with c-Src inhibitor PP2 significantly reduced TGF- β -induced invasion (Figure 5). However, it is also shown that PP2 can be non-selective by weakly inhibit EGFR and have other off-target effects [48, 49]. Further array analysis can be performed to understand the complete mechanism. Solving the mystery of the molecular interactions with other oncogenic signaling pathways associated with SMAD4 independent TGF- β signaling will provide great insight into the functional switch of TGF- β from a tumor suppressor to a promoter of tumor development. This knowledge may potentially enable anti-TGF- β therapies in combination with standard therapies and/or immunotherapy to become more efficiently used in the clinic. For example, although certain TGF- β inhibitory treatments have worked *in vivo* using mouse models, the results have not been particularly promising in clinical trials [62]. Targeting TGF- β carries a substantial risk as this pathway is implicated in multiple homeostatic processes and is known to have tumor-suppressor functions. Establishing the mechanism, and

determining a potential biomarker, should be priority before continuing anti-TGF- β clinical trials. The mechanisms for upregulation of TGF- β remain unknown. However, once malignant cells lose their growth inhibitory response to TGF- β and produce massive amounts of TGF- β (as seen in the MUC1-high cells-Figure 1), the increased expression of TGF- β provides a discerning advantage for tumor cell survival. If MUC1 can be shown as a correlative biomarker, as our data suggests, we may

alleviate some of the complications associated with anti-TGF- β therapies, especially in SMAD4 independent PDA cases. The data presented here is just the beginning in establishing why certain patients may be more suitable candidates for TGF- β targeted therapies than others may. We conclude that signaling through MUC1-CT plays a critical role in the switch of SMAD4 independent TGF- β function from a pro-apoptotic to a pro-invasion cytokine (Figure 6).

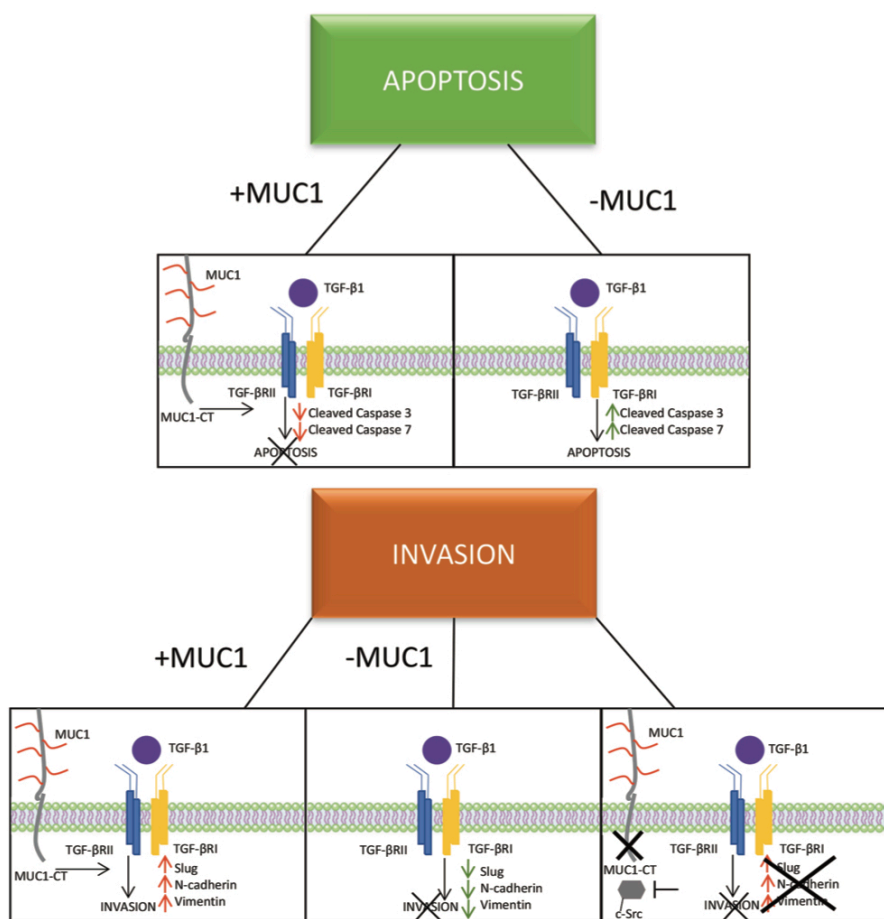


Figure 6: A schematic of the proposed mechanism of MUC1 mediating TGF- β signaling. Schematic showing that MUC1-CT plays an important role in switching the role of TGF- β from a tumor suppressor to a tumor promoter in PDA, specifically in BxPC3 cells.

EXPERIMENTAL PROCEDURES

Cell lines and culture

CHO.MUC1, CHO.Neo, CHO. Y0, BxPC3.MUC1, BxPC3.Neo, BxPC3.Y0 were generated as previously described [30]. HPAF-II and MIA Paca-2 were obtained from American Type Culture Collection and cultured as instructed. Cell lines were maintained in Roswell Park Memorial Institute 1640 medium (RPMI; with, L-glutamine; ThermoFisher). RPMI was supplemented with 10% fetal bovine serum (FBS; Hyclone), 3.4 mM L-glutamine, 90 units (U) per ml penicillin, 90 µg/ml streptomycin, and 1% Non-essential amino acids (Cellgro). RPMI was also supplemented with Geneticin (G418; Invitrogen, Carlsbad, CA, USA). Cells were kept in a 5% CO₂ atmosphere at 37°C. The antibiotic G418 (50 mg/ml) was added to every passage of BxPC3.Neo and BxPC3.MUC1 to ensure positive selection of MUC1 positive cells. For all experiments, cell lines were passaged no more than 10 times.

Western blotting

Cellular lysate preparation and Western blotting was done as previously described [30]. The cells were either treated as such: no treatment, 10 ng/ml of TGF-β1 (Peprotech, Rocky Hill, NJ, USA), or 100µM of Etoposide for 48 hours due to more pronounced signaling. 1:500 Armenian hamster monoclonal anti-human MUC1 cytoplasmic tail (CT2) antibody was used to probe for MUC1 in phosphate-buffered-saline-Tween 20 (PBS-T) with 5% BSA. CT2 antibody recognizes the last 17 amino acids (SSLSYNTPAVAATSANL) of the cytoplasmic tail (CT) of human MUC1 [38]. 1:10,000 TAB004 (OncoTAB, Charlotte, NC) was used to detect the N-terminus extracellular domain of MUC1 [24, 51]. Membranes were also probed with the following antibodies from Cell Signaling (1:1000): Smad4 (Rabbit, 38454), Smad 2/3 (Rabbit, 5678), Vimentin (Rabbit, 5741), Snail (Rabbit, 3879), Slug (Rabbit, 9585), N-cadherin (Rabbit, 13116), Cleaved Caspase 3 (Rabbit, 9664), Caspase 3 (Rabbit, 9665), Cleaved Caspase 7 (Rabbit, 8438), Caspase 7 (Rabbit, 12827), and β-Actin (Mouse, 3700). Other antibodies used include TGF-βRI (Abcam, 1:200, Rabbit, ab31013) and TGF-βRII (Abcam, 1:1000, Rabbit, ab61213). Densitometric analysis was conducted using the ImageJ software and percent change is calculated accordingly: First, each density unit for the particular protein was normalized to their respective β-actin density. Percent change was determined by formula (TGF-β treated – No treatment/ No treatment) * 100. If the final answer was negative, this was percentage decrease (suggesting that the protein level remained unchanged with treatment).

ELISA

Cells plated in duplicates in 6 well plates were cultured for 6, 12, and 24 hours. At the indicated time point, the culture supernatant was collected and concentrated using Amicon ultra-centrifugal filters (3KDa cutoff). The protein retentate was reconstituted up to 0.5ml with PBS. TGF-β1 levels in the supernatant were assessed using a specific ELISA (R&D systems, Minneapolis, MN), according to the manufacturer's recommended protocol. The total protein concentration was determined by BCA. The TGF-β1 levels were normalized to the total protein content of each sample. Results were expressed as TGF-β1 pg/ml concentration.

Apoptosis assay

Cells that were serum starved for 18 hours were left untreated or treated with 10ng/ml of TGF-β1 (Peprotech, Rocky Hill, NJ, USA) and 100µM of Etoposide (as a positive control). 24 hours after treatment began; the cells were harvested and stained with Annexin V and PI (Annexin V/Dead Cell Apoptosis Kit, Life Technologies, Eugene, Oregon). The cells were analyzed using BD FORTESSA and FlowJo Version 8.8.7. Fold-change was calculated as TGF-β treated percent apoptosis/control percent invasion.

Invasion assay

Cells were serum starved 18 hours before plating for the invasion assay. 50,000 cells in serum-free media were plated over transwell inserts (BD Biosciences, San Jose, CA, USA) precoated with diluted reduced growth factor Matrigel in serum free media, plus or minus TGF-β1 (Peprotech, Rocky Hill, NJ, USA). The cells were allowed to invade through the Matrigel for 48 hours towards the serum contained in the bottom chamber. After 48 hours, only the control wells were swabbed with a cotton swab, followed by staining of all inserts with coomassie blue. The excess stain was washed off and the inserts were allowed to dry. The membrane was cut and dipped in 10% acetic acid for 10 minutes to elute the dye, which was read by UV/Vis Spectrophotometer at 562µM. Percent invasion was calculated as sample absorbance/control absorbance X 100. Fold-change was calculated as TGF-β treated percent invasion/untreated percent invasion.

Treatment with c-Src inhibitor

BxPC3.MUC1, Neo, and Y0 cells were serum starved 18 hours before plating for the invasion assay. 50,000 cells were plated as in the invasion assay protocol. Cells were either left untreated, treated with 10 ng/ml of TGF-β1 (Peprotech, Rocky Hill, NJ, USA), or the c-Src inhibitor PP2 (Tocris), or a combination of 10 ng/ml of

TGF- β 1 and PP2. The invasion assay was performed as described above.

Statistics

Graphpad Prism 5 and ImageJ were used to analyze the western data. Graphpad Prism 5 was used to create the graphs and perform statistical analysis.

Footnotes

The content is solely the responsibility of the authors and does not necessarily represent the official views of the National Institutes of Health.

Abbreviations

PDA= Pancreatic Ductal Adenocarcinoma; TGF β = Transforming Growth Factor Beta; MUC1= Mucin 1; MUC1.CT= Mucin 1 cytoplasmic tail; BxPC3.MUC1= BxPC3 cell line overexpressing human MUC1 protein; PP2= c-Src inhibitor; CHO= Chinese Hamster Ovarian cell line; TGF β RI= Transforming Growth Factor Beta Receptor I; TGF β RII= Transforming Growth Factor Beta Receptor II; EMT= Epithelial- Mesenchymal Transition; COX-2= cyclooxygenase-2; PDGF= Platelet Derived Growth Factor; VEGF= Vascular Endothelial Growth Factor; CT= cytoplasmic tail; CHO.MUC1= Chinese Hamster Ovarian cell line overexpressing human MUC1 protein; BxPC3.Y0= BxPC3 cell line expressing Mucin 1 protein where all 7 tyrosines are mutated; CHO.Y0= Chinese Hamster Ovarian cell line expressing Mucin1 protein with 7 mutated tyrosines; Y0= mutated tyrosines; PanIN= Pancreatic intraepithelial lesions; LTBP1= Latent Transforming Growth Factor Beta Binding Protein.

Author contributions

PG and SN served as lead authors for data collection and analysis and are co-first authors on the manuscript. SN and PM conceived the idea for the project. SN conducted the ELISA experiment and created the BxPC3 and CHO MUC1, Neo, and Y0 cell lines and conducted some of the critical experiments. MDN aided in data analysis and writing the paper. RZ aided in the use of the FORTESSA and flow cytometry analysis. MA provided technical assistance for the collection of data.

ACKNOWLEDGMENTS

We thank the members of the Mukherjee Lab for advice and help throughout the project.

CONFLICTS OF INTEREST

The authors declare that they have no conflicts of interest with the contents of this article.

FUNDING

This work was supported in whole or part by NIH/ NCI grant CA166910-01A1 and CA118944-01A1 and the Belk Endowment at UNCC.

REFERENCES

1. Hezel AF, Kimmelman AC, Stanger BZ, Bardeesy N, Depinho RA. Genetics and biology of pancreatic ductal adenocarcinoma. *Genes Dev.* 2006; 20: 1218-49. <https://doi.org/10.1101/gad.1415606>.
2. Howlader N, Noone AM, Krapcho M, Miller D, Bishop K, Altekruse SF, Kosary CL, Yu M, Ruhl J, Tatalovich Z, Mariotto A, Lewis DR, Chen HS, Feuer EJ, Cronin KA (eds). SEER Cancer Statistics Review, 1975-2013. National Cancer Institute. 2016.
3. Rahib L, Smith BD, Aizenberg R, Rosenzweig AB, Fleshman JM, Matrisian LM. Projecting cancer incidence and deaths to 2030: the unexpected burden of thyroid, liver, and pancreas cancers in the United States. *Cancer Res.* 2014. <https://doi.org/10.1158/0008-5472.can-14-0155>.
4. Siegel RL, Miller KD, Jemal A. Cancer statistics, 2016. *CA Cancer J Clin.* 2016; 66: 7-30. <https://doi.org/10.3322/caac.21332>.
5. Macias-Silva M, Abdollah S, Hoodless PA, Pirone R, Attisano L, Wrana JL. MADR2 is a substrate of the TGF β receptor and its phosphorylation is required for nuclear accumulation and signaling. *Cell.* 1996; 87: 1215-24. [https://doi.org/http://dx.doi.org/10.1016/S0092-8674\(00\)81817-6](https://doi.org/http://dx.doi.org/10.1016/S0092-8674(00)81817-6).
6. Zhang Y, Feng X, We R, Derynck R. Receptor-associated Mad homologues synergize as effectors of the TGF-beta response. *Nature.* 1996; 383: 168-72. <https://doi.org/10.1038/383168a0>.
7. Shi Y, Massague J. Mechanisms of TGF-beta signaling from cell membrane to the nucleus. *Cell.* 2003; 113: 685-700.
8. Souchelnytskyi S, Tamaki K, Engstrom U, Wernstedt C, ten Dijke P, Heldin CH. Phosphorylation of Ser465 and Ser467 in the C terminus of Smad2 mediates interaction with Smad4 and is required for transforming growth factor-beta signaling. *J Biol Chem.* 1997; 272: 28107-15.
9. Katz LH, Li Y, Chen JS, Munoz NM, Majumdar A, Chen J, Mishra L. Targeting TGF-beta signaling in cancer. *Expert Opin Ther Targets.* 2013; 17: 743-60. <https://doi.org/10.1517/14728222.2013.782287>.
10. Neuzillet C, Tijeras-Raballand A, Cohen R, Cros J, Faivre S, Raymond E, de Gramont A. Targeting the TGF β pathway for cancer therapy. *Pharmacol Ther.* 2015; 147: 22-31. <http://doi.org/10.1016/j.pharmthera.2014.11.001>.
11. Fink SP, Mikkola D, Willson JK, Markowitz S. TGF-beta-induced nuclear localization of Smad2 and Smad3 in Smad4 null cancer cell lines. *Oncogene.* 2003; 22: 1317-23. <https://doi.org/10.1038/sj.onc.1206128>.

12. Hahn SA, Schutte M, Shamsul Hoque AT, Moskaluk CA, da Costa LT, Rozenblum E, Weinstein CL, Fischer A, Yeo CJ, Hruban RH, Kern SE. DPC4, a candidate tumor suppressor gene at human chromosome 18q21.1. *Science*. 1996; 271: 350-3. <https://doi.org/10.1126/science.271.5247.350>.
13. Hansel DE, Kern SE, Hruban RH. Molecular pathogenesis of pancreatic cancer. *Annu Rev Genomics Hum Genet*. 2003; 4: 237-56. <https://doi.org/10.1146/annurev.genom.4.070802.110341>.
14. Xie L, Law BK, Chytil AM, Brown KA, Aakre ME, Moses HL. Activation of the Erk pathway is required for TGF- β 1-induced EMT *in vivo*. *Neoplasia*. 2004; 6: 603-10. <http://doi.org/10.1593/neo.04241>.
15. Kalluri R, Weinberg RA. The basics of epithelial-mesenchymal transition. *J Clin Invest*. 2009; 119: 1420-8. <https://doi.org/10.1172/JCI39104>.
16. Thiery JP. Epithelial-mesenchymal transitions in tumour progression. *Nat Rev Cancer*. 2002; 2: 442-54.
17. Truty MJ, Urrutia R. Basics of TGF- β and pancreatic cancer. *Pancreatol*. 2007; 7: 423-35. <http://doi.org/10.1159/000108959>.
18. Assoian RK, Komoriya A, Meyers CA, Miller DM, Sporn MB. Transforming growth factor-beta in human platelets. Identification of a major storage site, purification, and characterization. *J Biol Chem*. 1983; 258: 7155-60.
19. Ikeda T, Lioubin MN, Marquardt H. Human transforming growth factor type beta 2: production by a prostatic adenocarcinoma cell line, purification, and initial characterization. *Biochemistry*. 1987; 26: 2406-10.
20. Derynck R, Lindquist PB, Lee A, Wen D, Tamm J, Graycar JL, Rhee L, Mason AJ, Miller DA, Coffey RJ. A new type of transforming growth factor-beta, TGF-beta 3. *EMBO J*. 1988; 7: 3737-43.
21. Buijs JT, Stayrook KR, Guise TA. The role of TGF-[beta] in bone metastasis: novel therapeutic perspectives. *Bonekey Rep*. 2012.
22. Nath S, Mukherjee P. MUC1: a multifaceted oncoprotein with a key role in cancer progression. *Trends Mol Med*. 2014; 20: 332-42. <https://doi.org/10.1016/j.molmed.2014.02.007>.
23. Kufe DW. Functional targeting of the MUC1 oncogene in human cancers. *Cancer Biol Ther*. 2009; 8: 1197-203.
24. Zhou R, Curry JM, Roy LD, Grover P, Haider J, Moore LJ, Wu ST, Kamesh A, Yazdanifar M, Ahrens WA, Leung T, Mukherjee P. A novel association of neuropilin-1 and MUC1 in pancreatic ductal adenocarcinoma: role in induction of VEGF signaling and angiogenesis. *Oncogene*. 2016. <https://doi.org/10.1038/onc.2015.516>.
25. Li Y, Ren J, Yu WH, Li Q, Kuwahara H, Yin L, Carraway KL, Kufe D. The epidermal growth factor receptor regulates interaction of the human DF3/MUC1 carcinoma antigen with c-Src and β -catenin. *J Biol Chem*. 2001; 276: 35239-42. <https://doi.org/10.1074/jbc.C100359200>.
26. Li Y, Kuwahara H, Ren J, Wen G, Kufe D. The c-Src tyrosine kinase regulates signaling of the human DF3/MUC1 carcinoma-associated antigen with GSK3 β and β -catenin. *J Biol Chem*. 2001; 276: 6061-4. <https://doi.org/10.1074/jbc.C000754200>.
27. Sahraei M, Roy LD, Curry JM, Teresa TL, Nath S, Besmer D, Kidiyoor A, Dalia R, Gendler SJ, Mukherjee P. MUC1 regulates PDGFA expression during pancreatic cancer progression. *Oncogene*. 2012; 31: 4935-45. <https://doi.org/10.1038/onc.2011.651>.
28. Kaur S, Kumar S, Momi N, Sasson AR, Batra SK. Mucins in pancreatic cancer and its microenvironment. *Nat Rev Gastroenterol Hepatol*. 2013; 10: 607-20. <https://doi.org/10.1038/nrgastro.2013.120>.
29. Nath S, Daneshvar K, Roy LD, Grover P, Kidiyoor A, Mosley L, Sahraei M, Mukherjee P. MUC1 induces drug resistance in pancreatic cancer cells via upregulation of multidrug resistance genes. *Oncogenesis*. 2013; 2: e51. <https://doi.org/10.1038/oncsis.2013.16>.
30. Roy LD, Sahraei M, Subramani DB, Besmer D, Nath S, Tinder TL, Bajaj E, Shanmugam K, Lee YY, Hwang SI, Gendler SJ, Mukherjee P. MUC1 enhances invasiveness of pancreatic cancer cells by inducing epithelial to mesenchymal transition. *Oncogene*. 2011; 30: 1449-59. <https://doi.org/10.1038/onc.2010.526>.
31. Nath S, Roy LD, Grover P, Rao S, Mukherjee P. Mucin 1 regulates Cox-2 gene in pancreatic cancer. *Pancreas*. 2015; 44: 909-17. <https://doi.org/10.1097/mpa.0000000000000371>.
32. Kufe DW. Mucins in cancer: function, prognosis and therapy. *Nat Rev Cancer*. 2009; 9: 874-85. <https://doi.org/10.1038/nrc2761>.
33. Tinder TL, Subramani DB, Basu GD, Bradley JM, Schettini J, Million A, Skaar T, Mukherjee P. MUC1 enhances tumor progression and contributes toward immunosuppression in a mouse model of spontaneous pancreatic adenocarcinoma. *J Immunol*. 2008; 181: 3116-25.
34. Singh PK, Hollingsworth MA. Cell surface-associated mucins in signal transduction. *Trends Cell Biol*. 2006; 16: 467-76. <http://doi.org/10.1016/j.tcb.2006.07.006>.
35. Thompson EJ, Shanmugam K, Kotlarczyk KL, Hatstrup CL, Gutierrez A, Bradley JM, Mukherjee P, Gendler SJ. Tyrosines in the MUC1 cytoplasmic tail modulate oncogenic signaling pathways. *Cancer Res*. 2005; 65: 222.
36. Hollingsworth MA, Swanson BJ. Mucins in cancer: protection and control of the cell surface. *Nat Rev Cancer*. 2004; 4: 45-60. http://www.nature.com/nrc/journal/v4/n1/supinfo/nrc1251_S1.html.
37. Ren J, Raina D, Chen W, Li G, Huang L, Kufe D. MUC1 Oncoprotein functions in activation of fibroblast growth factor receptor signaling. *Mol Cancer Res*. 2006; 4: 873-83. <https://doi.org/10.1158/1541-7786.MCR-06-0204>.

38. Roce MV, Isla-Larriain M, Remes-Lenicov F, Colussi AG, Lacunza E, Kim KC, Gendler SJ, Segal-Eiras A. MUC1 cytoplasmic tail detection using CT33 polyclonal and CT2 monoclonal antibodies in breast and colorectal tissue. *Histol Histopathol.* 2006; 21: 849-55.
39. Massague J. TGFbeta in Cancer. *Cell.* 2008; 134: 215-30. <https://doi.org/10.1016/j.cell.2008.07.001>.
40. Porter AG, Janicke RU. Emerging roles of caspase-3 in apoptosis. *Cell Death Differ.* 1999; 6: 99-104. <https://doi.org/10.1038/sj.cdd.4400476>.
41. Agata N, Ahmad R, Kawano T, Raina D, Kharbanda S, Kufe D. MUC1 oncoprotein blocks death receptor-mediated apoptosis by inhibiting recruitment of caspase-8. *Cancer Res.* 2008; 68: 6136-44. <https://doi.org/10.1158/0008-5472.CAN-08-0464>.
42. Chen Q, Li D, Ren J, Li C, Xiao ZX. MUC1 activates JNK1 and inhibits apoptosis under genotoxic stress. *Biochem Biophys Res Commun.* 2013; 440: 179-83. <https://doi.org/10.1016/j.bbrc.2013.09.055>.
43. Moz S, Basso D, Bozzato D, Galozzi P, Navaglia F, Negm OH, Arrigoni G, Zambon CF, Padoan A, Tighe P, Todd I, Franchin C, Pedrazzoli S, et al. SMAD4 loss enables EGF, TGFβ1 and S100A8/A9 induced activation of critical pathways to invasion in human pancreatic adenocarcinoma cells. *Oncotarget.* 2016; 7: 69927-44. <https://doi.org/10.18632/oncotarget.12068>.
44. Carson DD. The cytoplasmic tail of MUC1: a very busy place. *Sci Signal.* 2008; 1: pe35.
45. Thompson EJ, Shanmugam K, Hatrup CL, Kotlareczyk KL, Gutierrez A, Bradley JM, Mukherjee P, Gendler SJ. Tyrosines in the MUC1 cytoplasmic tail modulate transcription via the extracellular signal-regulated kinase 1/2 and nuclear factor-kappaB pathways. *Mol Cancer Res.* 2006; 4: 489-97.
46. Bartscht T, Rosien B, Rades D, Kaufmann R, Biersack H, Lehnert H, Gieseeler F, Ungefroren H. Dasatinib blocks transcriptional and promigratory responses to transforming growth factor-beta in pancreatic adenocarcinoma cells through inhibition of Smad signalling: implications for *in vivo* mode of action. *Mol Cancer.* 2015; 14: 199. <https://doi.org/10.1186/s12943-015-0468-0>.
47. Al Masri A, Gendler SJ. Muc1 affects c-Src signaling in PyV MT-induced mammary tumorigenesis. *Oncogene.* 2005; 24: 5799-808. <https://doi.org/10.1038/sj.onc.1208738>.
48. Kong L, Deng Z, Shen H, Zhang Y. Src family kinase inhibitor PP2 efficiently inhibits cervical cancer cell proliferation through down-regulating phospho-Src-Y416 and phospho-EGFR-Y1173. *Mol Cell Biochem.* 2011; 348: 11-9. <https://doi.org/10.1007/s11010-010-0632-1>.
49. Brandvold KR, Steffey ME, Fox CC, Soellner MB. Development of a highly selective c-Src kinase inhibitor. *ACS Chem Biol.* 2012; 7: 1393-8. <https://doi.org/10.1021/cb300172e>.
50. Nagata K, Horinouchi M, Saitou M, Higashi M, Nomoto M, Goto M, Yonezawa S. Mucin expression profile in pancreatic cancer and the precursor lesions. *J Hepatobiliary Pancreat Surg.* 2007; 14: 243-54. <https://doi.org/10.1007/s00534-006-1169-2>.
51. Curry JM, Thompson KJ, Rao SG, Besmer DM, Murphy AM, Grdzlishvili VZ, Ahrens WA, McKillop IH, Sindram D, Iannitti DA, Martinie JB, Mukherjee P. The use of a novel MUC1 antibody to identify cancer stem cells and circulating MUC1 in mice and patients with pancreatic cancer. *J Surg Oncol.* 2013; 107: 713-22. <https://doi.org/10.1002/jso.23316>.
52. Li Q, Liu G, Shao D, Wang J, Yuan H, Chen T, Zhai R, Ni W, Tai G. Mucin1 mediates autocrine transforming growth factor beta signaling through activating the c-Jun N-terminal kinase/activator protein 1 pathway in human hepatocellular carcinoma cells. *Int J Biochem Cell Biol.* 2015; 59: 116-25. <https://doi.org/10.1016/j.biocel.2014.11.012>.
53. Imbert-Fernandez Y, Radde BN, Teng Y, Young WW Jr, Hu C, Klinge CM. MUC1/A and MUC1/B splice variants differentially regulate inflammatory cytokine expression. *Exp Eye Res.* 2011; 93: 649-57. doi: <http://doi.org/10.1016/j.exer.2011.08.004>.
54. Norris AM, Gore A, Balboni A, Young A, Longnecker DS, Korc M. AGR2 is a SMAD4-suppressible gene that modulates MUC1 levels and promotes the initiation and progression of pancreatic intraepithelial neoplasia. *Oncogene.* 2013; 32: 3867-76. <https://doi.org/10.1038/onc.2012.394>.
55. Jakowlew SB. Transforming growth factor-beta in cancer and metastasis. *Cancer Metastasis Rev.* 2006; 25: 435-57. <https://doi.org/10.1007/s10555-006-9006-2>.
56. Kim TA, Kim SJ. Mechanisms of TGF-β-Induced Apoptosis in Cancer Cells. *Transforming Growth Factor-β in Cancer Therapy, Volume I: Basic and Clinical Biology.* (Totowa, NJ: Humana Press). 2008; 199-211.
57. Kerr JF, Wyllie AH, Currie AR. Apoptosis: a basic biological phenomenon with wide-ranging implications in tissue kinetics. *Br J Cancer.* 1972; 26: 239-57.
58. Lebrun JJ. The dual role of TGF in human cancer: from tumor suppression to cancer metastasis. *ISRN Mol Biol.* 2012; 2012: 28. <https://doi.org/10.5402/2012/381428>.
59. Fullerton PT, Creighton CJ, Matzuk MM. Insights into SMAD4 loss in pancreatic cancer from inducible restoration of TGF-β signaling. *Mol Endocrinol.* 2015; 29: 1440-53. <https://doi.org/10.1210/me.2015-1102>.
60. Zhao Q, Piyush T, Chen C, Hollingsworth MA, Hilken J, Rhodes JM, Yu LG. MUC1 extracellular domain confers resistance of epithelial cancer cells to anoikis. *Cell Death Dis.* 2014; 5: e1438. <https://doi.org/10.1038/cddis.2014.421>.
61. Gaspar NJ, Li L, Kapoun AM, Medicherla S, Reddy M, Li G, O'Young G, Quon D, Henson M, Damm DL, Muir GT, Murphy A, Higgins LS, et al. Inhibition of transforming

growth factor beta signaling reduces pancreatic adenocarcinoma growth and invasiveness. *Mol Pharmacol.* 2007; 72: 152-61. <https://doi.org/10.1124/mol.106.029025>.

62. Connolly EC, Freimuth J, Akhurst RJ. Complexities of TGF- β targeted cancer therapy. *Int J Biol Sci.* 2012; 8: 964-78. <https://doi.org/10.7150/ijbs.4564>.

RESEARCH ARTICLE

Early detection of pancreatic cancer in mouse models using a novel antibody, TAB004

Shu-ta Wu¹, Chandra D. Williams², Priyanka A. Grover¹, Laura J. Moore¹, Pinku Mukherjee^{1*}

1 Department of Biological Sciences, University of North Carolina at Charlotte, Charlotte, North Carolina, United States of America, **2** Department of Animal Laboratory Resources, University of North Carolina at Charlotte, Charlotte, North Carolina, United States of America

* pmukherj@uncc.edu



OPEN ACCESS

Citation: Wu S-t, Williams CD, Grover PA, Moore LJ, Mukherjee P (2018) Early detection of pancreatic cancer in mouse models using a novel antibody, TAB004. *PLoS ONE* 13(2): e0193260. <https://doi.org/10.1371/journal.pone.0193260>

Editor: Juri G. Gelovani, Wayne State University, UNITED STATES

Received: September 26, 2017

Accepted: February 7, 2018

Published: February 20, 2018

Copyright: © 2018 Wu et al. This is an open access article distributed under the terms of the [Creative Commons Attribution License](https://creativecommons.org/licenses/by/4.0/), which permits unrestricted use, distribution, and reproduction in any medium, provided the original author and source are credited.

Data Availability Statement: All relevant data are within the paper and its Supporting Information files.

Funding: OncoTAB Inc. only provided the antibody TAB004 for this study. OncoTAB did not play a role in the study design, data collection and analysis, decision to publish, or preparation of the manuscript and did not provide any financial support to any of the authors. All funding for this manuscript came from CPCP Levine UNCC Pancreatic Cancer Pilot Project, National Institutes of Health, National Cancer Institute (NIH-NIC grant

Abstract

Pancreatic ductal adenocarcinoma (PDA) is the fourth-leading cause of cancer death in the United States with a 5-year overall survival rate of 8% for all stages combined. But this decreases to 3% for the majority of patients that present with stage IV PDA at time of diagnosis. The lack of distinct early symptoms for PDA is one of the primary reasons for the late diagnosis. Common symptoms like weight loss, abdominal and back pains, and jaundice are often mistaken for symptoms of other issues and do not appear until the cancer has progressed to a late stage. Thus the development of novel imaging platforms for PDA is crucial for the early detection of the disease. MUC1 is a tumor-associated antigen (tMUC1) expressed on 80% of PDA. The goal of this study was to determine the targeting and detection capabilities of a tMUC1 specific antibody, TAB004. TAB004 antibody conjugated to a near infrared fluorescent probe was injected intraperitoneally into immune competent orthotopic and spontaneous models of PDA. Results show that fluorophore conjugated TAB004 specifically targets a) 1 week old small tumor in the pancreas in an orthotopic PDA model and b) very early pre-neoplastic lesions (PanIN lesions) that develop in the spontaneous PDA model before progression to adenocarcinoma. Thus, TAB004 is a promising antibody to deliver imaging agents directly to the pancreatic tumor microenvironment, significantly affecting early detection of PDA.

Introduction

Incidence and mortality trends predict pancreatic cancer will become the second-leading cause of cancer related deaths by 2020 in the United States. The mean expectation of life is less than six months and there are few long-term survivors. According to the Annual Cancer Statistics Review, patients with pancreatic carcinoma have the lowest 5-year survival rate [1,2]. Poor prognosis for patients is mainly due to late diagnosis, as a result of the lack of distinct early symptoms and effective diagnostics [3]. Only 15–18% of pancreatic cancer cases are resectable, and surgery offers the only single modality for potential cure. These patients have a two-year survival rate of 20%–40% with surgery, but despite surgical resection, local

RO1 CA118944-01A1), UNC Charlotte Faculty Research Grant, and The Williams States Lee College of Engineering Center for Biomedical Engineering and Science IVIS Imaging System Award.

Competing interests: Dr. Pinku Mukherjee is the co-founder and Chief Scientific Office of OncoTAB, Inc. The affiliation with OncoTAB does not alter our adherence to PLOS ONE policies on sharing data and materials.

recurrence or metastasis occurs in more than 50% of the patients (predominantly liver and peritoneum). Adjuvant therapy in patients with resectable pancreatic cancer including radiation and chemotherapy is a subject of controversy with randomized trials showing contradictory results. Very often the cancer becomes resistant to such therapies. Several of these therapies also produce undesirable side effects and in some instances damage to major organs. Overall survival from PDA is only possible with surgery and adjuvant treatment when detected early [4,5]. Thus, development of an effective and targeted detection platform is essential in order to improve the survival of PDA patients. Infiltrating PDA accounts for over 95% of all exocrine pancreatic malignancies. Activating mutations in the KRAS proto-oncogene are found in over 90% of invasive PDA and are thought to represent an initiating event. Recently a transgenic mouse model has been created that expresses physiological levels of oncogenic KRAS with a glycine to aspartate substitution at codon 12 (KRAS^{G12D}) in the progenitor cells of mouse pancreas. These mice develop the full spectrum of pancreatic ductal adenocarcinoma from preinvasive neoplasias (PanINs) to invasive and metastatic disease (designated as the Cre-LSL-KRAS^{G12D} or PDA mice).

Mucin-1 (MUC1), is a transmembrane protein with a heavily glycosylated extracellular domain [6]. Normal expression of MUC1 can be found on all glandular epithelial cells of the mammary gland, esophagus, stomach, duodenum, uterus, prostate, lung, and pancreas [7]. The negatively charged glycosylated extracellular domain of MUC1 in normal healthy tissues creates a physical barrier and an anti-adhesive surface, preventing pathogenic colonization [8]. However, in 80% of PDA, the extracellular domain of MUC1 is hypoglycosylated and the protein overexpressed [9]. This alteration of the structure and expression of MUC1 is associated with higher metastasis and poor prognosis [10,11] but also makes it the 2nd most targetable tumor antigen [12].

We have generated the PDA.MUC1 mice by breeding the Cre-LSL-KRAS^{G12D} to a human MUC1.Tg mice (designated KCM mice) that develop the entire spectrum of PanIN lesions and adenocarcinoma mimicking the human disease [13]. We generated cell lines from these KCM mice (KCM cells) [11,14,15] and developed a novel monoclonal antibody, TAB004 (OncoTAB, Inc., Charlotte, NC), which specifically targets the hypoglycosylated/tumor-associated form of MUC1 (tMUC1) [16–19].

Using the syngeneic KCM cell lines, we demonstrate that TAB004 specifically binds to tMUC1 expressing orthotopic KCM tumors in immunocompetent mice. Further, we show that TAB004 specifically targets the pancreas in the spontaneous tumor model (the KCM mice) at the early PanIN lesion stage much before the development of invasive PDA. We show that accumulation of TAB004 is significant at the tumor site but not so at other glandular epithelial organs. TAB004 can be further developed as a diagnostics imaging tool for early detection of PDA.

Methods

Cell culture and generation KCM-Luc cells

KCM cell line was generated by the Mukherjee lab from spontaneous PDA tumors from KCM mice [14]. This cell line expresses both mouse Muc1 and human MUC1 and was maintained in Dulbecco's modified Eagle's medium (DMEM, 11965–092, Gibco, Waltham, MA). KCM-Luc cell line was generated by retroviral transduction of KCM cells with MSCV Luciferase PGK-Hygro (MSCV Luciferase PGK-hygro was a gift from Scott Lowe, Addgene plasmid # 18782, Cambridge, MA) was performed by transfecting GP2-293 cells with the MSCV Luciferase PGK-Hygro and pVSV-G vectors and using the subsequent viral supernatant to infect KCM cells. Growth media for these cell lines were supplemented with 10% fetal bovine serum

(FBS, Gibco, Waltham, MA), 3.4mM L-glutamine, 90 units (U) per ml penicillin, and 90μg/ml streptomycin (Cellgro, Corning, Manassas, VA).

TAB004 production and comparison

TAB004 antibody (patent US 8518405 B2 and US 9090698 B2 provided by OncoTAB, Charlotte, NC) [16,18–22]. Parental Murine TAB004 (mTAB004) is a mouse IgG1 monoclonal antibody created from a hybridoma. Chimeric TAB004 (cTAB004) is a chimeric IgG1 antibody with mouse ScFv and human Fc regions. cTAB004 was cloned into a Lake Pharma high expression stable cell line mammalian vector system (CHO cells). After two rounds of cell screening, three top performing CHO cells expressing the antibody were selected for production runs to assess the characteristics of the final stable cell line. The production of all versions of TAB-004 is currently conducted by LakePharma Inc., Belmont, CA. Comparison of mTAB004 and cTAB004 binding profiles were performed by ELISA. 100μl of 3μg/ml in 1x PBS of each antibody was used to coat 96-well ELISA plates (07-200-721, Fisher Scientific, Pittsburgh, PA) for 24 hours at 4°C. Varying concentrations of KCM cell lysate were incubated for 1 hour at room temperature. Following incubation, detection antibody conjugated to HRP was added and incubated for 1 hour at room temperature. After 100μl of TMB (P137574, Thermo Scientific, Waltham, MA) was allowed to incubate for 30 minutes, 50μl of Stop solution (SS03, Invitrogen, Waltham, MA) was added. All steps were followed by 5x washed with 1x wash buffer.

Conjugation of TAB004 to fluorophore

TAB004 conjugation to indocyanine green (ICG) was performed using the ICG Labeling Kit-NH₂ (LK31-10, Dojindo Molecular Technologies, Inc., Washington, D.C.). All conjugations were performed using manufacturer protocols.

Confocal microscopy

Tumor/pancreas sections were treated with NucBlue Fixed Cell ReadyProbes Reagent (ThermoFisher, Waltham, MA) for 5 minutes and Wheat Germ Agglutinin-488 (Molecular Probes, Waltham, MA) for 20 minutes. The slides were then washed with PBS for 5 minutes (3x) and fixed with 4% formaldehyde. Prolong Gold Antifade reagent with DAPI (P36935, Molecular Probes, Waltham, MA) was applied to mount coverslips. Images were acquired on an Olympus Fluoview FV 1000 confocal microscope.

In vivo experiments

C57Bl/6 mice were purchased from Jackson Laboratory and housed at UNC Charlotte's vivarium. For the orthotopic tumor model, C57/Bl6 female mice were injected in the pancreas with 5×10^5 KCM-Luc cells and allowed to recuperate for 7 days before any experiments were performed. For tumor and antibody visualization, orthotopic KCM-Luc tumor bearing C57/Bl6 mice were injected with 125μl of Redijet D-Luciferin (760504, Perkin Elmer, Waltham, MA) intraperitoneally and imaged 25 minutes later. For groups injected with antibody, 12.5μg of IgG1 Isotype conjugated to ICG or TAB004 conjugated to ICG was injected intraperitoneally and imaged at various time points with a Perkin Elmer IVIS Spectrum. KCM mice were generated in the Mukherjee lab. This mouse model is a triple transgenic cross of LSL-KRASG12D x P48-Cre x Human MUC1.Tg that will develop PDA spontaneously and express human MUC1 in a tissue specific manner [13]. The P48-Cre mice have a tamoxifen inducible promoter and therefore, oncogenesis is initiated only when mice are treated with tamoxifen (75 mg/kg in 100ul of corn oil, 1 injection per day for 2 weeks [10 days]. T5648-1G, Millipore Sigma,

St. Louis, MO) as recommended by Jackson labs (<https://www.jax.org/research-and-faculty/tools/cre-repository/tamoxifen>). Mice were euthanized at the end of all imaging studies. This study and all procedures were performed after approval from the Institutional Animal Care and Use Committee of UNC Charlotte.

Image analysis

All fluorescent slide images were analyzed using Image-J (National Institutes of Health, Bethesda, Maryland). All mice and organ images were processed in Living Imagine 4.3.1 (Caliper Life Sciences, Waltham, MA).

Immunohistochemistry

The pancreases of KCM mice were collected and samples fixed in buffered formalin and embedded in paraffin, and 5- to 6- μ m-thick sections were obtained. Standard H&E staining protocol was performed and the tissue slides were then assessed by light microscopy to determine the PanIN lesions and progression to PDA at increasing disease stage. Microphotographs were taken using a DP70 camera and the Olympus Software Suite (Olympus, Waltham, MA).

Results

Targeting of tMUC1 in immunocompetent orthotopic PDA model with TAB004-ICG

Control groups. Four control groups were imaged alongside TAB004 injected groups. Radiance efficiency (RE) values were collected using the Region of Interests (ROIs) for all images.

Control group 1 comprised of normal C57/Bl6 mice with nothing injected that had their organs imaged using the IVIS (S1 Fig). The purpose of Control group 1 was to determine background fluorescence (of ICG) levels in C57/Bl6 mice (Fig 1). Background fluorescence of the interior of the mice (in-situ) where the tumor is normally located (S1A Fig) and each organ (S1B Fig) is shown. The remaining imaging groups would use the radiance efficiency values from Control group 1 for background normalization.

Control group 2 comprised of normal C57/Bl6 with orthotopic KCM-Luc tumors (S2 Fig). This group is to determine the RE of KCM-Luc tumor by itself without injection of TAB004-ICG. The KCM cell line is a syngeneic mouse PDA cell line that expresses high levels of tMUC1 [11,19,23,24] and therefore a good target for *in vivo* TAB004 [17]. Post luciferin injection, exterior bioluminescent image in live mice confirmed the presence of KCM tumor at 7 days post KCM challenge (S2A Fig). One representative image is shown with $n = 3$ mice showing similar images. After imaging of the live mice, mice were euthanized and the organs of the mice in-situ photographed confirming the location of tumor in the pancreas (S2B Fig). Additionally, IVIS images confirmed that KCM tumors (S2C Fig) do not auto fluoresce. RE values of organs from Control group 2 were recorded (S2D Fig) and compared with RE values of Control group 1. There was no significant increase in RE values between in-situ and organ images of Control group 1 and 2 (Fig 1), therefore background RE values do not increase if an orthotopic tumor is present.

Control group 3 and 4. Next, we were interested in seeing if a control IgG isotype antibody conjugated to ICG would accumulate in any regions of the mice. Control group 3 consisted of normal non-tumor bearing C57/Bl6 mice that were injected with IgG1-ICG (Fig 2). Exterior ICG images taken 24 hours post injection of the IgG1-ICG show no fluorescent signal stronger than the background of the control (Fig 2A). Interior (Fig 2B) and organ (Fig 2C) ICG RE

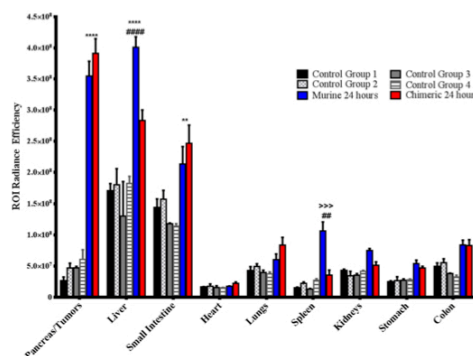


Fig 1. Quantification of ROI values from all imaging groups. The ROI radiance efficiency values for organs from all groups were quantified using Living Image software. * denotes significance between TAB004 (both Murine and Chimeric) and control groups, # denotes significance between Murine and Chimeric TAB004 groups, > denotes significance between Murine TAB004 and other control groups. Data shown is mean \pm SEM (n = 3) and determined by 2-way ANOVA with Tukey post hoc test, *p<0.05, **p<0.01, ***p<0.001, ****p<0.0001.

<https://doi.org/10.1371/journal.pone.0193260.g001>

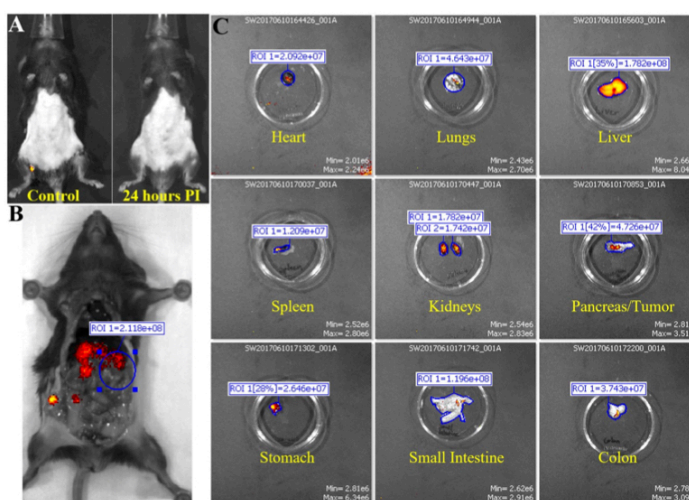


Fig 2. Fluorescent IVIS images of organs from mouse in control group 3. Representative images for non-tumor bearing mice injected with mouse IgG1 isotype control are shown. (A) Fluorescent IVIS image of before (control) and 24 hours post injection of IgG1 conjugated with ICG. 24 hours PI fluorescence is normalized to its own control fluorescence. (B) The mouse is imaged with filter pair ICG on the IVIS Spectrum. Background has been removed and the ROI measurements for the area where tumor would have been are shown. (C) Organs from mouse are imaged individually in the IVIS Spectrum. Intensity of the red-yellow fluorescence in ROI measurements indicate background and antibody accumulation for each organ.

<https://doi.org/10.1371/journal.pone.0193260.g002>

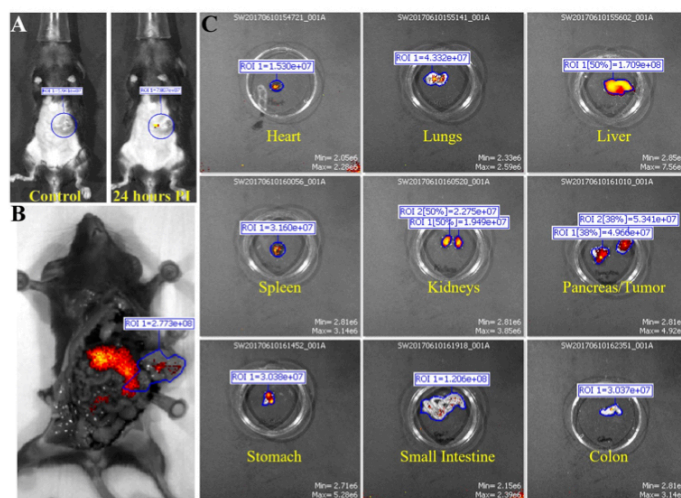


Fig 3. Fluorescent IVIS images of organs from mouse in control group 4. Representative images for tumor bearing mice injected with wtG1 isotype control are shown. (A) Fluorescent IVIS image of before (control) and 24 hours post injection of IgG1 conjugated with ICG. 24 hours PI fluorescence is normalized to its own control fluorescence. (B) The mouse is imaged with filter pair ICG on the IVIS Spectrum. Background has been removed and the ROI measurements for the tumor is shown. (C) Organs from mouse are imaged individually in the IVIS Spectrum. Intensity of the red-yellow fluorescence in ROI measurements indicate background and antibody accumulation for each organ.

<https://doi.org/10.1371/journal.pone.0193260.g003>

values display no significant increase over values of Control group 1 or 2 (Fig 1). Control group 4 comprised of orthotopic KCM tumor-bearing C57/Bl6 mice injected with IgG1-ICG (Fig 3). Exterior ICG images taken 24 hours after injection of the IgG1-ICG showed no significant increase in fluorescence at the tumor site (Fig 3A). Additionally, no significant increase in RE values from interior (Fig 3B) and organ (Fig 3C) images was observed between all the control groups (Fig 1). Therefore, the injection of an isotype control antibody with ICG does not increase background ICG RE values and any increase in ICG RE values seen in TAB004-ICG injected mice can be unequivocally taken as true accumulation of TAB004 at tumor region.

TAB004-ICG experimental groups. Murine monoclonal TAB004 antibody: The first treatment group consisted of KCM tumor-bearing C57/Bl6 mice injected with mTAB004-ICG (Figs 4 and 5). Exterior ICG images taken as early as 1 minute post injection (PI) show accumulation of the mTAB004 at the tumor site (Fig 4A). The accumulation appears to increase 14 hours PI but decreases after 24 hours (Fig 4A). Exterior bioluminescent image of the same mouse confirm the location of the tumor (Fig 4B). In-situ photograph (Fig 5A) confirms the location of the tumor and IVIS images show significant accumulation of mTAB004-ICG at the tumor site (Fig 5B). The larger region of red-yellow fluorescence indicates accumulation of mTAB004 at the tumor (Fig 5B). Significant increases in RE values (Fig 5C) was observed in the pancreatic tumor, liver, small intestine, and spleen (Fig 1) which indicates the accumulation of mTAB004 selectively in those organs. RE values at the tumor site were ~ 3.5 fold higher and ~2 fold higher at the liver and small intestine site compared to the control groups (Fig 1).

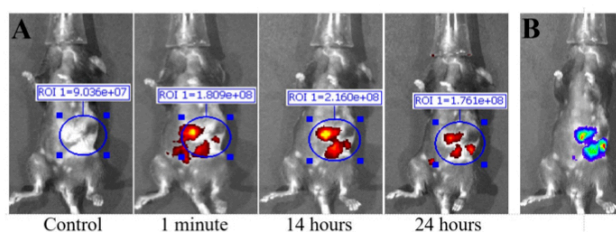


Fig 4. Fluorescent IVIS images taken at different time points of mouse injected with murine monoclonal TAB004. Representative images are shown. (A) Fluorescent IVIS image with filter pair ICG of before (control) 1 minutes, 14 hours, and 24 hours post injection of Parental TAB004 with ICG. Fluorescence images taken after injection are normalized to their own control fluorescence. Background has been removed and the ROI measurements for antibody fluorescence are shown. Intensity of the red-yellow fluorescence in ROI measurements indicates background and antibody accumulation. (B) Bioluminescent image of orthotopic tumor in same mouse.

<https://doi.org/10.1371/journal.pone.0193260.g004>

The increase in RE values in the liver is expected [25] from an IgG antibody. While the increase in RE values in the small intestines and spleen would suggest mTAB004 accumulation at the organs, and could be explained by some residual tumor in those organs that could not be completely dissected from the organ. Taken together, mTAB004 showed high specificity to the tumor and proves to be useful for detection of PDA by imaging.

Chimeric TAB004. Due to promising results with mTAB004, we generated a chimeric version of the antibody which shared an identical binding profile to mTAB004 in an ELISA

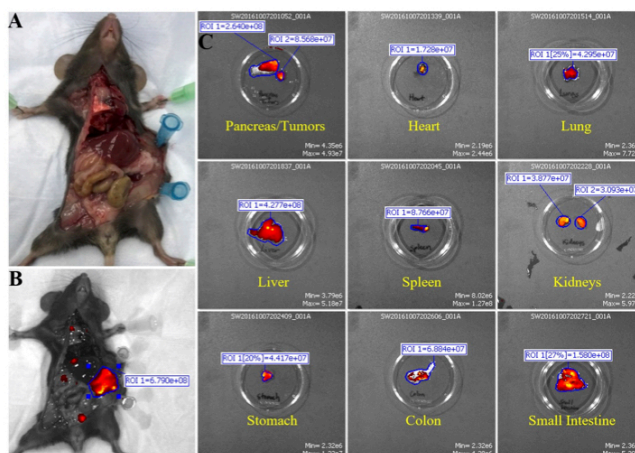


Fig 5. Fluorescent IVIS images of organs from mouse injected with murine monoclonal TAB004. Representative images are shown. (A) Photograph images of mouse to show location of tumor. (B) The mouse is imaged with filter pair ICG on the IVIS Spectrum. Background has been removed and the ROI measurements for the tumor are shown. (C) Organs from mouse are imaged individually in the IVIS Spectrum. Intensity of the red-yellow fluorescence in ROI measurements indicates background and antibody accumulation for each organ.

<https://doi.org/10.1371/journal.pone.0193260.g005>

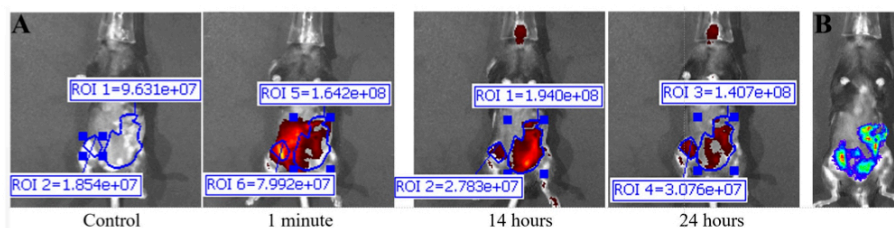


Fig 6. Fluorescent IVIS images taken at different time points of mouse injected with chimeric TAB004. Representative images are shown. (A) Fluorescent IVIS image with filter pair ICG of before (control) 1 minutes, 14 hours, and 24 hours post injection of Chimeric TAB004 with ICG. Fluorescence images taken after injection are normalized to their own control fluorescence. Background has been removed and the ROI measurements for antibody fluorescence are shown. Intensity of the red-yellow fluorescence in ROI measurements indicates background and antibody accumulation. (B) Bioluminescent image of orthotopic tumor in same mouse.

<https://doi.org/10.1371/journal.pone.0193260.g006>

(S3 Fig). A shift to humanize the antibody is essential for further development of any antibody-based targeted imaging for diagnostics or for targeted therapy. We acquired a chimeric version of TAB004, cTAB004, which comprises of murine antigen recognition moiety in a human IgG1 backbone. KCM orthotopic tumor-bearing C57/Bl6 mice were injected with cTAB004-ICG (Figs 6 and 7). Similar to the mTAB004-ICG (Fig 4), exterior ICG images taken as early as 1 minute post injection show accumulation of the cTAB004 at the tumor site (Fig 6A). The accumulation increases 14 hours PI but decreases post 24 hours (Fig 6A), similar to

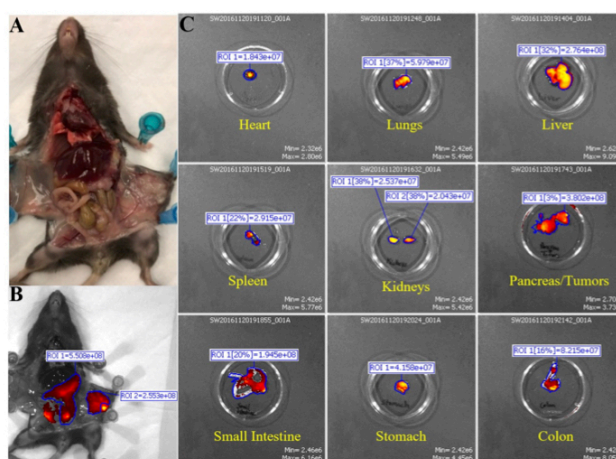


Fig 7. Fluorescent IVIS images of organs from mouse injected with chimeric TAB004. Representative images are shown. (A) Photograph images of mouse to show location of tumor. (B) The mouse is imaged with filter pair ICG on the IVIS Spectrum. Background has been removed and the ROI measurement for the tumor is shown. (C) Organs from mouse are imaged individually in the IVIS Spectrum. Intensity of the red-yellow fluorescence in ROI measurements indicates background and antibody accumulation for each organ.

<https://doi.org/10.1371/journal.pone.0193260.g007>

mTAB004 injected mice. Exterior bioluminescent image of the same mouse confirm the location of the tumor (Fig 6B). In-situ photograph of a cTAB004 injected mouse confirms the location of the tumor (Fig 7A). IVIS in-situ image shows accumulation in the tumor and few other organs (Fig 7B). Dissected organs were imaged separately by IVIS to calculate the RE. The larger region of red-yellow fluorescence indicates accumulation of cTAB004 at the tumor (Fig 7B). Significant increases in RE values were observed in the pancreatic tumor, liver, and small intestine (Fig 1); however, unlike mTAB004, there was minimal accumulation of the cTAB004 in the spleen. RE values at the tumor were ~ 3.5 fold higher while ~ 0.5 fold higher in the liver and ~2.5 fold higher in the small intestine compared to control RE values (Fig 1). As with mTAB004, RE values in the liver is expected to be higher [25] with an IgG antibody; however, the liver was significantly lower in the cTAB004 compared to mTAB004 injected mice, possibly due higher uptake of chimeric antibody by macrophages [26]. The RE values of cTAB004 in the small intestines is the same as the mTAB004 treatment group, where residual secondary tumor bodies could not be removed from the organ.

All experiments shown in Figs 2–7 were conducted with $n = 3$ mice per experimental group and representative images from 1 mouse is shown for all groups. Fig 1 shows the ROI RE values plotted for $n = 3$ mice per group and significance are represented as p value.

Tumors from 24h post cTAB004-ICG injected mice were removed, fixed, paraffin embedded, sectioned (4micron sections) and imaged under a confocal microscope to determine the cellular localization of cTAB004 ICG (Fig 8). Tumors from 3 cTAB004-ICG mice are shown alongside a control tumor from mice that were not injected with cTAB004-ICG. Tumor sections from the cTAB004-ICG injected mice display significantly more ICG fluorescent signal

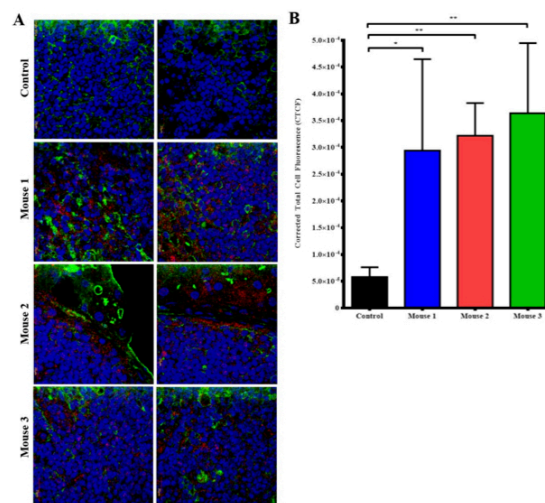


Fig 8. Confocal imaging of tumor sections from Chimeric TAB004 injected mice. Representative images shown. (A) Tumor sections from Chimeric TAB004 injected mice were sectioned into slides imaged. Blue = nucleus (DAPI), Green = cell membrane (Alexa Fluor 488), Red = Chimeric TAB004-ICG. (B) Quantification of fluorescent signal from Chimeric TAB004-ICG using Image J. Data shown is mean \pm SEM ($n = 3$) and determined by unpaired t-test. * $p < 0.05$, ** $p < 0.01$.

<https://doi.org/10.1371/journal.pone.0193260.g008>

(red) than control tumors without TAB004 ICG (Fig 8A) in all 3 mice. The blue and green fluorescent signals are DAPI (nucleus) and wheat germ agglutinin (membrane) respectively. Red ICG fluorescence was noted within the tumor bed as well as in the edges of the tumor. Most of staining seems to be localized in the surface and cytoplasm of the tumor cells. Green fluorescence suggests the disorganized membrane staining typical of undifferentiated tumors. Quantification of the red fluorescence showed significant increase in the corrected total cell fluorescence (Fig 8B).

Overall, we have shown that cTAB004 behaves nearly identical to mTAB004 when binding to the pancreas/tumor site, with no loss in accumulation index, which was determined by the RE values (summarized in Fig 7). Expected accumulation in other organs, besides the liver, was not significantly higher than control groups. cTAB004 is highly specific for the tumor and provides rationale for further development of this platform technology for targeted imaging of PDA.

Targeting the pancreas before PDA develops in the KCM mice

Although we determined the specific targeting in an orthotopic tumor model, the question remains if this antibody can be developed for early detection of pre-neoplastic lesions prior to the development of PDA. As a starting point to address this question, we generated KCM mice by crossing the LSL-KRAS^{G12D} with the tamoxifen inducible P⁴⁸Cre with the human MUC1. Tg mice [13]. These triple transgenic KCM mice develop spontaneous PDA when induced with tamoxifen. As controls, we generated KC mice that are double transgenic cross between LSL-KRAS^{G12D} x tamoxifen-inducible P⁴⁸Cre mice. KC mice do not express the human MUC1. Tamoxifen was injected in KCM and KC mice to initiate oncogenesis while control KCM mice remained without tamoxifen (therefore no initiation of oncogenesis). The 3 groups of mice (tamoxifen-induced or un-induced KCM and KC mice) were injected with cTAB004-ICG and imaged 24 hours PI (Fig 9). Both KC and KCM mice without tamoxifen induction did not display any ICG fluorescence signal in the pancreas from the exterior (Fig 9A and 9B left) or interior (Fig 9A and 9B right) IVIS images where the pancreas was imaged at its original and secondary positions. Secondary position represents moving the pancreas in situ using a forceps to confirm that any fluorescence signal is originating from the pancreas and nowhere else. As early as 3-weeks post tamoxifen induction, KCM mice showed ICG fluorescent signal over background from the exterior (Fig 9C left) and interior (Fig 9C right) IVIS images. Moving the pancreas from behind the liver and stomach displays a clearer ICG fluorescent signal over background (Fig 9C far right). Organs from these animals were also imaged with the pancreas possessing the highest level of RE over other organs, similar to the orthotopic tumor model (S3 Fig). None of the other organs showed fluorescence signal above background levels. It must be noted that in these KCM mice, all other glandular epithelial organs express normal human MUC1 but TAB004-ICG only accumulates in the pancreas post initiation of oncogenesis suggesting the high specificity of TAB004 to transformed/tumor associated form of MUC1. Based on our previous publication, we infer that at 3-weeks post completion of tamoxifen treatment, the mice have PanIN lesions 1a and b [13]. Additionally, KCM mice 11 weeks post tamoxifen induction, which develop PanIN 2 lesions at this point, were also injected with cTAB004-ICG to determine if it was possible to track disease progression (Fig 9D). By this time, the pancreas is larger and the TAB004-ICG fluorescent signal shows accumulation at the pancreas as well. Moving the pancreas from its primary location provides a clear image of the TAB004-ICG signal in the pancreas (Fig 9D). The control tamoxifen un-induced KCM and tamoxifen-induced KC mice at the same age showed no TAB004-ICG fluorescence in the pancreas or any other organ (S4 Fig). The data clearly suggests that cTAB004-ICG is binding to tMUC1 at very early stages in PDA initiation (at the early PanIN stage)

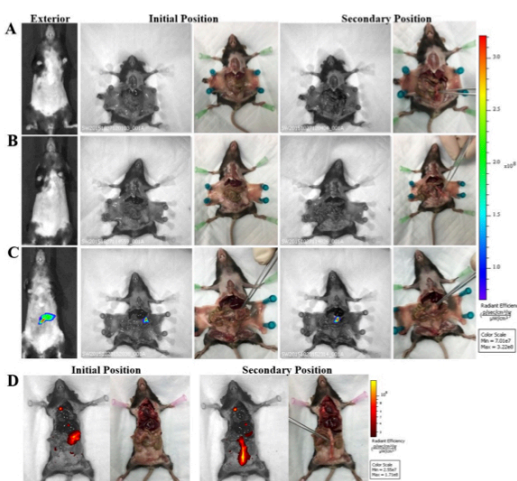


Fig 9. IVIS images of KC and KCM spontaneous mice (3 and 11 weeks PI of tamoxifen) injected with TAB004. Representative images are shown. Left to Right: Exterior IVIS images with ICG filter pair, IVIS image with ICG filter pair with pancreas in original position, photograph of original position, IVIS image with ICG filter pair with pancreas moved to secondary position, photo graph of secondary position. Forceps indicate location of pancreas. (A) KC mouse (lacks MUC1 transgene). (B) KCM mouse w/o tamoxifen treatment. (C) KCM 3 weeks post tamoxifen treatment. (D) KCM mouse 11 weeks post tamoxifen treatment. Rainbow fluorescence intensity indicates background and antibody accumulation in A-C. Red-yellow fluorescence intensity indicates background and antibody accumulation in D.

<https://doi.org/10.1371/journal.pone.0193260.g009>

and is effective in tracking disease over time. All images are representative of $n = 3$ mice per group. Finally, H&E section of the pancreas 5, 8, 11, 22, and 33 weeks post tamoxifen injection confirms the formation of abnormal ducts at 3 weeks and PanIN lesions as early as 8 weeks (Fig 10).

Discussion

The concept of molecularly targeted diagnostic approaches would be very valuable toward the goal of precision medicine. The ability to monitor preneoplastic lesions and progression on a molecular level not defined by the presence of a palpable tumor mass and before any overt physiologic symptoms have developed would permit early and more adequate therapeutic intervention. This study addresses this need by examining the possibility of predictive diagnostics for PDA in a genetically engineered mouse model of pancreatic cancer. tMUC1 is overexpressed in over 80% of pancreatic cancer patients [27,28] and is also expressed in pancreatic intraepithelial neoplasia (PanIN) lesions, precursors of PDA [13]. This makes it a promising target for early detection and diagnostics of PDA. Specifically, we illustrate the detection of the changes in the expression profile of the molecular biomarker tMUC1 with a noninvasive imaging approach. By focusing on early disease, i.e., the PanIN lesion, we explore a scenario in which the molecular changes in tMUC1 precede changes in anatomical and physiologic signs of tumor development. This study extends our prior work in breast cancer, which demonstrated that changes in MUC1 antigen that occur in breast cancer development could be detected *in vivo* using TAB004 as a carrier for imaging agent [17,29]. By broadening the application of

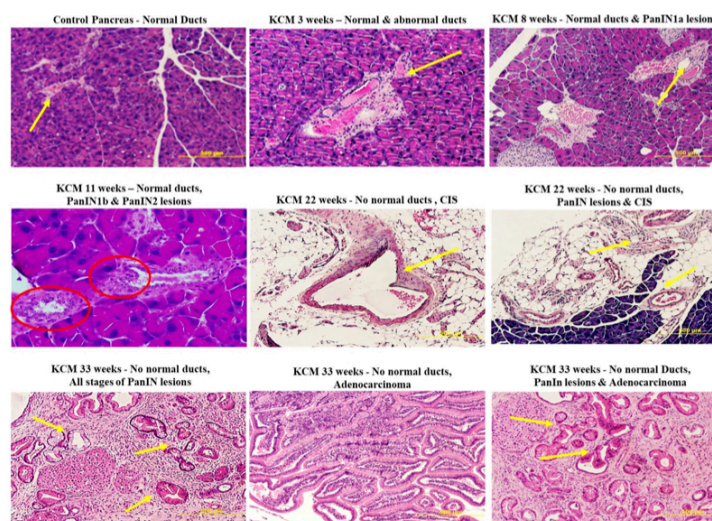


Fig 10. Immunohistochemistry images of pancreas from KCM mice. Representative images are shown. At different weeks post tamoxifen treatment, the progression from abnormal ducts to full adenocarcinoma is identified by H&E staining.

<https://doi.org/10.1371/journal.pone.0193260.g010>

this methodology to pancreatic cancer, we move closer to establishing the value of tMUC1 as a wide-ranging cancer biomarker.

Progress has already been made in the direction of targeted cancer diagnostics. An example includes screening for the BRCA mutation for the assessment of breast cancer risk. With regard to noninvasive imaging, the development of dynamic MRI techniques, magnetic resonance spectroscopy and positron emission tomography have contributed to progress. Still, none of these technologies probes for specific molecular biomarkers expressed by cells in proportion to their potential for malignancy. Consequently, this highly specific molecular imaging approach has the potential for capturing the earliest signs of neoplastic transformation and in the future permit predictive diagnosis and response to therapy.

Our results from the orthotopic tumor model demonstrate that TAB004 is highly specific in targeting the PDA tumor and does not accumulate in other organs. In control group 1 (normal C57/Bl6 mice) and 2 (KCM-Luc tumor bearing mice—no TAB004 injected), we established background fluorescence levels for the mice and used these values to determine antibody accumulation at the tumor site and other organs. Control groups 3 (non-tumor bearing mice injected with isotype IgG1-ICG) and 4 (KCM-Luc tumor bearing mice injected with isotype IgG1-ICG) displayed no significant increase in fluorescence levels in all regions when compared to control groups 1 and 2, suggesting that from an imaging standpoint, non-targeting antibody at the chosen concentration clears from the mice in 24 hours. The significant increase in RE within the pancreas/tumor in mTAB004 and cTAB004 injected groups clearly demonstrates the retention of the targeting antibody. The livers from TAB004 injected groups displayed significant increase in RE over the control groups as well, with mTAB004 showing a greater increase over cTAB004. This appears to be a specific effect, possibly due to the presence

of hepatic metastases from pancreatic cancer [30]. It also appears that TAB004 accumulates in the small intestine and spleen of mice, due to the increase in RE (Fig 7). Due to the orthotopic nature of the tumor, we have evidenced outgrowth of the primary pancreatic tumor into the surrounding organs including the spleen and small intestine due to their proximity to the pancreas. Whether this outgrowth is due to true metastasis or dissemination of tumor cells while injection is not clear at this time. Cells from the initial injection may leak out and cause many secondary tumors in the intraperitoneal space. Furthermore, we confirm that TAB004-ICG accumulates in the margins and within the pancreatic tumor bed (Fig 8). Other studies have attempted to target tMUC1 for diagnostic, imaging, and targeted therapy [17,31–33]. However, due to the non-specificity of most of the MUC1 antibodies, we believe that TAB004 can improve the specific visualization of pancreatic tumor. Furthermore, fluorescent-tagged antibody may be useful in defining the tumor margins improving patient outcome that are eligible for resection [34].

Finally, we utilized a genetically engineered mouse model that spontaneously induced human tMUC1-positive pancreatic cancer (in KCM mouse) (Figs 9 and 10). The data from the KCM mice show that TAB004 can target tMUC1 being expressed in the pancreas before PDA develops. Examination of the pancreas from KCM mice show no evidence of a primary tumor, but IHC sections from these mice show the presence of PanIN 2 lesions. PanIN 2 lesions are the first stage in the development of PDA that is associated with significant genetic and molecular changes [35]. This early detection of the PanIN lesions can be translated into early detection of PDA and significantly improve disease outcome [5,36]. Recent studies have shown there is an association of pancreatic cancer with new onset diabetes [37–39]. In some studies, diabetes was determined to be present in nearly half of the pancreatic cancer patients at diagnosis, with 75%–88% of the cases of diabetes being new onset [40,41]. It is also interesting that other studies have shown that patients with new onset diabetes have a higher chance of developing pancreatic cancer [42–44]. Perhaps the methods used in this study can be adapted for early detection of pancreatic cancer in people with new onset diabetes.

The use of ICG as an imaging agent is a limitation in this proof of concept study demonstrating the ability of TAB004 to target early stages of PDA its tumors in an immune competent model. While ICG imaging is effective in mice, it may not be as effective in humans. As an advantage, ICG has a high photon count rate, but its depth of penetration is estimated to be between 2 and 4 cm [45], limiting its utility to imaging near the surface of the patients skin or patients undergoing surgery. There is a trend to shift from fluorescent imaging to radiolabeling targeting agents such as antibodies [46] to overcome this penetrance limitation. Single-photon emission computed tomography (SPECT) and positron emission tomography (PET) are the two major molecular imaging modalities based on the detection of radioactive decay. Both PET and SPECT do not have limits in regards to their penetration depth and the image data is highly quantifiable [47–49]. For future studies we propose to use a fully humanized version of TAB004 with radioisotope labeling to target human xenograft tumors in immune compromised mice. Presently, this is outside the scope of this study.

As tMUC1 expression has global relevance in adenocarcinomas including pancreatic cancer, this study focused on applying our imaging approach to pancreatic cancer, as it has the lowest survival rate among all common cancers.

Supporting information

S1 Fig. Fluorescent IVIS images of organs from normal C57/Bl6. Representative images are shown. (A) The mouse is imaged with filter pair ICG on the IVIS Spectrum. Background has been removed and the ROI measurement for the area where tumor would have been present is shown. (B) Organs from mouse are imaged individually in the IVIS Spectrum. Intensity of the

red-yellow fluorescence in ROI measurements indicate background levels for each organ. (TIF)

S2 Fig. Fluorescent and bioluminescent IVIS images of organs from normal C57/Bl6 with orthotopic KCM-Luc tumors without TAB004 ICG injection. Representative images are shown. (A) Bioluminescent image of tumor. Rainbow indicates tumor site. (B) Photograph images of mouse to show location of tumor. (C) The mouse is imaged with filter pair ICG on the IVIS Spectrum. Background has been removed and the ROI measurements for the area where tumor is present and would have been present are shown. (D) Organs from mouse are imaged individually in the IVIS Spectrum. Intensity of the red-yellow fluorescence in ROI measurements indicates background levels for each organ. (TIF)

S3 Fig. Binding profiles of murine and chimeric TAB004. The binding profiles of mTAB004 (red) and cTAB004 (blue) were determined by ELISA and the OD values graphed against concentrations of KCM lysate. (TIF)

S4 Fig. Fluorescent IVIS images of organs from KCM mice. Representative images are shown. (A) IVIS images with ICG filter pair of organs from KCM Spontaneous mouse 3 weeks post tamoxifen induction, KCM Spontaneous mouse w/o tamoxifen, and a KC mouse. B) Organs from a KCM Spontaneous mouse 11 weeks post tamoxifen induction. Left—photograph of organs, Middle—Legend, Right—IVIS images with ICG filter pair. Intensity of the red-yellow fluorescence in ROI measurements indicates background and antibody accumulation for each organ. (TIF)

S5 Fig. Quantification of ROI values from control imaging groups. The ROI radiance efficiency values for organs from control groups were quantified used Living Image software. Data shown is mean \pm SEM (n = 3), except for Mouse IgG1 in KCM group (n = 1, only 1 mouse was available for this experiment). (TIF)

Acknowledgments

This work was supported by the CPCP Levine UNCC Pancreatic Cancer Pilot Project, National Institutes of Health, National Cancer Institute (NIH-NIC Grant RO1 CA118944-01A1), UNC Charlotte Faculty Research Grant, and UNC Charlotte, The Williams States Lee College of Engineering, Center for Biomedical Engineering and Science IVIS Imaging System Award. The authors thank Laura J. Moore and the UNC Charlotte's Vivarium staff, A. Perez and H. Gordils, for their support in caring for the animals. We also thank OncoTAB, Inc., for supplying TAB004 that was used in this research.

Author Contributions

Conceptualization: Shu-ta Wu, Pinku Mukherjee.

Data curation: Shu-ta Wu.

Funding acquisition: Pinku Mukherjee.

Investigation: Shu-ta Wu, Priyanka A. Grover.

Methodology: Shu-ta Wu, Chandra D. Williams, Laura J. Moore, Pinku Mukherjee.

Project administration: Shu-ta Wu, Pinku Mukherjee.

Resources: Pinku Mukherjee.

Supervision: Pinku Mukherjee.

Validation: Shu-ta Wu, Pinku Mukherjee.

Visualization: Shu-ta Wu, Pinku Mukherjee.

Writing – original draft: Shu-ta Wu.

Writing – review & editing: Shu-ta Wu, Pinku Mukherjee.

References

1. Siegel RL, Miller KD, Jemal A (2017) Cancer statistics, 2017. *CA: A Cancer Journal for Clinicians* 67: 7–30.
2. Melisi D, Budillon A (2012) Pancreatic cancer: between bench and bedside. *Curr Drug Targets* 13: 729–730. PMID: 22458518
3. Tamburrino A, Piro G, Carbone C, Tortora G, Melisi D (2013) Mechanisms of resistance to chemotherapeutic and anti-angiogenic drugs as novel targets for pancreatic cancer therapy. *Front Pharmacol* 4: 56. <https://doi.org/10.3389/fphar.2013.00056> PMID: 23641216
4. Yeo CJ, Cameron JL (1998) Prognostic factors in ductal pancreatic cancer. *Langenbeck's Archives of Surgery* 383: 129–133. PMID: 9641885
5. Shimizu Y, Yasui K, Matsueda K, Yanagisawa A, Yamao K (2005) Small carcinoma of the pancreas is curable: new computed tomography finding, pathological study and postoperative results from a single institute. *J Gastroenterol Hepatol* 20: 1591–1594. <https://doi.org/10.1111/j.1440-1746.2005.03895.x> PMID: 16174079
6. Hatrup CL, Gendler SJ (2008) Structure and function of the cell surface (tethered) mucins. *Annu Rev Physiol* 70: 431–457. <https://doi.org/10.1146/annurev.physiol.70.113006.100659> PMID: 17850209
7. Gendler SJ (2001) MUC1, The Renaissance Molecule. *Journal of Mammary Gland Biology and Neoplasia* 6: 339–353. PMID: 11547902
8. Yolken RH, Peterson JA, Vonderfecht SL, Fouts ET, Midhun K, et al. Human milk mucin inhibits rotavirus replication and prevents experimental gastroenteritis. *The Journal of Clinical Investigation* 90: 1984–1991. <https://doi.org/10.1172/JCI116078> PMID: 1331178
9. Burdick MD, Harris A, Reid CJ, Iwamura T, Hollingsworth MA (1997) Oligosaccharides expressed on MUC1 produced by pancreatic and colon tumor cell lines. *J Biol Chem* 272: 24198–24202. PMID: 9305871
10. Patton S, Gendler SJ, Spicer AP (1995) The epithelial mucin, MUC1, of milk, mammary gland and other tissues. *Biochim Biophys Acta* 1241: 407–423. PMID: 8547303
11. Roy LD, Sahraei M, Subramani DB, Besmer D, Nath S, et al. (2011) MUC1 enhances invasiveness of pancreatic cancer cells by inducing epithelial to mesenchymal transition. *Oncogene* 30: 1449–1459. <https://doi.org/10.1038/ncr.2010.526> PMID: 21102519
12. Cheever MA, Allison JP, Ferris AS, Finn OJ, Hastings BM, et al. (2009) The Prioritization of Cancer Antigens: A National Cancer Institute Pilot Project for the Acceleration of Translational Research. *Clinical Cancer Research* 15: 5323–5337. <https://doi.org/10.1158/1078-0432.CCR-09-0737> PMID: 19723653
13. Tinder TL, Subramani DB, Basu GD, Bradley JM, Schettini J, et al. (2008) MUC1 enhances tumor progression and contributes toward immunosuppression in a mouse model of spontaneous pancreatic adenocarcinoma. *J Immunol* 181: 3116–3125. PMID: 18713982
14. Besmer DM, Curry JM, Roy LD, Tinder TL, Sahraei M, et al. (2011) Pancreatic ductal adenocarcinoma mice lacking mucin 1 have a profound defect in tumor growth and metastasis. *Cancer Res* 71: 4432–4442. <https://doi.org/10.1158/0008-5472.CAN-10-4439> PMID: 21558393
15. Sahraei M, Roy LD, Curry JM, Teresa TL, Nath S, et al. (2012) MUC1 regulates PDGFA expression during pancreatic cancer progression. *Oncogene* 31: 4935–4945. <https://doi.org/10.1038/ncr.2011.651> PMID: 22266848
16. Curry JM, Thompson KJ, Rao SG, Besmer DM, Murphy AM, et al. (2013) The use of a novel MUC1 antibody to identify cancer stem cells and circulating MUC1 in mice and patients with pancreatic cancer. *J Surg Oncol* 107: 713–722. <https://doi.org/10.1002/jso.23316> PMID: 23335066
17. Moore LJ, Roy LD, Zhou R, Grover P, Wu ST, et al. (2016) Antibody-Guided In Vivo Imaging for Early Detection of Mammary Gland Tumors. *Transl Oncol* 9: 295–305. <https://doi.org/10.1016/j.tranon.2016.05.001> PMID: 27567952

18. Curry JM, Thompson KJ, Rao SG, Besmer DM, Murphy AM, et al. (2013) The Use of a Novel MUC1 Antibody to Identify Cancer Stem Cells and Circulating MUC1 in Mice and Patients With Pancreatic Cancer. *Journal of surgical oncology* 107: <https://doi.org/10.1002/jso.23316> PMID: 23335066
19. Nath S, Daneshvar K, Roy LD, Grover P, Kidlyoor A, et al. (2013) MUC1 induces drug resistance in pancreatic cancer cells via upregulation of multidrug resistance genes. *Oncogenesis* 2: e51. <https://doi.org/10.1038/oncsis.2013.16> PMID: 23774063
20. Fokas E, O'Neill E, Gordon-Weeks A, Mukherjee S, McKenna WG, et al. (2015) Pancreatic ductal adenocarcinoma: From genetics to biology to radiobiology to oncoimmunology and all the way back to the clinic. *Biochim Biophys Acta* 1855: 61–82. <https://doi.org/10.1016/j.bbcan.2014.12.001> PMID: 25489989
21. Zhou R, Curry JM, Roy LD, Grover P, Haider J, et al. (2016) A novel association of neuropilin-1 and MUC1 in pancreatic ductal adenocarcinoma: role in induction of VEGF signaling and angiogenesis. *Oncogene*.
22. Zhou R, Curry JM, Roy LD, Grover P, Haider J, et al. (2016) A novel association of neuropilin-1 and MUC1 in pancreatic ductal adenocarcinoma: role in induction of VEGF signaling and angiogenesis. *Oncogene* 35: 5608–5618. <https://doi.org/10.1038/ncr.2015.516> PMID: 26804176
23. Von Hoff DD, Ervin T, Arena FP, Chiorean EG, Infante J, et al. (2013) Increased Survival in Pancreatic Cancer with nab-Paclitaxel plus Gemcitabine. *The New England journal of medicine* 369: 1691–1703. <https://doi.org/10.1056/NEJMoa1304369> PMID: 24131140
24. Von Hoff DD, Ervin T, Arena FP, Chiorean EG, Infante J, et al. (2013) Increased survival in pancreatic cancer with nab-paclitaxel plus gemcitabine. *N Engl J Med* 369: 1691–1703. <https://doi.org/10.1056/NEJMoa1304369> PMID: 24131140
25. Schneider DW, Heitner T, Alicke B, Light DR, McLean K, et al. (2009) In Vivo Biodistribution, PET Imaging, and Tumor Accumulation of 86Y- and 111In-Antimirdin/RG-1, Engineered Antibody Fragments in LNCaP Tumor-Bearing Nude Mice. *Journal of Nuclear Medicine* 50: 435–443. <https://doi.org/10.2967/jnumed.108.055608> PMID: 19223400
26. Overdijk MB, Verploegen S, Ortiz Buijse A, Vink T, Leusen JH, et al. (2012) Crosstalk between human IgG isotypes and murine effector cells. *J Immunol* 189: 3430–3438. <https://doi.org/10.4049/jimmunol.1200356> PMID: 22956577
27. Qu CF, Li Y, Song YJ, Rizvi SM, Raja C, et al. (2004) MUC1 expression in primary and metastatic pancreatic cancer cells for in vitro treatment by (213)Bi-C595 radioimmunoconjugate. *Br J Cancer* 91: 2086–2093. <https://doi.org/10.1038/sj.bjc.6602232> PMID: 15599383
28. Winter JM, Tang LH, Klimstra DS, Brennan MF, Brody JR, et al. (2012) A novel survival-based tissue microarray of pancreatic cancer validates MUC1 and mesothelin as biomarkers. *PLoS One* 7: e40157. <https://doi.org/10.1371/journal.pone.0040157> PMID: 22792233
29. Dreau D, Moore LJ, Alvarez-Berrios MP, Tarannum M, Mukherjee P, et al. (2016) Mucin-1-Antibody-Conjugated Mesoporous Silica Nanoparticles for Selective Breast Cancer Detection in a Mucin-1 Transgenic Murine Mouse Model. *Journal of Biomedical Nanotechnology* 12: 2172–2184. <https://doi.org/10.1166/jbn.2016.2318> PMID: 28522938
30. Katada T, Hashidate H, Yokoyama N, Sudo N, Mitsuma K, et al. (2017) Initial Features of Hepatic Metastases From Pancreatic Cancer: Histological and Radiological Appraisal of Hepatic Micrometastases Detected by Real-Time Fluorescent Imaging. *Pancreas* 46: 1196–1201. <https://doi.org/10.1097/MPA.0000000000000915> PMID: 28902791
31. Pascual L, Cerqueira-Coutinho C, Garcia-Fernandez A, de Luis B, Bernardes ES, et al. (2017) MUC1 aptamer-capped mesoporous silica nanoparticles for controlled drug delivery and radio-imaging applications. *Nanomedicine*.
32. Santos do Carmo F, Ricci-Junior E, Cerqueira-Coutinho C, Albernaz MS, Bernardes ES, et al. (2017) Anti-MUC1 nano-aptamers for triple-negative breast cancer imaging by single-photon emission computed tomography in induced animals: initial considerations. *Int J Nanomedicine* 12: 53–60. <https://doi.org/10.2147/IJN.S118482> PMID: 28053523
33. Park JY, Hiroshima Y, Lee JY, Maawy AA, Hoffman RM, et al. (2015) MUC1 selectively targets human pancreatic cancer in orthotopic nude mouse models. *PLoS One* 10: e0122100. <https://doi.org/10.1371/journal.pone.0122100> PMID: 25815753
34. Yeh R, Steinman J, Luk L, Kluger MD, Hecht EM (2017) Imaging of pancreatic cancer: what the surgeon wants to know. *Clin Imaging* 42: 203–217. <https://doi.org/10.1016/j.clinimag.2016.10.002> PMID: 28110203
35. Buchholz M, Braun M, Heidenblut A, Kestler HA, Kloppel G, et al. (2005) Transcriptome analysis of microdissected pancreatic intraepithelial neoplastic lesions. *Oncogene* 24: 6626–6636. <https://doi.org/10.1038/sj.onc.1208804> PMID: 16103885

36. Zhou B, Xu JW, Cheng YG, Gao JY, Hu SY, et al. (2017) Early detection of pancreatic cancer: Where are we now and where are we going? *Int J Cancer* 141: 231–241. <https://doi.org/10.1002/ijc.30670> PMID: 28240774
37. Pannala R, Basu A, Petersen GM, Chari ST (2009) New-onset diabetes: a potential clue to the early diagnosis of pancreatic cancer. *Lancet Oncol* 10: 88–95. [https://doi.org/10.1016/S1470-2045\(08\)70337-1](https://doi.org/10.1016/S1470-2045(08)70337-1) PMID: 19111249
38. Illes D, Terzin V, Holzinger G, Kosar K, Roka R, et al. (2016) New-onset type 2 diabetes mellitus—A high-risk group suitable for the screening of pancreatic cancer? *Pancreatol* 16: 266–271. <https://doi.org/10.1016/j.pan.2015.12.005> PMID: 26777407
39. Tantau A, Negrean V, Alexescu T, Para I, Tarmure S, et al. (2014) Two different types of diabetes mellitus in pancreatic cancer population. Comparative study between new onset and long standing diabetes mellitus on 76 patients with pancreatic cancer. *Rom J Intern Med* 52: 18–23. PMID: 25000673
40. Pannala R, Leirness JB, Bamlet WR, Basu A, Petersen GM, et al. (2008) Prevalence and clinical profile of pancreatic cancer-associated diabetes mellitus. *Gastroenterology* 134: 981–987. <https://doi.org/10.1053/j.gastro.2008.01.039> PMID: 18395079
41. Chari ST, Klee GG, Miller LJ, Raimondo M, DiMagno EP (2001) Islet amyloid polypeptide is not a satisfactory marker for detecting pancreatic cancer. *Gastroenterology* 121: 640–645. PMID: 11522748
42. Chari ST, Leibson CL, Rabe KG, Ransom J, de Andrade M, et al. (2005) Probability of pancreatic cancer following diabetes: a population-based study. *Gastroenterology* 129: 504–511. <https://doi.org/10.1053/j.gastro.2005.05.007> PMID: 16083707
43. Damiano J, Bordier L, Le Berre JP, Margery J, Dupuy O, et al. (2004) Should pancreas imaging be recommended in patients over 50 years when diabetes is discovered because of acute symptoms? *Diabetes Metab* 30: 203–207. PMID: 15223996
44. Ogawa Y, Tanaka M, Inoue K, Yamaguchi K, Chijiwa K, et al. (2002) A prospective pancreatographic study of the prevalence of pancreatic carcinoma in patients with diabetes mellitus. *Cancer* 94: 2344–2349. PMID: 12015758
45. Marshall MV, Rasmussen JC, Tan IC, Aldrich MB, Adams KE, et al. (2010) Near-Infrared Fluorescence Imaging in Humans with Indocyanine Green: A Review and Update. *Open surgical oncology journal (Online)* 2: 12–25. <https://doi.org/10.2174/1876504101002010012> PMID: 22924087
46. Wallberg H, Stahl S (2013) Design and evaluation of radiolabeled tracers for tumor imaging. *Biotechnol Appl Biochem* 60: 365–383. <https://doi.org/10.1002/bab.1111> PMID: 24033592
47. Condeelis J, Weissleder R (2010) In vivo imaging in cancer. *Cold Spring Harb Perspect Biol* 2: a003848. <https://doi.org/10.1101/cshperspect.a003848> PMID: 20861158
48. Levin CS (2005) Primer on molecular imaging technology. *Eur J Nucl Med Mol Imaging* 32 Suppl 2: S325–345.
49. Tolmachev V, Ortova A (2010) Influence of labelling methods on biodistribution and imaging properties of radiolabelled peptides for visualisation of molecular therapeutic targets. *Curr Med Chem* 17: 2636–2655. PMID: 20491631

CONTRIBUTIONS, HONORS, AND AWARDS

Awards

06/2019	Chosen as one of 100 Leaders of Tomorrow in Biotechnology by the Gap Summit and the Global Biotech Revolution. Will present solutions to Biotechnology problems to world-class academics, industry leaders, and government officials.
05/2019	Chosen as the commencement speaker for the May 2019 Doctoral Hooding ceremony, UNCC
12/2018	Chosen as Graduate Marshal for the December Doctoral Hooding Ceremony, UNCC
Fall 2018	Spring Graduate Professional Student Government Travel Award given * Cash prize \$500
05/2018	1 st place in 2018 UNC Charlotte College of Bioinformatics and Engineering Competition * Cash travel prize of \$500
Spring 2018	2 nd place in Poster Category of Physical and Natural Sciences at UNCC Graduate Research Symposium * Cash prize \$150
Fall 2017	Spring Graduate Professional Student Government Travel Award given * Cash prize \$500
Fall 2016-current	GASP Tuition Award for PhD students for each academic year
Spring 2015	UNCC CBES Graduate Student Travel Award * Cash prize \$500
Fall 2015	Spring Graduate Professional Student Government Travel Award given * Cash prize \$500
Fall 2014	UNCC Masters Student Tuition Award
Spring 2014	UNCC Masters Student Tuition Award

- 05/2014 2nd place in 2014 UNC Charlotte College of Bioinformatics and Engineering Competition
* Cash prize of \$300
- 05/2014 Nominated for Teaching Award for 1000 and 2000 levels category for Spring 2014

Leadership

- 06/2018 – current President for Graduate & Professional Student Government (GPSG) of UNCC.
* Winner of first popular election vote for GPSG. Chosen to advocate for the interests of the graduate community on and off UNCC campus.
* Led the Independence of the graduate student government from the undergraduate student government to better represent the UNCC graduate students. Vote passed with 91% in favor campuswide. The only precedence in the NC system is UNC-Chapel Hill.
- 05/2018 – current Vice-President of Association of Biological Sciences Graduate Students, UNCC
- 05/2017 – 05/2018 President of Association of Biological Sciences Graduate Students, UNCC
* Organizer of the 5th Annual Biological Sciences Symposium of UNCC
- Spring 2017 Leadership Graduate Module, Graduate School of UNCC
* Will provide distinction on transcript
- 09/2016 – 05/2017 Secretary of Association of Biological Sciences Graduate Students, UNCC

Committees

- 03/2018 – current Inaugural committee member of Reynolds Award for Leadership, UNCC Graduate School
- 08/2018 – current Graduate Representative of the Graduate Council, UNCC
* Provides the Graduate Student perspective as the only student on the council.

Fall 2018 – current	Steering committee member of the Chancellor’s Diversity Fund Grant – “Changing the Lens: Graduate Scientists Building Student Science Capital in Title 1 K12 Classrooms”
Fall 2018	Member of the Harshini V. De Silva Graduate Mentor Award Committee
08/2017 – 05/2018	Member of Graduate Finance Committee, Graduate School of UNCC * One of four in charge of \$110,000 budget for graduate student activities and travel at UNCC
Spring 2017	Member of Graduate Dinner Committee, Graduate School of UNCC

Memberships

06/2016 – current	American Association for the Advancement of Science
04/2014 – current	American Society of Clinical Oncologists
12/2013 – current	American Association of Cancer Research, Associate Member * Member of AACR – Women in Cancer Research
09/2013 – current	Association of Biological Sciences Graduate Students, Department of Biological Sciences, UNCC
09/2013 – current	Graduate & Professional Student Government, UNCC

Speaking

June 5-7 2018	2018 St. Jude Future Fellow Research Conference * From over 1,500 students invited to apply for the 2018 St. Jude symposia, I am one of 21 students selected by a faculty review committee to attend.
04/21/2018, 04/29/2017	Invited speaker at Project GENES Symposium, Pfeiffer University, North Carolina * Project GENES invites science interested, Charlotte-area high school students who will be the first of their family to attend college. I have the privilege of discussing cancer research to them and their families.

04/13/2018 Guest Lecturer in UNCC BIOL 2140 Lab Recitation
 * Discuss Biological Sciences research with freshmen and sophomores of UNCC.

Mentorships

Undergraduates

01/2019 – current Benjamin Jaques, UNCC Biology student

08/2018 – current student Chelsea Maccow – UNCC Honors Biology Research
 * Will complete Honors Research Thesis project

Summer 2018 Paul Slota, Case Western Reserve University

2014-2016 Haohiep Nyugen, former UNCC student
 *Currently, medical student at St. George's University in Grenada

High School

Summer 2017 Rhea Gopali

Summer 2015-16 Coral Levkovitz

Summer 2015 Vijay Rachakonda

Summer 2014 Aditya Banerji

Papers

1. **Priyanka Grover**, Monica D Nye, Mahboubeh Yazdanifar, Mohammad Ahmad, Ru Zhou, Lopamudra Das Roy, Kajal Grover, Shu-ta Wu, Sritama Nath, Pinku Mukherjee. 'MUC1 regulates TGF- β function in Pancreatic Cancer.' Manuscript in preparation.
2. Mahboubeh Yazdanifar, Ru Zhou, **Priyanka Grover**, Chandra Williams, Mukulika Bose, Shu-ta Wu, Richard Chi, Didier Dreau and Pinku Mukherjee. 'Developing a novel anti-MUC1 CAR T cell for treating pancreatic cancer and breaking the resistance by combination therapy.' Manuscript in preparation.
3. Jennifer M Curry*, Dahlia M Besmer*, Timothy K. Erick, Lopamudra D. Roy, **Priyanka Grover**, Shanti Rao, Sritama Nath, Pinku Mukherjee. 'Combinational treatment with MUC1 vaccine and indomethacin reduces breast tumor burden via a COX-independent pathway.' Manuscript submitted.

4. Shu-ta Wu, Chandra D. Williams, **Priyanka A. Grover**, Laura J. Moore, Pinku Mukherjee. Early detection of pancreatic cancer in mouse models using a novel antibody, TAB004. PLOS One (2018) 12(2): e0193260. <https://doi.org/10.1371/journal.pone.0193260>
5. **Priyanka Grover***, Sritama Nath*, Monica D. Nye, Ru Zhou, Mohammad Ahmad, Pinku Mukherjee. 'SMAD4-independent regulation of TGF- β by MUC1 in a human pancreatic cancer cell line.' *Oncotarget*. 2018 Jan 5;9(6):6897-6910. doi: 10.18632/oncotarget.23966. eCollection 2018 Jan 23.
6. Laura Jeffords Moore, Lopamudra Das Roy, Ru Zhou, **Priyanka Grover**, Shu-ta Wu, Jennifer M. Curry, Lloye M. Dillon, Priya M. Puri, Mahboubeh Yazdanifar, Rahul Puri, Pinku Mukherjee, and Didier Dréau. 'Antibody-Guided In Vivo Imaging for Early Detection of Mammary Gland Tumors.' *Translational Oncology* (2016) v9 (4) 295-305; DOI: <http://dx.doi.org/10.1016/j.tranon.2016.05.001>
7. R Zhou, J Curry, L D Roy, **P Grover**, J Haider, L J Moore, S-t Wu, A Kamesh, M Yazdanifar, W A Ahrens, T Leung, P Mukherjee. 'A novel association of neuropilin-1 and MUC1 in pancreatic ductal adenocarcinoma: role in induction of VEGF signaling and angiogenesis.' *Oncogene* (2016) 35(43): 5608-5618. PMCID: PMC4960005
8. Sritama Nath, Lopamudra Das Roy, **Priyanka Grover**, Shanti Rao, Pinku Mukherjee. 'MUC1 regulates COX-2 gene expression in pancreatic cancer.' *Pancreas* (2015) 44(6): 909-917. PMCID: PMC4500655
9. Sritama Nath, Kaveh Daneshvar, Lopamudra Das Roy, **Priyanka Grover**, Logan Mosley, Amritha Kidiyoor, Mahnaz Sahraei, and Pinku Mukherjee. 'MUC1 induces drug resistance in pancreatic cancer cells via upregulation of multidrug resistance genes.' *Oncogenesis* (2013) 2, e51

Conference presentations

1. **Priyanka Grover**, Ru Zhou, Mahboubeh Yazdanifar, Mohammad Ahmad, Johanna Sanders, Kajal Grover, and Pinku Mukherjee. 'MUC1 regulates TGF- β function in Pancreatic Cancer.' Abstract presented to American Association of Cancer Research, Atlanta, 2019
2. Mahboubeh Yazdanifar, Ru Zhou, Shu-ta Wu, **Priyanka Grover**, Didier Dreau, Richard Chi, and Pinku Mukherjee. 'Developing a novel engineered T cell to target resistant pancreatic cancer.' Abstract presented to American Association of Cancer Research, Atlanta, 2019

3. **Priyanka Grover**, Mahboubeh Yazdanifar, Mohammad Ahmad, Ru Zhou, Angat Puri, Kajal Grover, Xinghua Shi, and Pinku Mukherjee. 'MUC1 regulates TGF- β function in Pancreatic Cancer.' Abstract presented UNC Charlotte College of Biological Engineering and Sciences Poster Competition, University of North Carolina at Charlotte, 2018.
 - **1st place overall**
4. **Priyanka Grover**, Mahboubeh Yazdanifar, Mohammad Ahmad, Ru Zhou, Angat Puri, Kajal Grover, Xinghua Shi, and Pinku Mukherjee. 'MUC1 regulates TGF- β function in Pancreatic Cancer.' Abstract presented to American Association of Cancer Research, Chicago, 2018
5. **Priyanka Grover**, Monica D. Nye, Mehoubeh Yazdanifar, Mohammad Ahmad, Lopamudra Das Roy, Kajal Grover, and Pinku Mukherjee. 'MUC1 regulates TGF- β function in Pancreatic Cancer.' Abstract presented at Graduate Research Symposium, University of North Carolina at Charlotte, 2018
 - **2nd place in Poster category for Natural and Physical Sciences**
6. **Priyanka Grover**, Monica D. Nye, Mehoubeh Yazdanifar, Mohammad Ahmad, Lopamudra Das Roy, Kajal Grover, and Pinku Mukherjee. 'MUC1 regulates TGF- β function in Pancreatic Cancer.' Abstract presented to UNC Charlotte College of Biological Engineering and Sciences Poster Competition, University of North Carolina at Charlotte, 2017
7. **Priyanka Grover**, Monica D. Nye, Mehoubeh Yazdanifar, Mohammad Ahmad, Lopamudra Das Roy, Kajal Grover, and Pinku Mukherjee. 'MUC1 regulates TGF- β function in Pancreatic Cancer.' Abstract presented to American Association of Cancer Research, Washington D.C., 2017
8. **Priyanka Grover**, Sritama Nath, Mohammad Ahmad, Pinku Mukherjee. 'In Pancreatic Cancer, MUC1 regulates function of TGF- β and thus enhances metastasis.' Abstract presented to American Association of Cancer Research, Philadelphia, 2015
9. **Priyanka Grover**, Sritama Nath, Mohammad Ahmad, Emily Ashkin, Pinku Mukherjee. 'In Pancreatic Cancer, MUC1 regulates function of TGF- β and thus enhances metastasis.' Abstract presented to UNC Charlotte College of Biological Engineering and Sciences Poster Competition, University of North Carolina at Charlotte, 2014

10. Ru Zhou, Jennifer Curry, **Priyanka Grover**, Lopamudra Das Roy, TinChung Leung, Pinku Mukherjee. 'MUC1 enhances neuropilin-1 signaling in pancreatic ductal adenocarcinoma.' Abstract presented to American Association of Cancer Research, San Diego, 2014
11. Sritama Nath, Lopamudra Das Roy, **Priyanka Grover**, Shanti Rao, Pinku Mukherjee. 'MUC1 regulates COX-2 gene expression in pancreatic cancer cells.' Abstract presented to Graduate Research Symposium, University of North Carolina at Charlotte, 2013
12. Sritama Nath, Lopamudra Das Roy, Shanti Rao, **Priyanka Grover**, Pinku Mukherjee. 'MUC1 regulates COX-2 gene expression in pancreatic cancer cells.' Abstract presented to American Association of Cancer Research, Washington, D.C., 2013
13. Jennifer M Curry, Dahlia M Besmer, Lopamudra D. Roy, **Priyanka Grover**, Sritama Nath, Shanti Rao, Pinku Mukherjee. 'Combinational MUC1 vaccine therapy and Indomethacin treatment reduces breast tumor burden via a COX-independent pathway.' Abstract presented to American Association of Cancer Research, Washington, D.C., 2013